

**The Development of Precast Concrete Beam-to-Column
Connections under Static, Cyclic and Sustained Loading**

Vera Agustriana Noorhidana

Submitted in accordance with the requirements for the degree of
Doctor of Philosophy

The University of Leeds
School of Civil Engineering
September 2017

The candidate confirms that the work submitted is her own, except where work which has formed of jointly-authored publications has been included. The contribution of the candidate and the other authored work has been explicitly indicated herein. The candidate confirms that appropriate credit has been given within the thesis where reference has been made to the work of others.

The work presented in Chapter 4 and 5 of the thesis has appeared in the following publication:

Noorhidana, V.A. and Forth, J.P. 2016. An experimental study on precast concrete beam-to-column connection using interlocking bars. Proceeding of the Second International Conference on Concrete Sustainability Madrid, Spain.

The candidate was responsible for generating and collecting the experimental data and the data analysis. The candidate wrote the manuscript with guidance from the co-author.

The work presented in Chapter 1, 4 and 5 of the thesis has appeared in the following publication:

Noorhidana, V.A. and Forth, J.P. 2016. Precast Concrete Beam-To-Column Connection Using Interlocking Bars, An Alternative. Concrete Plant International (CPI), December 2016.

The candidate was responsible for the experimental data and the data analysis. The candidate wrote the manuscript with guidance from the co-author.

This copy has been supplied on the understanding that it is copyright material and that no quotation from the thesis may be published without proper acknowledgement.

@2017 The University of Leeds and Vera Agustriana Noorhidana.

The right of Vera Agustriana Noorhidana to be identified as Author of this work has been asserted by her in accordance with the Copyright, Designs and Patents Act 1988.

Acknowledgements

I would like to express my sincere gratitude to my supervisor, Prof John Forth for his support, supervision, critical reviews and motivation to become an independent researcher during the various stages of the research. I would also like to acknowledge the advice provided on my research by my co-supervisor Dr Nikolaos Nikitas.

I wish to thank the technical staff (Mr. Norman Harmon, Mr. Peter Flatt, Mr. Steve Holmes, Mr. Marvin Wilman and Mr. Robert Clarke) who facilitated so much of this work.

I would like to thank my beloved mother and my late father for their blessing and encouragement throughout my study, to my husband Tas'an Junaedi, my lovely kids (Muhammad Verdy Rizaldi Noorghifari, Razan Danendra Noor Muhammad, and Raditya Ananta Noorkhairan) for their patience, understanding and love during our stay in Leeds, which without their support these achievements would not have been possible. I would also like to thank my sisters and brothers for their moral support.

I gratefully acknowledge the financial support given by the Ministry of Research Technology and Higher Education, Republic of Indonesia, and the School of Civil Engineering, University of Leeds.

Last but not least, my sincere gratitude goes to my fellow PhD students, my research colleagues who worked in the George Earle laboratory, my office mates in Room 4.12 of the Civil Engineering building and my Indonesian friends for making this place a second home away home.

Abstract

This study investigates the experimental and theoretical behaviour of an exterior precast concrete beam-column (PCBC) connection. The experimental test specimens consisted of a precast reinforced concrete beam, a precast reinforced concrete column, interlocking bars and cast-in-place (CIP) concrete. The aim of this study was to develop a ductile exterior PCBC connection, which will be comparatively simple to construct on site and be suitable for building structures in seismic zones.

Five PCBC connection specimens (namely: P1, P2, P3, P4 and P5) were tested. Two principal factors were investigated: the applied loadings and the steel fibre content contained in the CIP connections. Specimens P1, P2 and P5 contained no steel fibre ($V_f = 0\%$) in the CIP concrete. Specimens P3 and P4 contained 0.5% and 1% of steel fibre content in their CIP concrete, respectively. Specimen P1 was subjected to static loading. Specimens P2, P3 and P4 were subjected to quasi-static loading. Specimen P5 was subjected to long-term loading. All specimens had identical reinforcement details and dimensions. The beam column joint was designed based on ACI 318-2011 Sec. 21, which is proposed for earthquake-resistant structures. The connection performance was evaluated in terms of the load carrying capacity, energy dissipation, stiffness and crack propagation.

The results showed that the exterior PCBC connections failed in flexure when they were subjected to static and quasi-static loadings. Plastic hinges formed in the end of the beam (adjacent to the column); these satisfied the seismic resistant moment resisting frame requirements. The PCBC connection had 67% of the joint rigidity in comparison with a monolithic beam-column joint; this led it to have less secant stiffness and greater beam deflection. In spite of this the connection satisfied the acceptance criteria stated in ACI 374.1.-05.

The rotation of the beam-column connection did not stop when the initial loading was applied; it continued during sustained loading, which generated a bigger deflection of the PCBC connection. A modification of the ACI long-term deflection equation has been proposed taking into account 67% of the joint rigidity. As a result of the modification the theoretically predicted deflection was found to be in agreement with that measured in experiments.

The steel fibre contained in the CIP connection delayed the onset of cracking and slowed down the rate of crack propagation, causing shorter cracks in the joint core and the beam core. Furthermore, SFRC improved the energy dissipation of the connections.

A finite element analysis was performed on an exterior PCBC connection using MIDAS FEA software under static loading. The results showed that the model could predict the load-deflection relationship until the yield point under static loading. A further finite element analysis was performed on an interior PCBC connection. The results showed that the interior PCBC connection behaved in a similar manner to a conventional reinforced concrete member under static loading.

Table of Contents

Acknowledgements	iii
Abstract	iv
Table of Contents	vi
List of Figures	x
List of Tables	xx
Notation	xxii
Abbreviation	xxv
Chapter 1 Introduction	1
1.1 Background	1
1.2 A New Precast Concrete Beam-to-Column Connection	3
1.3 Research Aims and Objectives	8
1.4 Outline of Thesis	10
Chapter 2 Literature Review	11
2.1 Introduction	11
2.2 Precast Concrete	11
2.2.1 Advantages of precast concrete	11
2.2.2 Design criteria for precast concrete connections	13
2.2.3 Seismic design concepts for precast concrete in buildings	14
2.2.4 Types of precast concrete connections	16
2.2.5 Research on precast concrete beam-column connections	17
2.3 Time-Dependent Behaviour of Reinforced Concrete Beams	28
2.3.1 Effect of shrinkage	28
2.3.2 The effect of creep	29
2.4 Bond Strength between Old Concrete and New Concrete	32
2.5 Shear Reinforcement of Beam-Column Joints	34
2.5.1 Horizontal stirrups	35
2.5.2 Intermediate column bars	36
2.5.3 Diagonal bracing bars	38
2.6 Fibre Reinforced Concrete	40

2.6.1 SFRC and bond strength	45
2.6.2 Application of FRC in seismic beam-column joints	48
2.7 Summary	58
Chapter 3 Experimental Programme	62
3.2 Introduction	62
3.3 Design of PCBC Specimens	62
3.3 Description of Specimens	65
3.3.1 Experimental programme	65
3.3.2 Description of test specimens	67
3.3.3 Geometry and reinforcement details	69
3.3.4 Materials	76
3.3.5 PCBC specimen construction	79
3.4 Test Setup and Instrumentation	83
3.4.1 Test setup	83
3.4.2 Instrumentation (LVDT, strain gauge, DEMEC points)	85
3.5 Summary	88
Chapter 4 Precast Concrete Beam-Column Connection under Static Loading	91
4.1 Introduction	91
4.2 Detail of Test Specimen P1	91
4.2.1 Mechanical properties of concrete	92
4.2.2 Loading procedure – A description of the test	93
4.3 Test Results	94
4.3.1 Load-deflection curve	94
4.3.2 Observation of cracking	98
4.3.3 Internal behaviour of Specimen P1	100
4.4 Discussion	110
4.4.1 Load-deflection relationship and failure mode	110
4.4.2 Bond strength between old concrete (U-beam) and new concrete (CIP core)	116
4.4.3 Curvatures of the U-beam	116
4.4.4 Joint core response	119
4.4.5 Theoretical calculation of nominal moment of beam	123
4.5 Conclusions	127

Chapter 5 Precast Concrete Beam-Column Connection under Quasi-Static Loading	129
5.1 Introduction	129
5.2 Acceptance Criteria	130
5.3 Detail of Test Specimen P2.....	132
5.3.1 Geometry and reinforcement detail	132
5.3.2 Test setup and instrumentation/loading procedure.....	132
5.3.3 Mechanical properties of concrete	134
5.4 Test Results.....	135
5.4.1 Failure mode.....	135
5.4.2 Load-deflection curves.....	140
5.5 Discussion	144
5.5.1 Beam-column connection behaviour with reference to the ACI Acceptance Criteria	144
5.5.2 Theoretical calculation of nominal moment of beam.....	148
5.5.3 Internal behaviour of Specimen P2	153
5.6 Conclusions	160
Chapter 6 Precast Concrete Beam-Column Connection Incorporating with Steel Fibre Reinforced Concrete	162
6.1 Introduction	162
6.2 Material.....	164
6.3 Test Results.....	166
6.3.1 Mechanical properties of concrete	166
6.3.2 Beam-Colum Connection	176
6.4 Discussion	193
6.4.1 Beam-column connection behaviour with reference to the ACI Acceptance Criteria.....	193
6.4.2 The effect of the steel fibre in the CIP-connection on the behaviour of the beam-column connections	196
6.5 Conclusions	203
Chapter 7 Precast Concrete Beam-Column Connection under Sustained Loading	205
7.1 Introduction	205
7.2 Detail of Test Specimen P5.....	206
7.2.1 Mechanical properties of the concrete	206

7.2.2	Test setup and instrumentation/loading procedure.....	207
7.3	Test Results.....	208
7.3.1	Immediate and long-term deflection	208
7.3.2	Observation of cracking	209
7.3.3	Strain development (long-term creep strain) of the U- beam.....	215
7.4	Discussion	224
7.4.1	Theoretical immediate deflection.....	224
7.4.2	Theoretical long-term deflection.....	230
7.4.3	Long-term curvatures of the U-beam	238
7.5	Conclusions	243
Chapter 8	Finite Element Modelling	245
8.1	Introduction.....	245
8.2	Material Constitutive Model.....	246
8.2.1	Concrete	246
8.2.2	Steel reinforcement	251
8.3	Modelling of Exterior PCBC Connection.....	253
8.3.1	FE model	253
8.3.2	Results and discussion	259
8.4	Modelling of Monolithic Exterior BC Joint	269
8.4.1	FE model	269
8.4.2	Results and discussion	270
8.5	Modelling of Interior PCBC Connection.....	272
8.5.1	FE Model	272
8.5.2	Result and discussion	274
8.6	Conclusions	276
Chapter 9	Conclusions and Recommendation for Future Studies	278
9.1	Introduction.....	278
9.2	Conclusions	278
9.3	Recommendation for Future Studies.....	287

List of Figures

Figure 1-1 Description of system concept	6
Figure 1-2 Detail 1 (exterior beam-column joint)	6
Figure 1-3 Detail 2 (interior beam-column joint)	7
Figure 1-4 Isometric of the beam-column specimen.....	8
Figure 2-1 Moment resisting frames with horizontal seismic loading mechanisms (Bull & Park, 1986).....	14
Figure 2-2 Moments at a beam-column joint (MacGregor, 2009)	15
Figure 2-3 Exterior beam-column connections (Ertas et al., 2006)	19
Figure 2-4 Monolithic beam-column specimens (Ertas et al., 2006)	20
Figure 2-5 Specimen hysteresis loops (Li et al., 2003).....	21
Figure 2-6 Specimen details (Li et al., 2003).....	22
Figure 2-7 Connection details of typical precast specimens (Li et al., 2003).....	23
Figure 2-8 Dimensions and details of the monolithic specimen (Park et al., 2008)	25
Figure 2-9 Dimensions and details of precast specimens (Park et al., 2008)	27
Figure 2-10 Shrinkage effect on the reinforced concrete beam	29
Figure 2-11 Effects of creep on the strain of a single reinforced section in bending (Gilbert, 2011)	30
Figure 2-12 Effect of compression reinforcement on deflections under sustained loading (Washa and Fluck, 1952; MacGregor, 1992)	31
Figure 2-13 Geometry and reinforcement detail (Kaung and Wong, 2011)	36
Figure 2-14 Column sections of Unit 4, 5 and 9 (Park and Keong, 1979)	37
Figure 2-15 Column sections of Unit 11, 12 and 13	37
Figure 2-16 Unit 4 (Park and Keong, 1979).....	38
Figure 2-17 Unit 11 at the end of loading cycles (Park and Keong, 1979)	38
Figure 2-18 Reinforcement of interior precast concrete beam-column connections (Parastesh et al., 2014).....	39

Figure 2-19 Typical failure in joint cores of (a) interior monolithic specimen (b) interior precast connection (Parastesh et al., 2014)	40
Figure 2-20 Load-deflection curves for matrix (plain concrete) and FRC (ACI 544.1 R, 1996)	41
Figure 2-21 Geometries of steel fibre (ACI 544.1 R, 1996)	42
Figure 2-22 Classification of FRC composites based on tensile stress-strain responses (Naaman and Reinhardt, 2003)	44
Figure 2-23 Deflection-softening or deflection-hardening of FRC	44
Figure 2-24 Pull-out test setup (Ganesan et al., 2014b)	46
Figure 2-25 Pull-out failures (Ganesan et al., 2014b)	47
Figure 2-26 Yielding failure (Ganesan et al., 2014b)	47
Figure 2-27 Typical beam-column T-specimen (Soubra and Naaman, 1993)	49
Figure 2-28 Reinforcement for T-specimens (Soubra and Naaman, 1993)	49
Figure 2-29 Isolated exterior beam-column connection (Marthong and Marthong, 2016)	51
Figure 2-30 Hysteresis responses of BWF and BWFSF (Marthong and Marthong, 2016)	51
Figure 2-31 Reinforcement details of specimens (a) BWF, (b) BWS and (c) CWS (Marthong and Marthong, 2016)	52
Figure 2-32 Test specimen details (Gencoglu and Eren, 2002)	54
Figure 2-33 Set-up of beam-column testing (Gencoglu and Eren, 2002)	54
Figure 2-34 Displacement controlled cyclic loading (Gencoglu and Eren, 2002)	55
Figure 2-35 Hysteresis loops of specimens #1 and #3 (Gencoglu and Eren, 2002)	55
Figure 2-36 Total dissipated energy (Gencoglu and Eren, 2002)	56
Figure 2-37 Reinforcement of BC specimens (Ganesan, <i>et al.</i> , 2007)	57
Figure 2-38 Test setup (Ganesan, <i>et al.</i> , 2007)	57
Figure 2-39 Beam-column specimens after failure (Ganesan, <i>et al.</i> , 2007)	58
Figure 3-1 Anchorage into exterior columns (ACI 318-2011)	64
Figure 3-2 Hooked bar details for the development of standard hooks (ACI 318-2011)	64
Figure 3-3 Experimental programme	66

Figure 3-4 (a) Reinforcement details of the PCBC specimen; (b) Corbel details	70
Figure 3-5 Cross section of the beam core of PCBC Specimen P1	71
Figure 3-6 Cross section of the beam core of PCBC Specimens P2 – P5.....	71
Figure 3-7 Isometrics of precast concrete beam-column connections	72
Figure 3-8 Precast U-beam.....	73
Figure 3-9 Precast column.....	73
Figure 3-10 Precast U-beam seated on the corbel of the precast column.....	74
Figure 3-11 Reinforcement detail of the joint core.....	75
Figure 3-12 Reinforcement detail in the CIP beam core of Specimen P1	75
Figure 3-13 Reinforcement cage of the precast U-beam.....	80
Figure 3-14 Joint core covered by a form before casting	82
Figure 3-15 Exterior beam-column sub assemblages (Said and Nehdi, 2004; Kalogeropoulos et al., 2016).	84
Figure 3-16 Test setup of PCBC specimens	85
Figure 3-17 Strain gauge arrangements on PCBC specimens	87
Figure 3-18 DEMEC points arrangement on PCBC specimens	87
Figure 4-1 Strain profile of the beam core	94
Figure 4-2 Load vs. beam deflection of Specimen P1	95
Figure 4-3 Beam moment vs. beam curvature	96
Figure 4-4 Load vs. strain response of the longitudinal bars of the beam in Specimen P1.....	97
Figure 4-5 Crack pattern of Specimen P1	98
Figure 4-6 Crack pattern of beam-column specimen subjected to static loading (Specimen P1)	99
Figure 4-7 Location of strain gauges on the reinforcing bars of Specimen P1	100
Figure 4-8 Load vs. strain response of the beam stirrup in Specimen P1	102
Figure 4-9 Load vs. strain response of the joint-core stirrups in Specimen P1	103
Figure 4-10 Position of DEMEC points in the joint core and the U- beam (horizontally)	104
Figure 4-11 Position of DEMEC points in the joint core (vertically).....	104

Figure 4-12 Strain development of Position I (the joint core) in Specimen P1	105
Figure 4-13 Strain development of Position II (the U-beam) of Specimen P1	105
Figure 4-14 Strain development on Position III (the U-beam) of Specimen P1	106
Figure 4-15 Strain development of Position IV (the U-beam) of Specimen P1	106
Figure 4-16 Strain development of Position V (the U-beam) of Specimen P1	107
Figure 4-17 Strain development of Position VI (the U-beam) of Specimen P1	107
Figure 4-18 Strain development of Position VII (the joint core) of Specimen P1	108
Figure 4-19 Strain development of Position VIII (the joint core) of Specimen P1	108
Figure 4-20 Strain development of Position IX (the joint core) of Specimen P1	109
Figure 4-21 Beam section before cracking: elastic behaviour	111
Figure 4-22 Test result of precast beam-column connection under gravity loads (Hasan et al., 2011)	114
Figure 4-23 Photo of cracks on the top surface of the beam core of Specimen P1	115
Figure 4-24 Cracks of the precast U-beam at the supports	115
Figure 4-26 Curvatures of the surface strain of the U-beam of Specimen P1	117
Figure 4-25 Strain profiles of the beam	117
Figure 4-27 Curvatures of the beam core and the precast U-beam for Specimen P1	119
Figure 4-28 (a) Joint core strain distribution based on DEMEC's readings, (b) Internal forces and (c) Joint shear equilibrium.....	120
Figure 4-29 Mechanism of joint shear resistance at an exterior beam-column joint (Paulay and Scarpas, 1981).....	121
Figure 4-30 Horizontal shear in an exterior joint (Uma and Prasad, 1996)	121
Figure 4-31 Cross-sectional dimensions, distribution of strain and stresses in the composite beam at the load level of 56 kN.....	124
Figure 4-32 Load vs. strain of longitudinal steel bars (SG1, SG2 and SG3).....	125

Figure 5-1 Quantities used in evaluating acceptance criteria (ACI 374.1-05, 2005)	131
Figure 5-2 Relative Energy Dissipation Ratio (β) based on ACI 374.1-05 (2005)	131
Figure 5-3 Unacceptable hysteretic behaviour (ACI 374.1-05, 2005)	132
Figure 5-4 Exterior beam-column joints (Said and Nehdi, 2004; Kalogeropoulos et al., 2016)	133
Figure 5-5 Load history for reversed cyclic load test used for Specimen P2	134
Figure 5-6 Crack-pattern of Specimen P2	137
Figure 5-7 Cracks on the joint core of Specimen P2 at the end of the test.....	137
Figure 5-8 Crack width on the beam core of Specimen P2	138
Figure 5-9 Opening between the precast U-beam and the column	139
Figure 5-10 U-beam condition Specimen P2 at the end of displacement level of 60 mm (2 nd cycle)	139
Figure 5-11 Crack-pattern on the beam-column connection (Specimen P2).....	140
Figure 5-12 Load-displacement relationship of Specimen P2	141
Figure 5-13 Bauschinger effect for steel under reverse loading (Park and Paulay, 1975)	142
Figure 5-14 Load vs. deflection loops of Specimen P2 at the displacement level of 18mm	143
Figure 5-15 Load vs. strain of top longitudinal bar of Specimen P2 at the displacement level of 18mm	143
Figure 5-16 Load-deflection curve (at 2 nd cycle) of Specimen P2 at drift ratio of 3.5% (equal with deflection level of 36mm)	147
Figure 5-17 Secant stiffness at 2 nd cycle of 60 mm displacement ($\pm 5.83\%$ of DR).....	147
Figure 5-18 Strain and stress profile of the composite beam of Specimen P2 at the displacement level of 18mm (negative bending moment).....	149
Figure 5-19 Strain and stress profile of the composite beam of Specimen P2 at the displacement level of 18mm (positive bending moment).....	151
Figure 5-20 Location of strain gauges on the reinforcing bars of Specimen P2	154
Figure 5-21 Strain response of the top interlocking bar of the beam in Specimen P2	155

Figure 5-22 Strain response of the bottom interlocking bar of the beam in Specimen P2.....	155
Figure 5-23 Strain response of the longitudinal bar of the precast U-beam in Specimen P2.....	156
Figure 5-24 Strain response of longitudinal bar of the precast column of Specimen P2.....	157
Figure 5-25 Load vs. strain response of longitudinal bar of the precast column of Specimen P2	158
Figure 5-26 Strain response of the joint stirrup (top) in Specimen P2 ...	159
Figure 5-27 Load vs. strain response of the joint stirrup (top) in Specimen P2	159
Figure 6-1 Typical measured hysteresis loops for reinforced concrete beam-column sub-assemblages Park (1988)	163
Figure 6-2 Steel fibres	165
Figure 6-3 Dimensions of the steel fibre.....	165
Figure 6-4 Flexural test set-up	169
Figure 6-5 Failure mode of the flexural test of the prism	170
Figure 6-6 MOR test of PCBC Specimen P3.....	172
Figure 6-7 MOR test of PCBC Specimen P4.....	172
Figure 6-8 Deflection-hardening and deflection-softening behaviour (Naaman and Reinhardt, 1996)	173
Figure 6-9 Load-deflection comparison between CIP connections of Specimen P3 ($V_f = 0.5\%$) and P4 ($V_f = 1.0\%$)	175
Figure 6-10 Crack pattern of beam-column Specimen P3.....	176
Figure 6-11 Crack pattern of beam-column Specimen P4.....	177
Figure 6-12 Applied load vs. load cell output readings (National Weighing & Sampling Association, 2013)	178
Figure 6-13 Load-deflection hysteresis loops of PCBC Specimen P3 containing the errors in the positive load.....	179
Figure 6-14 Load-deflection hysteresis loops of PCBC Specimen P3 containing the errors in the positive load.....	179
Figure 6-15 Load-deflection hysteresis loops of PCBC Specimen P2 ...	180
Figure 6-16 Load-deflection hysteresis loops of PCBC Specimen P3 ...	180
Figure 6-17 Load-deflection hysteresis loops of PCBC Specimen P4 ...	181
Figure 6-18 Secant stiffness (Ertas et al., 2006)	183
Figure 6-19 Secant stiffness degradation of the PCBC specimens	184
Figure 6-20 Stiffness degradation (Ganesan et al., 2014a)	185

Figure 6-21 Stiffness degradation (Marthong and Marthong, 2016)	187
Figure 6-22 Definition of normalized dissipated energy normalizing hysteretic energy dissipation at each load cycle (Parastesh et al., 2014)	188
Figure 6-23 Cumulative energy dissipation of PCBC specimens.....	189
Figure 6-24 Percentage increase of cumulative energy dissipation (refer to Specimen P2).....	189
Figure 6-25 Normalized energy dissipation (NED) of PCBC specimens P2, P3 and P4.....	190
Figure 6-26 Crack-pattern on the top surface of the beam core (CIP-concrete) at the deflection level of 3mm.....	191
Figure 6-27 Normalized energy dissipation capacity of PCBC specimens (Parastesh et al., 2014).....	192
Figure 6-28 Load-deflection curves of precast concrete beam-column specimens (Soubra and Naaman, 1993)	192
Figure 6-29 Manufacturing the U-beam	198
Figure 6-30 Crack-pattern in the joint core (CIP-concrete)	199
Figure 6-31 Load-deflection curves of Specimen P2 P3 and P4 at the displacement level of 60mm	201
Figure 6-32 Curvatures of the beam core and the precast U-beam for specimens P2, P3 and P4	202
Figure 7-1 Load vs. deflection of Specimen P5 due to an initial load of 20kN (immediate deflection)	208
Figure 7-2 Long-term deflection of PCBC Specimen P5	209
Figure 7-3 First-crack in the beam core of Specimen P5	211
Figure 7-4 Crack-pattern in the beam core	212
Figure 7-5 Crack-pattern of the beam at the end of the test	212
Figure 7-6 No cracks occurred in the joint core/column	213
Figure 7-7 Crack-pattern in the U-beam.....	214
Figure 7-8 Position of DEMEC points in the joint core and the U-beam of Specimen P5 (horizontally)	215
Figure 7-9 Position of DEMEC points in the joint core of Specimen P5 (vertically).....	216
Figure 7-10 Strain development of Position I (the joint-core) of Specimen P5	216
Figure 7-11 Strain development of Position II (the U-beam) of Specimen P5	217

Figure 7-12 Strain development of Position III (the U-beam) of Specimen P5	217
Figure 7-13 Strain development of Position IV (the U-beam) of Specimen P5	218
Figure 7-14 Strain development of Position V (the U-beam) of Specimen P5	218
Figure 7-15 Strain development of Position VI (the joint core) of Specimen P5	219
Figure 7-16 Strain development of Position VII (the joint core) of Specimen P5	219
Figure 7-17 Strain development of Position VIII (the joint core) of Specimen P5	220
Figure 7-18 Position I (the joint core): (a) The rate of strain increase of Specimen P5; (b) The strain development of Specimen P1	222
Figure 7-19 Position III: (a) The rate of strain increase of Specimen P5; (b) The strain development of Specimen P1	223
Figure 7-20 Position V: (a) The rate of strain increase of Specimen P5; (b) The strain development of Specimen P1	223
Figure 7-21 Theoretical and experimental of the load vs. deflection relationship	226
Figure 7-22 Ideal load-deflection curve (Branson, 1977).....	227
Figure 7-23 Comparison between PCBC and MBC (monolithic beam-column) joint	228
Figure 7-24 Theoretical (including the rigidity factor of 0.67) and experimental of the load vs. deflection relationship	229
Figure 7-25 Time dependent factor (MacGregor, 1992)	231
Figure 7-26 Comparison the test result of Specimen P5 and the predicted values	234
Figure 7-27 Theoretical and experimental deflection of Specimen P5 for the time-dependent factor (ξ) multiplied by 1.5	234
Figure 7-28 Moment-curvature relationship.....	236
Figure 7-29 Deformation configuration of composite beam-column connection (Hasan et al., 2011)	237
Figure 7-30 Load-deflection relation of GR1 (Hasan et al., 2011)	237
Figure 7-32 Curvature developments of the surface strain of the U-beam of Specimen P5	239
Figure 7-31 Strain profiles of the beam (Higgins et al., 2013)	239

Figure 7-33 Curvatures of the surface strain of the U-beam of Specimen P1	240
Figure 7-34 Shrinkage effect on the reinforced concrete beam	241
Figure 7-35 Effects of creep on the strain a single reinforced section in bending (Gilbert, 2011)	241
Figure 8-1 Constitutive model of material provided by Midas FEA	246
Figure 8-2 Total strain crack parameters used in this study	247
Figure 8-3 Thorenfeldt compression curve (Thorenfeldt et al., 1987) ...	248
Figure 8-4 Reduction factor due to lateral cracking (Vecchio and Collins, 1986).....	249
Figure 8-5 Hordijk tension model (Hordijk, 1991)	249
Figure 8-6 Hysteresis model (Hordijk, 1991)	250
Figure 8-7 Shear stiffness model	251
Figure 8-8 Model proposed by (Menegotto and Pinto, 1973)	252
Figure 8-9 Auto-mesh Solid in Midas FEA	254
Figure 8-10 FE meshes of the exterior PCBC connection: (a) 25mm, (b) 50mm, (c) 75mm and (d) 100mm	255
Figure 8-11 Interface mesh.....	256
Figure 8-12 Shear stress against normal stress distribution at the interface (Lampropoulos et al., 2007)	257
Figure 8-13 Properties of interface elements used in MIDAS.....	257
Figure 8-14 Boundary condition and reinforcement of exterior PCBC specimen	258
Figure 8-15 Comparison of load-deflection curves of PCBC connection between experimental and numerical results	260
Figure 8-16 Load-deflection curves with different friction angle of the interface (i.e. 2, 5 and 30 Degrees).....	261
Figure 8-17 Load-deflection curves with different cohesion (C) of the interface (i.e. 1, 1.38, 2 and 5 N/mm ²)	262
Figure 8-18 Reinforcement stresses at failure.....	263
Figure 8-19 Cyclic loading used for the exterior PCBC connection	265
Figure 8-20 Load history for reversed cyclic load test used for Specimen P2	265
Figure 8-21 Comparison of load-deflection curves of PCBC connection between experimental and numerical results	267
Figure 8-22 Load-displacement envelopes	267

Figure 8-23 Reinforcement stresses at failure due to negative moment	268
Figure 8-24 Reinforcement stresses at failure under positive moment	268
Figure 8-25 Mesh and reinforcement detail of the monolithic beam-column joint	270
Figure 8-26 Comparison of load-deflection curves of PCBC connection and the monolithic beam-column joint.....	271
Figure 8-27 Loading arrangement of static loading for the interior PCBC connection	273
Figure 8-28 FE meshes and the boundary conditions of the interior PCBC connection	273
Figure 8-29 Reinforcement arrangement of the interior PCBC connection	274
Figure 8-30 Load-deflection relationship of the interior PCBC connection under static loading	275
Figure 8-31 Deflection of the interior PCBC connection under static loading.....	275
Figure 8-32 Reinforcement stresses of the interior PCBC connection under static loading.....	276

List of Tables

Table 2-1 Test specimen details (Park et al., 2008)	25
Table 2-2 Specimen details (Kaung and Wong, 2011)	35
Table 2-3 Fibre properties (Ganesan et al., 2014b).....	45
Table 2-4 Characteristics of individual beam-column sub- assemblages	48
Table 2-5 Concrete mix characteristics (Gencoglu and Eren, 2002)	55
Table 3-1 Description of beam-column connection test.....	67
Table 3-2 Sieve analyses of fine aggregate	76
Table 3-3 Sieve analyses of coarse aggregate	77
Table 3-4 Material composition of precast concrete and CIP concrete (kg/m ³)	78
Table 3-5 Concrete compressive strength (trial mixes)	79
Table 4-1 Material composition of CIP concrete.....	92
Table 4-2 Mechanical properties of concrete of Specimen P1	93
Table 4-3 Experiment results	95
Table 5-1 Average value of mechanical properties of concrete of Specimen P2	135
Table 5-2 Peak load for every cycle of testing of Specimen P2.....	141
Table 5-3 Comparison between test results of P2 and Acceptance Criteria ACI 374.1-05	146
Table 5-4 Data of the composite beam of Specimen P2	148
Table 5-5 Comparison of the maximum load of Specimen P2.....	153
Table 6-1 Material composition of CIP-connection of specimens P2, P3 and P4.....	164
Table 6-2 Properties of the steel fibres	164
Table 6-3 Average of compressive strengths	167
Table 6-4 Average modulus of elasticity	168
Table 6-5 Average modulus of rupture (MOR)	171
Table 6-6 Comparison of the mechanical properties of the CIP connection of the PCBC specimens.....	174
Table 6-7 Peak loads at each cycle	182
Table 6-8 Secant stiffness of specimen P2, P3, P4.....	184
Table 6-9 Detail of specimens (Ganesan et al., 2014a)	186

Table 6-10 Ratio of the maximum load at the second cycle to the maximum load for each loading direction.....	194
Table 6-11 Calculation of Relative Energy Dissipation Ratio (β)	194
Table 6-12 Ratio of the secant stiffness at a drift ratio of 0.035 to the initial stiffness	195
Table 6-13 Result of Specimen P2, P3 and P4 with reference to the Acceptance Criteria in ACI 374.1-05.....	195
Table 6-14 Maximum load of specimens P2, P3 and P4 for each loading direction	196
Table 7-1 Average value of mechanical properties of concrete of Specimen P5	206
Table 8-1 Mechanical properties of concrete*	259

Notation

a	: depth of equivalent rectangular stress block
A_c	: area of concrete section
A_s	: area of steel reinforcement
A_h	: area of the hysteresis loop
A_j	: effective cross-sectional area
b	: beam width
c	: distance from extreme-compression fibre to neutral axis
C_c	: compression force resulted from concrete
C_{bc}	: compression force resulted from the beam core
C_{Ub}	: compression force resulted from the wall of the U-beam
d	: effective depth of reinforced beam
E_c	: modulus of elasticity of concrete
E_e	: the effective modulus of elasticity of concrete
E_{ea}	: adjusted effective modulus elasticity of concrete
E_s	: modulus of elasticity of steel reinforcement
f_c'	: cylinder compressive strength of concrete
f_k	: characteristic concrete strength
f_m	: target mean concrete strength
f_s	: the steel stress at particular load
f_t	: the modulus of rupture or flexural strength
f_y	: yield strength of steel
h	: height of beam;
I_{cr}	: second moment of area of cracked section
I_{eff}	: effective second moment of area for computation of deflection
I_g	: second moment of area of gross concrete section
K	: initial stiffness for positive loading for first cycle
K'	: initial stiffness for negative loading for first cycle
$K_{0.035}$: secant stiffness at drift ratio of 3.5%
K_a	: a factor that depends on the loading and support conditions
M	: bending moment

M_a	: service moment/applied moment
M_{cr}	: cracking moment
M_n	: nominal moment
M_{max}	: the maximum applied moment
n	: modular ratio
P_n	: nominal load
P_u	: ultimate load
P_{cr}	: first-crack load
T	: force in tension reinforcement
V_f	: volume fraction of fibre;
V_{jh}	: joint shear force
V_{jn}	: nominal joint shear strength
V_{col}	: column shear
y_t	: distance from centroidal axis of cross section to extreme fibre tension
β	: relative energy dissipation;
δ_y	: yield deflection
Δ_i	: immediate deflection
$\Delta_{(cr+sh)}$: long-term deflection due to creep and shrinkage
Δ_{tot}	: total deflection of a beam
δ_u	: deflection assuming an un-cracked section
δ_c	: deflection assuming a fully cracked section
δ_s	: deflection due to sustained loading
ε_c	: strain in concrete
ε_s	: strain in steel
ε_y	: yield strain of steel;
ρ	: tension reinforcement ratio
ρ'	: compression reinforcement ratio
Φ	: creep coefficient
φ_{ucr}	: curvature of the un-cracked beam
φ_{cr}	: curvature of the cracked beam
φ_s	: curvature due to sustained loading

ζ : distribution coefficient which allows the effects of tension stiffening at the section

Abbreviation

FRC	:	Fibre Reinforced Concrete
SFRC	:	Steel Fibre Reinforced Concrete
LVDT	:	Linear Variable Differential Transformer
MOR	:	Modulus of Rupture
PCBC	:	Precast Concrete Beam-Column
CIP	:	Cast-in-Place
PC	:	Precast Concrete
SD	:	Standard Deviation
DR	:	Drift Ratio
SG	:	Strain Gauge
CED	:	Cumulative Energy Dissipation
NED	:	Normalized Energy Dissipation

Chapter 1

Introduction

1.1 Background

Precast concrete systems continue to develop and have become more popular in the last few decades. These systems are believed to be an alternative solution to many of the problems in the construction industry, because they offer advantages in terms of quality, time and cost, in comparison with cast-in-situ construction (Bull and Park (1986); (Gibb, 1999; Choi et al., 2013)).

Precast systems are used in many different types of infrastructure projects, e.g. housing, multi-storey buildings, bridges, etc. Time savings in comparison with conventional systems are around 30% (Nurjaman et al., 2011). Cost savings are around 20% compared to those of conventional systems (Abduh, 2007). Furthermore, the manufacture of precast units in a controlled factory environment improves the quality of the material selection, mixing, moulding and the curing process, such that the quality and strength can be guaranteed. These advantages make precast systems more appealing to the construction industry.

The structural behaviour of a precast concrete structure is dictated by the method and efficiency of the connection between the precast elements (Choi et al., 2013). This is particularly the case in seismic regions, where precast concrete structures have to be designed to withstand earthquakes. A moment resistant structure which is designed using the 'strong column-weak beam' principle will have a 'sway mechanism' of collapse due to

lateral forces; the structure will have to have ductility and produce a ductile failure (Paulay and Scarpas, 1981).

In terms of precast concrete moment resisting frames, many types of beam-column connection have been developed. These include bolted, welded, pre-stressed, cast-in-place (CIP) connections, or a combination of two or more of these. Each type of connection has its own advantages and disadvantages.

Welded connections, although satisfying strength and stiffness requirements, can introduce excessive heat which can damage or cause cracks in the adjacent precast concrete (Bhatt and Kirk, 1985; Ochs and Ehsani, 1993; Stanton et al., 1991; Yee, 1991). Furthermore, the implementation of this type of connection will need skilled site staff who can guarantee the quality of the welding in the connection (Ertas et al., 2006).

Bolted connections are the easiest method used to connect precast elements on site. Unfortunately, this method requires a high degree of precision in placing the channels or steel plates before casting the precast elements. It is also not easy to achieve due to the sliding risk (Ertas et al., 2006). Another study negated the sliding risk by providing additional tolerances in the bolt holes. However, this caused an initial loss of stiffness in the connection (Li et al., 2003).

The cast-in-place (CIP) concrete method can achieve a more monolithic connection and is recommended for seismic designed buildings (Bull and Park, 1986). It also allows more tolerance in the precast connections. Unfortunately, it takes longer as the concrete has to gain strength and it needs additional formwork and scaffolding on site. All of these factors will lead to an increase in cost and time for the construction.

In other words, precast systems still face several technical problems, especially in terms of the connections required on site. A connection

system which has a high degree of precision; such as a complex connection with steel box or pipe and involving bolting or welding, should be avoided. Such systems could cause difficulties in implementation, which can extend the construction time and increase the construction cost. Therefore, further innovation and further development, particularly in the area of the beam-to-column connections, is required.

1.2 A New Precast Concrete Beam-to-Column Connection

There are several problems associated with the implementation of precast concrete on site. Abduh (2007) mentioned that the complexity of the connection can lead to poor quality connections and slower construction time. Complex connections involve the use of steel boxes or pipes (Choi et al., 2013; Ertas et al., 2006), welding (Bhatt and Kirk, 1985), bolts (Li et al., 2003) and complex reinforcement. Therefore, the method of assembly of the precast elements on the project site is also an important factor to be considered in the design of the connection (Bull and Park, 1986).

The connection developed and discussed here in this study was designed as a ductile connection. Figure 1-1 presents a description of the system. Figure 1-2 and Figure 1-3 present details of an exterior and interior connection, respectively, which could be found in a moment resisting frame.

The precast concrete moment resisting frame suggested here consists of multi-storey (potentially 3 storeys) precast columns connected to horizontal elements (precast beams) using interlocking bars and cast-in-place concrete. The detail of the system is explained below (Noorhidana and Forth, 2016b):

a. Columns

It is expected that the precast reinforced concrete columns will typically be a length equivalent to 3 storeys; the intention here is to accelerate the erection work for the precast concrete system. The column is designed to have corbels that can support the precast beams during the installation process thereby minimising the need for scaffolding. There will be a gap (see Figure 1-4) in the concrete of the column at each intended floor level (the column steel will be continuous through this gap); the corbel will be located at the bottom of the gap – see Figure 1-2. The column will be braced across the gap to maintain its stiffness; the height of the gap is equal to the beam depth.

In order to avoid any difficulties that may be present when casting corbels on three or four faces, it is likely that corbels will be cast monolithically only on two opposite sides of the column. If further corbels are required these will be in the form of steel corbels, bolted to the side of the column (see Figure 1-3).

b. Beams

The precast beams (see Figure 1-4) are U-shaped at both ends (this is part of the connection) and solid in between. The U-shaped part of the beam acts as permanent formwork and is not connected directly to the column. The connection between the column and the beam is made using interlocking bars which are located in the U-section and extend into the gap in the column and cast in situ concrete (see c. below).

c. Interlocking Bars and Cast-in-Place (CIP) Concrete

For an exterior joint, interlocking bars are used as longitudinal reinforcement, which connect the precast beam and the column/joint core (see Figure 1-2). The function of these bars is to withstand the sagging and hogging moments. These bars are also designed to ensure the continuity of the top and bottom reinforcement of the precast concrete beam into the joint core. (Normally, the

discontinuities of the bottom reinforcement of the beam in many current systems causes a lower moment capacity of the beam (Li et al., 2003).

For beams spanning orthogonally to the one mentioned in the previous paragraph, to avoid any clash of reinforcing bars in the joint core, the connecting bars will pass through the column joint at the lower level, as can be seen in Figure 1-3. The connection regions (the joint core and beam core) are then filled with CIP concrete.

The new connection offers several advantages; this connection will negate the need for high precision engineering, thereby improving practicality; reduce the use of formwork due to the use of a precast partial U-beam (acting as permanent formwork); and lower the volume of cast-in-place concrete. The use of corbels, which support the precast beam, will minimize the need for scaffolding. This new connection also avoids the use of welding, bolts and pre-stressing, which therefore leads to a reduced need for skilled labour and a reduction in the construction time. Overall, this new connection can be expected to offer a more economical and practical solution (Noorhidana and Forth, 2016a).

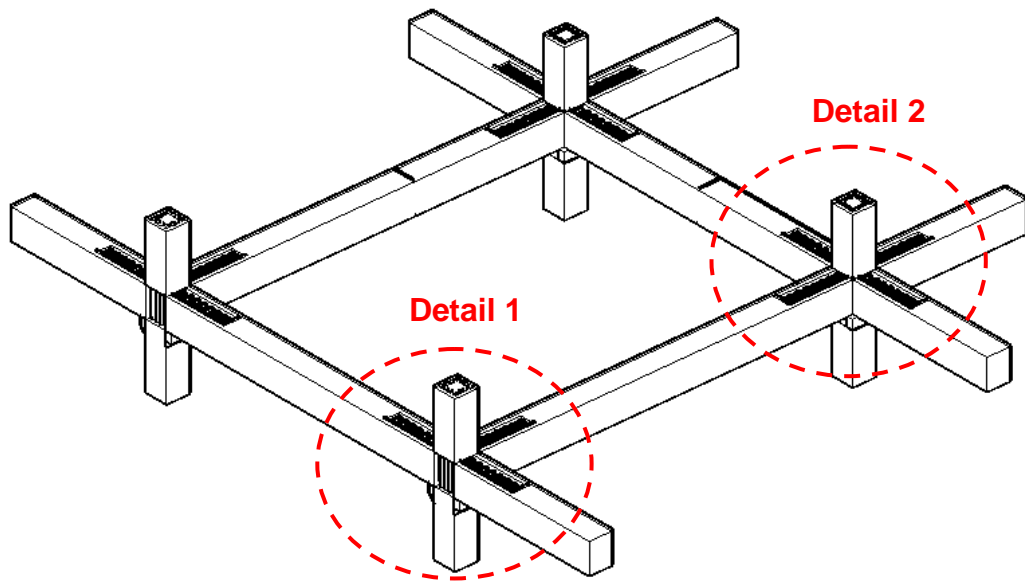


Figure 1-1 Description of system concept

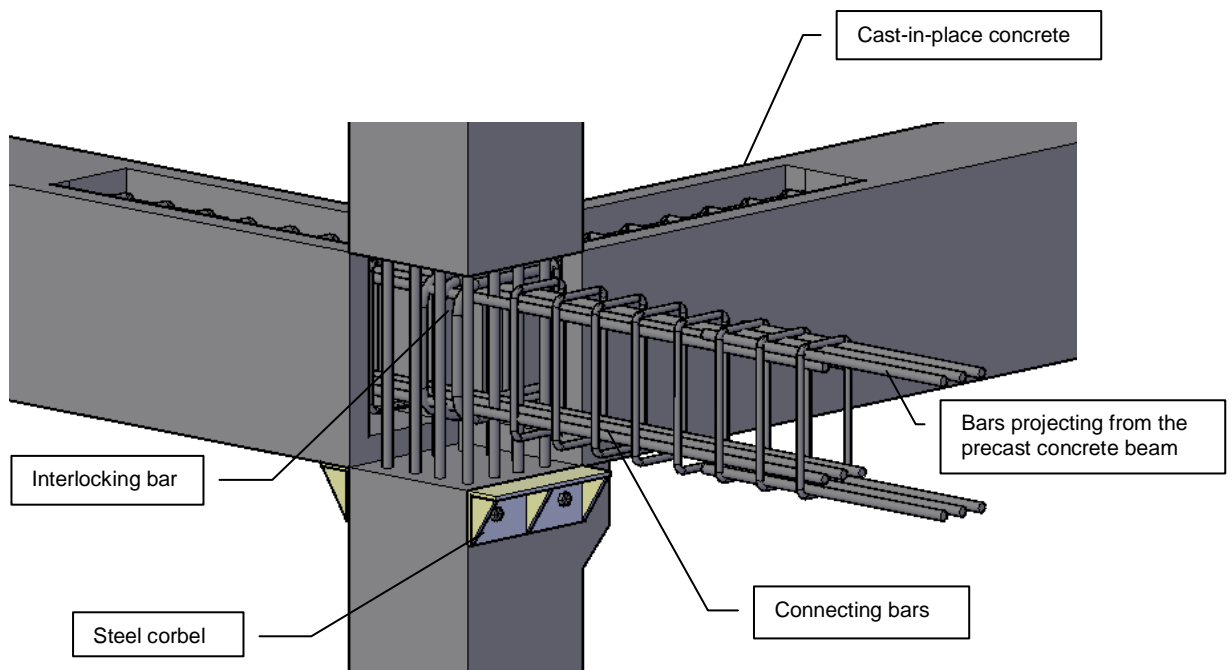


Figure 1-2 Detail 1 (exterior beam-column joint)

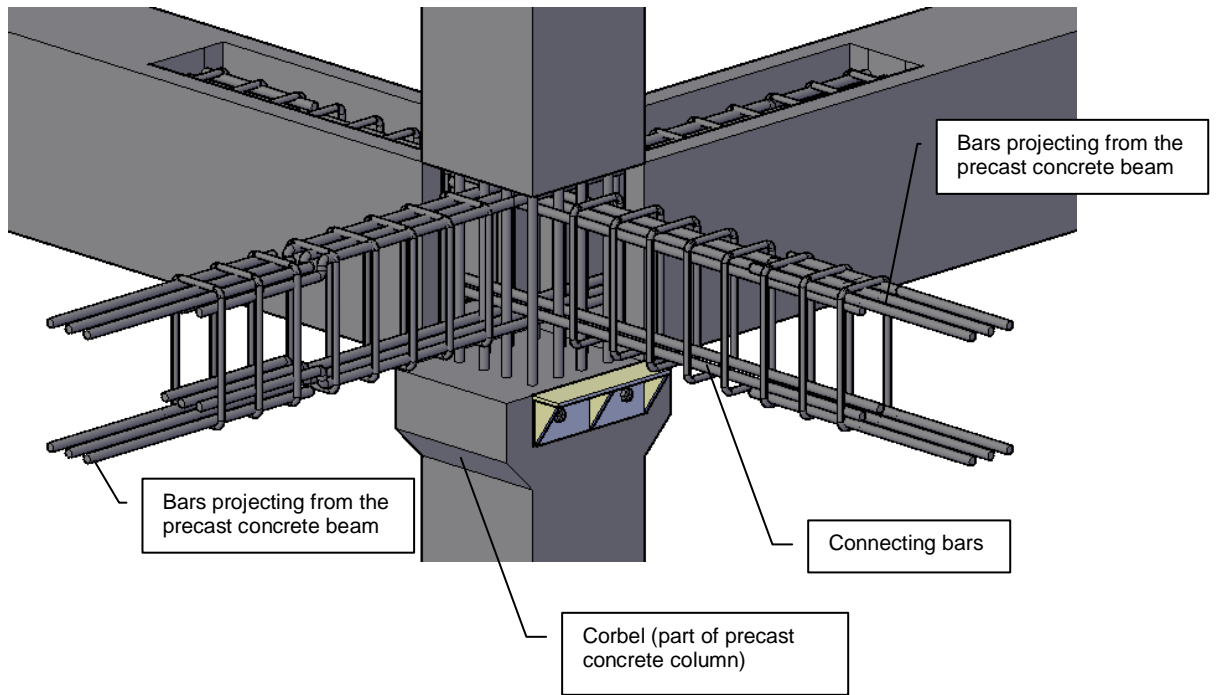


Figure 1-3 Detail 2 (interior beam-column joint)

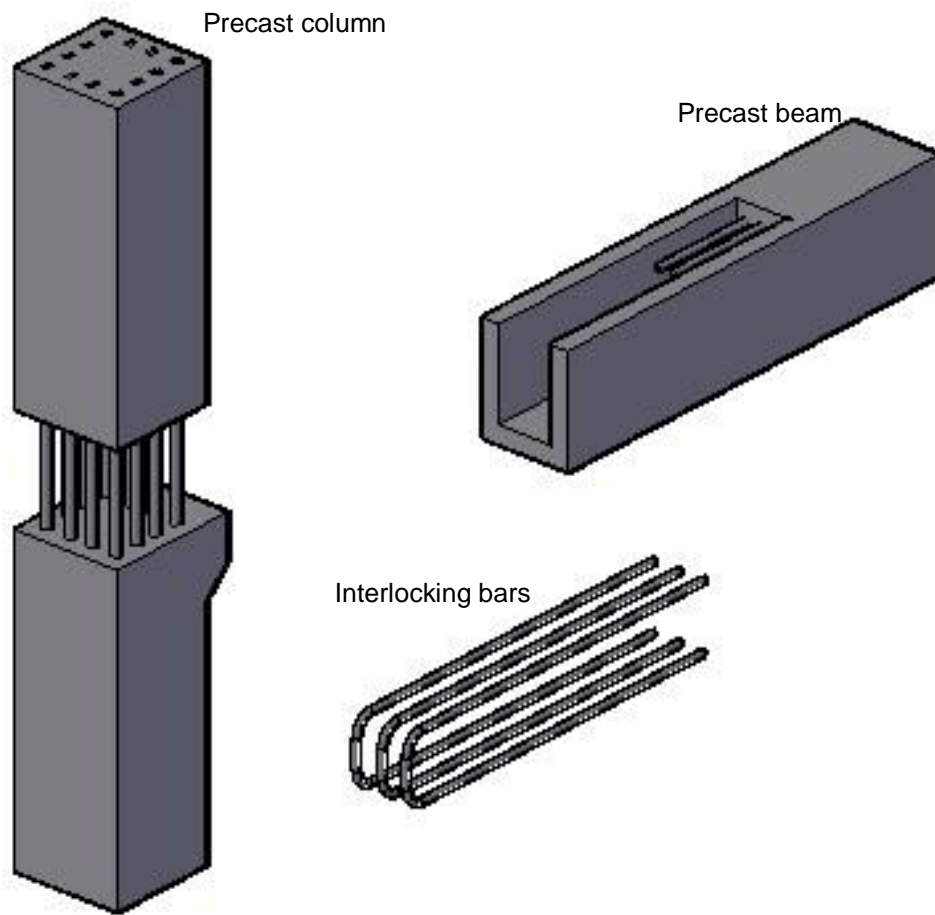


Figure 1-4 Isometric of the beam-column specimen

1.3 Research Aims and Objectives

Five tests were carried out on the beam-column connections under different types of loading (i.e. static, quasi-static and long-term loading) in the George Earle Laboratory at the School of Civil Engineering, University of Leeds. The specimen represents an exterior beam-to-column connection of a two-dimensional moment resisting frame (see Figure 1-4). The specimen consists of a precast reinforced concrete beam, a precast reinforced concrete column, interlocking steel reinforcing bars and cast-in-place (CIP) concrete.

The use of interlocking steel reinforcing bars provides ductility to the connection. Hence, when inelastic deformation occurs in the connection, the precast members are still in the elastic state and therefore the joint still has sufficient strength and stiffness to withstand the earthquake load. Furthermore, the performance of the precast concrete beam-to-column connection is determined by the action of friction/bonding between the interlocking bars and the cast-in-place (CIP) concrete. So, the use of steel fibre reinforced concrete (FRC) as the CIP concrete should enhance the bonding strength, which in turn can improve the performance of the beam-to-column connection.

The aim of this research is to develop a ductile exterior precast concrete beam-to-column (PCBC) connection, which will be suitable for precast structures in seismic zones and which has an ease of implementation.

The following objectives are set in order to achieve the aim of this study:

1. To identify the structural behaviour of the exterior PCBC connection under static loading.
2. To identify the structural behaviour of the exterior PCBC connection under quasi-static loading.
3. To evaluate the hysteresis behaviour of the exterior PCBC connection using the Acceptance Criteria for Moment Frames Based on Structural Testing and Commentary (ACI 374.1-05, 2005).
4. To quantify the behaviour of the exterior PCBC connection incorporating steel fibre reinforced concrete (SFRC) used as the cast-in-place (CIP) concrete, in terms of the load carrying capacity, energy dissipation, stiffness degradation and crack propagation.
5. To identify the behaviour of the exterior PCBC connection under sustained loading, which use normal concrete as the material of CIP connection.
6. To develop a finite element based computational model of a PCBC connection, validated using the results from the testing of the beam-

column connection specimens the laboratory, to explore the behaviour of an interior PCBC connection.

1.4 Outline of Thesis

The thesis consists of nine chapters including this introduction chapter. Chapter 2 contains a literature review, concentrating on the precast concrete system and the beam-column connection.

Chapter 3 presents the experimental program; this includes the stages of the experiments, details of the material and equipment that was used in the laboratory and the test set-up of the PCBC specimens. It also includes an evaluation of the erection process of the precast elements into the laboratory test rig.

Chapter 4 discusses the structural behaviour of the exterior PCBC connection under static loading. Chapter 5 discusses the structural behaviour of the exterior PCBC connection under cyclic loading and its evaluation using the acceptance criteria stated in the ACI 374.1-05, 2005.

Chapter 6 discusses the contribution of the CIP steel fibre reinforced concrete material in the exterior PCBC connection subjected to cyclic loading, specifically in terms of the hysteresis loop of the load-deflection relationship, energy dissipation, stiffness degradation and crack propagation.

Chapter 7 discusses the behaviour of the exterior PCBC connection under sustained loading.

Chapter 8 presents the modelling of the exterior PCBC connection using MIDAS finite element software and validates the developed models against the experimental results.

Chapter 9 present the findings and conclusions of this investigation and also the recommendations for future work.

Chapter 2

Literature Review

2.1 Introduction

This chapter reviews current research in the development of exterior precast concrete beam-column (PCBC) connections. Section 2.2 focuses on precast concrete, advantages and disadvantages, design criteria and design considerations and categories of precast concrete connections. Section 2.3 expands on the need for shear reinforcement in beam-column joints. Section 2.4 focuses on mechanical properties of fibre reinforced concrete (FRC) when compared to plain concrete (without fibres). This section expands on research where FRC is applied in beam-column joints/connections. Finally, a summary and critical review of this chapter is presented in Section 2.5.

2.2 Precast Concrete

2.2.1 Advantages of precast concrete

Precast concrete can be defined as ready for casting and curing in a location which is not its final destination, usually in a controlled factory environment where reusable moulds are utilised (Elliot, 2002). Precast concrete components are jointed to other components using a connection system to form a complete structure. Precast concrete systems are used for repetitive structural systems such as wall panels, floors, beams, columns, staircases, pipes, tunnels, etc.

Precast concrete members are advantageous when compared to cast-in-place concrete members, in terms of (1) quality, (2) construction time and (3) construction cost (Gibb, 1999; Bull and Park, 1986; Seckin and Fu, 1990; Soubra et al., 1991; Soubra, 1993):

1. **Quality:** Precast elements are manufactured in controlled environments, where mixing, placement and curing are controlled and monitored properly. Weather effects, when casting can be eliminated, improving the quality of precast elements. Therefore, the overall process of making precast members produces a stronger and durable concrete thanks to harmonised batching, enhancing consistent quality control.
2. **Speed of construction:** when precast units are delivered to site, they can be installed immediately. It is not necessary to wait for the concrete to gain compressive strength as in the case with cast-in-place concrete. The heating/ curing of precast members at the precast manufacturing stage, accelerates concrete strength, thereby reducing the time between casting members and its final use.
3. **Economy:** Economic advantages can be realised both at the manufacturing and site-construction stages. Manufacturers can bulk buy materials for multiple projects at lower prices, leading to lower construction costs. In addition, product repetition/duplication using the same precast products, means attaining added value from existing moulds and set-up, for future projects. Also, handling precast concrete involves less labourers, less formwork and scaffolding-setup when compared to cast-in-place construction. However, some economies can be lost, as special erection and support procedures may be needed for precast concrete structures.

However, precast concrete systems have their limitations, i.e.:

1. They can be uneconomical for small precast productions. The precast industry requires high investment to provide facilities for manufacturing and handling erections on site.
2. They require high levels of accuracy in manufacturing of precast elements to avoid large deviations between elements.
3. In seismic zones, precast concrete connections require special designs as they must transfer seismic loads properly.

2.2.2 Design criteria for precast concrete connections

For the design of precast concrete components such as floor slabs, beams, columns and walls, special attention should be given to connection components. These connections have to distribute construction loads and they must integrate the precast concrete components to become one united structure (Negro and Toniolo, 2012).

For a satisfactory performance, connections should meet specific design criteria:

- Connections must withstand the ultimate load in a ductile behaviour.
- The precast components should be simple to manufacture and be economical, easy to transport and easy to assemble on site. Similarly, they must endure tolerances which cannot be jeopardised in service.
- The final appearance of a connection must satisfy fire resistance regulations, must be durable and conform to visual requirements.

Besides fulfilling these design criteria, connections must satisfy other design requirements including those relating to strength, ductility and volume changes (due to creep and shrinkage).

2.2.3 Seismic design concepts for precast concrete in buildings

In the design of precast concrete moment resisting frames, connection systems should provide adequate stiffness, strength, ductility and structural stability. Loadings during construction, serviceability and ultimate limit states within the lifetime of the structure, must be taken into account (Bull and Park, 1986).

As a seismic resistant structure for a monolithic moment resisting frame, a precast concrete structure is required to behave in a ductile manner under seismic loading (Park, 2002). A beam side-sway mechanism (Figure 2-1) is recommended for post-elastic behaviour, rather than a column side-sway mechanism. Beam side-sway mechanisms result from strong column-weak beam design. The plastic hinges form at the ends of the beams. The required ductility of the plastic hinges in the beams and at the column is moderate and can be provided during design stages.

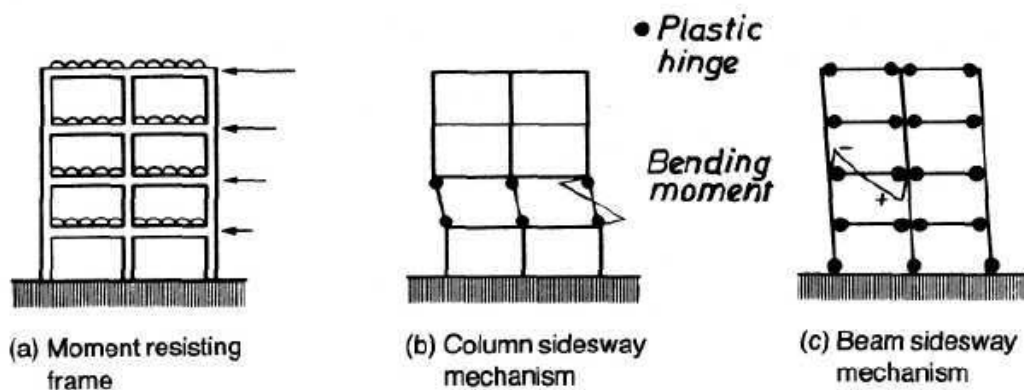


Figure 2-1 Moment resisting frames with horizontal seismic loading mechanisms (Bull & Park, 1986)

A column side-sway mechanism is not practical as it requires very large ductility at the plastic hinges in the columns in the critical storey. This mechanism, which is also called a soft storeys mechanism, can lead to collapse during earthquakes.

To avoid column side-sway mechanisms, columns are designed to have a higher bending moment capacity than the connecting beams. Similarly, to avoid flexure in undesirable parts of the structure, or shear failure occurring anywhere in the structure, an over-strength factor is applied during the design stages of the flexural strength of the beam.

This flexural over-strength (ϕ) is taken as 1.25 (NZS, 1997) or 1.2 (ACI, 2011), where M_{nb} is the nominal flexural strength of the beam. This factor considers the additional longitudinal steel strength due to strain hardening at large deformation. Therefore, strong column-weak beam behaviours (Figure 2-2) can be ensured by satisfying Equation (2-1).

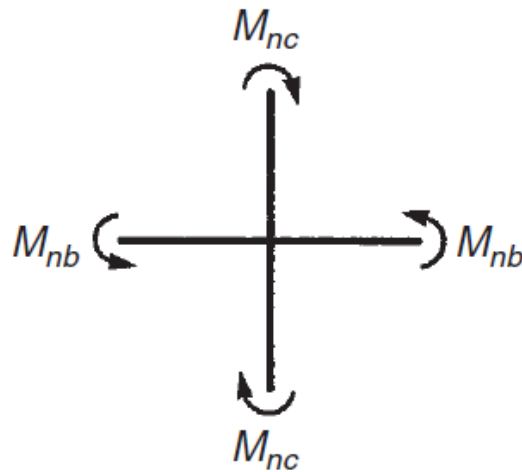


Figure 2-2 Moments at a beam-column joint (MacGregor, 2009)

$$\sum M_{nc} \geq \sum \phi M_{nb} \quad (2-1)$$

Where,

$\sum M_{nc}$ = the sum of nominal flexural strengths of columns framing into the joint, evaluated at the faces of the joint.

$\sum M_{nb}$ = the sum of the nominal flexural strengths of the beams framing into the joint, evaluated at the faces of the joint.

2.2.4 Types of precast concrete connections

The connections between precast concrete elements are commonly divided into two types, i.e.

1. Dry connections
Dry connections usually use steel plates and bolts or welding to connect precast elements. These connections require special analysis and computer modelling because the connections between elements are not monolithic in nature.
2. Wet connections
Wet connections use cast-in-place concrete to connect precast elements. Each precast element has protruding bars in connection regions. These bars are connected to each other by mechanical joints, mechanical couples (or splice sleeves), or by development length within CIP concrete. Then connection regions are filled by cast-in-place concrete. The connections created are monolithic in nature, therefore wet connections should be recommended for seismically resistant buildings.

Other categorisations of precast connections are mentioned in the US-PRESS program:

1. Rigid connections/strong connections
These connections are designed to have more strength than precast elements in terms of flexure and shear. Consequently, plastic hinges will be formed outside connection regions while the connections remain in the elastic range (Ghosh et al., 1997).
2. Ductile connections.
These connection regions are weaker than the precast elements, or in other words, the precast elements are designed to have greater strengths than the connections. This allows the plastic hinges to

remain in the connection regions while precast elements remain undamaged.

2.2.5 Research on precast concrete beam-column connections

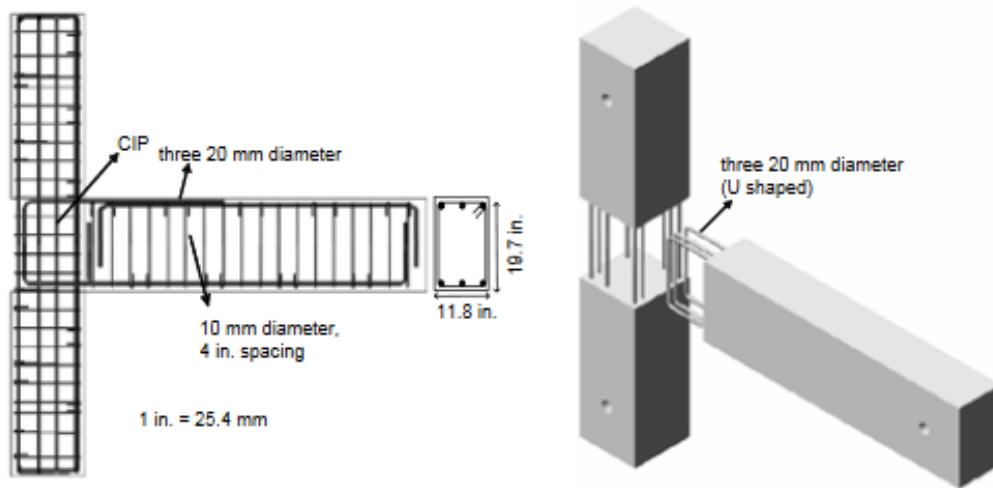
Several experimental research projects, conducted in the last two decades, have significantly improved our understanding of the behaviour of connections between precast elements (Ghosh et al., 1997). The performance and capacity of designed connections in seismic regions have been well evaluated. In some research programmes, precast elements have been connected at beam-to-column joint regions; whereas in others, elements have been connected at mid-span (in the case of beams) and at mid-height in the case of columns (Choi et al., 2013; Korkmaz and Tankut, 2005; Elliott, 2002).

Several types of beam-column connections have been studied and developed to resist earthquake-loading simulations. Bhatt and Kirk (1985) developed welded connections for use in precast concrete structures, where the connections performed properly under loading. These beam-column specimens required significant welding of the beam and column reinforcement. Unfortunately, the welding process generated excessive heat that caused damage to the steel bar bonding and led to cracking of the adjacent precast concrete. Therefore, the use of welding in precast concrete construction should be minimised.

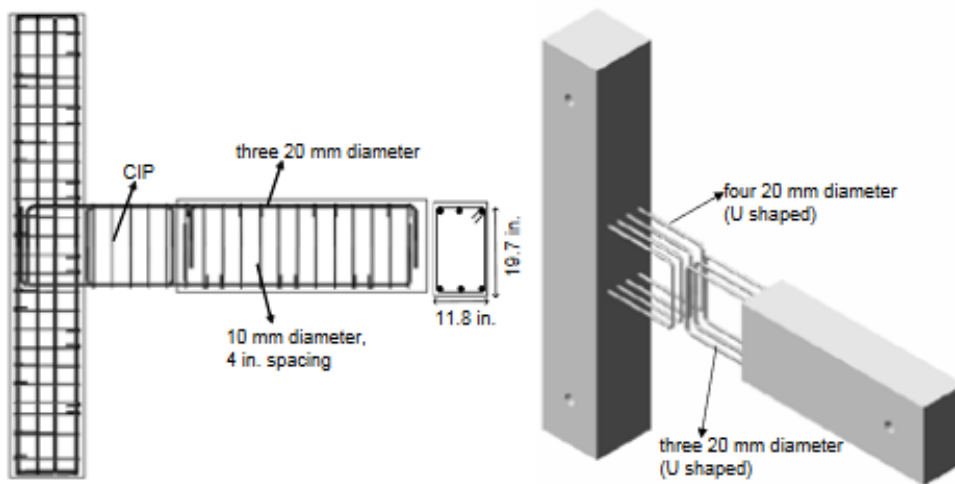
Ertas et al. (2006) investigated connections which were modelled as exterior beam-column joints in a multi-storey building. Figure 2-3 shows examples of developed connections, i.e. (a) cast-in-place (CIP) in column, (b) cast-in-place (CIP) in beam, (c) composite and (d) bolted connections. Specimens were subjected to cyclic loading and the results compared to monolithic joints (Figure 2-4). All specimens showed good performance in terms of strength and energy dissipation, which are key factors in high

seismic zones. However, for bolted connections, a sliding potential of steel boxes or pipes in precast beams was observed, suggesting proper and precise detailing of steel boxes/pipes to avoid sliding risks.

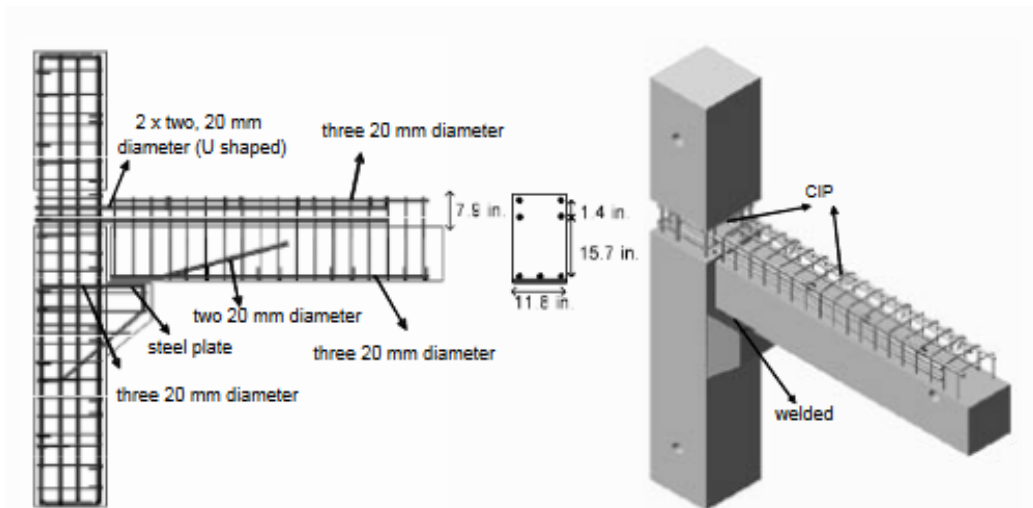
In addition, the use of bolted plates in connections may cause an initial connection stiffness loss due to the tolerance of the holes (Li *et al*, 2003). In contrast, CIP connections require extra formwork on site which could lead to increases in time and construction costs.



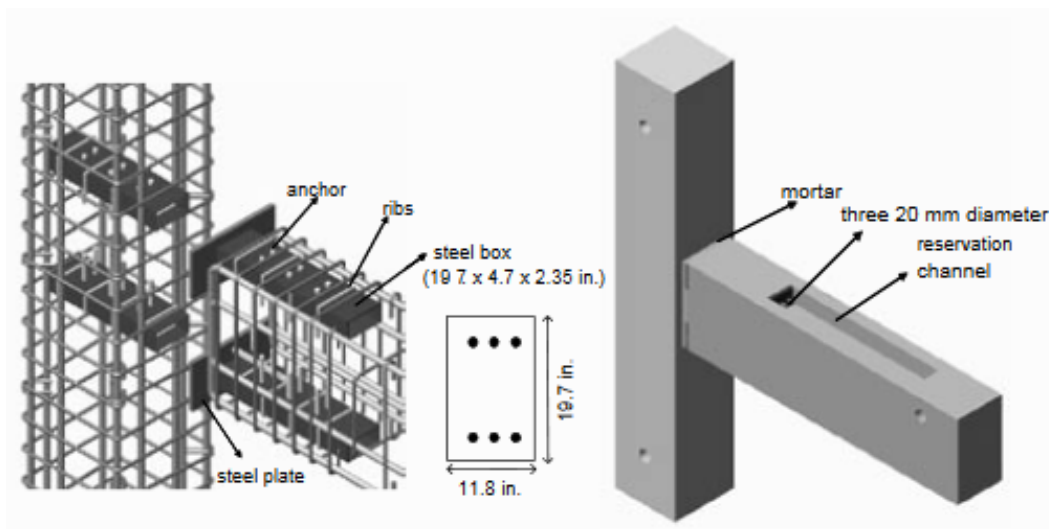
a. Cast-in-place in column connection



b. Cast-in-place in beam connection



c. Composite connection



d. Bolted connection

Figure 2-3 Exterior beam-column connections (Ertas et al., 2006)

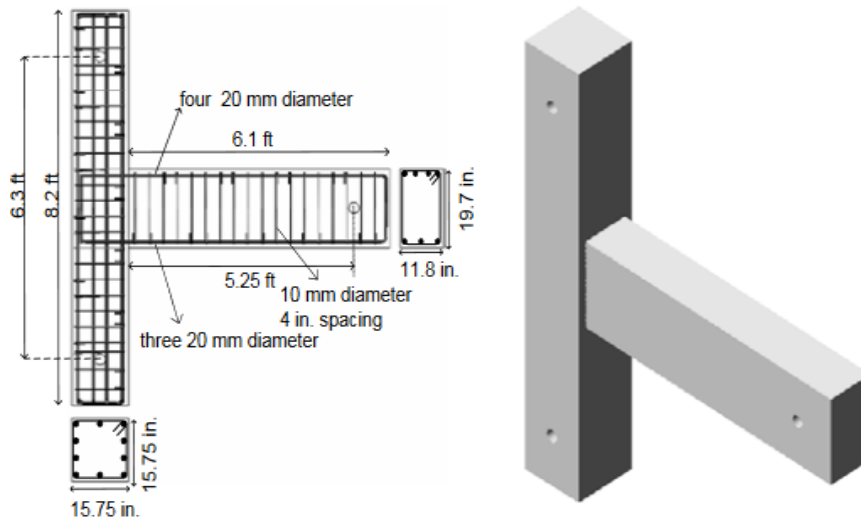
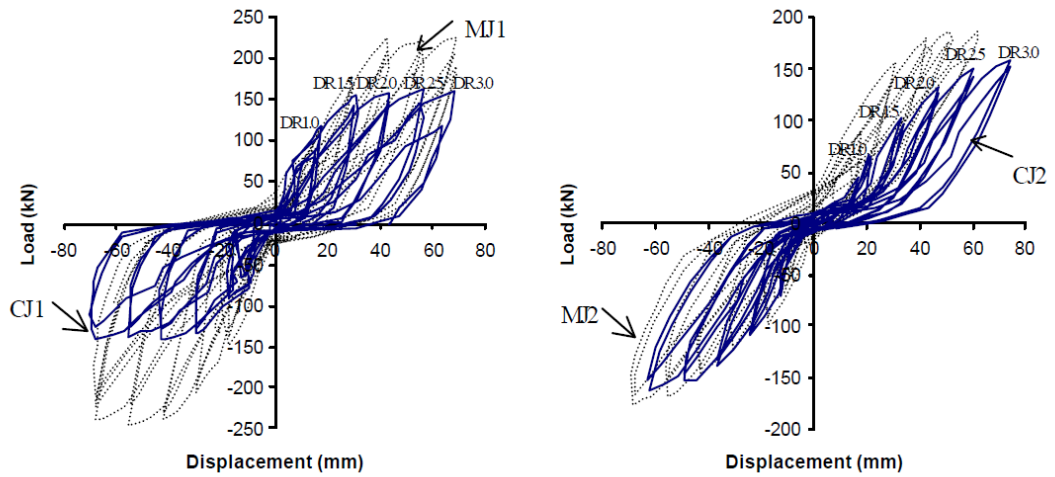


Figure 2-4 Monolithic beam-column specimens (Ertas et al., 2006)

The development of hybrid-steel concrete connections for precast concrete frames was carried out by Li et al. (2003). The specimens consisted of 2 monolithic interior beam-column joints (MJ1 and MJ2) and 2 interior precast concrete beam-column connections (CJ1 and CJ2). MJ1 and MJ2 were identical in column orientation with respect to beams framing into columns. Specimen CJ1 was compared to MJ1 while CJ2 was compared to MJ2. Figure 2-6 and Figure 2-7 show the specimens and isometry of the connections.

The researchers used a combination of bolt and cast-in-situ concrete as connections between precast beams and precast columns. The top longitudinal reinforcement of the precast beams continued across the column joints, while the bottom reinforcement stopped at the face of the column and was continued by bolted connections (using steel plates) to the column. The specimens were subjected to reverse cyclic loading to evaluate behaviour in terms of ductility, strength and energy dissipation capacity. The results showed that the precast specimens performed consistent hysteresis loops which were similar to the monolithic specimens. However, the precast specimens had lower load capacities when compared to monolithic specimens (Figure 2-5). This was caused by a discontinuity of the bottom reinforcement of the precast beams, which

caused the formation of a reduced lever arm; leading to a lower moment capacity of the specimens. These data suggested that the continuity of longitudinal reinforcing bars of precast beams to the column is important.



- a. Specimen CJ1 (compared to MJ1) b. Specimen CJ2 (compared to MJ2)

Figure 2-5 Specimen hysteresis loops (Li et al., 2003)

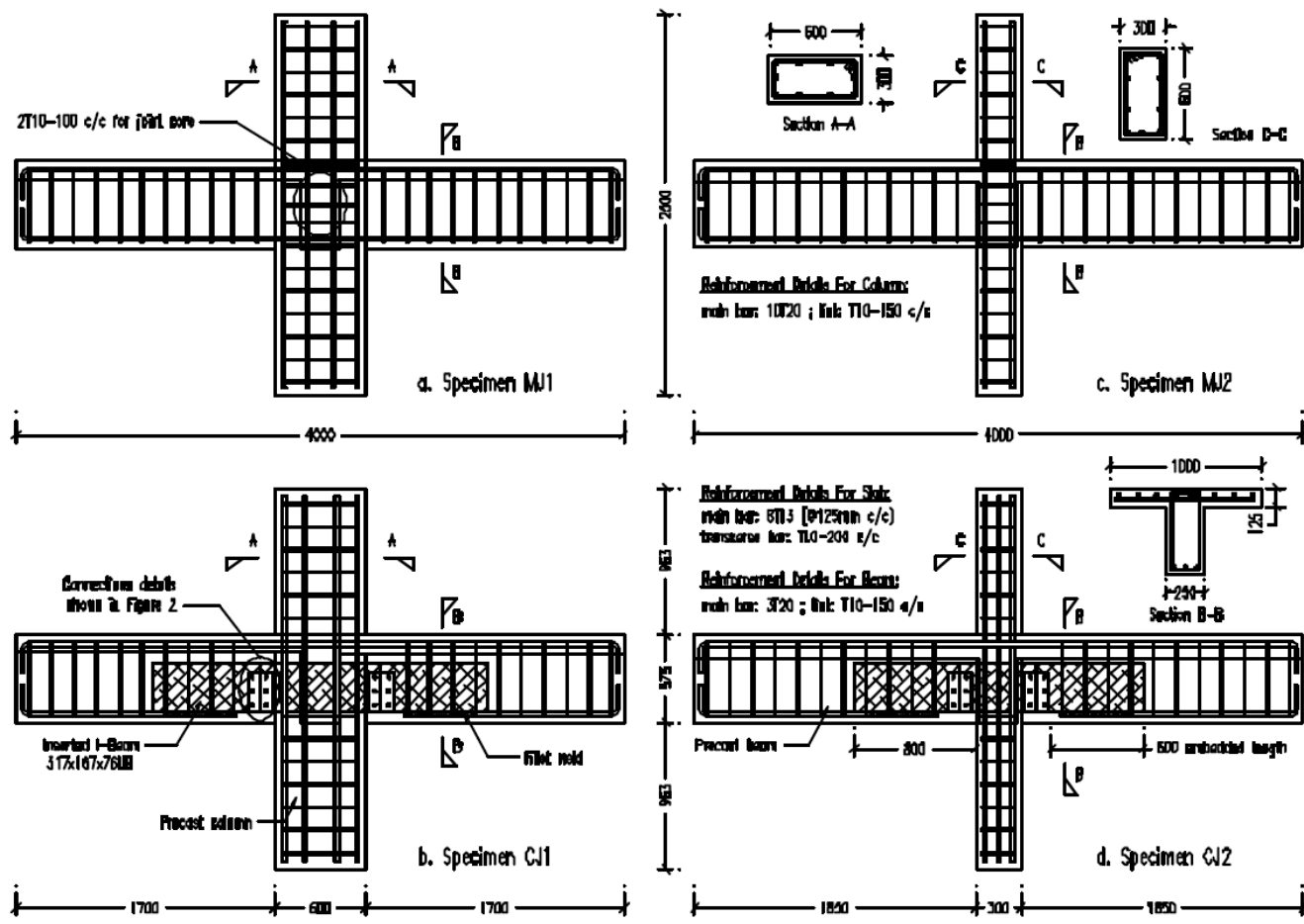


Figure 2-6 Specimen details (Li et al., 2003)

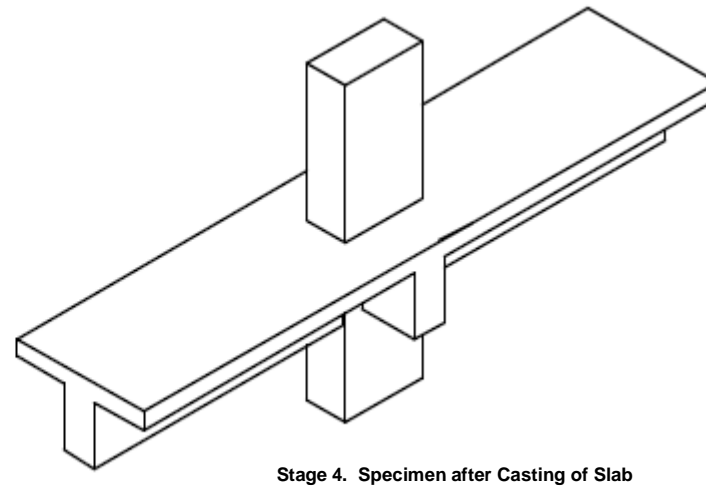
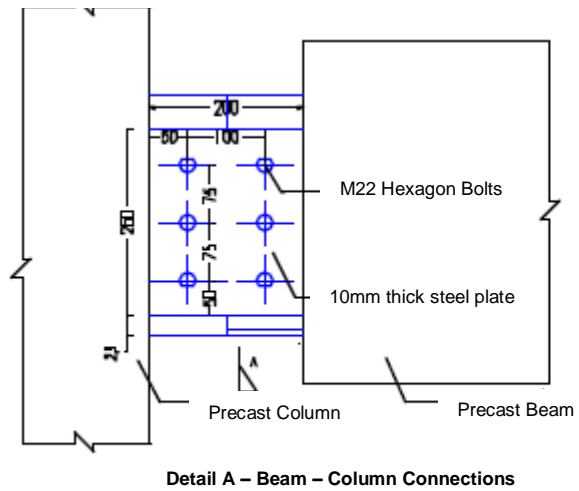
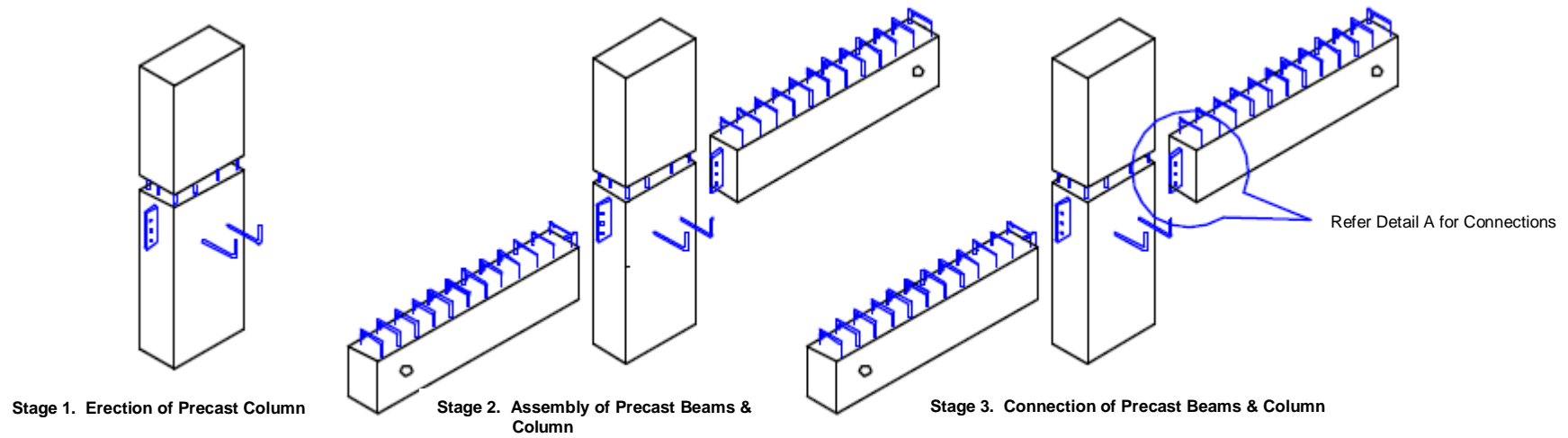


Figure 2-7 Connection details of typical precast specimens (Li et al., 2003)

Park et al. (2008) investigated several full scale interior precast beam-column connections to understand earthquake resistance. The specimens consisted of one monolithic and five precast concrete specimens (Table 2-1, Figure 2-9 and Figure 2-8). The precast beam had U-shaped cross sections. The beam core and the beam-column connections were monolithically constructed with cast-in-place concrete. Five precast concrete specimens and one conventional monolithic specimen were tested for cyclic loading.

Connection behaviours were observed with respect to the following parameters; i.e. the reinforcement detail for the precast beam shell, stirrup spacing in the beams, and length of the beam shell seated on the column. Although there were no significant strength degradations in the precast connections at large inelastic deformations, the energy dissipation capacities and stiffness of the precast connections were significantly less than those of the conventional monolithic specimen. Concrete spalling in the column occurred in some precast specimens due to a lack of steel angles, which would be used to strengthen the contact surface between the U-shell beam and the column.

Generally, at the beginning of tests, initial flexural cracks were observed in the beams of the precast specimens. At higher load levels, the first diagonal cracks were observed at the beam-column joints. At the upper stages, diagonal crack widths increased in the beam-column connection and severe concrete spalling occurred at the top and bottom of the connections. Even though the precast specimens reached their yield load, the flexural cracks did not propagate significantly in the plastic hinge of the beam and bond-slip of the rebars occurred in the beam-column joints. It indicated that yielding of the longitudinal bars in the beams occurred in the joints. Furthermore, the bond-slip behaviour of the re-bars occurred in the joints, which was confirmed by gaps opening between the column faces and the U-shell beams. On the other hand, the monolithic specimens had different crack patterns. Flexural cracks developed in the plastic hinge

region of the beam, while diagonal shear cracks were minimised in the beam-column joints.

Table 2-1 Test specimen details (Park et al., 2008)

Specimens	Reinforcement in Beams			Seated length of U-beam shell	Steel Angle-Strengthening for U-beam end
	Top reinforcement (ratio, %)	Bottom reinforcement (ratio, %)	Stirrups		
CP	4-D32(1.23)	2-D25,2-D29 (0.89)	D13@160 (0.22)	-	
SP1	4-D32(1.23)	4-D32(1.66)	D13@120 (0.30)	50mm	
SP2	4-D32(1.23)	4-D32(1.66)	D13@120 (0.30)	50mm	o
SP3	4-D32(1.23)	4-D32(1.66)	D13@160 (0.22)	50mm	o
SP4	4-D32(1.23)	4-D32(1.66)	D13@120 (0.30)	65mm	
SP5	4-D35(1.49)	4-D35(1.99)	D13@120 (0.30)	50mm	o

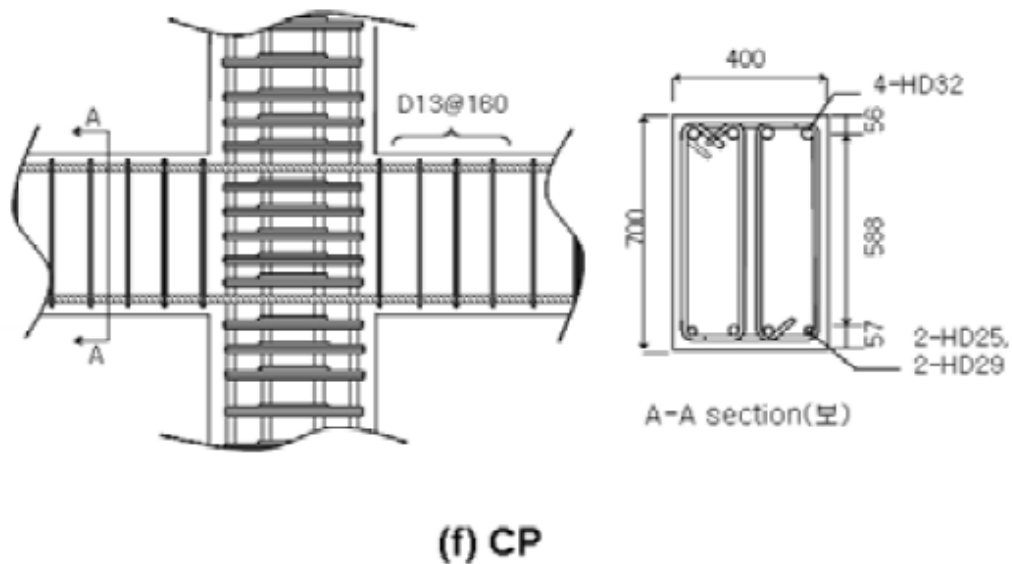
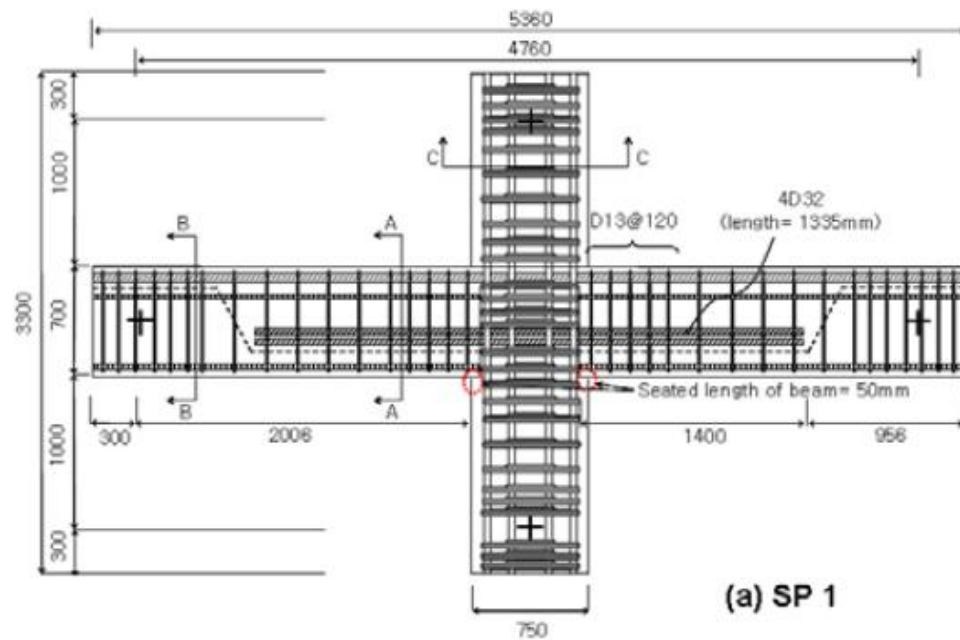
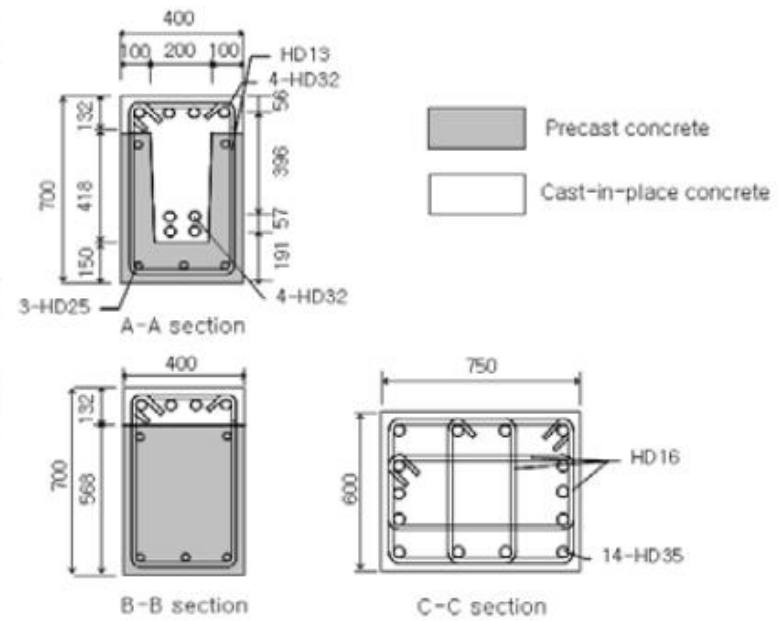


Figure 2-8 Dimensions and details of the monolithic specimen (Park et al., 2008)



(a) SP 1



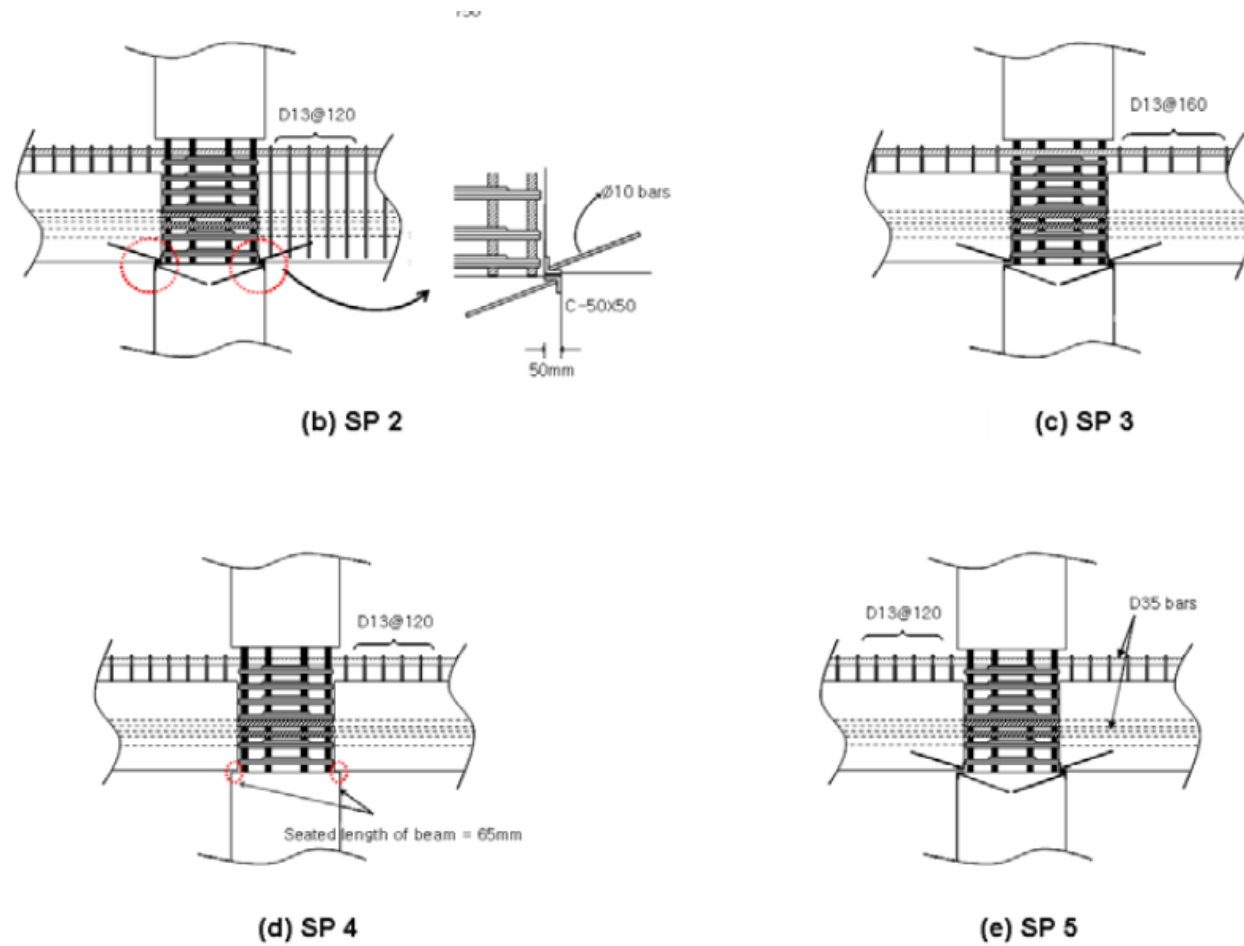


Figure 2-9 Dimensions and details of precast specimens (Park et al., 2008)

Park *et al.* (2008) found that the unexpected behaviour of precast specimens in comparison with the monolithic specimen (CP) was caused by: (a) the seating of U-shell beams on the column reducing the effective shear area of the beam-column connection; (b) the use of large diameter re-bars resulting in greater shear force being applied to the beam-column joint, thereby requiring greater embedment length. Because of these factors, diagonal shear cracks and the bond-slip of re-bars occurred in precast beam-column specimens, thereby decreasing the energy dissipation capacity.

2.3 Time-Dependent Behaviour of Reinforced Concrete Beams

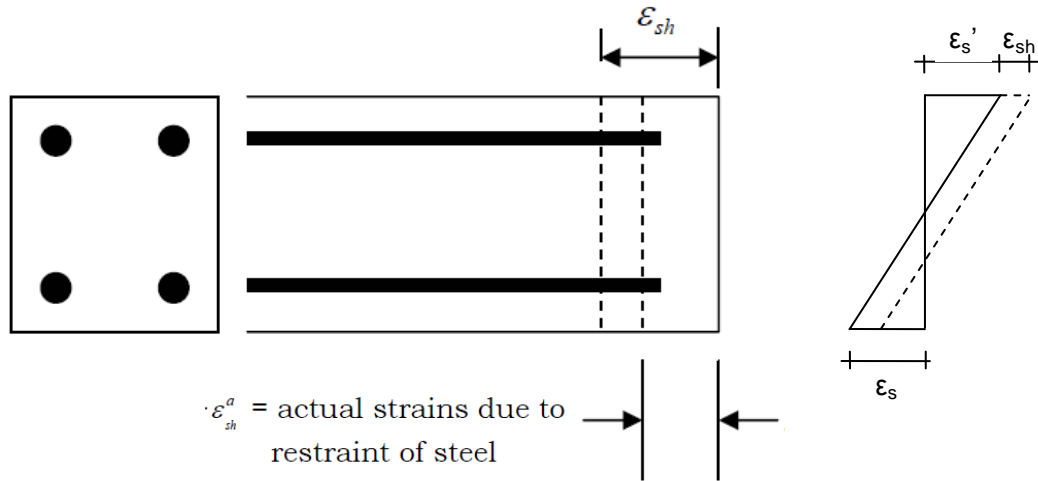
A reinforced concrete structure must perform its intended function throughout its working life. The behaviour of reinforced concrete structures during this period is complicated and is influenced by cracking, tension stiffening, creep and shrinkage (Gilbert, 2011). For instance, the deflection of a beam under sustained loading is affected by both shrinkage and creep and this long-term deflection could be several times larger than the instantaneous value.

2.3.1 Effect of shrinkage

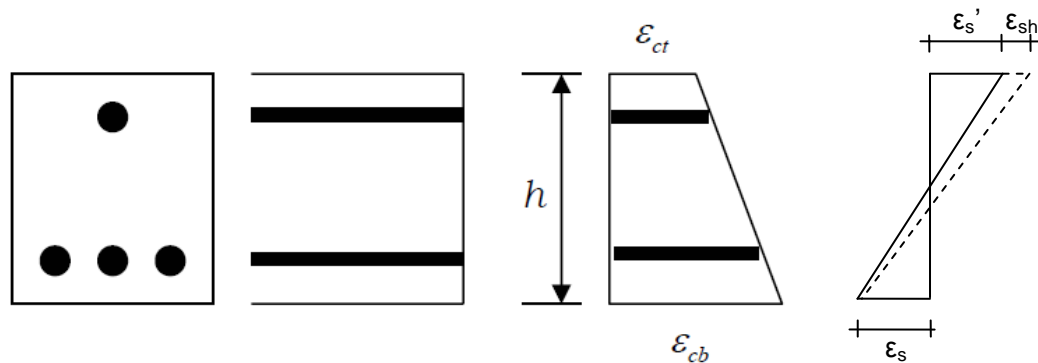
The steel reinforcement embedded in the concrete restrains shrinkage. As seen in Figure 2-10 (a), the symmetrically reinforced concrete beam section has the same shrinkage strains in both compression and tension zone. The neutral axis drops but the curvature remains same.

In the un-symmetrically reinforced concrete beam section (Figure 2-10 (b)), where the tension reinforcement is greater than the compression reinforcement, the shrinkage in the tension zone is lower than in the

compression zone. This is because the tension steel provides a greater restraint to movement than the compression reinforcement. Consequently, the neutral axis drops slightly and the curvature increases.



a. Symmetrical reinforced beam



b. Unsymmetrical reinforced beam

Figure 2-10 Shrinkage effect on the reinforced concrete beam

2.3.2 The effect of creep

Under sustained load, concrete experiences creep and the curvature of a beam cross-section increases; consequently there is an increase in the deflection of the beam (Gilbert, 2011; MacGregor, 1992).

Figure 2-11 presents the effects of creep on the un-cracked and cracked sections of a reinforced concrete beam. The interaction of the compression and tension zone works according to the compatibility requirement that plane sections must remain plane. The neutral axis depth varies along the beam length depending on the un-cracked and the cracked sections.

As seen in Figure 2-11(a), creep increases the compressive and tensile strain in the un-cracked section. This causes an increase in the curvature of the beam section. In the cracked section (Figure 2-11(b)), creep in the compression zone increases the compressive strain, whereas the tensile strain remains the same because there is no concrete in this zone to creep. Therefore, creep increases the neutral axis depth (measured from the top surface) and the curvature as well, but reduces the compressive stress level.

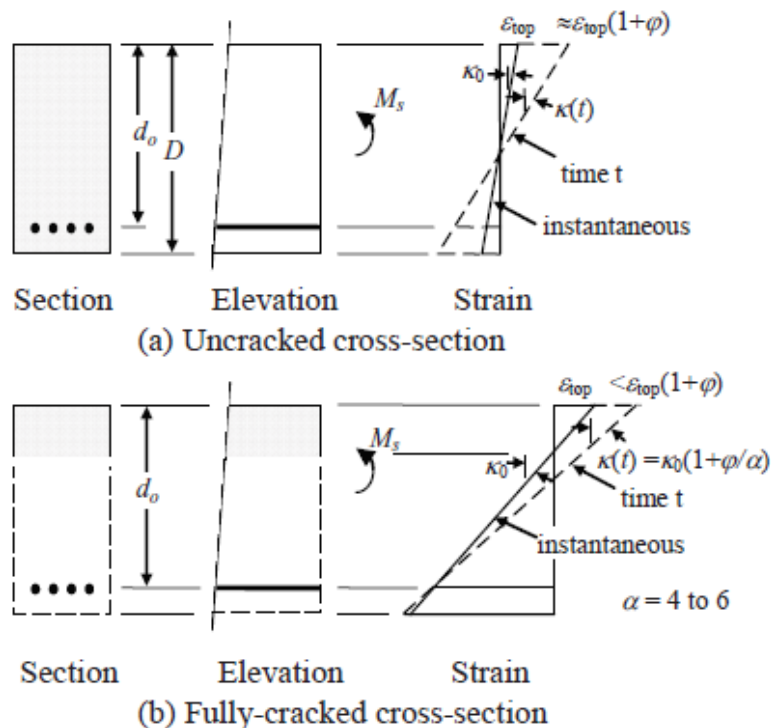


Figure 2-11 Effects of creep on the strain of a single reinforced section in bending (Gilbert, 2011)

Compression steel can reduce creep strains. Creep of the concrete in the compression zone transfers some of the compressive force from the concrete to the compression steel (so the stress in the compression steel increases). Hence, the compressive stress in the concrete decreases and the creep is reduced. In other words, the addition of compression steel reduces the long-term deflection of a reinforced concrete beam subjected to sustained loads (MacGregor, 1992).

Larger ratios of the compression steel ($\rho' = A_s'/bd$) will also further increase the reduction in creep. Figure 2-12 presents deflection-time relationships for beams with and without compression reinforcement. Washa and Fluck (1952) showed that the beam without compression steel ($\rho' = 0$) had 195% additional deflection with time, whereas the beam with compression steel ($\rho' = \rho$) had 99% additional deflection with time in comparison with the initial deflection.

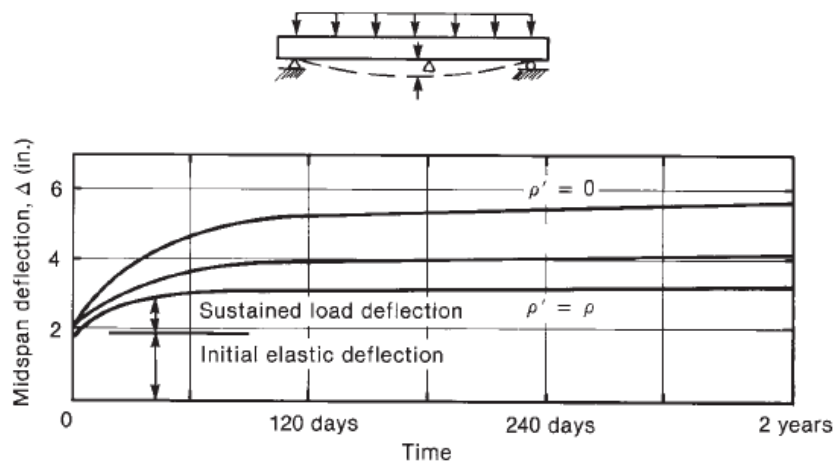


Figure 2-12 Effect of compression reinforcement on deflections under sustained loading (Washa and Fluck, 1952; MacGregor, 1992)

Many experimental studies have been conducted to investigate the long-term deflection of concrete beams under a 4-point bending test arrangements. The effect of the compression steel in reducing the long-

term deflection has been studied by Washa and Fluck (1952) and Paulson et al. (1991). The time dependent deformation of reinforced concrete beams, strengthened externally with FRP, was investigated by Al Chami et al. (2009), Hong and Park (2016), Mazzotti and Savoia (2007) and Sobuz et al. (2012). Arockiasamy et al. (2000) studied the long-term behaviour of concrete beams reinforced with CFRP bars. There has been no experimental work to investigate the long-term deflection of a cantilevered reinforced concrete beam.

2.4 Bond Strength between Old Concrete and New Concrete

The bond strength at the interface between old concrete and new concrete has been investigated by some researchers. The interface is the weakest link for composite behaviour and a place where a premature failure could happen.

The strength of the interface is effected by several factors, such as the moisture and/or the Saturated Surface Dry (SSD) or air-dry condition of the old concrete surface, the w/c ratio of the new concrete (Shin and Wan, 2010), and the surface condition (roughness) of the old concrete (Gillette (1963) in (Shin and Wan, 2010). Shin and Wan (2010) proved that the SSD condition of the old concrete results in higher shear bond strength of the interface (almost double) in comparison with the old concrete with air-dry surface condition. Chorinsky (mentioned in Austin et al. (1999)) concluded that too wet or too dry concrete always generates a weak interface.

Current design codes (EN 1992, ACI Committee 318-2008) only consider factors such as the concrete compressive strength, the normal stress at the interface and the amount of reinforcement crossing the interface and the roughness of the substrate surface. The expressions are based on

shear-friction theory. Santos and Júlio (2011) found that the bond strength and failure mode of concrete-to-concrete interfaces of reinforced concrete members (cast at different ages) is also determined by the curing condition. The curing of concrete influences the differential shrinkage and differential stiffness at the interface between old and new concrete.

The increase in the difference of ages will also increase the differential shrinkage at the interface, and therefore, increase the stresses in the interface (Santos and Júlio, 2011). As a result, the bond strength of the interface is supposed to decrease.

The difference in compressive strength and hence the elastic modulus of each concrete layer can cause a difference in the stiffness of the composite concrete member (Santos and Júlio, 2011). Some researchers (Julio et al., 2006; Austin et al., 1999) stated that the increase in the difference between the stiffness of the two layers changes the stress distribution at the interface, and stress concentrations can potentially occur at both ends.

Julio et al. (2004) evaluated the effect of the roughness on the concrete-to-concrete bond strength through slant shear tests and pull-off tests. They compared some roughening techniques which were commonly used in practice, such as (1) surface cast against steel formwork; (2) surface prepared with steel brush; (3) surface partially chipped; (4) as in (3) plus water saturation 24 h prior to casting the concrete and (5) surface treated with sand blasting. The results showed that the sand-blasting method provided the highest values of the bond strength in shear and in tension.

The behaviour of the interface between old concrete and new concrete in composite beams subjected to cyclic loading was shown by Bull and Park (1986). They investigated precast beam-column connections using a precast U-beam and cast-in-place reinforced concrete beams. The inside surface of the precast beam was roughened using a chemical retarder in order to remove the surface cement paste and hence increase the bond

strength of the interface between the precast U-beam and cast-in-place reinforced concrete beam core. Composite action of the beam can develop only if shear can be transferred across the interface between the precast concrete and the cast-in-place concrete through concrete adhesion, interlocking or mated roughened surfaces and friction, or a combination of these.

Under seismic loading, the interface bond between the cast-in-place and precast beam may break down which reduces the available negative moment flexural strength to less than the composite section value. Because of that, it is suggested that at the beam end, the cast-in-place reinforced concrete beam core is designed to provide the negative moment flexural strength. While away from the end, the negative moment flexural strengths will be provided by the composite section.

As well the shear strength of beams at the beam ends (in the plastic hinge regions), the cast-in-place reinforced concrete beam should be designed to have sufficient transverse reinforcement to resist the design shear force. While away from either end of the beams, the whole composite section could be designed to provide the shear resistance.

2.5 Shear Reinforcement of Beam-Column Joints

Specific criteria within beam-column joints are required to increase shear resistance of the joints, since they experience significant shear forces under seismic loading, when compared to those under gravity loading. Park and Paulay (1975) stated that joint shear reinforcement is important in both horizontal and vertical directions. Horizontal joint shear reinforcement is provided by horizontal stirrup ties, while vertical directions are reinforced by intermediate column bars which pass through joints.

2.5.1 Horizontal stirrups

In most countries, where earthquake probabilities are small, e.g. the UK, Hong Kong and many European countries, structural engineers do not include seismic considerations in their designs. Kaung and Wong (2011) investigated the effectiveness of horizontal stirrups in joint cores of full scale reinforced beam-column joints using non-seismic designs.

Six exterior beam-column joints were made with variations in the number of horizontal stirrups (Table 2-2 and Figure 2-13). The specimens were subjected to cyclic loading. The results showed that horizontal stirrups in joint cores improved seismic behaviour and enhanced joint shear strengths. These authors concluded that providing a joint stirrups ratio of more than 0.4% would not be effective in increasing shear strength. These observations were in agreement with Kitayama et al. (1989), who stated the optimum percentage of hoop ratio for interior beam-column joints was 0.4%.

Table 2-2 Specimen details (Kaung and Wong, 2011)

Specimen	Beam section: mm	Concrete cube strength f_{cu} (f'_c): N/mm ²	Transverse steel in joint core	
			Stirrup	Stirrup ratio (%)
BS-450	260 X 450	38.6 (30.9)	Nil	0
BS-450-H1T10	260 X 450	41.6 (33.3)	1T10	0.14
BS-450-H2T10	260 X 450	52.6 (42.1)	2T10	0.27
BS-600	260 X 600	45.5 (36.4)	Nil	0
BS-600-H2T8	260 X 600	52.7 (41.8)	2T8	0.13
BS-600-H4T8	260 X 600	37.1 (29.7)	4T8	0.26

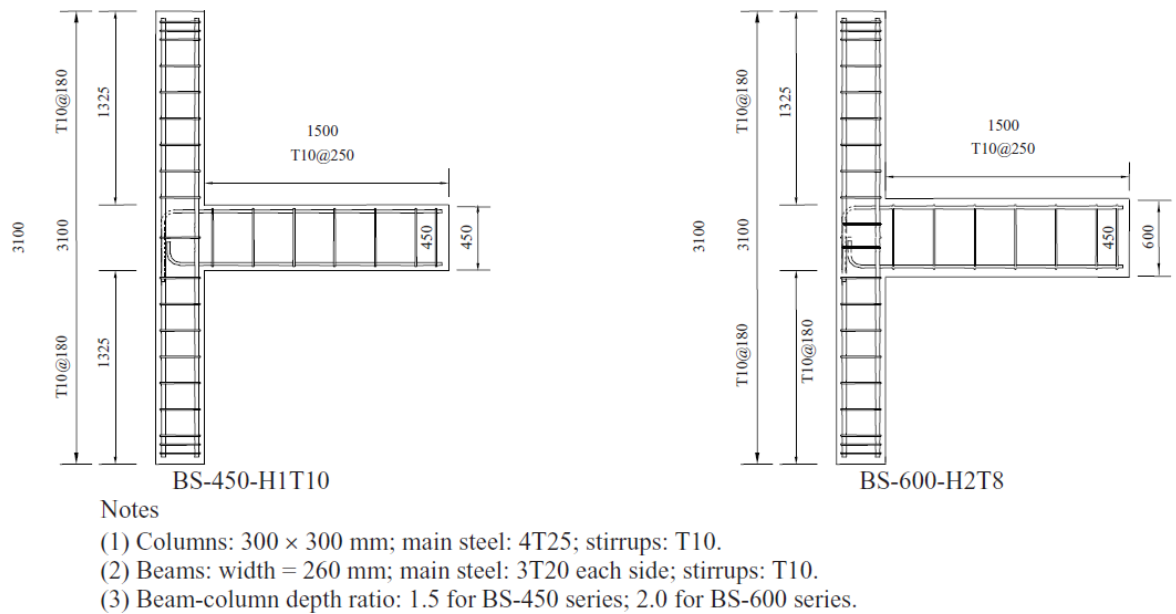


Figure 2-13 Geometry and reinforcement detail (Kaung and Wong, 2011)

2.5.2 Intermediate column bars

The importance of intermediate column bars as vertical joint shear reinforcements was experimentally shown by Park and Keong (1979). They compared two groups of interior beam-column joints. The first group consisted of 3 specimens (Unit 4, 5 and 9), where columns contained only 4 longitudinal (corner) bars (Figure 2-14). These specimens had been studied by Park and Thompson (1977) previously.

The second group consisted of 3 specimens (Unit 11, 12 and 13), which shared the same flexural strengths as those columns in the first group, unless they contained intermediate longitudinal bars (Figure 2-15). Static cyclic loadings were applied to joint specimens.

The results showed significant improvements in hysteretic responses and joint failures. As seen in Figure 2-16, there was extensive damage in the joint core of Unit 4, whereas the diagonal cracks in the joint core of Unit 11

were relatively small and the plastic hinges occurred in the beam (see Figure 2-17).

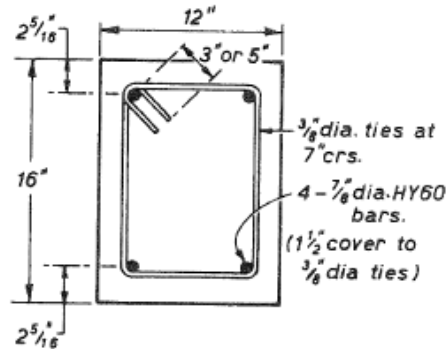


Figure 2-14 Column sections of Unit 4, 5 and 9 (Park and Keong, 1979)

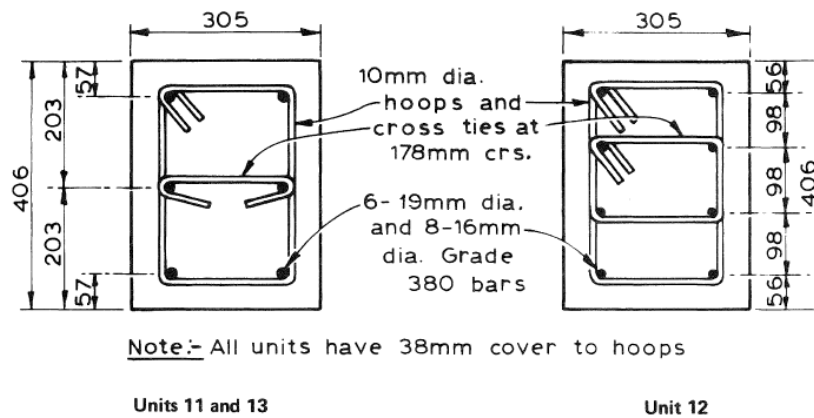


Figure 2-15 Column sections of Unit 11, 12 and 13

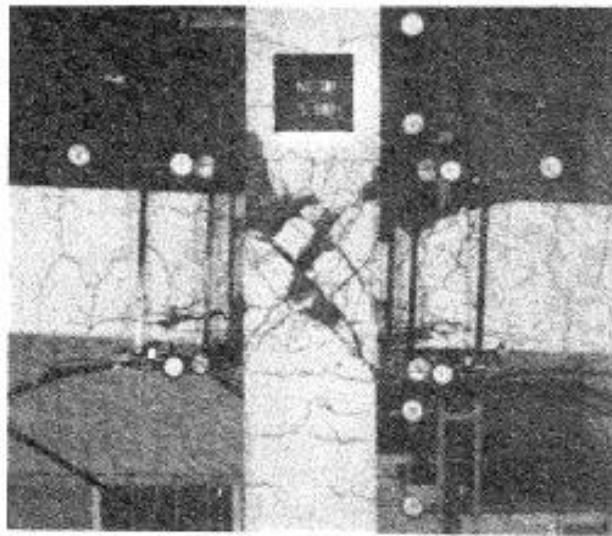


Figure 2-16 Unit 4 (Park and Keong, 1979)

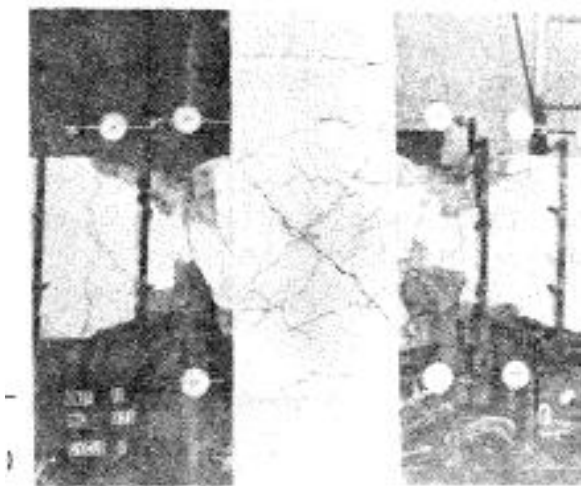


Figure 2-17 Unit 11 at the end of loading cycles (Park and Keong, 1979)

2.5.3 Diagonal bracing bars

Another type of reinforcement that increases shear joint resistance is the diagonal bracing bar. These bars are placed into beam-column joint cores and behave like truss elements, providing strength and stability during the installation process. The contribution of diagonal bars to increased shear resistance in joints has been shown by Parastesh et al. (2014). In their

work, diagonal bars were installed in both exterior and interior beam-column precast specimens, whereas diagonal bars were not installed in monolithic specimens. Figure 2-18 shows how the diagonal bracing bars were placed into interior joints. Again, cyclic loadings were applied to specimens. Diagonal shear cracks were observed initially at the beam-column joint core at different levels of drift ratio for every specimen; the monolithic specimen occurred at a drift ratio of 2.5%, while the precast specimens were at 3% and 3.5% of drift ratio. The monolithic specimen showed higher damage in the joint core (Figure 2-19). This suggested that diagonal bracing bars placed in the joint core, could delay diagonal crack propagation in the joint core of the precast specimens when compared to monolithic specimens.

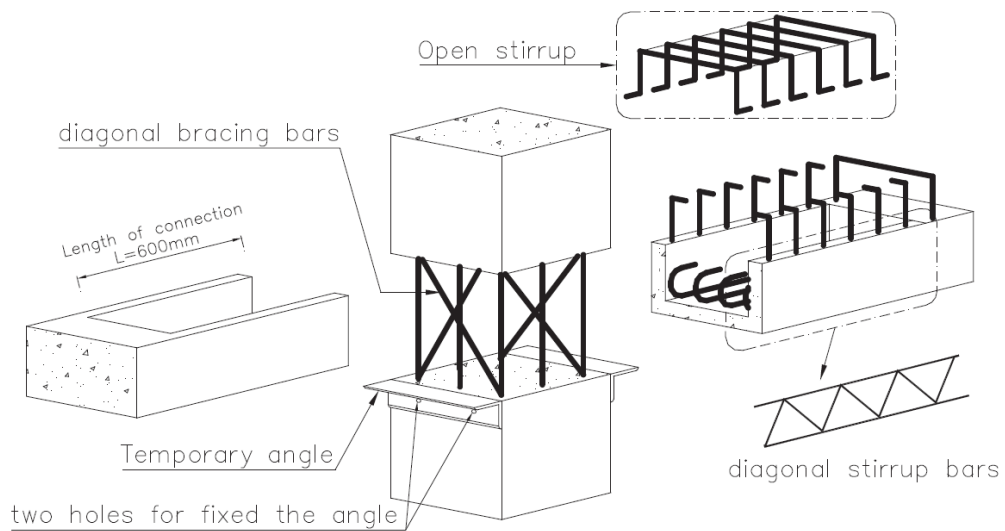


Figure 2-18 Reinforcement of interior precast concrete beam-column connections (Parastesh et al., 2014)

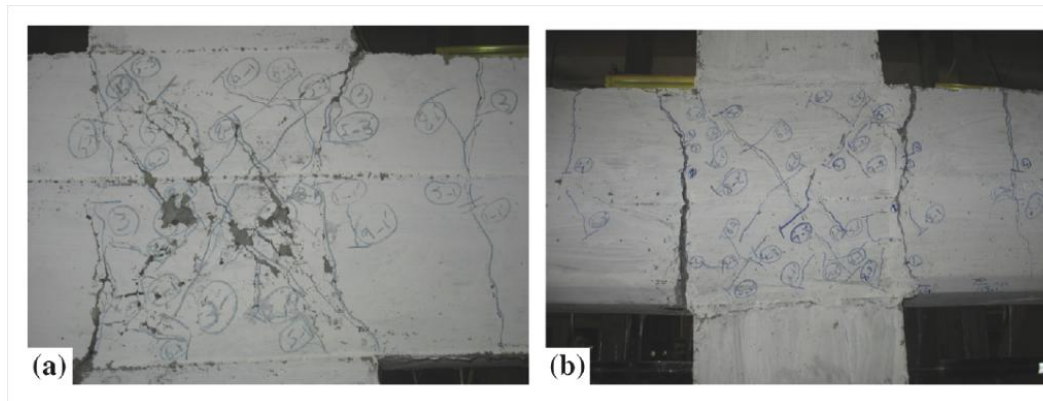


Figure 2-19 Typical failure in joint cores of (a) interior monolithic specimen (b) interior precast connection (Parastesh et al., 2014)

The advantages of diagonal bars in beam-column joint performance was emphasised by Kularni and Patil (2013). These authors studied column crossed inclined reinforcements (CCIR) in the exterior beam-column joints in conjunction with, (1) concrete grade, (2) tie ratio and (3) joint aspect ratio.

A nonlinear finite element analysis package, ANSYS 13.0, was used to develop a 3D model of external beam-column joints. The authors concluded that external beam-column joints with CCIRs exhibited better performances in terms of energy dissipation, joint shear capacity and load resistance. Important factors which may affect joint shear capacity include: (1) concrete compressive strength, (2) joint aspect ratio (h_b/h_c), (3) anchorage of beam longitudinal reinforcement, and (4) the number of stirrups within the joint.

2.6 Fibre Reinforced Concrete

Fibre reinforced concrete (FRC) is a cement based material reinforced with short randomly distributed fibres. Currently, fibres are produced from several materials such as steel, glass, carbon, and steel combined with synthetic fibres (nylon, acrylic, polyester, etc.). Research has shown that FRC has better mechanical properties when compared to plain concrete

(Ezeldin and Balaguru, 1992; Lee and Barr, 2004). The fibres, which are dispersed homogeneously in the concrete, can bridge cracks and distribute tensile and shear stresses so that crack sizes become smaller and are spread evenly (Altun et al., 2007). The fibres also can control crack formation, delay crack propagation and improve the ductility of the concrete. In addition, the presence of fibres in concrete can enhance bond strength between concrete and deformed steel bars (Chao et al., 2009; Ganesan et al., 2014b).

Introducing fibres into concrete can change the properties of concrete from a more brittle material to a more ductile material. As can be seen in Figure 2-20, concrete without fibres (unreinforced matrix) has no significant post-cracking ductility, whereas fibre reinforced concrete (FRC) has significant ductility after cracking, which increases concrete toughness.

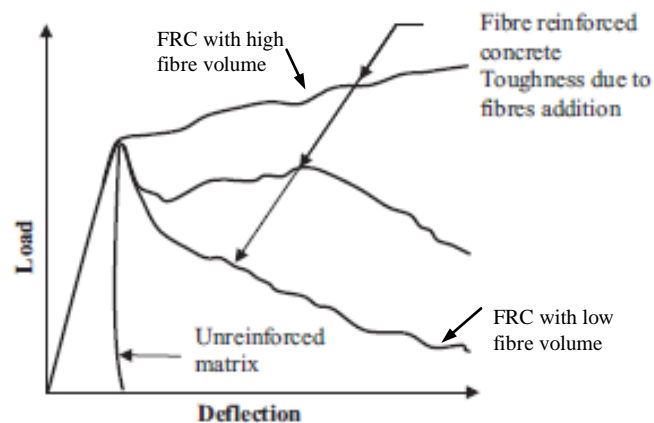


Figure 2-20 Load-deflection curves for matrix (plain concrete) and FRC (ACI 544.1 R, 1996)

Fibres in concrete could bridge cracks, requiring more energy for debonding and pull-out; thereby increasing concrete toughness. Toughness is defined as the area under the load-deflection curve, which indicates the energy absorption capability of a material (ACI 544.1 R, 1996). Steel fibres have been fabricated using several geometries (Figure 2-21) that are intended to increase the bond strength between the steel fibres and the matrix, thereby increasing concrete toughness.

Fibres in concrete can improve its mechanical properties, especially the tensile strength. These fibres cannot replace the reinforcing bars in the structural members, however they are beneficial in controlling the development and widening of micro-cracks (Maidl and Dietrich, 1995) through de-bonding and pull-out mechanisms.

Fibres in concrete can also improve ductility and the energy absorption capacities of concrete. In addition, fibres increase toughness, strength, dynamic resistance and cracking resistance of cement composites (Neville and Brooks, 2010). Fibres also enhance shear and bending resistance in structural members due to improvements in bond strength between reinforcing bars and concrete under monotonic and cyclic loading.

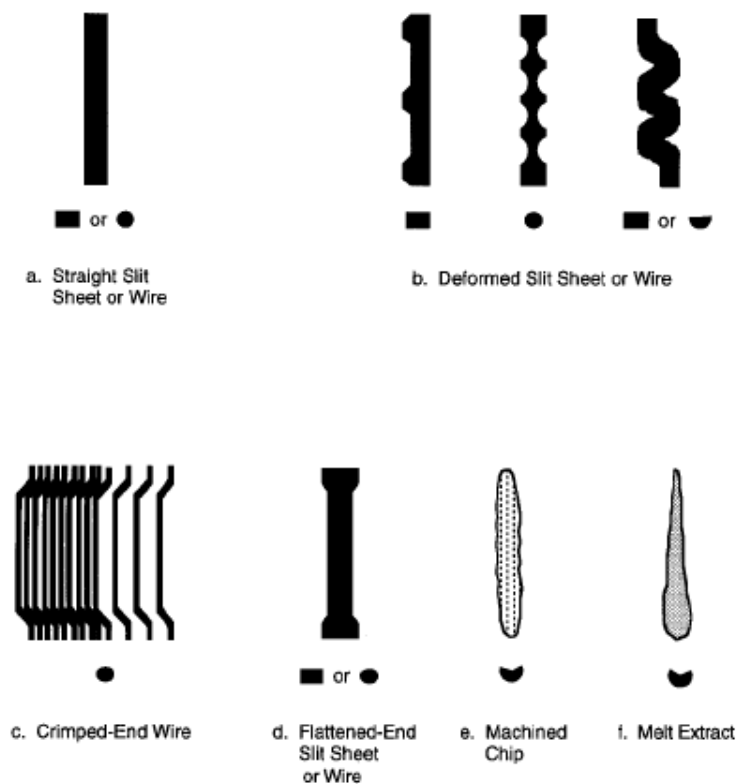


Figure 2-21 Geometries of steel fibre (ACI 544.1 R, 1996)

The effectiveness of fibres in enhancing mechanical properties of concrete depends on several factors, such as fibre type, fibre modulus, fibre aspect ratio, fibre strength, fibre surface bonding characteristics, fibre content, fibre orientation, aggregate size and the strength of the concrete matrix itself (ACI 544.1 R, 1996). The formation of end anchorage by the hooked ends of steel fibres can increase the pull-out forces significantly, when compared to straight fibres; they increase the energy absorption capacity and concrete toughness (Soroushian and Bayasi, 1991).

Naaman and Reinhardt (2003) proposed a classification of high performance fibre reinforced concrete (HPFRC), based on tensile responses (Figure 2-22). The tensile responses of FRC can be categorised into two groups based on their behaviour after first-crack; i.e. strain hardening and strain softening. While flexural behaviour of FRC is categorised into deflection-hardening and deflection-softening (Figure 2-23). Deflection-hardening properties of FRC is beneficial for flexural member applications, while deflection softening properties are useful in controlling plastic shrinkage cracking of concrete (i.e. in pavements or slabs) (Naaman and Reinhardt, 2006).

Post-cracking responses depend on the fibre content incorporated into concrete. As can be seen in Figure 2-20, the higher the fibre content, the greater the concrete toughness. However, the optimum fibre content as recommended by ACI Committee 544.1R-96 (ACI 544.1 R, 1996) was 2%, and was made for practical reasons. Concrete mixes with high fibre contents, tended to be less workable. Also, there was a tendency for fibre-balling during mixing. Both factors led to the potential generation of voids in the hardened concrete.

There are further drawbacks to the use of steel fibres in structural applications. They are vulnerable to corrosion and fire, therefore they are not suitable for exposed infrastructure applications (e.g. bridge decks). In addition, the presence of fibres has been shown to increase concrete density, leading to increased structure weight (Jiang et al., 2014).

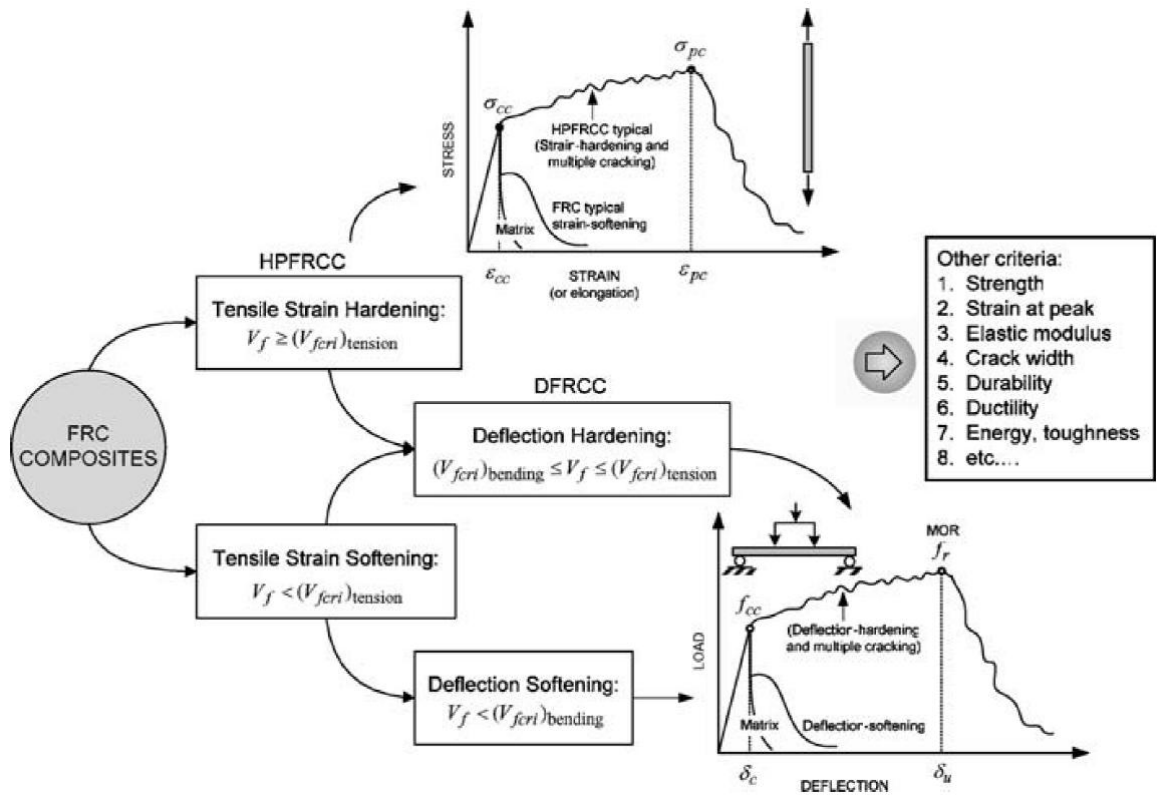


Figure 2-22 Classification of FRC composites based on tensile stress-strain responses (Naaman and Reinhardt, 2003)

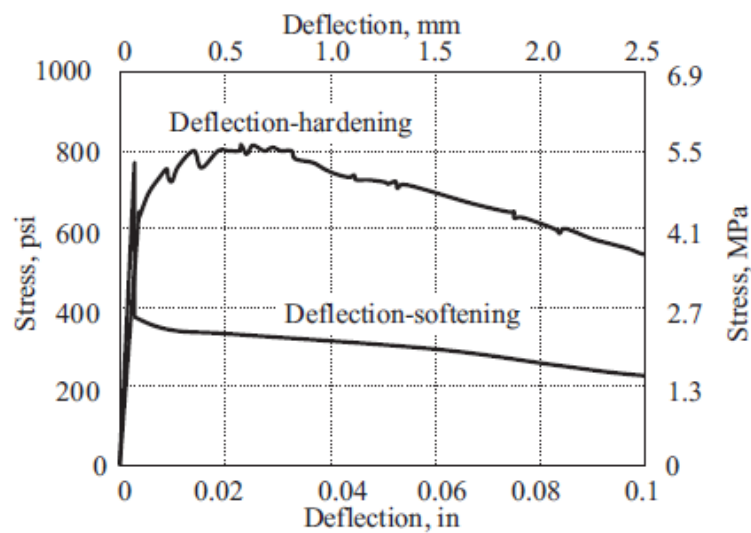


Figure 2-23 Deflection-softening or deflection-hardening of FRC

2.6.1 SFRC and bond strength

Choi et al. (2013) stated that the interface bond strengths between concrete and reinforcing bars is one of most important properties of reinforced concrete Choi et al. (2013). The interface transfers forces among the two materials, ensuring strain compatibility and composite action. Weak bonds at the interface can decrease load carrying capacity and stiffness of a structure.

Bond performances are affected by several factors. According to previous studies (Mathey and Watstein, 1961; Valcuende and Parra, 2009), these include; concrete strength, concrete thickness, surrounding reinforcing bars, confinements due to transverse reinforcements and bar geometries.

The bond strength of reinforcing bars embedded in hybrid fibre reinforced high performance concrete (HFRHPC) was studied by Ganesan et al. (2014b) using pull out test methods, incorporating a total of 96 cube specimens. Each specimen consisted of a concrete cube with a single reinforcing bar embedded vertically. Figure 2-24 shows the test setup of the pull-out test. The variables under test were volume fractions of steel fibre (i.e. 0.5% and 1.0%), volume fractions of polypropylene fibre (i.e. 0.1% and 0.15%, and diameters of steel reinforcement bars (i.e. 10 mm, 12 mm, 16 mm and 20 mm). A cube size of 100 mm was used for 10 mm and 12 mm diameter bars, while a cube size of 150 mm was used for 16 mm and 20 mm diameter bars. Table 2-3 lists the properties of the fibres. To achieve the required workability, a naphthalene based super plasticiser was used.

Table 2-3 Fibre properties (Ganesan et al., 2014b)

Type of fibre	Length (mm)	Diameter (mm)	Aspect ratio	Ultimate tensile strength (MPa)
Crimped steel fibre	30	0.45	66	800
Polypropylene fibre	12	0.038	316	550-600

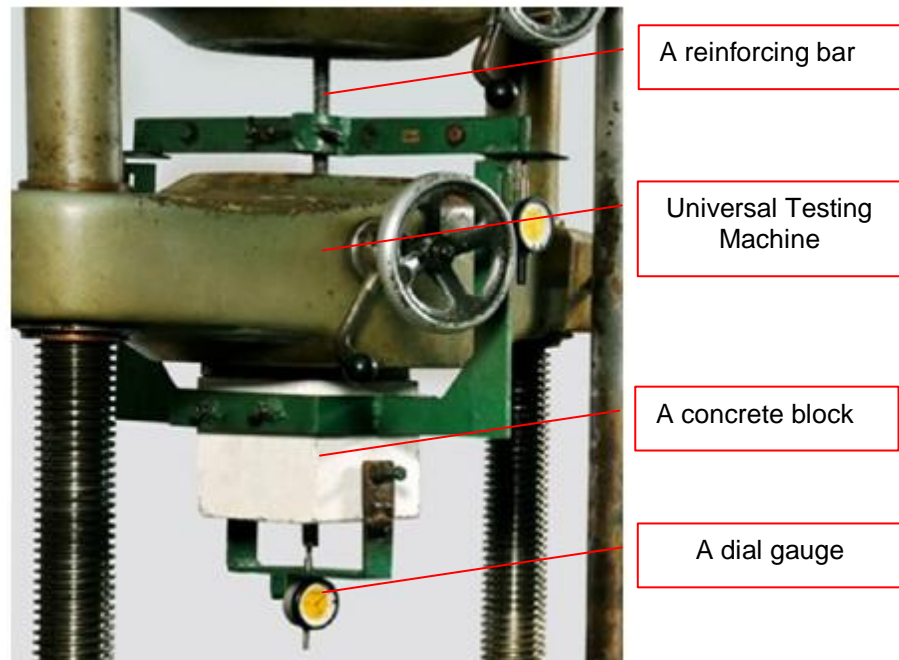
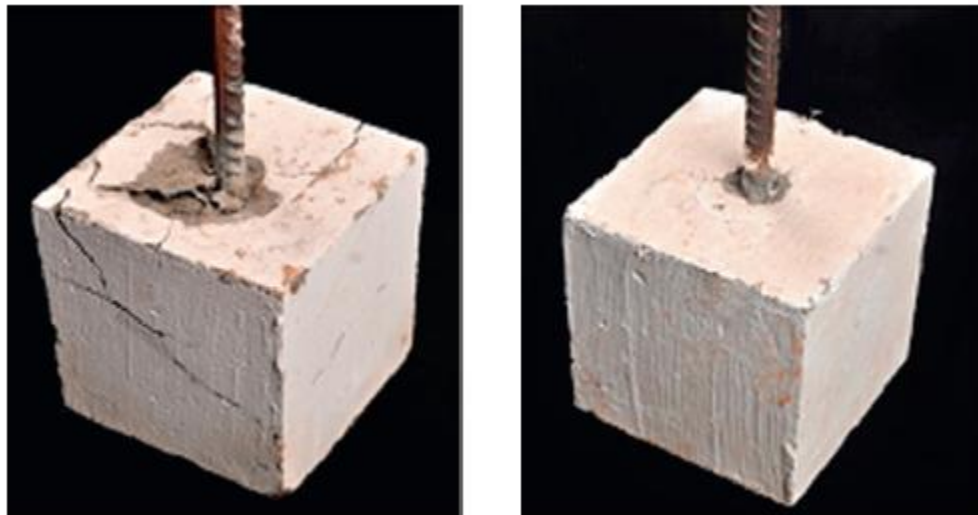


Figure 2-24 Pull-out test setup (Ganesan et al., 2014b)

Two failure types were observed in specimens, i.e. pull-out and yielding failures (Figure 2-25 and Figure 2-26). The specimen lacking fibres exhibited extensive cracking in the concrete (Figure 2-25a). The specimen containing fibres experienced pull-out failures with no significant cracks (Figure 2-25 b) and the yielding failure which the steel bar attained the maximum stress before reaching the ultimate bond stress (see Figure 2-26).

The optimum result was represented by a 1% volume fraction of steel fibres combined with a 0.10% volume fraction of polypropylene fibres. This combination improved bond stresses of 12 mm, 16 mm and 20 mm diameter bars by approximately 50%, 46% and 33% respectively. The fibre hybrid increased bond stress and reduced slip, which could be caused by polypropylene controlling micro-cracks, and steel fibres controlling macro-cracks. This study suggested that HFRHPC reduced the anchorage length requirements of deformed bars.



a. Specimen with no fibres

b. Specimen with fibres

Figure 2-25 Pull-out failures (Ganesan et al., 2014b)

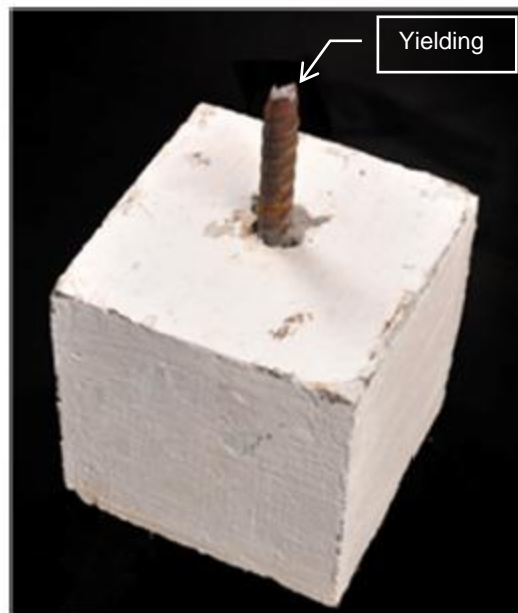


Figure 2-26 Yielding failure (Ganesan et al., 2014b)

The effect of fibre reinforced concrete on the length requirements of bars was demonstrated by Maya et al. (2013). These authors carried out a two-stage experimental programme to study the behaviour of precast elements connected using short reinforcement splice lengths. Ultra-high performance fibre reinforced concrete (UHPFRC) was used as the cast-in-place concrete. Flexural beam tests were carried out to assess the use of

short reinforcement splice lengths in the first experimental stage. For the next stage, short reinforcement splice lengths were applied to the beam-to-column connection for precast construction. The results showed that UHPFRC enabled reductions in splice length. A reinforcement splice length of $15d_b$, where d_b is the reinforcing bar diameter, achieved ultimate connection strengths in both flexural beam tests and beam-to-column connections.

2.6.2 Application of FRC in seismic beam-column joints

2.6.2.1 Research by Soubra and Naaman (1993)

Soubra and Naaman (1993) investigated four precast concrete beam-column sub-assemblages under cyclic loading. Each T-specimen consisted of two precast elements which were connected by a cast-in-place (CIP) connection. Figure 2-27 shows the typical beam-column T-specimen used in this study. Table 2-4 summarises CIP connection characteristics for every T-specimen. All T-specimens have the same reinforcement detail (Figure 2-28).

Table 2-4 Characteristics of individual beam-column sub-assemblages

Specimen	Properties of fibres in CIP connection		
	Type	Length (mm)	Volume fraction (%)
Control	-		0.0
Poly	Polypropylene	19	1.0
H50	Hooked (steel)	50	1.0
H30	Hooked (steel)	30	2.0

It was observed that steel FRCs in CIP connections improved displacement ductility of the specimens, increasing maximum loads (60% higher by using fibre volume fractions of 2%; Specimen H30), slowed

stiffness degradation, and improved the energy dissipation in comparison with the control specimen.

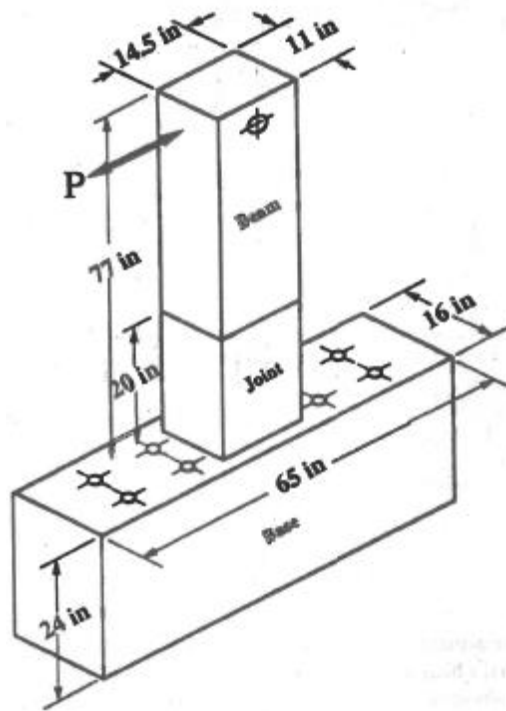


Figure 2-27 Typical beam-column T-specimen (Soubra and Naaman, 1993)

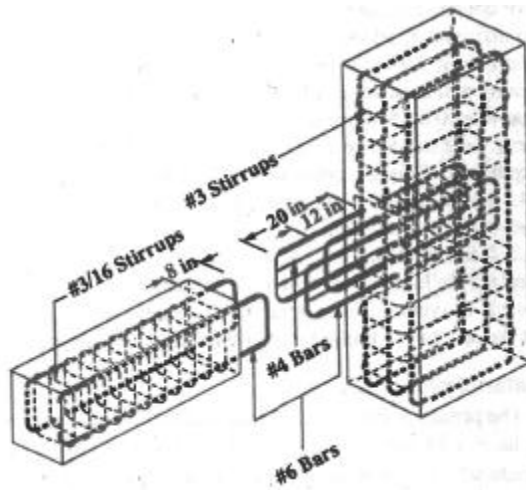


Figure 2-28 Reinforcement for T-specimens (Soubra and Naaman, 1993)

2.6.2.2 Research by Marthong and Marthong (2016)

In their experimental work, Marthong and Marthong (2016) studied one-third sized exterior reinforced concrete beam-column connections. The beam-column specimens were subjected to cyclic loading. A total of six beam-column specimens were cast and tested; three were used as reference specimens. They were categorised for three types of deficiency, (1) beam weak in flexure (BWF), (2) beam weak in shear (BWS) and (3) column weak in shear (CWS). Figure 2-29 and Figure 2-31 show an isolated exterior beam-column connection and steel reinforcement details of the beam-column specimens, respectively.

The reference specimens were designed using standard code practices (Indian Standard). Strong column-weak beam principles were adopted in designing BWF and BWS. The BWF beam was designed under reinforced sections, whereas the BWS beam was similar to that of BWF, except the beam shear reinforcement was reduced. The cross sectional dimensions of the CWS column was identical to BWF and BSF, but the beam cross section was increased to 80 mm x 150 mm. This made the beam stronger than the column (strong beam-weak column principle).

The other three specimens had similar geometries and reinforcement details similar to those of the reference specimens. They were cast with the same concrete mixes, but strengthened with Polyethylene terephthalate (PET) fibre-reinforced concrete or PFRC at the joint region (D-region); the specimens were called BWFSF (beam weak in flexure and strengthening with fibre), BWSSF (beam weak in shear and strengthening with fibre), and CWSSF (column weak in shear and strengthening with fibre),. The PET fibre content was 0.5% by concrete weight. The fibre aspect ratio was 25.

Figure 2-30 shows the comparison hysteresis loops between BWF and BWFSF specimens. It can be seen that BWFSF performed efficiently with maximum load capacities at the same beam tip displacement, with higher

stiffness and wider areas inside each loop in comparison with BWF. Overall, the authors concluded that PET fibre reinforced concrete (PFRC) in D-regions of beam-column connections, improved load resisting capacities, stiffness degradations, displacement ductility levels, energy dissipation, and damage tolerances in comparison to reference specimens.

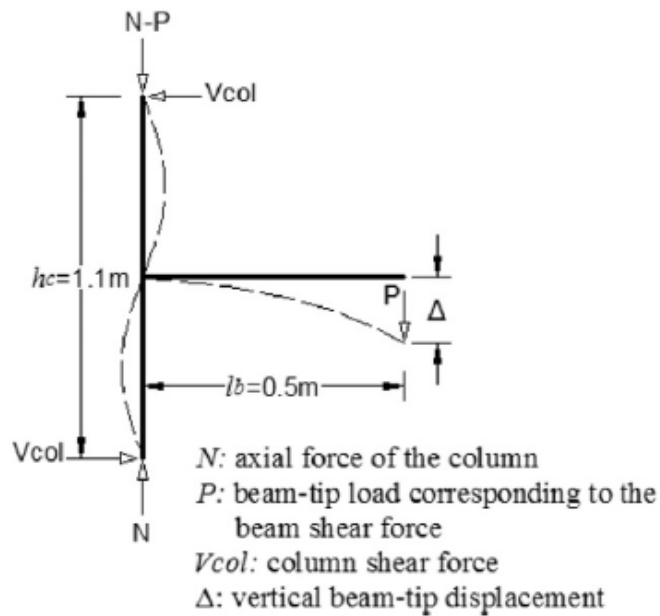


Figure 2-29 Isolated exterior beam-column connection (Marthong and Marthong, 2016)

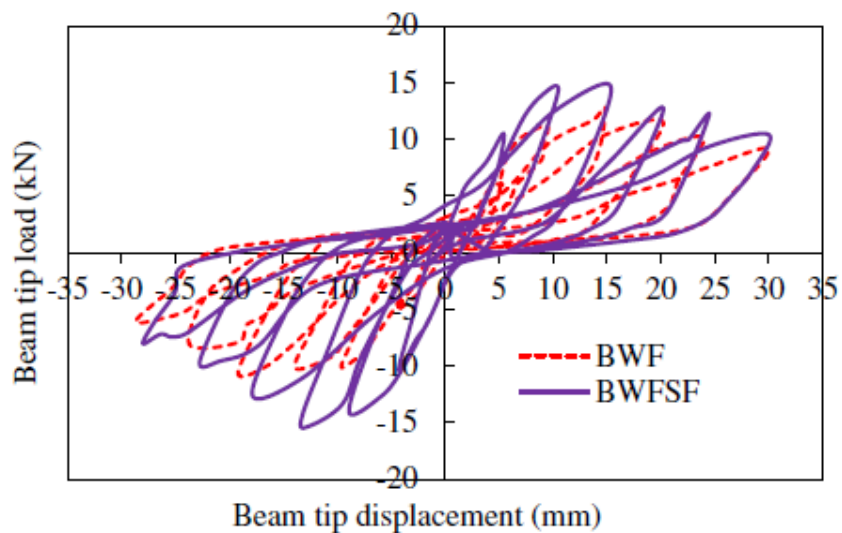


Figure 2-30 Hysteresis responses of BWF and BWFSF (Marthong and Marthong, 2016)

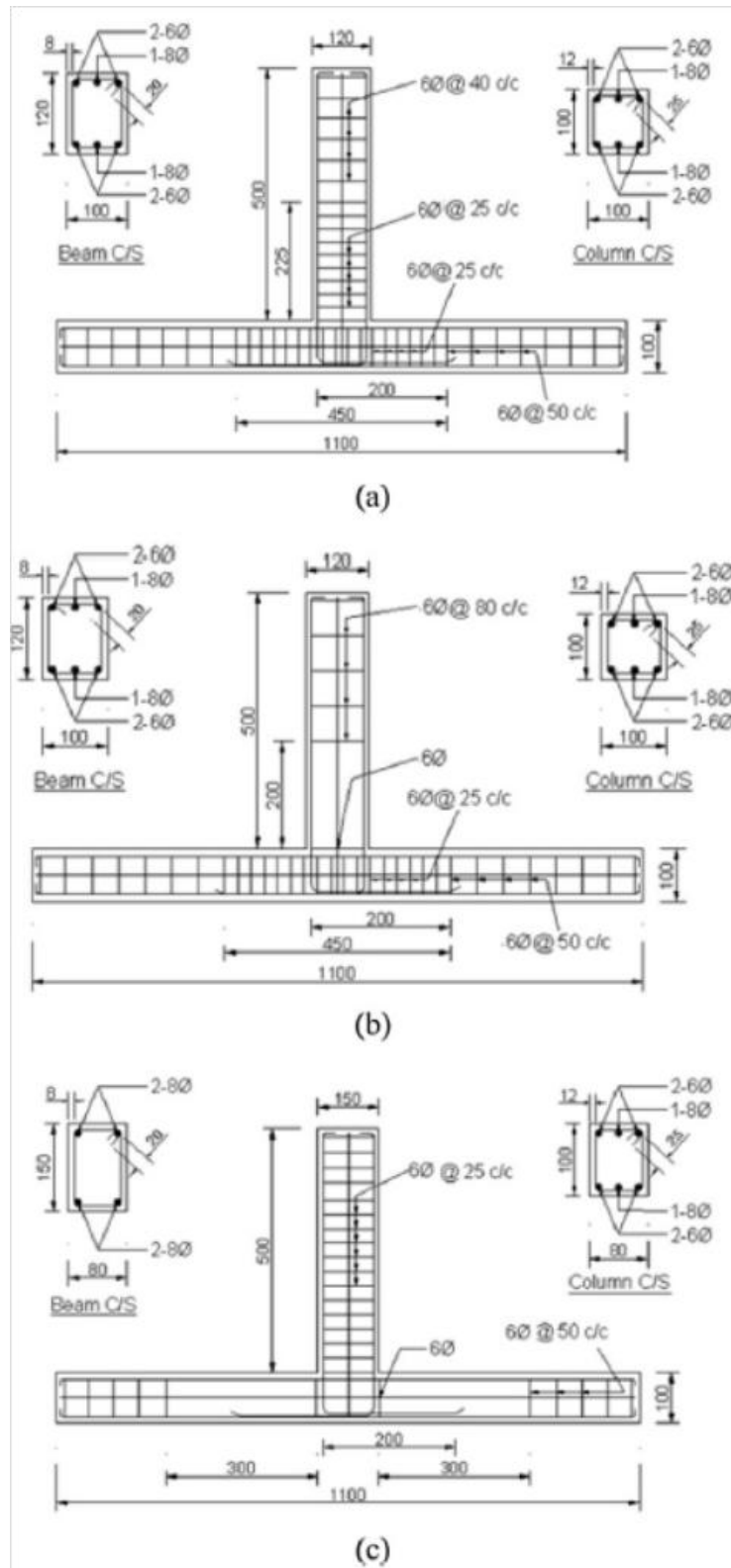


Figure 2-31 Reinforcement details of specimens (a) BWF, (b) BWS and (c) CWS (Marthong and Marthong, 2016)

2.6.2.3 Research by GENÇOĞLU and Eren (2002)

GENÇOĞLU and Eren (2002) studied steel fibre reinforced concrete (SFRC) in reducing the number of stirrups in beam-column joints. Four full-scale exterior beam-column specimens were tested under reversed cyclic loadings. Figure 2-32 shows reinforcement details of all test specimens. Specimen #1 and #2 were cast using plain concrete to understand the importance of closely spaced stirrups in joints. Specimen #3 and #4 were made using SFRC with fewer numbers of stirrups in joint cores. Table 2-5 shows the material composition of the plain concrete and SFRC specimens. The SFRC mix incorporated collated hooked-end steel fibres with the following specifications: 1% volume fraction of fibre, with dimensions; length 60 mm, diameter 0.8 mm, an aspect ratio of 75 and a yield strength of 1100MPa.

The beam-column specimens were tested according to Figure 2-33. Reversal loadings were applied to the beam-tip of the specimen in accordance with the loading history (Figure 2-34). An axial compressive load of 150kN was applied to the column to representative normal force.

The effectiveness of SFRC reducing stirrup numbers in the joint core was proven by this research. Specimen #3, with one stirrup in the joint core, had better hysteresis loops than those of Specimen #1, which contained 5 stirrups in the joint core (Figure 2-35). Figure 2-36 shows that Specimen #3 had the highest values in terms of total dissipated energy. It showed that SFRC in beam-column joints can be used as an alternative, in reducing congestion due to the transverse reinforcement and the cost of steel reinforcement and its installation.

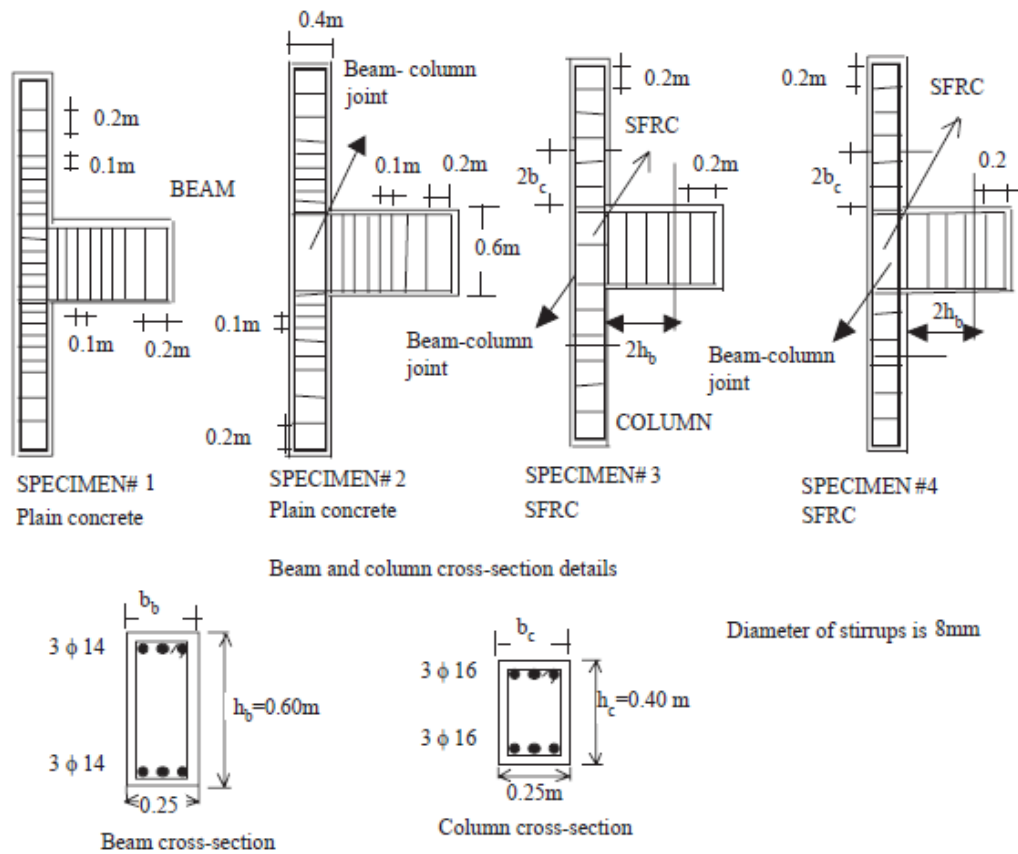


Figure 2-32 Test specimen details (Gencoglu and Eren, 2002)

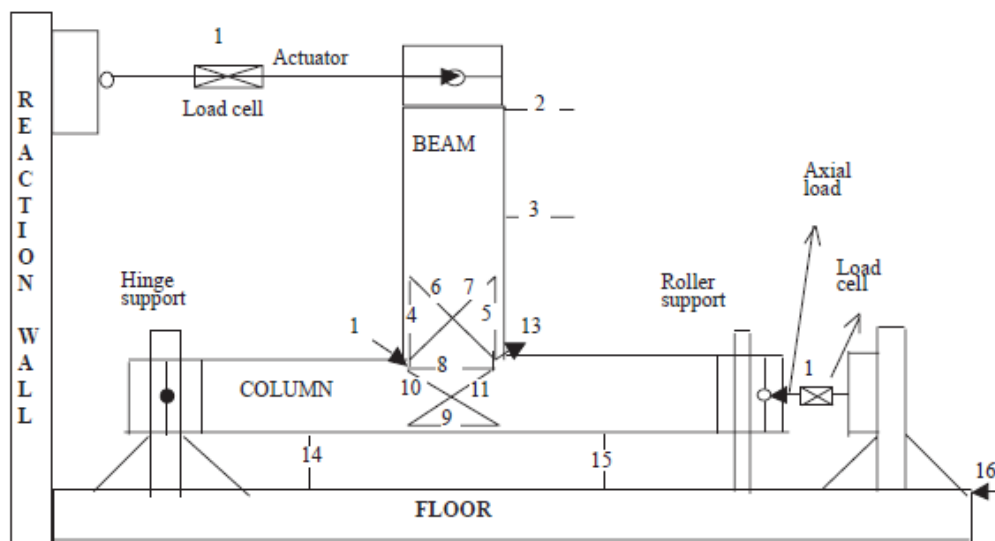


Figure 2-33 Set-up of beam-column testing (Gencoglu and Eren, 2002)

Table 2-5 Concrete mix characteristics (Gencoglu and Eren, 2002)

Materials	Unit	Plain concrete	SFRC
Cement	kg/m ³	340	340
Aggregate (10mm)	kg/m ³	906	906
Sand	kg/m ³	349	349
Water	kg/m ³	197	197
Supeplastisiser	ml/m ³	5000	5000
Stel fibre 60/0.8	kg/m ³		78

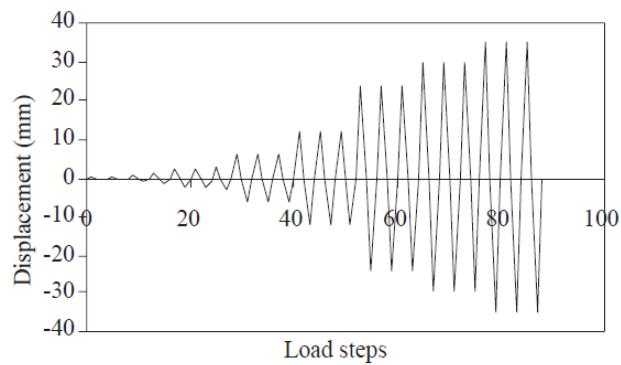


Figure 2-34 Displacement controlled cyclic loading (Gencoglu and Eren, 2002)

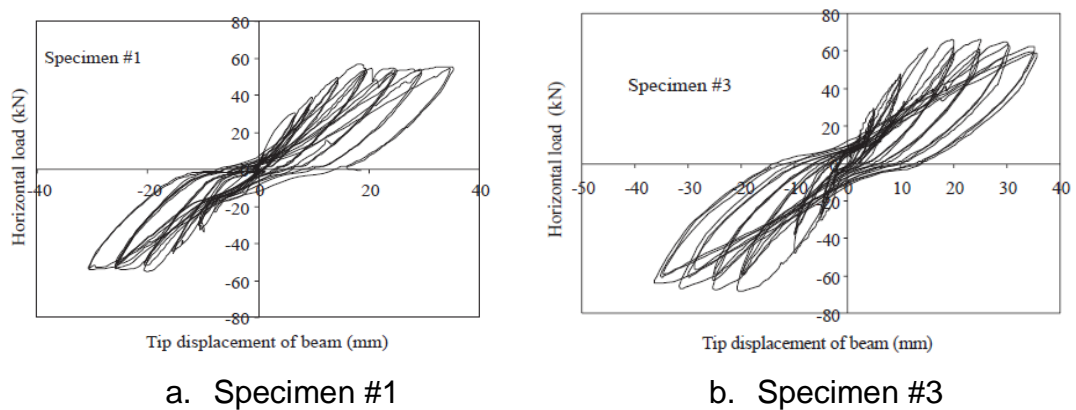


Figure 2-35 Hysteresis loops of specimens #1 and #3 (Gencoglu and Eren, 2002)

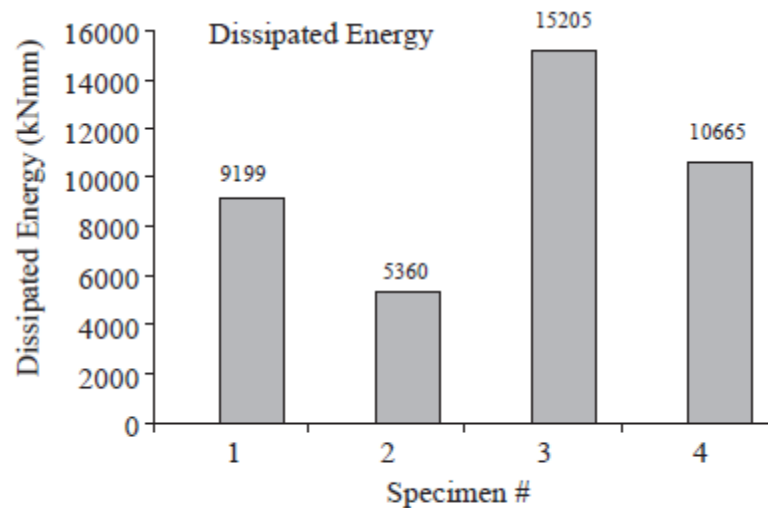


Figure 2-36 Total dissipated energy (Gencoglu and Eren, 2002)

2.6.2.4 Research by (Ganesan et al., 2007)

To investigate the effects of steel fibre reinforced high performance concrete (SFRHPC) on beam-column joints, Ganesan, *et al.* (2007) studied 10 exterior beam-column joints which were subjected to cyclic loading.

Beam-column specimens were made from M60 grade concrete which was designed using a modified ACI Method. The compositions consisted of cement (353 kg/m³), fly ash (98 kg/m³), silica fume 39 (kg/m³), sand 658 (kg/m³), coarse aggregate 1048 (kg/m³), water 162 (kg/m³) and super-plasticiser 10.78 (kg/m³). 30% cement was replaced by silica fume (10%) and fly ash (20%). Fibre volume fractions varied from 0 to 1% with increments of 0.25%. The specimens were called HP_r, F1HP_r, F2HP_r, F3HP_r and F4HP_r.

Figure 2-37 shows beam-specimen details. When testing, a constant load of 15.7kN or approximately 20% of the axial capacity of the column was applied. This held the specimen in position and stimulated the normal force of the column. The test arrangements are shown in Figure 2-38. The

cyclic loading (load-up and unload) was applied to the beam tip with increment loadings of 0.5kN.

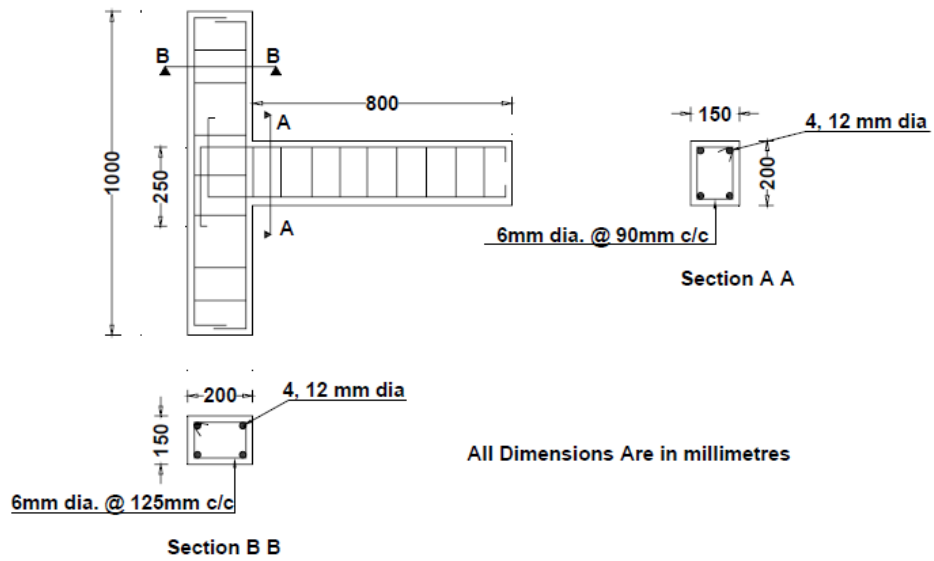


Figure 2-37 Reinforcement of BC specimens (Ganesan, *et al.*, 2007)



Figure 2-38 Test setup (Ganesan, *et al.*, 2007)

The failure patterns of HPC and SFHRPC beam-column joints are shown in Figure 2-39. Closely spaced fine cracks appeared in SFHRPC beam-column joint specimens. These crack-widths were smaller than those of the HPC beam-column joint specimen. The first crack load and the ultimate load increased with increases in steel fibre fraction. SFHRPC was shown to decrease the rate of stiffness-degradation, improve the dimensional stability and integrity of the joint and reduce the congestion of steel reinforcement in joint cores.

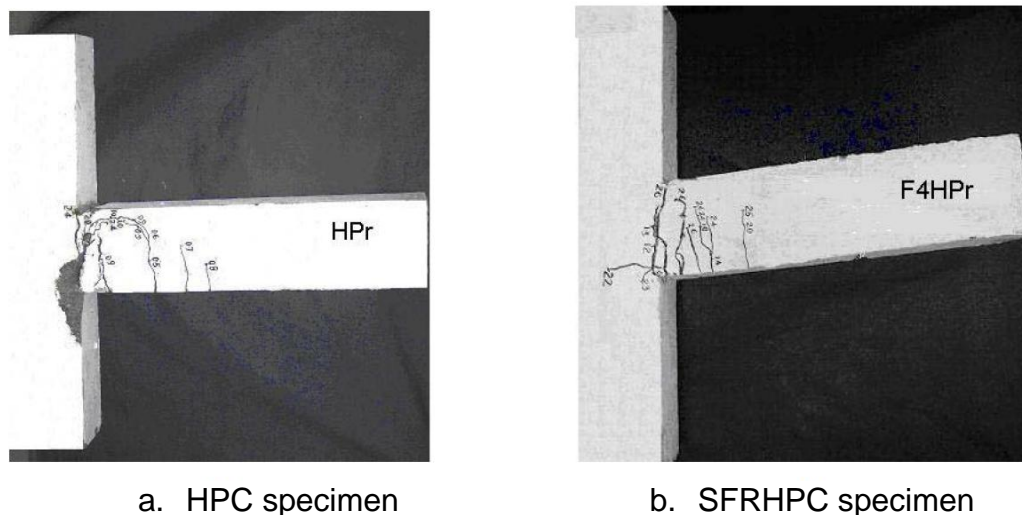


Figure 2-39 Beam-column specimens after failure (Ganesan, *et al.*, 2007)

2.7 Summary

The conclusions from this literature review are presented below and includes the base lines used to design experimental tests in this current study.

1. Economical and practical jointing methods in precast concrete systems have become important considerations in construction industries.

2. Precast concrete moment resisting frames should behave in a ductile manner due to seismic loading, through beam side-sway mechanisms, with plastic hinges forming at the ends of beams.
3. Several connection types have been developed, i.e. bolted/welded/pre-stressed/cast-in-place (CIP) connections or combinations of the above. Each connection has advantages and disadvantages in terms of strength, stiffness and ease of implementation.
4. Even though precast systems have advantages when compared to conventional systems in terms of time, quality and cost, they still face many technical problems, particularly in terms of connecting precast elements on site, which extend construction times and increase construction costs. Hence, increased development and innovation, especially with regard to beam-to-column connections, is needed.
5. For seismic resistance structure design, it is necessary to provide horizontal and vertical shear resistance in the joint cores. Vertical shear resistance in the joint is provided by intermediate column bars passing through joints, whereas horizontal shear resistance is provided by horizontal stirrups.
6. It is important to extend the longitudinal bars of precast beam into the column (the joint core) to achieve maximum moment capacity of the beam.
7. No investigation has focussed on research regarding exterior precast concrete beam-column connections. These consist of (1) interlocking bars acting as flexural reinforcements of beams which extend into gaps in precast columns, (2) precast U-beams as permanent formworks, and (3) stirrups which are located in both precast U-beam and beam-cores (Figure 3-4 and 3-7). There is therefore, a need to investigate these connection types. Based on Park 2008, the seated length of the precast U-beam (Table 2-1 and Figure 2-9) could

reduce effective shear areas of beam-column connections; therefore, to avoid this, the new connection would use corbel for placing the precast U-beam.

8. Steel fibres improve the mechanical properties of concrete, particularly flexural strength and post-crack performances. The use of steel fibre reinforced concrete (SFRC) in joint regions of beam-column joints has been extensively studied. The results have shown that SFRC could improve joint performance in terms of strength, ductility and energy dissipation. Therefore, SFRC has great potential for use as a material in CIP connections as it has better structural behaviour.

Each precast concrete connection type has a specific behaviour depending on the detail of the connection. Therefore, this study will investigate the structural behaviour of the new connection that has not been completely covered as following:

- a. Study the structural behaviour of the new connection under different loadings, i.e. static, quasi-static and sustained loading, to get a comprehensive understanding of the connection performance, especially to check the ductility and how the plastic hinges form at the end of beams.
- b. Currently, no study has investigated beam-column joint/connection under long-term loading experimentally, hence, the information and knowledge about their long-term behaviour is still limited. Therefore, the study of beam-column connection under sustained loading will increase the knowledge regarding the reinforced concrete structure under sustained loading.
- c. As SFRC has very good mechanical properties in comparison with plain concrete, especially in terms of the tensile strength, it is important to introduce the SFRC as the cast-in-place material in the

PCBC connection in order to get a better joint behaviour in terms of strength, ductility and energy dissipation.

- d. In general, there is an obvious lack of experimental investigation regarding the structural behaviour of the new type PCBC connection. This study will provide a better understanding of this connection's performance. Therefore, this study will increase the database of precast concrete beam-column connection results.

Chapter 3

Experimental Programme

3.2 Introduction

This chapter describes the experimental processes used in this study. It starts with the design of the geometry and reinforcement of the exterior precast concrete beam-column (PCBC) specimens, the number of PCBC specimens tested and their purpose, the materials, how to make PCBC specimens in the laboratory, and finally how to setup PCBC specimens in test rigs and associated instrumentation. All experimental works were carried out in the George Earle laboratory of the Civil Engineering School, University of Leeds.

3.3 Design of PCBC Specimens

Test specimens were representative of exterior beam-column joints of a prototype building. They were bounded by contra-flexure points in members. Beam-column joints were specifically designed for seismic loadings, therefore specimen designs followed strong column-weak beam principles. The over-strength factor was used in the columns to ensure failures occurred in the beams.

Currently, specific design recommendations for ductile precast connection are not available. Therefore, design recommendations for monolithic connections, as stated in ACI 318-11 (2011), were used as conservative guides for designing precast concrete beam-column connections.

Several requirements were used for designing beam-column specimens (based on ACI 318-2011):

1. The flexural strength of the column shall satisfy Equation (3-1). The over-strength factor in the reinforced concrete beam should not be less than 6/5 (Section 21.6.2.2).

$$\sum M_{nc} \geq \sum \left(\frac{6}{5}\right) M_{nb} \quad (3-1)$$

Where,

ΣM_{nc} = the sum of the nominal flexural strengths of columns framing into the joint, evaluated at the faces of the joint.

ΣM_{nb} = the sum of the nominal flexural strengths of the beams framing into the joint, evaluated at the faces of the joint.

2. The column dimensions shall not be less than 20 times the largest diameter of the longitudinal bars of the beam, which extends through a beam-column joint (Section 21.7.2.3).
3. The width of the beam framing into the joint shall be at least three-fourths the column width (Section 21.7.3.2).
4. The longitudinal reinforcement ratio (ρ) of the column is 1%-6% (Section 21.6.3.1)
5. The longitudinal reinforcement ratio (ρ) of the beam shall not be less than $1.4/f_y$ and not exceed 0.025 (Section 21.5.2.1)
6. The embedment length of the longitudinal bars of a beam extended through the joint (l_{dh} in Figure 3-1) shall not be less than d , or 12 times the diameter of the longitudinal bars of the beam (Section 12.12.3)

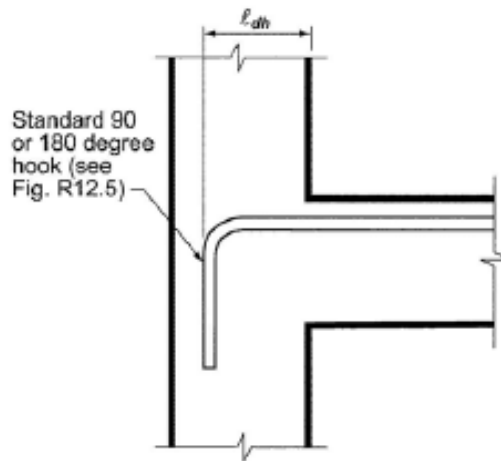


Figure 3-1 Anchorage into exterior columns (ACI 318-2011)

7. The development of standard hooks in tension (Section 12.5.1)

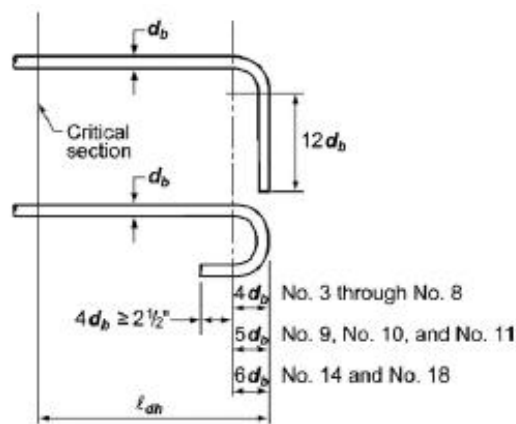


Figure 3-2 Hooked bar details for the development of standard hooks (ACI 318-2011)

8. The transverse reinforcements of joints shall have the same spacing with those of upper and lower columns (Section 21.7.3.1).

In considering these requirements, the dimensions and reinforcement details of the exterior PCBC specimens have been established (Figure 3-4).

Several assumptions were made for test specimens:

1. No axial force was subjected to columns. In real situations, columns of a structure retain axial forces resulting from gravity, live loads, and

sometimes seismic forces. These forces could improve beam-column joint shear strengths. Because this study focused on the behaviour of connections between precast beams and precast columns, it was not relevant to apply axial loads on column tops during testing.

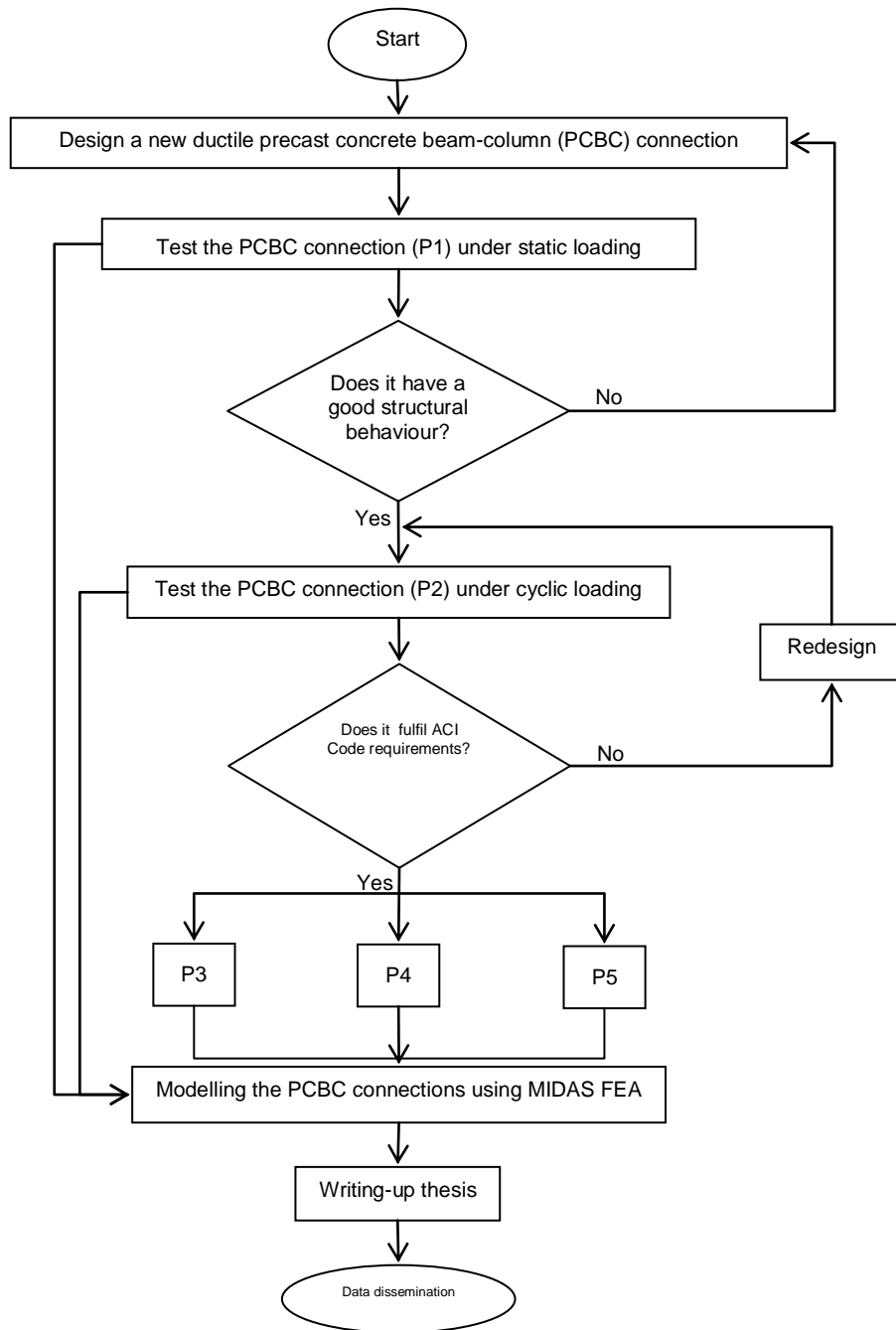
2. No floor systems were applied to PCBC specimens. The floor system of the prototype building used hollow-core slabs spanning two precast beams, with pins as the support assumption.
3. No transverse beams were framed into joints. The PCBC specimens represented exterior beam-column connections of two-dimensional moment resisting frames.

3.3 Description of Specimens

3.3.1 Experimental programme

Figure 3-3 presents the study work-plan; starting at the design stage of the precast concrete beam-column (PCBC) specimens, onto later test procedures. Five PCBC specimens were tested, including samples to measure the mechanical properties of the concrete.

This study concentrated solely on precast systems. The comparison with in-situ reinforced concrete joints was not done experimentally, but carried out using finite element modelling.



P3 is PCBC connection incorporating steel fibre ($V_f = 0.5\%$), subjected to cyclic loading.
 P4 is PCBC connection incorporating steel fibre ($V_f = 1.0\%$), subjected to cyclic loading.
 P5 is PCBC connection, no steel fibre, subjected to long-term loading.

Figure 3-3 Experimental programme

3.3.2 Description of test specimens

The specimens in this study represent the exterior precast concrete beam-column connections of a moment resisting frame, which is bound by contra-flexure points in vertical and horizontal members. There were five sets of precast concrete beam-column (PCBC) connection specimens in this study, with two variations, i.e. applied loadings and the concrete type used as the material of cast-in-place (CIP) connections.

One set of specimens consisted of one precast concrete beam and one precast concrete column that were joined using cast-in-place (CIP) concrete, to become an exterior beam-column joint. Table 3-1 shows the specimen details. Each variable consisted of one set of PCBC specimens. This was related to the size of specimen, time, and number of people involved in this process.

Table 3-1 Description of beam-column connection test

No.	Series	Cast-in-place concrete	Interlocking bars	Type of loading
1	P1	Plain concrete $f'_c = 45\text{MPa}$	4D12	Static
2	P2	Plain concrete $f'_c = 45\text{MPa}$	2D16 + 1D12	Quasi static
3	P3	FRC $f'_c = 45\text{MPa}$ $V_f = 0.5\%$ *	2D16 + 1D12	Quasi static
4	P4	FRC $f'_c = 45\text{MPa}$ $V_f = 1.0\%$ *	2D16 + 1D12	Quasi static
5	P5	Plain concrete $f'_c = 45\text{MPa}$	2D16 + 1D12	Long-term

* FRC is fibre reinforced concrete, $l_f/d_f = 35/0.55 = 65$

PCBC specimen descriptions are presented below:

a. PCBC Specimen 1 (P1)

Figure 3-4 and Figure 3-5 show PCBC Specimen P1. The specimen was subjected to static loading. The purpose of this specimen was to study the

behaviour of the PCBC connection under static loading. P1 was used as a control.

b. PCBC Specimen 2 (P2)

The details of PCBC Specimen P2 were similar to those of Specimen P1, unless specified; e.g. changes in diameter and numbers of interlocking bars (see Figure 3-6). The specimen was subjected to quasi-static loading. The purpose of specimen P2 was to study the behaviour of PCBC connections under cyclic loading. The test results of Specimen P2 were compared to Specimen P1.

c. PCBC Specimen 3 (P3)

Details of PCBC specimen P3 were identical to Specimen P2 unless specified; e.g. the specimen used steel fibre reinforced concrete (FRC) as a base material in cast-in-place (CIP) connections. The purpose of this specimen was to study the influence of the mechanical properties of CIP concrete on the performance of PCBC connections and to test the hypothesis that FRC can improve the strength and ductility of connections. Specimen P3 contained 0.5 % steel fibre ($V_f = 0.5\%$) and was subjected to quasi-static loading. The test results of Specimen P3 were compared to Specimen P2.

d. PCBC Specimen 4 (P4)

This specimen was similar to Specimen P3, unless specified; e.g. it contained 1.0% steel fibre in CIP connections. The purpose of this specimen was to study the influence of higher steel fibre contents, in the CIP connection on the behaviour of PCBC connections. The test results of Specimen P4 were compared to P2 and P3.

e. PCBC Specimen 5 (P5)

PCBC Specimen P5 were identical to Specimen P2. Specimen P5 was subjected to sustained loading. The purpose of P5 was to study the behaviour of PCBC connections under long-term loading, representing the serviceability stage of a structure.

3.3.3 Geometry and reinforcement details

Columns were designed to be stronger than beams in order to meet the requirements of strong column-weak beam principles. These principles are used in designing seismic resistance structures, ensuring flexural failures occur at the ends of the beam (adjacent to the column). All precast concrete beam-column (PCBC) specimens (i.e., P1 – P5) were of the same dimensions. Figure 3-4 shows reinforcement details of the PCBC specimens.

The cross section of the precast column was 300 mm x 300 mm, with total height, 2000 mm. 12 reinforcing bars of 16 mm-diameter were used as longitudinal reinforcements with a reinforcement ratio of 2.67%. This parameter satisfied ACI provisions which stated that the longitudinal steel bar ratio in a column should be between 1% and 6%. The 8 mm-diameter shear links with 100 mm-spacing were used along the height of the column.

The precast column is typically a multi-storey precast column. There was a gap at mid-height in the precast column (at the beam framing position), which was used for placing interlocking bars. The height of the gap was 300 mm, which was equal to beam depth. The precast column had a corbel which was used for seating precast U-beams.

The precast beam comprised two parts, i.e. the precast U-beam and the cast-in-place (CIP) reinforced concrete beam core. The outer dimensions of the precast U-beam were 250 mm x 300 mm and 1250 mm (length). The dimension of the CIP beam core was 150 mm x 250 mm with a length of 800 mm from the column face. The longitudinal bars of the beam core of PCBC Specimen P1 consisted of four interlocking bars of 12 mm-diameter, which acted as both negative and positive moment reinforcements (Figure 3-5). The 8 mm-diameter shear links with 100 mm spacing were used along the CIP beam core and the precast U-beam.

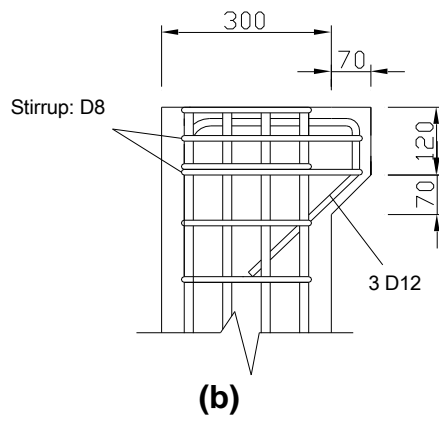
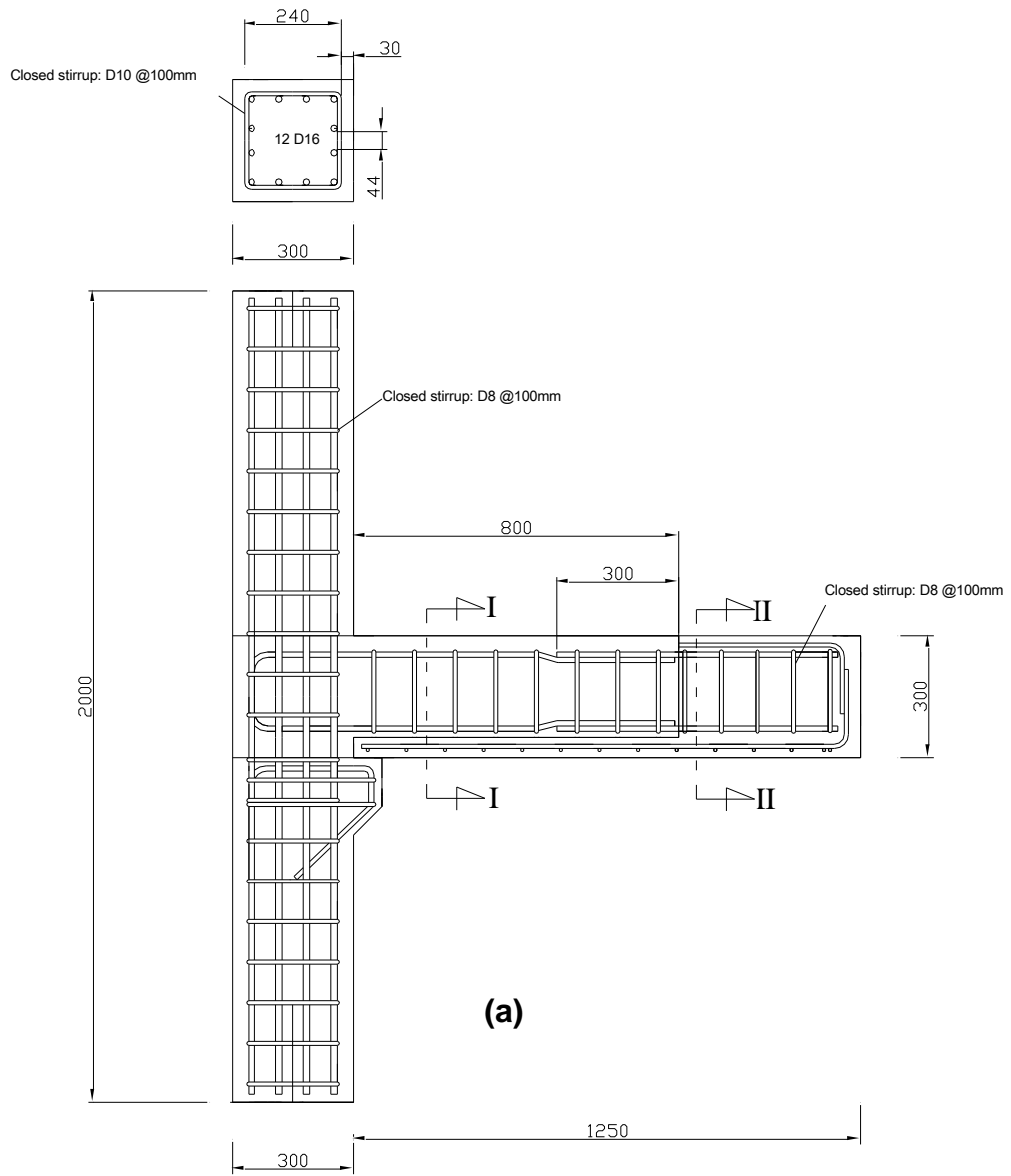


Figure 3-4 (a) Reinforcement details of the PCBC specimen; (b) Corbel details

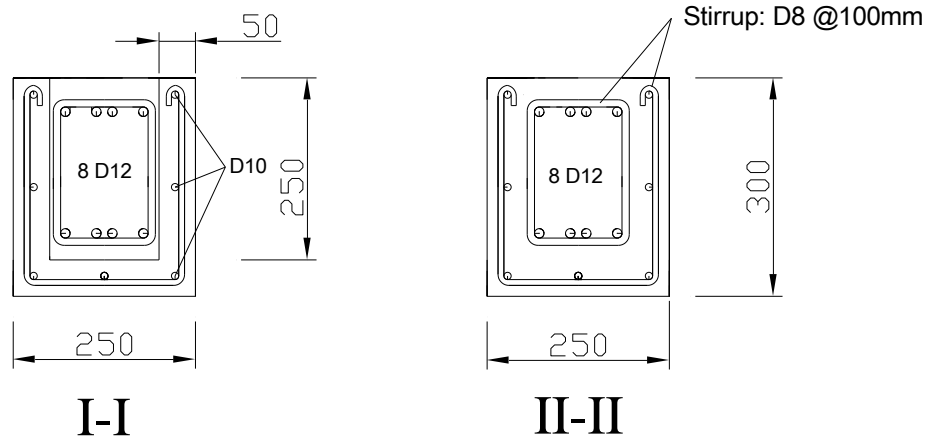


Figure 3-5 Cross section of the beam core of PCBC Specimen P1

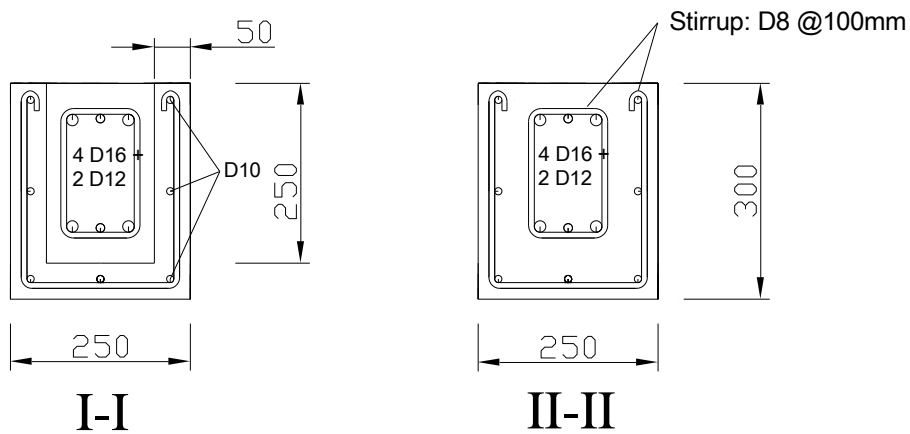


Figure 3-6 Cross section of the beam core of PCBC Specimens P2 – P5

The PCBC specimens P2 – P5 had similar geometry and reinforcement details to Specimen P1. Due to reinforcement congestion in the beam core of Specimen P1, which has 4 interlocking bars (4 D12), the number of interlocking bars was reduced to 3 bars (2 D16 and 1 D12) for the beam core of PCBC specimens P2 – P5. The reinforcement ratio was similar. Figure 3-6 shows the cross sectional details of the beam core of specimens P2-P5.

Figure 3-7 shows isometric details of the precast concrete beam-column specimen. Figure 3-8 to Figure 3-12 shows images of precast elements.

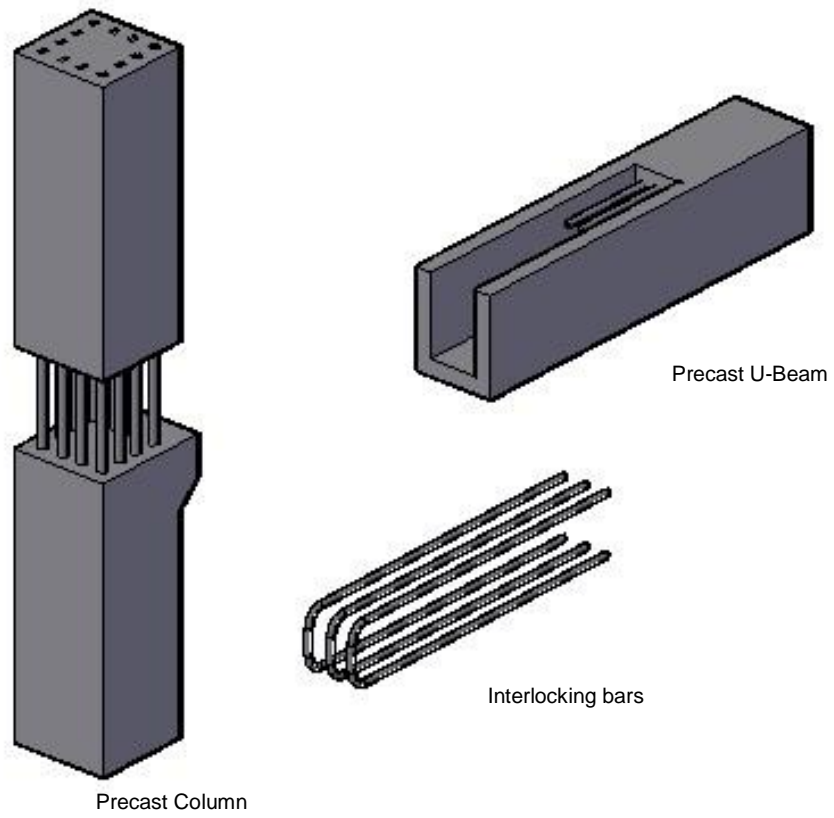


Figure 3-7 Isometrics of precast concrete beam-column connections



Figure 3-8 Precast U-beam



Figure 3-9 Precast column



Figure 3-10 Precast U-beam seated on the corbel of the precast column



Figure 3-11 Reinforcement detail of the joint core



Figure 3-12 Reinforcement detail in the CIP beam core of Specimen P1

3.3.4 Materials

Concrete mixes consisted of fine aggregate, coarse aggregate, cement, and water. The maximum aggregate size was 10 mm. This was to ensure the aggregate could get into the wall part of the U-beam. No super-plasticiser was added to concrete mixes.

Table 3-2 and Table 3-3 show the sieve analysis result of fine aggregate and coarse aggregate, respectively. The grading complied with the requirement of BS 882: 1992. The supplier of these materials was Tarmac Roadstone, Ltd. The coarse aggregate comprised uncrushed quartzitic aggregate of irregular shape and smooth surface.

Table 3-2 Sieve analyses of fine aggregate

BS sieve size	Weight retained (gram)	Cumulative percentage retained (%)	Cumulative percentage passing (%)	BS 882 grading zone M
>2.36 mm	21	4.2	100	-
2.36 mm	78	19.8	80.2	65-100
1.18 mm	52	30.2	69.8	45-100
600 µm	67	43.6	56.4	25-80
300 µm	173	78.2	21.8	5.0-48
150 µm	79	94	6	-
pan	30	100	0	-
total	500			

Table 3-3 Sieve analyses of coarse aggregate

BS sieve size	Cumulative percentage passing (%)	BS 882 grading
>10 mm	100	100 - 100
10	95	85 - 99
8	75	-
6.3	48	-
5	15	-
4	5	0 - 20
2.8	3	-
2	3	0 - 5
1	2	-
500	2	-
250	2	-
125	2	-
63	1	0.0 - 1.5

The precast concrete elements were cast using normal weight concrete with a target mean compressive strength of 30MPa. Two types of concrete mixes were used as cast-in-place (CIP) connections, i.e. plain concrete and steel fibre reinforced concrete (FRC). The target mean compressive strength of CIP (cast-in-place) concrete was 45MPa.

The material composition for precast concrete elements (target compressive strength of 30MPa) and CIP connection-without steel fibre (target compressive strength of 45MPa) are presented in Table 3-4. The trial mixes were done using the compositions presented in Table 3-4. The cube strengths tested at 14 days and 28 days for both mixes are presented in Table 3-5. The compressive strength observed satisfied the target compressive strength. Therefore, compositions from Table 3-4 were used for the PCBC specimens P1, P2 and P5. The compressive strength of precast elements of specimens P1-P5 will be presented in a later chapter.

The composition material of steel fibre reinforced concrete (SFRC) used for the CIP connections of Specimen P3 and P4 will be presented in Chapter 6. The mechanical properties of concrete for each PCBC specimen will be presented in a later chapter.

Table 3-4 Material composition of precast concrete and CIP concrete (kg/m³)

Materials	Precast concrete	CIP concrete
Coarse aggregate (kg/m ³)	1000.55	1028.4
Fine aggregate (kg/m ³)	818.63	685.6
Cement (kg/m ³)	335.82	441
Water (kg/m ³)	208	210
w/c	0.62	0.47

Table 3-5 Concrete compressive strength (trial mixes)

Age	14-day		28-day		% increase
No. samples	Compressive strength (MPa)	Average (MPa)	Compressive strength (MPa)	Average (MPa)	
Target compressive strength = 30 MPa					
1	34.10	33.89	36.54	36.93	8.20
2	33.23		36.01		
3	34.36		38.23		
Target compressive strength = 45 MPa					
1	47.68	46.52	49.42	48.37	3.82
2	45.16		47.02		
3	46.72		48.66		

Four different diameters of steel bar were used for the PCBC specimens, i.e. 8 mm, 10 mm, 12 mm, and 16 mm. The yield strength of the steel reinforcing bars was 500MPa; standard deviation was 30MPa and the yield strain was 0.0030. Strain gauges of 5mm length of the FLA-5-11 type were used to measure the strain of the reinforcing bars.

3.3.5 PCBC specimen construction

All PCBC specimens underwent the same initial design. Each PCBC specimen consisted of one precast concrete beam and one precast concrete column.

There were two times of casting for each PCBC specimen. The first casting encompassed the precast units (beam and column) and the second casting was for the cast-in-place (CIP) connection region, which included the beam core and the joint core. The second casting was carried out after the precast beam and the precast column had been set up. The following PCBC procedures were followed:

a. Making the precast units

Before casting, some strain gauges were mounted on reinforcing bars of precast units. All precast units were designed to have the same concrete strength. The precast U-beams and columns were cast on the same day. Due to the large volume of concrete required for both precast U-beams and columns, and the limited capacity of the concrete mixer, the casting of precast units was divided into 3 mixes.

The first and second mixes were used for casting the precast column element, whereas the third mix was used for the precast beam element. Specifically for PCBC Specimen P1, the precast units were cast using ready-mix concrete. A poker vibrator was used during the casting process to produce a compact form of concrete elements.

The precast column was cast in the horizontal position to make the casting process easier. The precast U-beam was cast in an upside down position with a block of polystyrene inside, to ensure concrete filled the horizontal part of the U-beam (see Figure 3-13). Together with the casting of precast elements, the samples for mechanical properties tests were also made.



Figure 3-13 Reinforcement cage of the precast U-beam

A day after casting, the samples (cubes, prisms, cylinders, etc.) were removed from their moulds. Precast columns and precast beams were still in their moulds; the mould bolts were un-tightened to avoid premature cracks in the concrete due to shrinkage in the early hardening processes.

All samples and precast elements were covered by a wet hessian material and plastic sheets to ensure consistent environmental conditions, for approximately 1 week.

At a minimum of one week after casting, the precast beams and column elements were removed from their moulds. They were cleaned to remove polystyrene, oil, and other unwanted material that could influence specimen quality.

b. The construction process of the precast units and casting of CIP Connections

Strain gauges were installed on the longitudinal bars (interlocking bars) of the beam core, on the stirrups located in the beam core and the joint core (Figure 3-17).

Precast columns were vertically set up in the test rig. Column ends were restrained by steel plates, which were bolted on to the test rig (Figure 3-10). One end of the precast U-beam was horizontally placed on the corbel, while the free end was supported by scaffolding.



Figure 3-14 Joint core covered by a form before casting

After the precast columns and precast U-beams were set up in the test rig and all reinforcements (interlocking bars and stirrups) in the joint-core and the beam-core were installed, the connection casting was carried out. The joint core was covered by the form and sealed to avoid concrete-mix leaking from the form (see Figure 3-14). The connection region was cast using cast-in-place (CIP) concrete (see Table 3-4), which had a higher compressive strength than the precast beam and column. This was because the connection region is vulnerable, and can experience stresses from applied loads. From the same CIP concrete mix, several cubes, cylinders, prisms, etc., were made to measure the mechanical properties of the CIP connection.

A day after casting, the CIP connection was covered by wet hessian material and plastic sheeting for a minimum of one week. The cubes, prisms, cylinders, etc. were taken from their moulds and placed on the floor around the PCBC specimens to ensure the same curing treatment/environment.

At a minimum of one day after casting, the joint core was grouted using non-shrink grout material to fill a gap between the hardened joint core concrete and the upper part of precast column.

The scaffolding was removed after 2 weeks and the PCBC specimens were ready to test after the CIP connection had aged a minimum of 28 days.

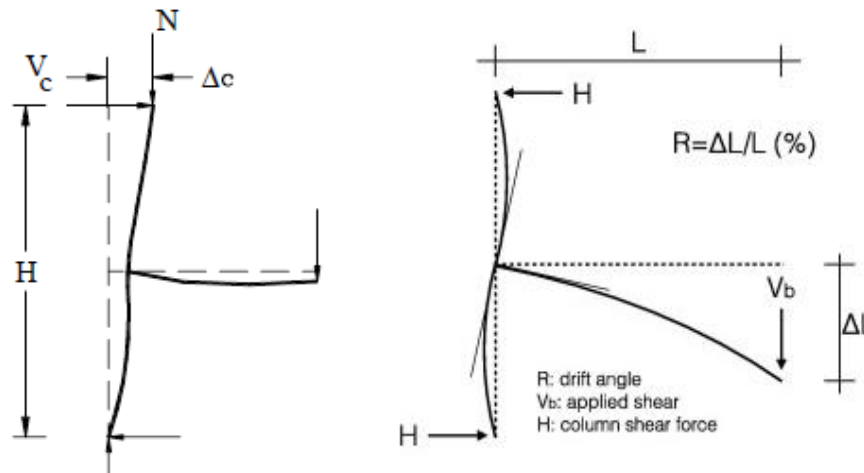
Evaluation of the construction method:

1. In real situations, scaffolding is not necessary. The precast U-beam can be placed directly on the corbels of the precast columns at both sides (left and right precast beam).
2. The cast-in-place (CIP) connection allows enough tolerance in dimension. Problems regarding precast elements installation, due to dimensional imprecision, can be minimised.
3. It is important that concrete-mixes fill all space within the joint core.
4. Grouting using non-shrink grout material in the joint core may help to achieve a compact joint core concrete.
5. Overall, the construction process of these PCBC connections is effective.

3.4 Test Setup and Instrumentation

3.4.1 Test setup

To emulate deformation of the exterior beam-column connections in the actual frame buildings, subjected to lateral seismic loading, the test specimens should be loaded to deform as shown in Figure 3-15 (a). However, to simplify the test setup, the beam-column specimens were loaded to deform according to Figure 3-15 (b). The equivalence of both deformed shapes is shown below:



(a) In actual displaced frame (b) In test rig

Figure 3-15 Exterior beam-column sub assemblages (Said and Nehdi, 2004; Kalogeropoulos et al., 2016).

For the exterior beam-column connection deformation that represents an actual structure (Figure 3-15a), the drift ratio (R) is defined as:

$$R = \frac{\Delta_c}{H} \quad (3-2)$$

Where Δ is the column relative displacement and H is the column height.

Whereas, for the simplified testing setup, the drift ratio (R) is defined as:

$$R = \frac{\Delta L}{L} \quad (3-3)$$

Where δ is the tip deflection of the beam and L is the clear beam span.

The test setup followed that of the simplified test setup (Figure 3-15 (b)) as illustrated in Figure 3-16. The vertical load was applied through an actuator on the beam tip of the PCBC specimen. Three types of loading tests were applied on the PCBC specimens in this study; i.e. static, quasi-static and long-term loading. The implementation of each test is described in chapters 4, 5, 6 and 7.

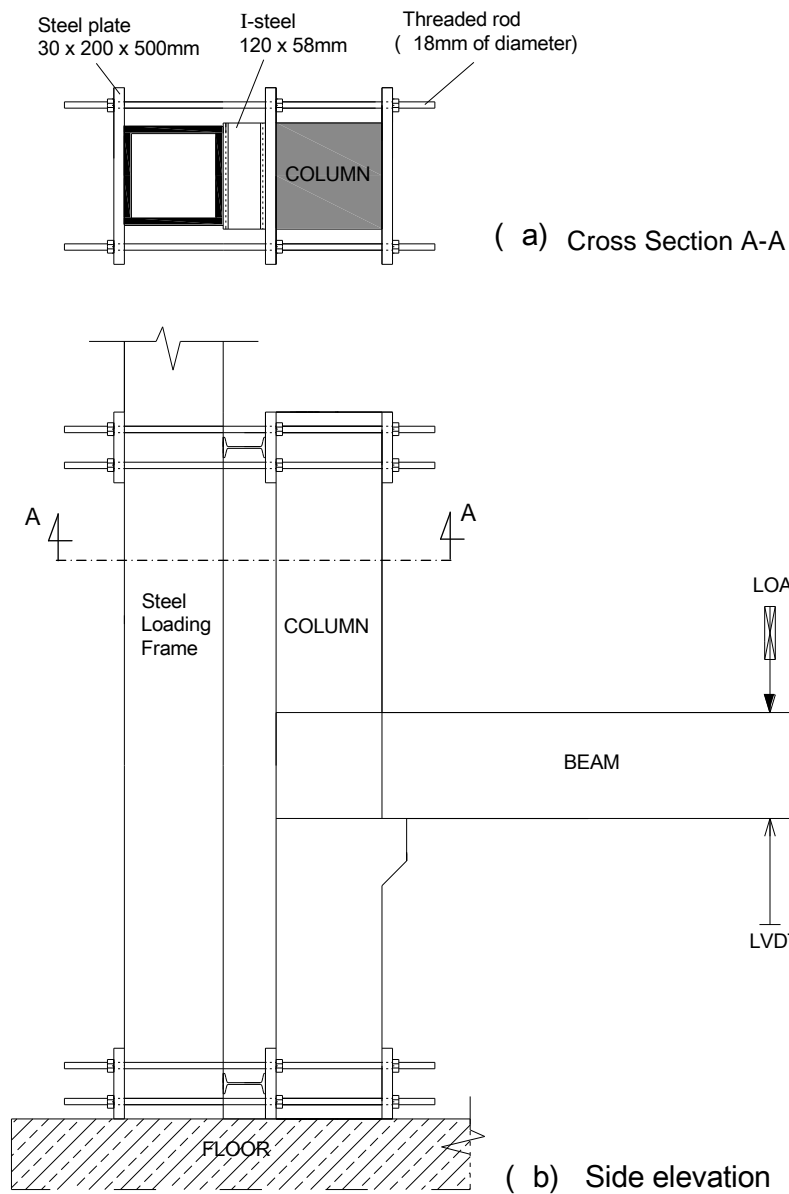


Figure 3-16 Test setup of PCBC specimens

3.4.2 Instrumentation (LVDT, strain gauge, DEMEC points)

To study the behaviour of PCBC connections during loading, several instruments were installed at critical points; an LVDT (Linear Variable Differential Transformer), electrical resistance strain gauges and measuring points for DEMEC (Demountable Mechanical) gauge measurements.

Some LVDTs were placed to measure deflections of the PCBC specimens. LVDT1 was placed at the beam tip (under the load position). LVDT2 and LVDT3 determined the horizontal deflection at the column base and the column top. Since both ends of the column are fixed, their horizontal deflections should be nearly zero during testing.

Figure 3-17 shows the location of electrical resistance strain gauges attached to the reinforcing bars. SG1, SG2 and SG3 were used to measure the strain in the flexural reinforcement in the beam core and the precast U-beam in the maximum moment region. SG5 was used to measure the strain of the flexural reinforcement in the precast column. SG4 and SG6 provided information on shear deformation in the beam core and the joint core.

DEMEC gauges were used to measure strain in different parts of the PCBC specimen surfaces as shown in Figure 3-18. The DEMEC points were glued to the concrete surface, at the top and bottom longitudinal reinforcement of the beam. These gauges were used to assess the elongation of the tensile and compression chords during the loading. At certain load levels, the strain between two DEMEC points was measured to assess how the strain changes were exerted at that position. The strain distribution obtained from the top and bottom DEMEC points reflected the change of neutral axis positions of the beam.

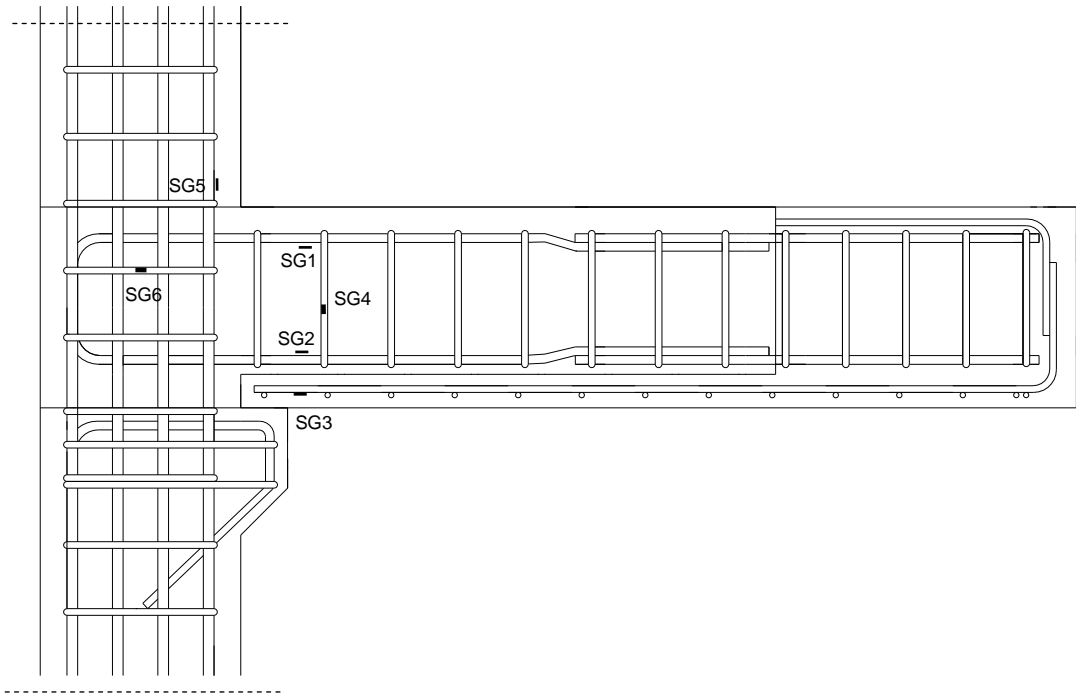


Figure 3-17 Strain gauge arrangements on PCBC specimens

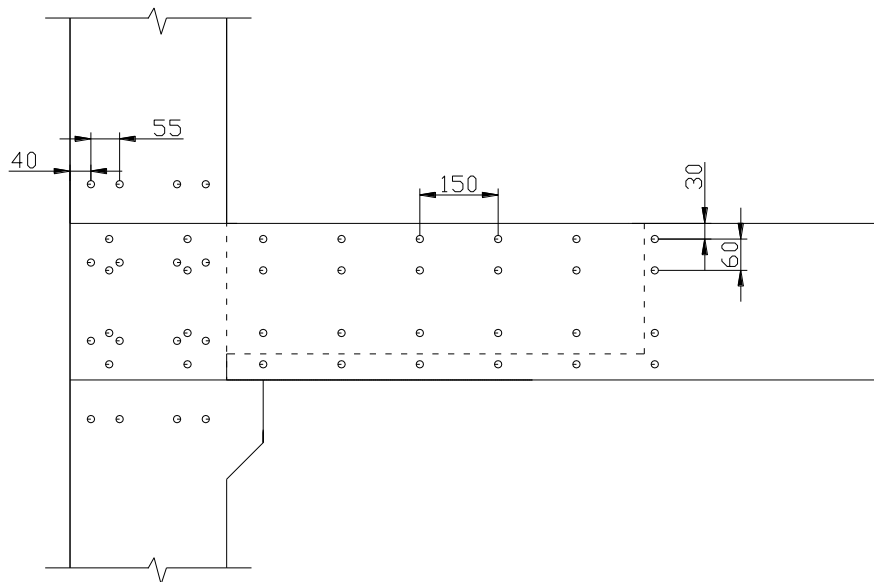


Figure 3-18 DEMEC points arrangement on PCBC specimens

3.5 Summary

The conclusion of this chapter are:

1. The exterior precast concrete beam-column (PCBC) connections developed here were designed using ACI 318-2011 which is intended for detailing monolithic connections.

2. Evaluation of the curing of precast elements:

Most precast concrete elements manufactured in factories are cured in a controlled environment, especially during the early stages of hardening and hydration. Accelerated curing methods are used to gain the compressive strength rapidly, such as conductive/convective heating, electrical resistance heating and steam curing, i.e. low and high pressure (Vollenweider, 2004). Soroka et al. (1978) concluded that steam curing affected adversely the concrete later-age strength. This is also confirmed by Naderi et al. (2009); the compressive strength obtained from the specimens cured using steam curing was lower than those using wet Hessian and polythene sheet at the age of 28 days. Considering these facts mentioned above, even though the precast beam and precast column in this study did not have high compressive strength at early age, curing was performed using wet hessian / polythene sheets such that they still had the expected compressive strength at the age of 28 days.

3. Evaluation of the curing of CIP connection:

The use of wet fabric to cure the CIP connection after casting did not totally prevent the concrete from autogenous and drying shrinkage during the hardening and hydration process. Some fine cracks were observed in the concrete surface and fine gaps were formed at the interface between the CIP beam core and the wall of the precast U-beam. It is possible that these cracks could have been avoided by keeping the surface continuously wet-100% relative humidity (this will be discussed in Chapter 7).

4. Five PCBC specimens were fabricated, P1, P2, P3, P4 and P5. Variables of precast concrete beam-column specimens included types of loading (i.e. static, quasi-static and long-term loading) and steel fibre contents incorporated in cast-in-place (CIP) concrete connections.
5. The test setup of beam-column joints was simplified from an actual frame building subjected to lateral seismic loading. Therefore, the test setup for this study was: both column ends were fixed by steel plates bolted into the test rig while the beam end was free. The load was applied on the beam end vertically.
6. No axial load was applied to columns in these tests, as it increased joint shear strength.
7. Some instrumentation, including strain gauges, LVDT, and DEMEC points were used in/on beam-column specimens to record the behaviour of specimens during testing.
8. The interlocking bars (4D12) placed in Specimen P1 caused congestion problems in the CIP beam, i.e., placing the steel bars as well as placing and compacting the concrete in the beam core. To improve this, the number of interlocking bars was reduced (although the steel area remained the same) to 2D16 bars and 1D12 bar. The new reinforcement ratio was applied in the CIP beam core of Specimen P2-P5.
9. The precast members of the PCBC specimens were relatively simple to fabricate. The connection process of the precast beam to the precast column allowed enough tolerances in dimension. The interlocking bars were easy to install. Therefore, no issues were encountered in the installation of precast members due to any imprecision of the dimensions. No welding, bolting and pre-stressing or special tools were required for the construction process. In

general, the construction of PCBC connections was feasible in term of construction technology.

Chapter 4

Precast Concrete Beam-Column Connection under Static Loading

4.1 Introduction

The aim of this chapter is to investigate the behaviour of the precast concrete beam-column (BC) connection under static-monotonic loading in terms of,

- The crack-pattern propagated during the test.
- The load capacity of the precast concrete beam-column connection.
- The deflection capacity of the BC connection.
- The failure mode
- To investigate whether there is a bonding problem between the beam core and the wall of the U-beam, based on the nominal moment calculation.
- To investigate whether the bottom-wall of the U-beam contributes to the strength of the beam-column connection under the negative moment.

This chapter presents the mechanical properties of the material used in Specimen P1, the procedure of the test and then the test result and the analysis. The reinforcement detail and the test set-up and instrumentation are presented in Chapter 3.

4.2 Detail of Test Specimen P1

The geometry and reinforcement detail for the precast concrete beam-column Specimen P1 are presented in Figure 3-4 and 3-5 (Chapter 3).

This section contains the mechanical properties used for the precast concrete units and CIP concrete.

4.2.1 Mechanical properties of concrete

The precast beam and column were cast using ready-mix concrete with a target design compressive strength of 30MPa. From the same mix, three cylinders, four cubes, three prisms, and two bobbins were made and used to examine the mechanical properties of the concrete, i.e. modulus of elasticity, compressive strength, flexural strength and direct tensile strength.

After assembling the precast beam and column to form the T-joint, the connection region (CIP concrete) was cast using fresh concrete mixed in the casting shop which had a higher design compressive strength; i.e. 45MPa. Table 4-1 provides the material proportions for the CIP concrete. From the same mix, cylinders, cubes and prisms were cast. Table 4-2 presents the mechanical properties of the precast units and CIP connection.

Table 4-1 Material composition of CIP concrete

Items	Weight (kg) per m³
Coarse Aggregate	1028.4
Fine Aggregate	685.6
Cement	441
Water	225

Table 4-2 Mechanical properties of concrete of Specimen P1

	Precast Units		CIP Connection	
	MPa	SD (MPa)	MPa	SD (MPa)
Average of Cube Strength	38.07	1.60	59.12	1.13
Average of Modulus of Elasticity	27200	1061.99	32400	1458.86
Average of Flexural Strength	-		3.96	0.51
Direct tensile Strength	1.85			

4.2.2 Loading procedure – A description of the test

A static-monotonic loading was applied to Specimen P1. The static load was applied using an actuator which was applied vertically downwards to the beam tip, in line with the gravity loading (see Figure 4-6). The loading rate was slow, between 0.2 – 0.5 mm/min, to permit DEMEC gauge readings to be taken. No axial load was applied to the column. Specimen P1 was loaded until failure.

The DEMEC gauge readings were taken manually every 2.5 KN, but after the first crack occurred, the readings were taken every 5 KN. The readings were stopped after the applied load reached 35 KN for safety reasons.

Crack propagation on all faces of the specimen was observed during the loading. The cracks were marked including the load level. Photographs were taken throughout the test. The computer recorded the electrical resistance strain gauge data, the LVDT data and load cell readings automatically.

4.3 Test Results

4.3.1 Load-deflection curve

The structural behaviour of the beam-column joint could be seen from the load-deflection and moment-curvature curves.

Figure 4-2 shows the curve of load vs. deflection, which was drawn based on the data recorded from the LVDT readings at the beam tip. Figure 4-3 presents the curve of moment-beam curvature relationship. The beam moment is calculated by multiplying every level of load with the distance of the point load to the critical cross section of beam (i.e. 1.03 m), which is in line with the corbel end. The beam curvature was calculated using the strain gauge data (SG1 and SG2) which were located on the interlocking bars (see Figure 4-7) and used in Equation (4-1).

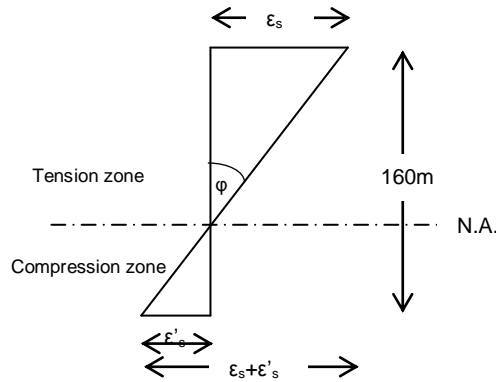


Figure 4-1 Strain profile of the beam core

$$\varphi = \frac{\varepsilon_s + \varepsilon'_s}{160} \quad (4-1)$$

Where, φ is the beam curvature; ε_s is the tensile strain of the steel bar (SG1 data); ε'_s is the compressive strain of the steel bar (SG2 data).

Based on the results in Figure 4-2 and Figure 4-3, the load, the beam moment, deflection, drift ratio and curvature can be drawn in terms of first crack, yield and ultimate conditions. All values are presented in Table 4-3.

Table 4-3 Experiment results

Items	Load (KN)	Deflection (mm)	Moment (KNm)	Curvature (rad)	Drift ratio (%)
First-crack	15.02	2.0	15.47	2.248E-06	0.194
Yield (Park, 1988)	51.88	16.0	53.46	11.61E-06	1.553
Yield-exp	57.68	20.0	59.41	12.99E-06	
Maximum	59.80	23.5	61.59	26.06E-06	2.233
Ultimate	49.41	46.5	50.89		4.515

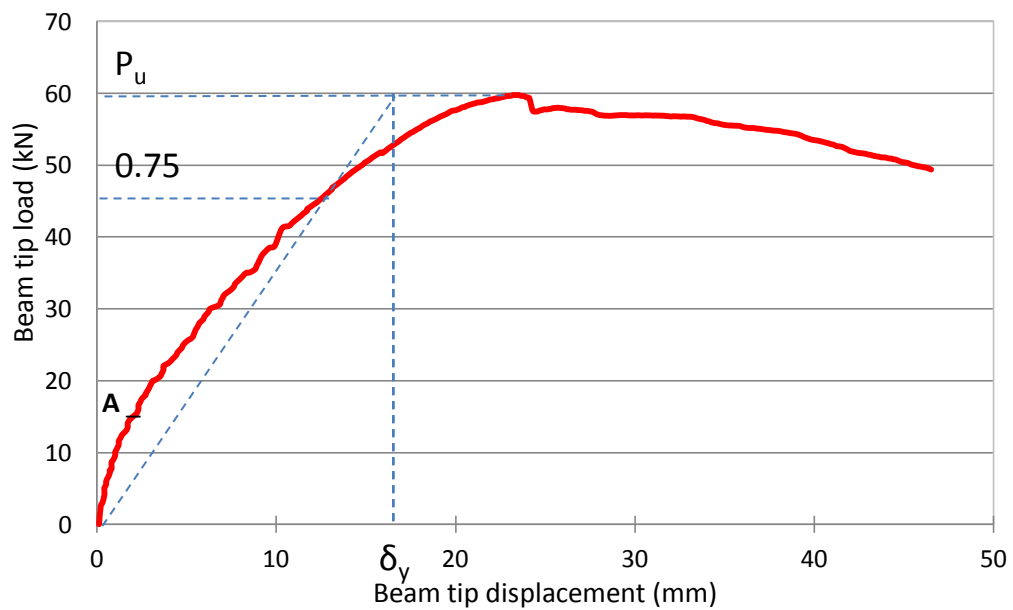


Figure 4-2 Load vs. beam deflection of Specimen P1

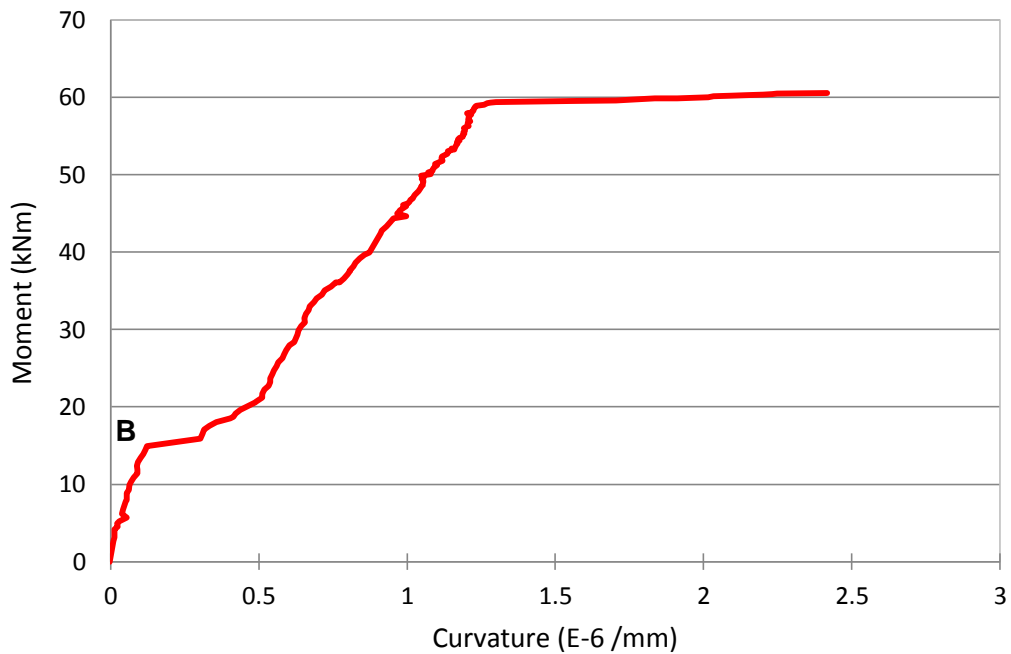


Figure 4-3 Beam moment vs. beam curvature

4.3.1.1 First crack

The first-crack load was determined when the first-crack appeared on the surface of the beam core. Other evidence of the first-crack load can be seen on the load vs. deflection graph, when the slope of the curve changes slightly (see point A in Figure 4-2).

Additionally, on the moment vs. curvature graph, there is a significant change in curvature when the first crack occurred (see point B in Figure 4-3). From this evidence, it can be concluded that the first-crack load is 15kN. The internal cracks could occur before a load of 15kN.

4.3.1.2 Yield

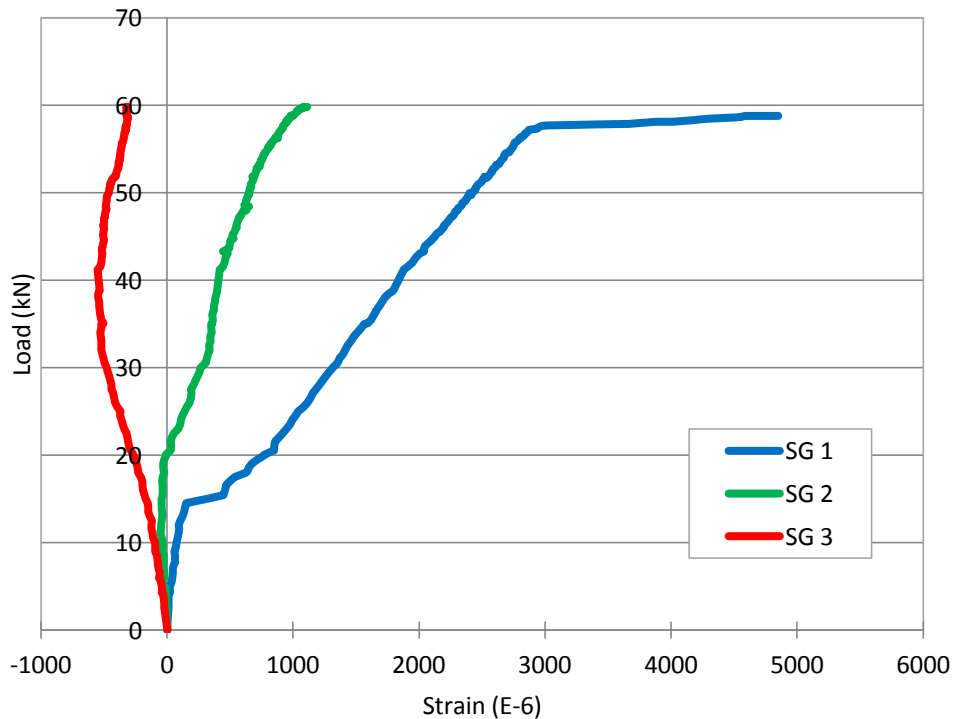
The yield condition was not clear either physically or from the graphs. Several researchers have tried to determine the yielding point of a load vs. deflection relationship, Park (1988); (Mahin and Bertero, 1976; Priestley

and Park, 1987). By using the theory that the yield deflection is determined from the secant stiffness at 75% of the ultimate lateral load (H_u) of the real system (Priestley and Park, 1987), the yield deflection of Specimen P1 is 16mm (see Table 4-3).

Alternatively, based on the experimental load vs. strain curve for the longitudinal bars in the beam (Figure 4-4), the strain at yield is approximately $3000E-06$, which corresponds to a load of 57.68kN. This is equivalent to a yield deflection of 20.0mm and being based on actual measured data, is more reasonable.

4.3.1.3 Ultimate

The ultimate condition can be determined easily from the load vs. deflection curve. The peak load is 59.80kN and the deflection is 23.5mm.



Note: the position of SG1, SG2 and SG3 is presented in Figure 4-7.

Figure 4-4 Load vs. strain response of the longitudinal bars of the beam in Specimen P1

4.3.2 Observation of cracking

Cracking was observed through-out the test. Figure 4-5 and Figure 4-6 illustrate the crack-pattern of the precast concrete beam-column joint specimen P1, which was subjected to the negative bending moment.

The first crack appeared on the surface of the beam core, in line with the tip of the corbel (where the maximum moment occurs), at a load of 15kN; the crack-width was 0.05 mm. This was followed by a delamination crack on the top surface of the beam core and the wall of the precast U-beam at a load of 15kN as well. The subsequent cracks again occurred on the beam core at a distance of 150 mm and 300 mm away from the column. In general, all cracks could be categorised as typical flexural cracks that occurred on the top surface of the beam; they were distributed at a distance of $2 \times$ the depth of beam (h) from the column face, which means $2 \times 300 \text{ mm} = 600 \text{ mm}$, which is the plastic hinge length stated in the ACI 318-08 (2008).

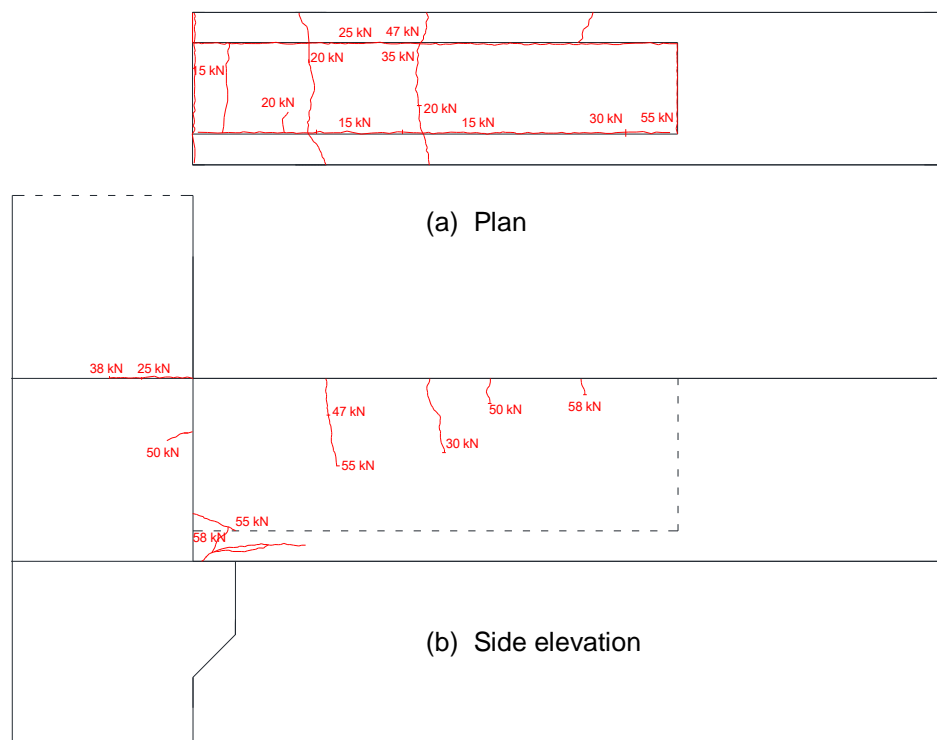


Figure 4-5 Crack pattern of Specimen P1



Figure 4-6 Crack pattern of beam-column specimen subjected to static loading (Specimen P1)

Cracks developed in the wall of the precast U-beam at a load of 20kN. The cracks propagated vertically, perpendicular to the beam axis, and became an extension of the crack in the beam core at the top surface of the beam.

The longitudinal bars of the U-beam started to slip at a fairly high load, i.e. 55kN. This slip was indicated by a horizontal crack in the bottom of the U-beam which extended from the support to a distance of 200 mm from the corbel. That means that the beam core and U-beam acted as a composite beam almost until failure and so there was therefore good bond between the walls of the U-beam and the beam cores.

No significant cracks occurred in the joint core. A small delamination crack appeared at the gap between the joint core and the upper precast concrete at a load of 25kN. The crack stopped in the middle of the column width.

The final width of the gap between the precast beam and the precast column at the end of the test was 8 mm. No cracks occurred in the corbel.

4.3.3 Internal behaviour of Specimen P1

The internal behaviour of Specimen P1 was evaluated from the data collected by electrical strain gauges and the DEMEC strain gauges. Figure 4-7 presents the position of the electrical strain gauges.

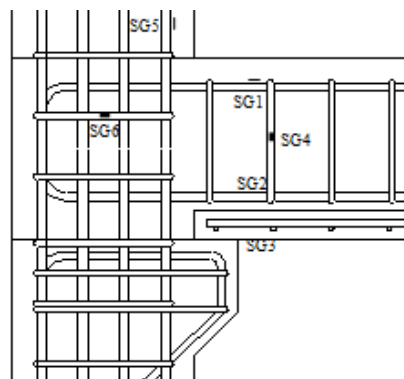


Figure 4-7 Location of strain gauges on the reinforcing bars of Specimen P1

4.3.3.1 Behaviour of the interlocking bars

Figure 4-4 presents the relationship between load and the strain in the longitudinal bars of the beam. SG1 represents the strain of the top reinforcement in the beam core (tension zone). When the first crack occurred in the beam, this bar experienced a large deformation. The strain of the bar reached the yield strain before the beam failure.

SG2 represents the strain of the bottom longitudinal bar of the beam core. In the beginning of the test, SG2 experienced a compression force, as can be seen in Figure 4-4. However, from the load of 20.56kN (after the first crack occurred) until the end of loading, the neutral axis depth of the composite beam section reduces gradually (measured from the bottom surface of the composite beam) which caused the bar to undergo tension; it did not yield even at the failure load of the joint.

In contrast to the previous two gauges, SG3, positioned on one of the bottom longitudinal bars of the U-beam was consistently in compression throughout the test.

4.3.3.2 Strain development in the beam stirrup

Figure 4-8 presents the load vs. strain of one of the beam core stirrups. The stirrup which would be subjected to the greater shear force during the test was chosen (see Figure 4-7 for its location). The stirrup exhibited almost zero strain until the load reached 20kN; after that, the stirrup went into tension until the beam failed, however, the stirrup did not yield even at joint failure. It can be concluded that the stirrup, with a diameter of 8 mm and a spacing of 100 mm, is sufficient to help prevent shear failure in the beam core.

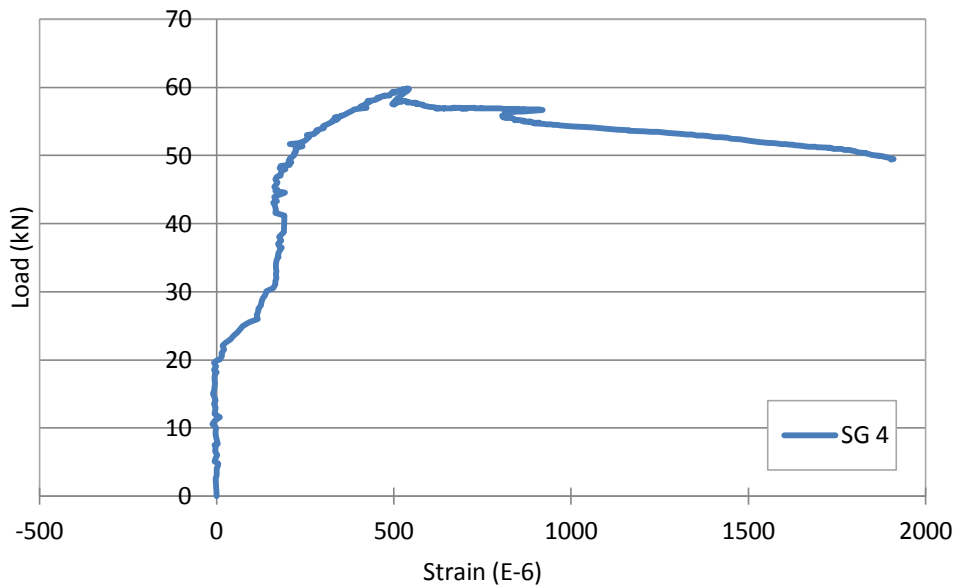


Figure 4-8 Load vs. strain response of the beam stirrup in Specimen P1

4.3.3.3 Strain development in the joint core stirrup

Figure 4-9 presents the load vs. strain of the joint-core stirrups. There were two strain gauges, which were mounted on the same stirrup/location in the joint core, namely SG6a and SG6b (see Figure 4-7 for their location). The purpose of these strain gauges was to evaluate the shear joint resistance of this specimen. As a note, SG6a was possibly damaged during the construction of the joint as its initial strain value was more than $-1000E-6$. The initial value of SG6b was $130E-6$, which is more reasonable. Nevertheless, both of the gauges behaved identically during the loading. As with the stirrup in the beam core, the stirrup in the joint core began to experience tension after a load of 20kN. The maximum strains of the stirrups were less than $700E-6$, which means that they never yielded during the test. From these results, it can be concluded that the two stirrups in the joint core of specimen P1 were enough to restrain the joint shear during loading.

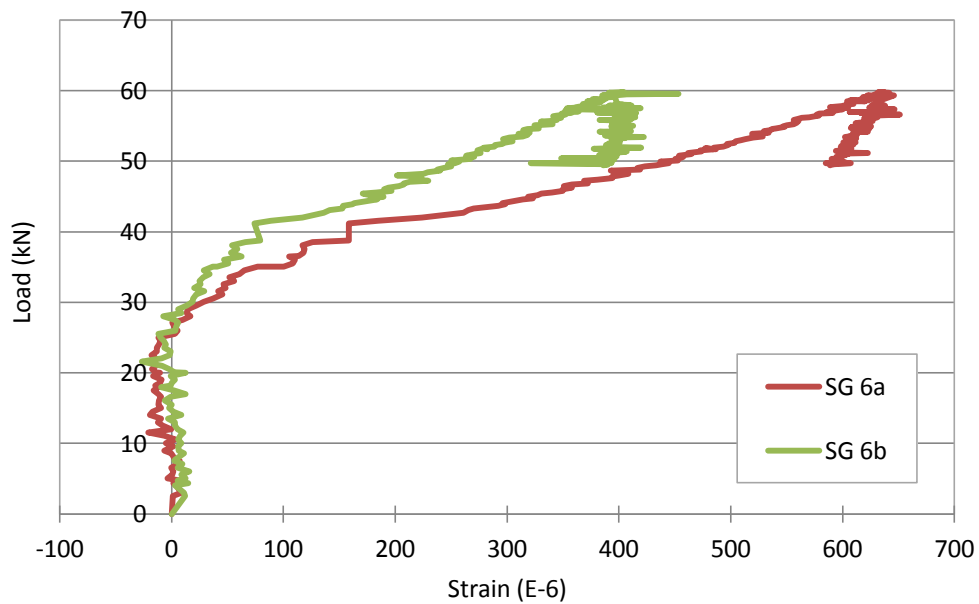


Figure 4-9 Load vs. strain response of the joint-core stirrups in Specimen P1

The shear steel percentage of the joint core of specimen P1 was 0.26% (if using the dimension of the cross section of the U-beam, i.e. 250 mm and 300 mm), or 0.54% (if using the dimension of the beam core, i.e. 150 mm and 250 mm). Kaung and Wong (2011) suggested that the horizontal stirrup steel ratio for enhancing the shear capacity of the section should be no more than 0.4%.

4.3.3.4 Strain development at the concrete surface

The measurements of the concrete surface strain were taken using a digital DEMEC strain gauge; DEMEC points were attached to the side of the U-beam as shown in Figure 4-10 and Figure 4-11.

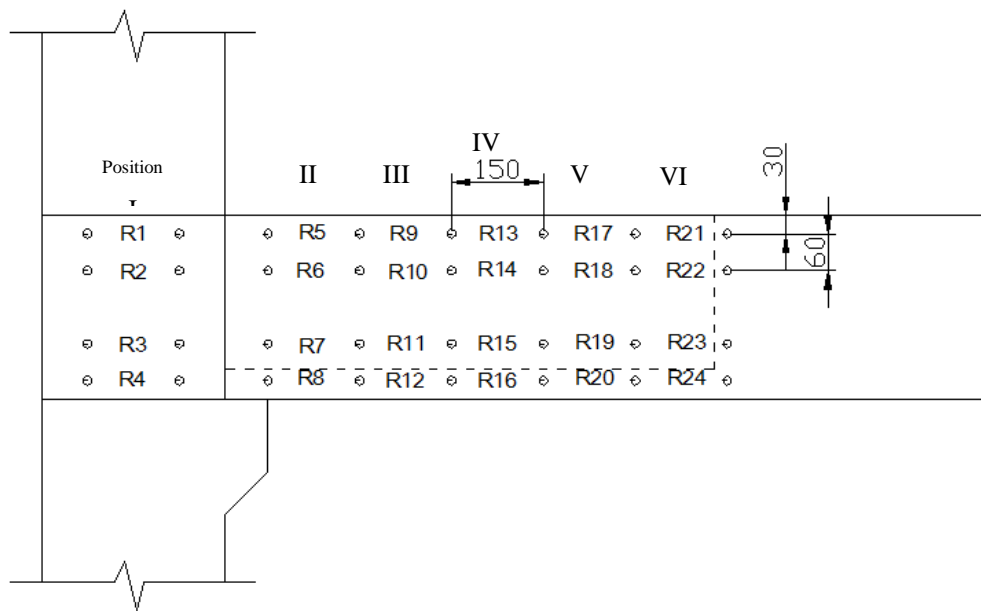


Figure 4-10 Position of DEMEC points in the joint core and the U-beam (horizontally)

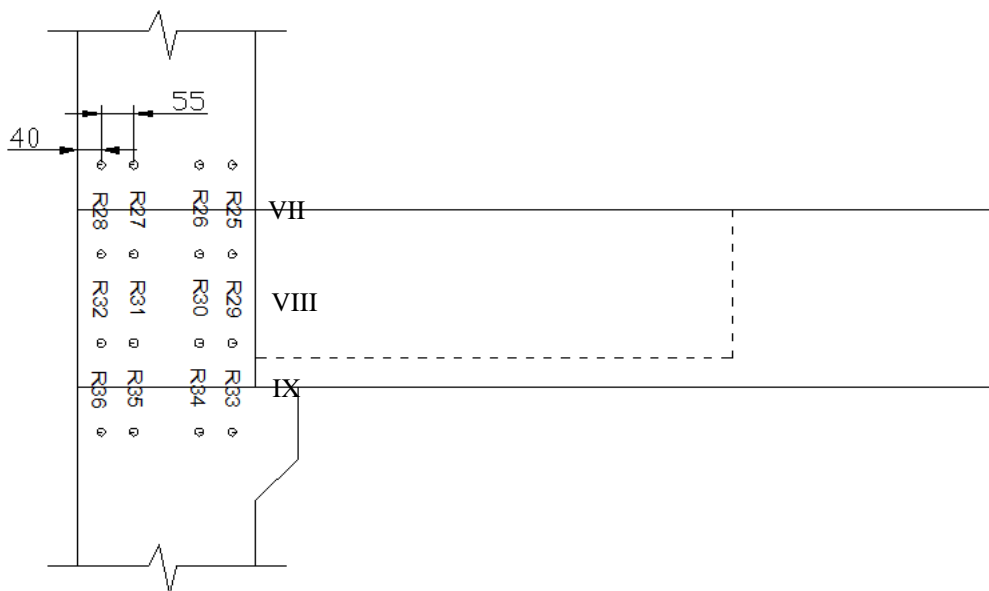


Figure 4-11 Position of DEMEC points in the joint core (vertically)

Strain readings were taken at six positions (horizontally) in the U-beam and the joint core. Vertically, strain was measured at 3 positions in the joint core. Each position consisted of 4 levels of DEMEC points, for which the top and the bottom levels represented the level of the longitudinal bars of the member (beam or column). The strain in the concrete surface of the

joint core and the U-beam are presented in Figure 4-12 - Figure 4-20. The strain values presented in these figures are the total measured strains minus the initial strains at zero loading.

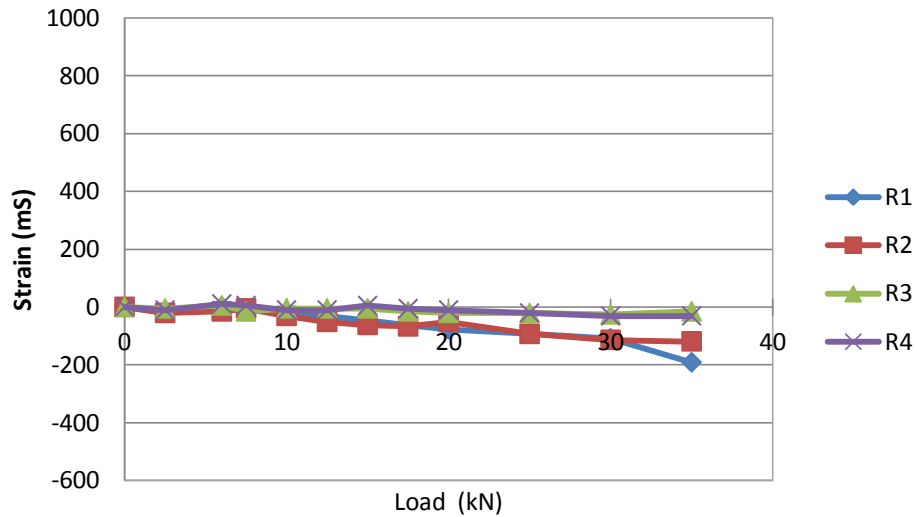


Figure 4-12 Strain development of Position I (the joint core) in Specimen P1

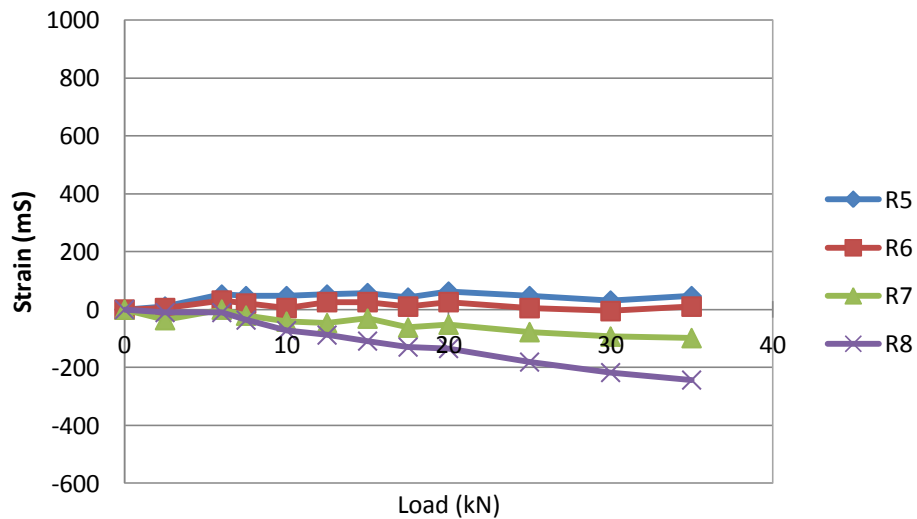


Figure 4-13 Strain development of Position II (the U-beam) of Specimen P1

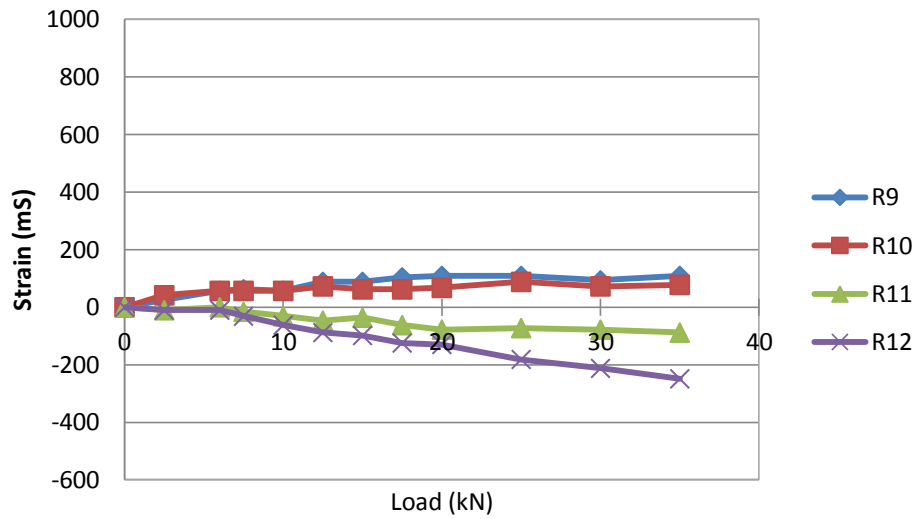


Figure 4-14 Strain development on Position III (the U-beam) of Specimen P1

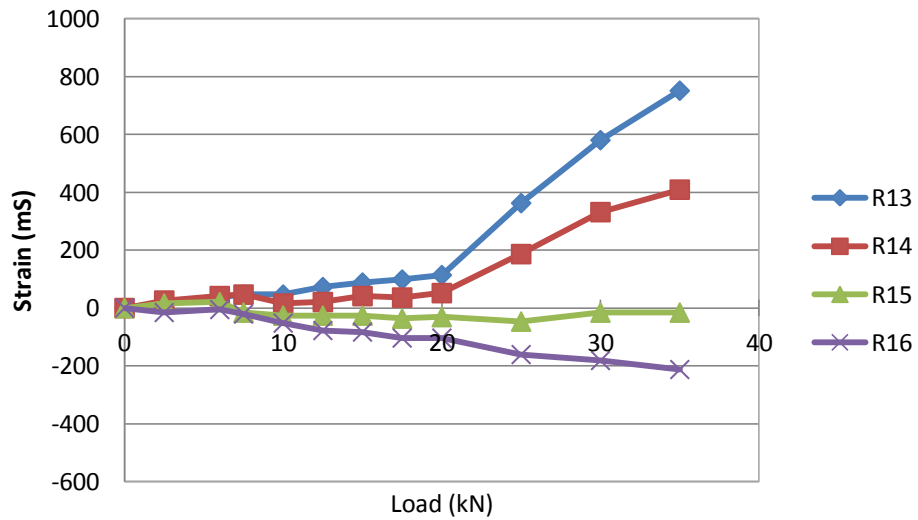


Figure 4-15 Strain development of Position IV (the U-beam) of Specimen P1

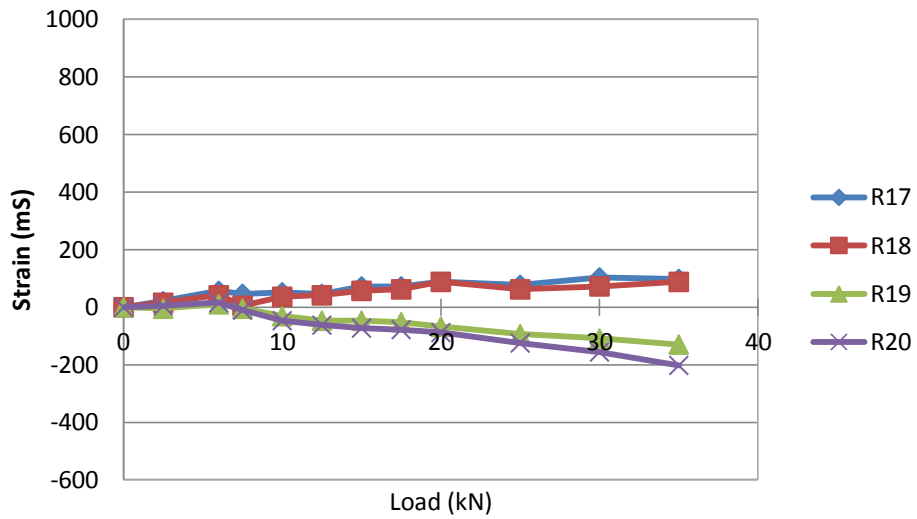


Figure 4-16 Strain development of Position V (the U-beam) of Specimen P1

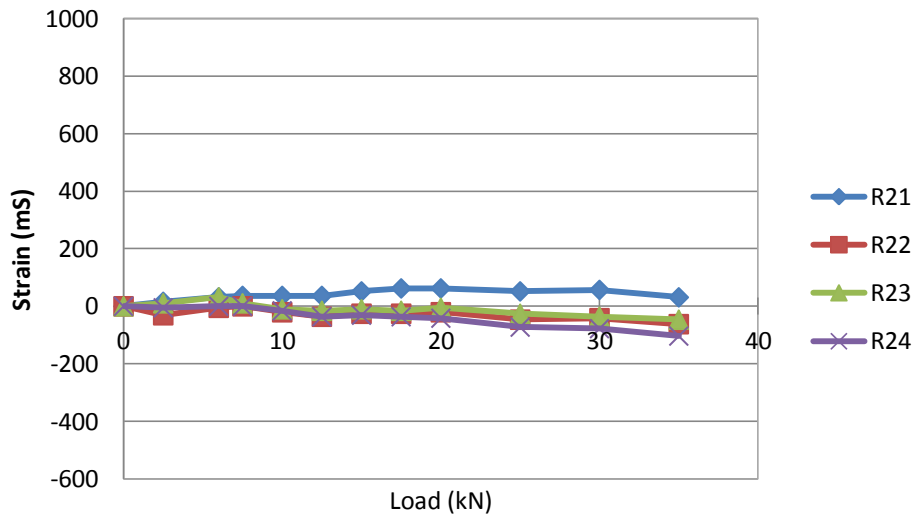


Figure 4-17 Strain development of Position VI (the U-beam) of Specimen P1

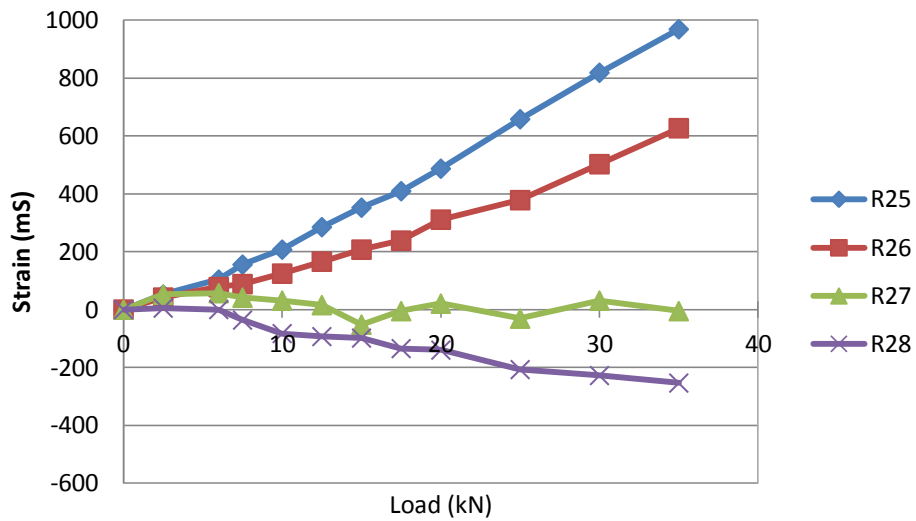


Figure 4-18 Strain development of Position VII (the joint core) of Specimen P1

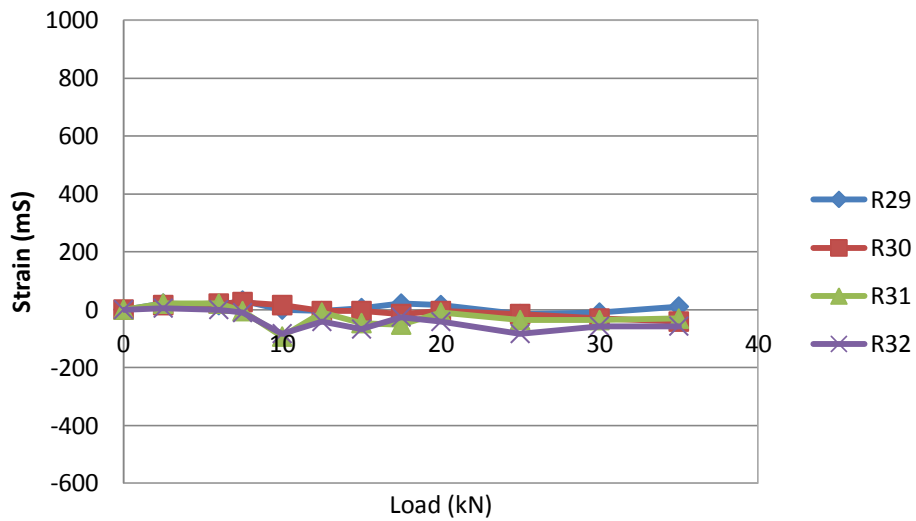


Figure 4-19 Strain development of Position VIII (the joint core) of Specimen P1

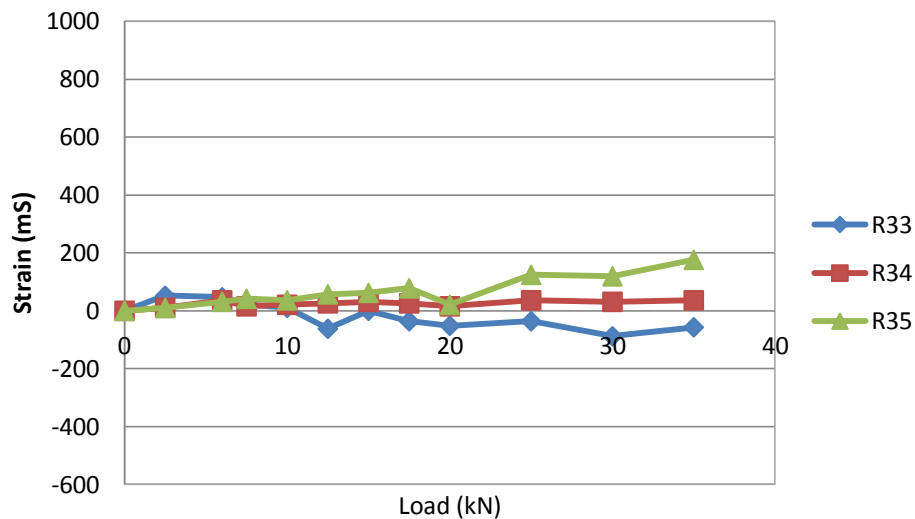


Figure 4-20 Strain development of Position IX (the joint core) of Specimen P1

All levels in Position I (the joint core – R1 to R4) experienced compressive strains (see Figure 4-12). R1 and R2 had higher strains than those of R3 and R4. The strains of R3 and R4 were nearly zero.

In Position II (R5 to R8), the strains of R5 and R6 were almost zero, while R7 and R8 experienced compressive strains (see Figure 4-13). No cracks occurred in the walls of the U-beam at this position during the test.

Position III and V exhibited similar strain development with respect to the applied load (see Figure 4-14 and Figure 4-15). Level R9 and R10 (in Position III) experienced tensile strain, while R11 and R12 exhibited compressive strains. This means that the neutral axis was located between R10 and R11. No cracks formed at this position until a load of 35kN was applied.

Figure 4-15 presents the strain development at Position IV. No significant strain development (recorded by R13 and R14) until the load reached 20kN, then, due to a crack occurring on the surface of the beam core which continued to the wall of the U-beam at this position (see Figure 4-5

and Figure 4-23) there was a large increase in compressive strains and a moderately large increase in the tensile strain (R16).

Figure 4-18, Figure 4-19 and Figure 4-20 present the vertical strain development in the joint core. The biggest tensile strain happened in R25 which suggests that the column bent to the right when the beam was loaded by the negative loading. Position VIII experienced compressive strain although the strain was small. At Position IX, R34 and R35 indicated tension, while R33 was under compression.

4.4 Discussion

4.4.1 Load-deflection relationship and failure mode

Theoretically, due to flexural moments, a reinforced concrete beam commonly has three stages before failure, (also known as the three linear phases), which can be seen in the load vs. deflection relationship (Nawy, 2000). In the first stage, the reinforced concrete beam has not cracked. The beam starts to enter the second stage once the first-crack has occurred. This second stage continues until a stabilised crack pattern has been achieved. The third stage finishes when the tension reinforcement reaches the limit state of yielding. In this discussion, the behaviour of beam-column Specimen P1 is compared to this theory in terms of the load vs. deflection relationship.

In Specimen P1, the first crack occurred at 15kN; it was located in the top surface of the cast-in-place (CIP) reinforced concrete beam core. The theoretical first-crack load can be calculated using the dimension of the composite beam (i.e. the beam core and the U-beam) and the modulus of rupture of the concrete (Table 4-2); the predicted load at first crack is 16.116kN. The theoretical first-crack load is greater than the experimental value (7.4% of difference). The calculation used the flexural strength of

concrete. Since the flexural strength of concrete is always higher than the direct tensile strength, the calculation using the flexural strength will result greater theoretical first-crack load.

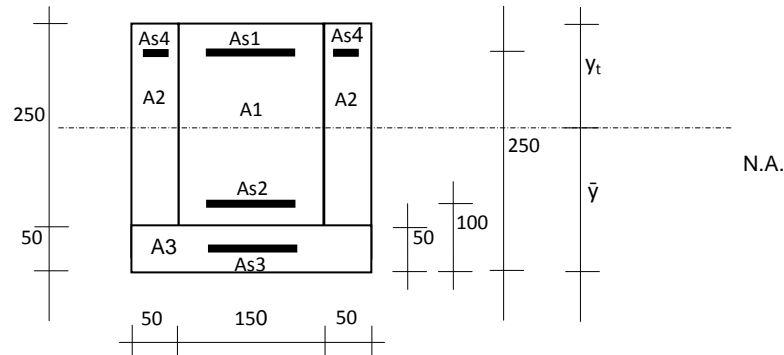


Figure 4-21 Beam section before cracking: elastic behaviour

The section in Figure 4-21 is analysed using elastic theory and the transformed section.

$$E_s = 200000 \text{ MPa}$$

$$E_c (\text{CIP}) = 32414 \text{ MPa (see Table 4-2)}$$

$$E_c (\text{PC}) = 27261 \text{ MPa (see Table 4-2)}$$

$$\text{The modular ratio } n = E_s / E_c$$

CIP connection:

$$n_1 = \frac{200000}{32414} = 6.170$$

$$A_1 = 150 \times 250 = 37500 \text{ mm}^2$$

$$A_{s1} = A_{s2} = 4\phi 12 = 452.16 \text{ mm}^2$$

$$\text{Transformed area: } (n_1 - 1)A_{s1} = (n_1 - 1)A_{s2} = 2337.737 \text{ mm}^2$$

Precast concrete U-beam:

$$n_2 = \frac{200000}{27261} = 7.336$$

$$A_2 = A_3 = 50 \times 250 = 12500 \text{ mm}^2$$

$$A_{s3} = 3\phi 10 = 235.5mm^2$$

$$\text{Transformed area: } (n_2 - 1)A_{s3} = 1492.216mm^2$$

$$A_{s4} = 2\phi 10 = 157mm^2$$

$$\text{Transformed area: } (n_2 - 1)A_{s4} = 994.811mm^2$$

Centroid of the transformed section is given by taking moments of the areas about the bottom edge of the section.

$$\bar{y} = \frac{\sum(Ay)}{\sum A}$$

$$\begin{aligned} \sum(Ay) &= 37500 \times \left(\frac{250}{2} + 50\right) + 2 \times 12500 \times \left(\frac{250}{2} + 50\right) + 12500 \times \frac{50}{2} \\ &\quad + 2337.737 \times 250 + 2337.737 \times 100 + 1492.216 \times 25 \\ &\quad + 994.811 \times 250 = 12354216mm^3 \end{aligned}$$

$$\begin{aligned} \sum A &= 37500 + 2 \times 12500 + 12500 + 2337.737 + 2337.737 + 1492.216 \\ &\quad + 994.811 = 82162.501mm^2 \end{aligned}$$

$$\bar{y} = \frac{12354216}{82162.501} = 150.363mm$$

Hence, the moment of inertia (gross) is given by

$$I_g = \sum I + \sum A y^2$$

$$\begin{aligned} I_g &= \frac{1}{12} \times 150 \times 250^3 + 37500 \times \left(150.363 - \frac{250}{2}\right)^2 + 2 \times \frac{1}{12} \times 50 \times 250^3 \\ &\quad + 2 \times 12500 \times (150.363 - 175)^2 + \frac{1}{12} \times 250 \times 50^3 + 12500 \\ &\quad \times (150.363 - 25)^2 + 2337.737 \times (150.363 - 250)^2 \\ &\quad + 2337.737 \times (150.363 - 100)^2 + 1492.216 \\ &\quad \times (150.363 - 25)^2 + 994.811 \times (150.363 - 250)^2 \\ &= 627244823mm^4 \end{aligned}$$

$$y_t = h - \bar{y}$$

$$y_t = 300 - 150.363 = 149.637mm$$

Cracking will occur when the modulus of rupture f_r is reached in the top fibre of the beam section.

$$f_r = 3.96MPa \text{ (see Table 4-2)}$$

$$M_{cr} = \frac{I_g f_r}{y_t} = 16599455 Nmm = 16.599 kNm$$

Hence the first crack load with the moment arm length of 1.03m is

$$P_{cr} = \frac{16.599}{1.030} = 16.116 kN$$

The flexural cracks propagated over the top surface of the beam core within a distance of 600mm from the column face. ACI 318-08 (2008) states that the plastic hinge length is $2h$; where h is the beam height. In this case, $2h = 2 \times 300\text{mm} = 600\text{mm}$. Therefore, the length over which crack propagation occurs in Specimen P1 was in agreement with the plastic hinge length stated in ACI 318-08 (2008).

In some literature, the load vs. displacement graph of the beam-column joint tests showed that after the yield point, the curve will slightly increase until the peak load is reached. Hasan et al. (2011) investigated the behaviour of interior precast concrete beam-column connections under gravity loading. There were three connections (GR1, GR2 and GR3) each with different reinforcement details (i.e. T1, T2 and T3). The curves of the load vs. deflection of the beams are presented in Figure 4-22. It shows that the curves of GR1 and GR2 increased slightly after the yield point (about 5%). The increase in the beam load level between the first yielding and the rupture load level will vary between 4% and 10% (Nawy, 2000).

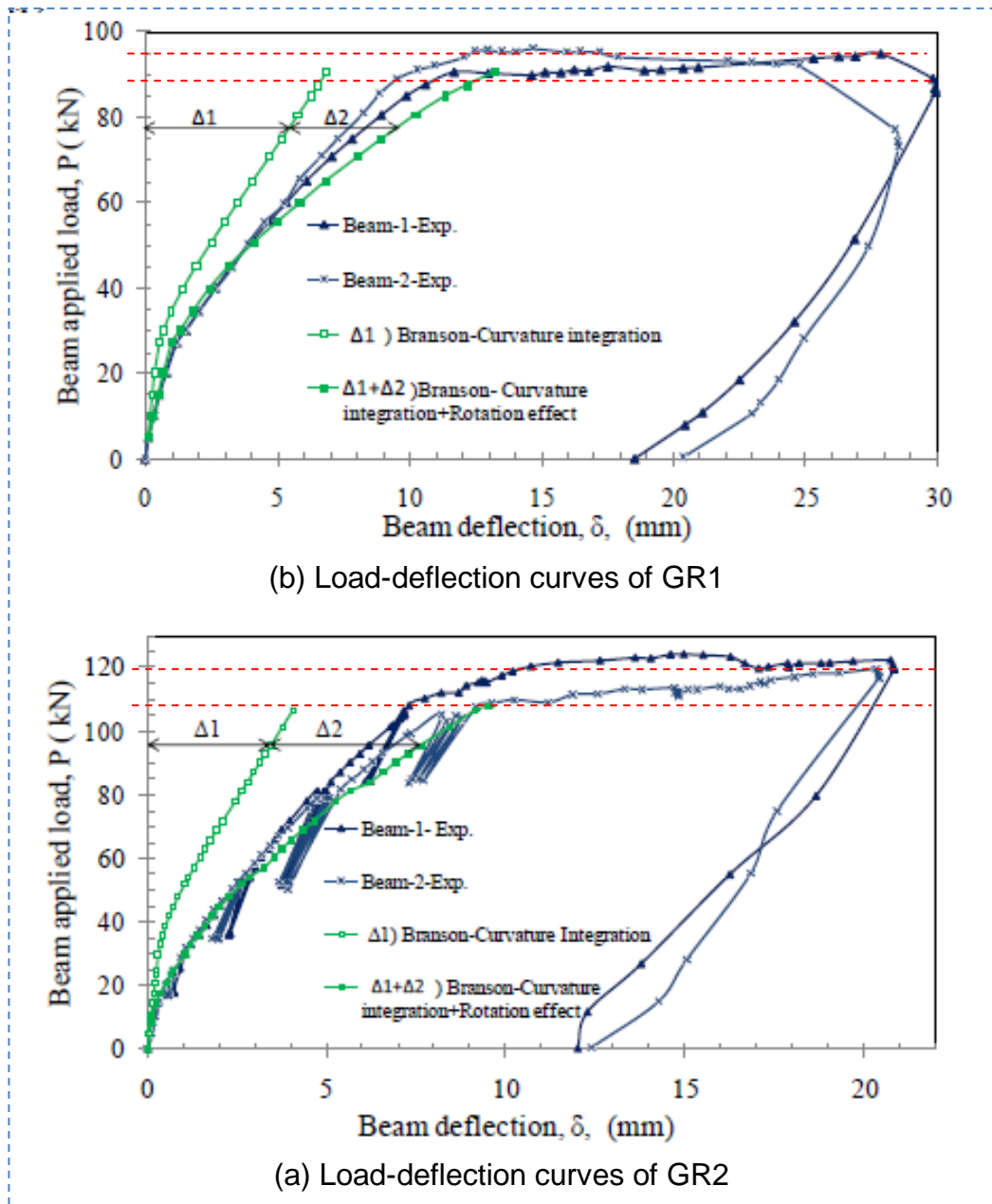


Figure 4-22 Test result of precast beam-column connection under gravity loads (Hasan et al., 2011)

The maximum load of Specimen P1 was 59.60kN. As seen in Figure 4-2, the results contradict that of Hasan et al. (2011), as after reaching the maximum load, the curve reduces until the maximum deflection is reached. The difference in behaviour is thought to be due to the fact that after yield it was apparent that the bond between the core and the U-beam had started to disintegrate. Figure 4-23 shows how the core broke into

two parts and the delamination present between the beam core and the wall of the U-beam. The load at the maximum deflection (i.e. 49.41kN) was still acceptable, because it was still over the 75% of maximum load which is allowable (ACI 374.1-05, 2005).



Figure 4-23 Photo of cracks on the top surface of the beam core of Specimen P1



(a) Side A



(b) Side B

Figure 4-24 Cracks of the precast U-beam at the supports

4.4.2 Bond strength between old concrete (U-beam) and new concrete (CIP core)

There are several factors which could affect the shear bond strength of the interface between the old concrete and new concrete surfaces, i.e. the moisture condition and/or the Saturated Surface Dry (SSD) or air-dry condition of the old concrete surface, the w/c ratio of the new concrete (Shin and Wan, 2010), and the surface condition (roughness) of the old concrete (Gillette, 1963 in Shin and Wan (2010)). Shin and Wan (2010) proved that the SSD condition of the old concrete results in higher shear bond strength of the interface (almost double) in comparison with the old concrete with air-dry surface condition.

In this experimental study, before the connection region of the beam-column joint was filled with the new concrete (CIP connection/beam core), the old concrete surface was sprayed with water in order to ensure that it satisfied the SSD condition. According to the conclusion of Shin and Wan (2010), by doing this, the interface between the old concrete and the new concrete should have had a good bond strength. Therefore, the assumption that the bond between the old concrete and the new concrete surface should be adequate up to peak load is reasonable. However, after peak load, delamination between the beam core and the wall of the U-beam occurred, which caused the load to decrease before failure.

4.4.3 Curvatures of the U-beam

Figure 4-25 and Equation (4-2) were used to calculate the curvature of the U-beam by using the strain data presented in Figure 4-12 to Figure 4-17. Figure 4-26 presents the curvatures as they develop in the joint core and the U-beam of Specimen 1.

$$\frac{1}{r} = \frac{R_a + R_b}{240} \quad (4-2)$$

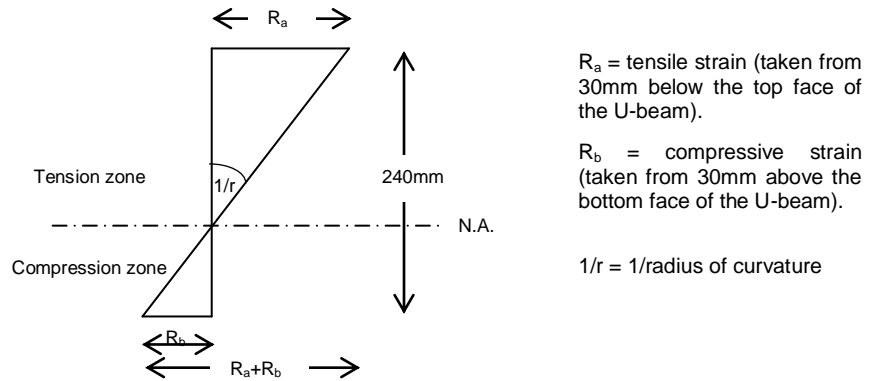


Figure 4-25 Strain profiles of the beam

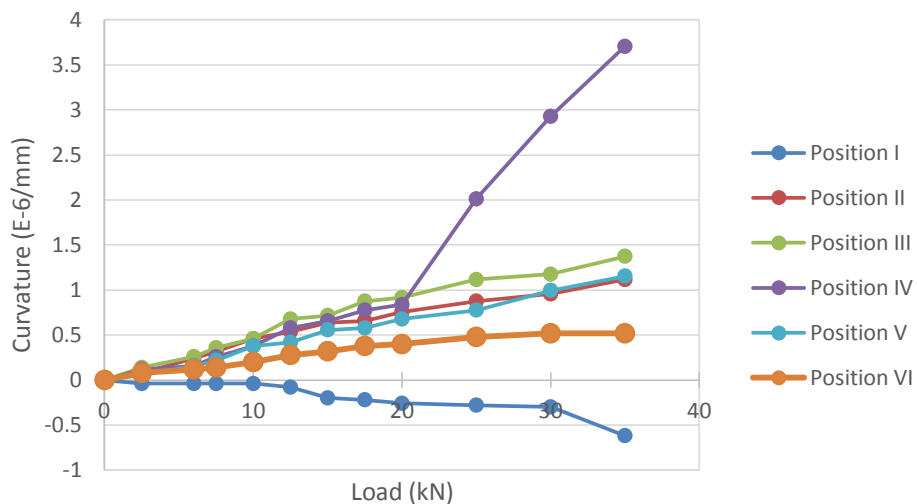


Figure 4-26 Curvatures of the surface strain of the U-beam of Specimen P1

As can be seen in Figure 4-26, the curvatures at Position II-VI (the U-beam) increased as the load increased. The curvatures at II, III and V appear to be similar; the curvature at Position IV was different in that it increased dramatically once a load of 20kN had been exceeded - at this

stage, the crack at the beam core surface extended into the wall of the U-beam. The curvature at Position VI is lower than the others because there was no crack at this position, either in the top surface of the beam core or the wall of the U-beam. This means that a crack occurring in the beam core will increase the curvature of the beam (even though the cracks did not appear in the U-beam wall at the observed load stages). The curves presented in Figure 4-26 also confirm that the curvature varied along the beam length; this was caused by the neutral axis depth fluctuation and strains between cracks (Park and Paulay, 1975).

The curvature in the joint core (Position I) decreased with increasing load. This is because the joint core is subjected to a compression strut mechanism from the negative bending moment.

The composite behaviour of the connection relies on the bond strength between the old (precast) concrete and the new concrete. Figure 4-27 presents the comparison of curvatures of Specimen P1 which were obtained from the electrical strain gauge data (attached on the interlocking bars within the beam core) and the DEMEC data (attached on the concrete surface of the U-beam at Position I). Both curves are similar, which indicates that the CIP beam core and the precast U-beam were probably behaving compositely.

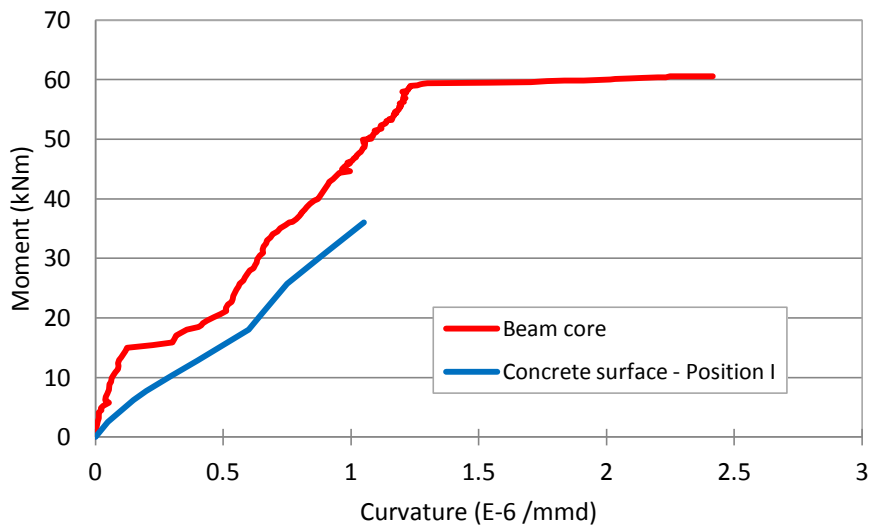


Figure 4-27 Curvatures of the beam core and the precast U-beam for Specimen P1

4.4.4 Joint core response

Using the strain data measured in the joint core (Figure 4-12, Figure 4-18, Figure 4-19 and Figure 4-20), tensile and compressive stresses in the joint core can be illustrated, as presented in Figure 4-28 (a). A diagonal compression strut has been formed due to the negative bending moment applied to the beam end. This is in agreement with the Compressive Strut Mechanism mentioned by Paulay and Scarpas (1981) for an exterior beam-column joint, as presented in Figure 4-27 (a).

Figure 4-29 (a) shows that the diagonal strut force, D_c in the joint core is introduced by the horizontal forces (consisting of the horizontal concrete force C_c , the horizontal steel compression force C_s and the column shear force (V_{col}') and the vertical forces (i.e. C_c'' , $\Delta T''$ and V_b) (Paulay and Scarpas, 1981).

Park and Paulay (1975) revealed that beam-column joints resist the shear force by the strut and truss mechanism (see Figure 4-29). The strut

mechanism depends on the compressive strength of the concrete, whereas the truss mechanism depends on the bond stress transfer along the beam and column reinforcement (Park and Paulay, 1975).

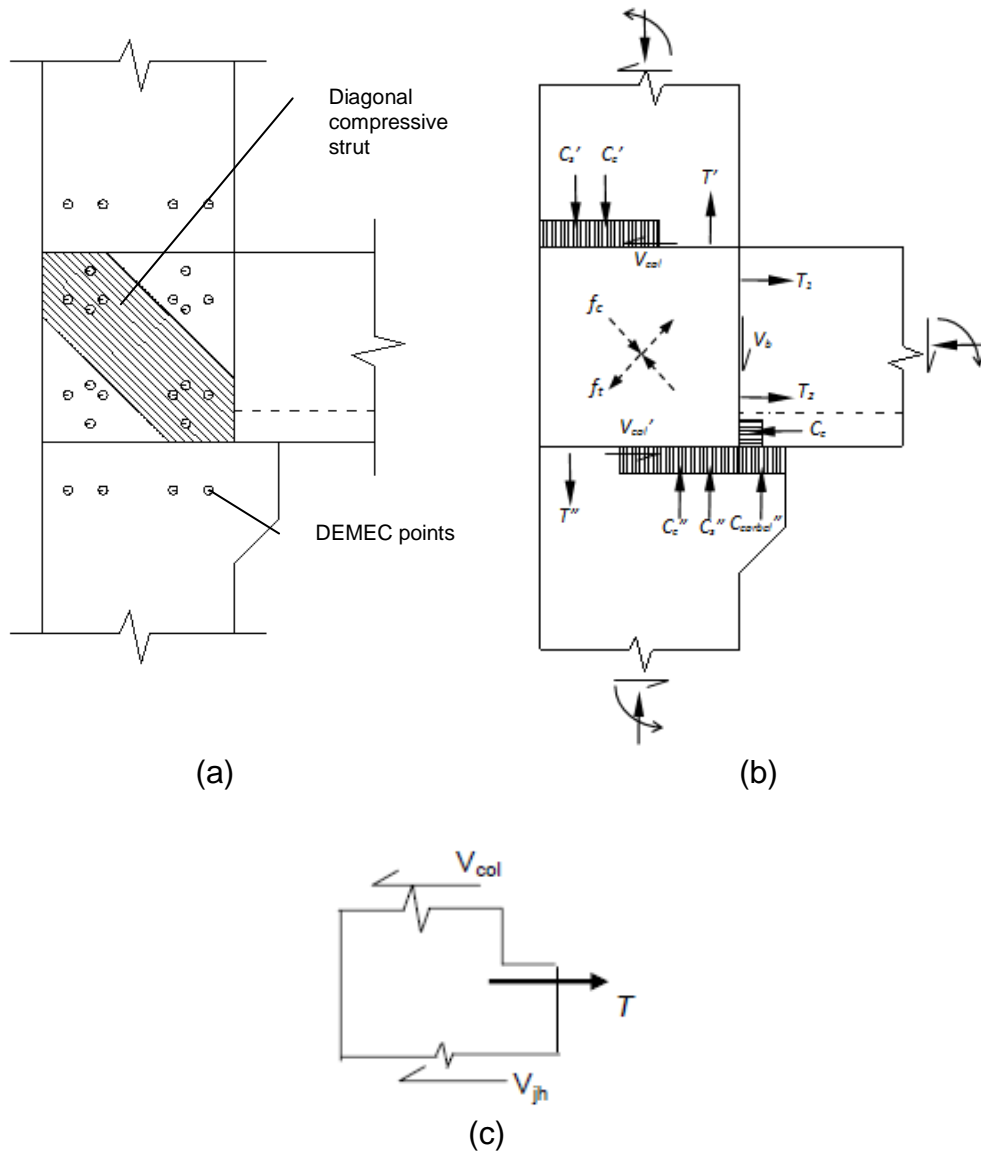


Figure 4-28 (a) Joint core strain distribution based on DEMEC's readings, (b) Internal forces and (c) Joint shear equilibrium

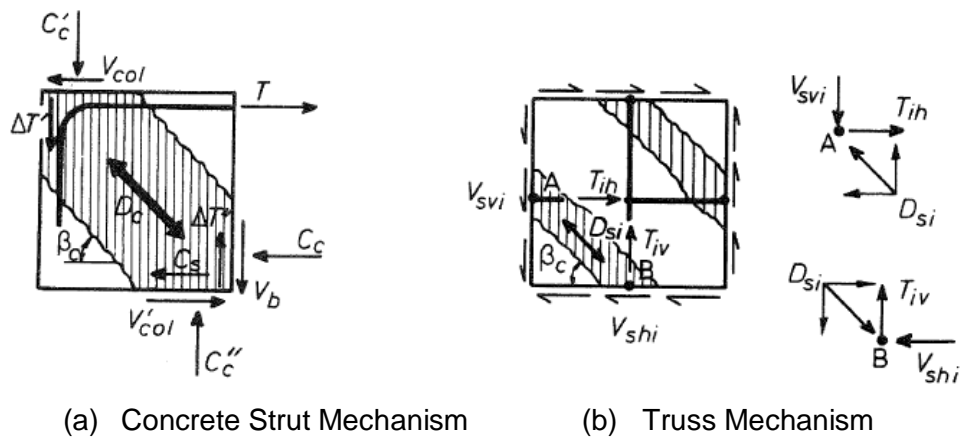


Figure 4-29 Mechanism of joint shear resistance at an exterior beam-column joint (Paulay and Scarpas, 1981)

A simple analysis was performed to estimate the joint shear force using the joint shear equilibrium in an exterior joint, see Figure 4-29 c. The joint shear force (V_{jh}), which is assumed to act on a horizontal plane passing through the joint, is

$$V_{jh} = T - V_{col} \quad (4-3)$$

In an exterior joint, the column shear V_{col} (see Figure 4-30) is

$$V_{col} = \frac{M_h}{l_c} \quad (4-4)$$

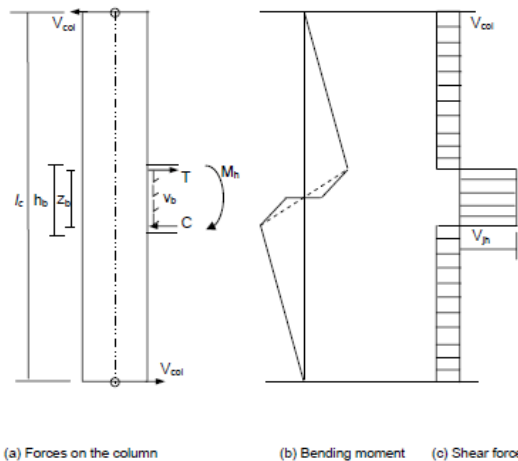


Figure 4-30 Horizontal shear in an exterior joint (Uma and Prasad, 1996)

ACI 318-08 (2008) defines the force due to tension reinforcement should include multiplying the steel yield stress by a factor of 1.25 to obtain the upper limit of shear on the joint. Therefore, T in Equation (4-3) is $1.25A_s f_y$.

ACI 318-08 requires that the actual horizontal joint shear force (V_{jh}) must be less than the nominal joint shear strength (V_{jn}). Regarding the exterior beam-column joint, the nominal shear strength of the joint (V_{jn}) is given in Equation (4-5) (ACI 318-08, using imperial units) or Equation (4-6) (SNI-2847-2002-(Indonesia, 2002), using metric units), where A_j is the effective cross-sectional area within a joint.

$$V_{jn} = 12A_j \sqrt{f_c'} \quad (4-5)$$

$$V_{jn} = 1.0A_j \sqrt{f_c'} \quad (4-6)$$

The horizontal joint force in this case is calculated using Equation (4-3) - (4-6), as follows

$T_1 = 226080\text{N}$ and $M_n = 56.71\text{kNm}$ (the calculation is presented in 4.4.5 in this chapter)

$$T = 1.25T_1 = 1.25 \times 226,080 = 282,600 \text{ N} = 282.6\text{kN}$$

$$M = 1.25M_n = 1.25 \times 56.71 \text{ kNm} = 70.888\text{kNm}$$

$$V_{col} = \frac{M}{h} = \frac{70.888}{2} = 35.444\text{kN}$$

$$\begin{aligned} V_{jh} &= T - V_{col} \\ &= 282.6 - 35.444 = 247.156\text{kN} \end{aligned}$$

The nominal joint shear strength is

$$\begin{aligned} V_{jn} &= 1.0A_j \sqrt{f_c'} \\ &= 1 \times (300 \times 300) \times \sqrt{47.296} = 618948.78\text{N} = 618.948\text{kN} \end{aligned}$$

Checking:

$$V_{jh} < V_{jn}$$

$$247.156kN < 618.948kN \dots\dots\dots OK!$$

According to the calculation above, the joint in Specimen P1 has enough shear strength to resist the applied load.

4.4.5 Theoretical calculation of nominal moment of beam

As shown in Figure 4-32, in the critical section of the beam, when the load level approached the peak load, both the interlocking bars contained within the beam core experienced tension while the longitudinal bars of the U-beam experienced compression. This shows that the behaviour of the precast beam was similar to a conventionally reinforced concrete beam. In this investigation, it was assumed that there was perfect bond between the old concrete and the new concrete until the maximum load was reached and therefore that the precast U-beam and the cast-in-place (CIP) reinforced concrete beam core behaved compositely. The internal force diagram for the beam-column joint is presented in Figure 4-28.

In order to test the assumption above that the two elements do indeed act compositely, a theoretical calculation based on Equation (4-7) was performed using the strain stress profiles of the beam cross-section recorded at a load of 56kN, i.e. just slightly under the peak load of 59.60kN. The concrete strength was taken from Table 4-2. Figure 4-31 presents the strain and stress distributions in the composite beam.

The analysis predicts that the theoretical nominal moment of the beam is 56.71kNm, which is equivalent to a load of 55.09kN (within 2% of the actual load of 56kN). As such, it is reasonable to assume that the precast U-beam and the CIP beam core act compositely similarly to a conventional reinforced concrete beam. The calculation detail is presented below.

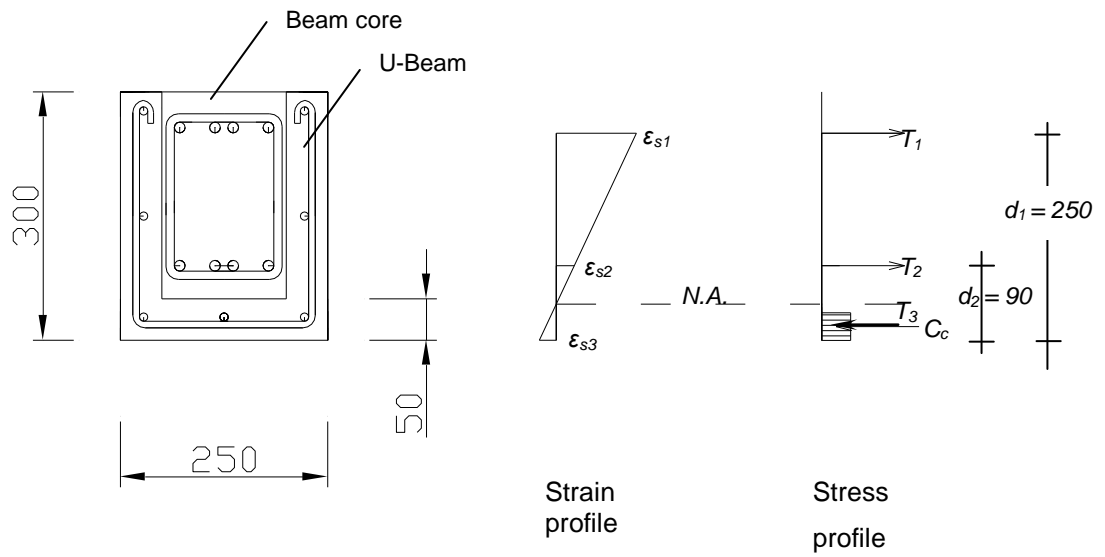


Figure 4-31 Cross-sectional dimensions, distribution of strain and stresses in the composite beam at the load level of 56 kN

$$T_1 + T_2 = C_c + T_3 = 0.85 f'_c ab + T_3 \quad (4-7)$$

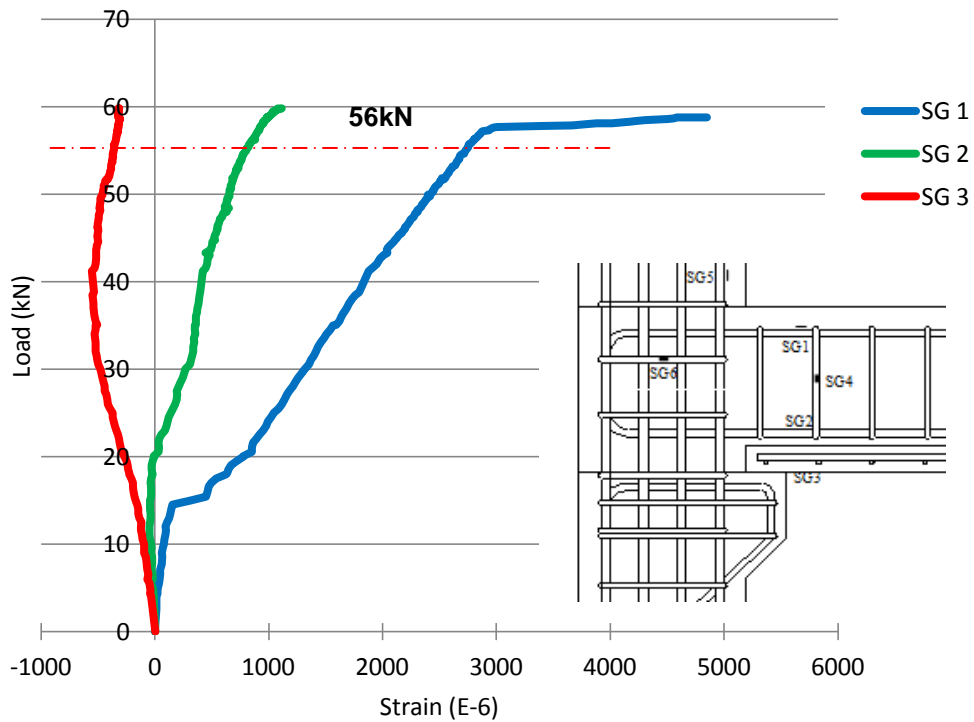


Figure 4-32 Load vs. strain of longitudinal steel bars (SG1, SG2 and SG3)

At a load of 56kN, the SG1 strain had reached the yield strain; SG2 and SG3 strains are used from the data as follows,

$$\varepsilon_{s2} = 884.82 \times 10^{-6}$$

$$\therefore f_{s2} = \varepsilon_{s2} E_s = 884.82 \times 10^{-6} \times 200,000 = 168.964 \text{ MPa}$$

$$\varepsilon_{s3} = -345.5 \times 10^{-6}$$

$$\therefore f_{s3} = \varepsilon_{s3} E_s = -345.5 \times 10^{-6} \times 200,000 = -69.1 \text{ MPa}$$

Material properties of steel and concrete as given in Table 4-2, as follows

$$f_y = 500 \text{ MPa}$$

$$f'_c = 59.12 \times 0.8 = 47.296 \text{ MPa}$$

$$f'_c = 38.07 \times 0.8 = 30.5 \text{ MPa}$$

The area of longitudinal bars are

$$A_{s1} = A_{s2} = 4\phi 12 = 452.16 \text{ mm}^2$$

$$A_{s3} = 3\phi 10 = 235.5 \text{ mm}^2$$

Hence, the nominal forces due to the longitudinal bars are:

$$T_1 = A_{s1} f_y = 452.16 \times 500 = 226,080 \text{ N}$$

$$T_2 = A_{s2} f_{s2} = 452.16 \times 168.964 = 76,379.76 \text{ N}$$

$$T_3 = A_{s3} f_{s3} = 235.5 \times 69.1 = 16,273.05 \text{ N}$$

Find a using Equation (4-7),

$$T_1 + T_2 = C_c + T_3 = 0.85 f'_c ab + T_3$$

$$226,080 + 76,379.76 = 0.85 \times 30.5 \times a \times 150 + 16,273.05$$

$$a = \frac{226,080 + 76,379.76 - 16,273.05}{0.85 \times 30.5 \times 150} = 44.2 \text{ mm}$$

Assume the compression force of T_3 works adjacent with compression force of C_c , hence, the nominal moment of the composite beam under positive bending moment applied to the beam end:

$$M_n = T_1 \left(d_1 - \frac{a}{2} \right) + T_2 \left(d_2 - \frac{a}{2} \right)$$

$$M_n = 226,080 \times 227.9 + 76,398.76 \times 67.9 = 56711108 \text{ Nmm}$$

$$= 56.71 \text{ kNmm}$$

Hence, the theoretical ultimate load of the composite beam with the moment arm length of 1.03m is

$$P_u = \frac{56.71}{1.03} = 55.059 \text{ kN}$$

In addition, it is apparent that the interlocking bars in this type of connection can connect the precast beam and the precast column, and can act as flexural reinforcement in the CIP reinforced concrete beam. The development length of the interlocking bars, that exceeds the plastic hinge

length, is considered sufficient to distribute the internal forces without bond slip occurring, as evidenced by the top interlocking bars which reached their yield strain.

4.5 Conclusions

The conclusions of this chapter are:

1. Specimen P1 (a precast concrete beam-column connection under static monotonic loading) behaved in a similar manner to traditional reinforced concrete elements. Flexural cracks occurred with the plastic hinge region of the beam, while the joint core had no significant cracks and the precast column was free of cracks. The specimen failed in flexural failure. Therefore, this design meets the strong column-weak beam concept.
2. The first crack occurred in the top surface of the beam core at a load of 15kN. The wall of the precast U-beam started to crack at 30kN, while the joint core cracked at 50kN. The maximum load and deflection were 59.80kN and 46.5mm, respectively.
3. The precast U-beam and the CIP beam core behave as a composite beam (the evidence for this were the extension cracks from the beam core through the wall of U-beam, the load-displacement curve and the moment-curvature curve). After the joint reached the yield phase, the bond strength of the interface between the precast U-beam and the beam core decreased.
4. The assumption that the bond between the old concrete and the new concrete existed until the yield point was correct; this was shown by theoretical analysis.
5. Based on the strain data, the top interlocking bars of the beam core experienced tensile stress during the test, while the bottom

longitudinal bars of the precast U-beam experienced compressive stress. The bottom interlocking bars experienced compressive stress from the beginning of the test until a load of 20kN, at which point it underwent tension until the end of loading. This is likely because, at the beginning of the test, the neutral axis position was between the top and the bottom interlocking bars. Once the first crack had occurred, the neutral axis depth decreased gradually (measured from the bottom surface of the beam).

6. Due to the negative loading, only the top interlocking bars reached the yield stage, whereas other reinforcement (i.e. the bottom interlocking bars, the longitudinal bar of the U-beam, the joint stirrups and the beam core stirrup) were still elastic.
7. The interlocking bars connecting the joint core and the beam core can act as flexural reinforcement for the beam core. The development length of the interlocking bars, i.e. 800 mm from the face of the column, is considered necessary to generate enough bond strength between the reinforcing bars and the concrete, so as to allow the interlocking bars to develop their tensile strength through to yield.

Chapter 5

Precast Concrete Beam-Column Connection under Quasi-Static Loading

5.1 Introduction

As explained in Chapter 4, the new precast concrete beam-column (PCBC) connection in this study performed well under static monotonic loading. The next stage of this study was to investigate the resistance of the new PCBC specimen connection to an equivalent seismic load. The seismic loading subjected to the PCBC specimen was in the form of a quasi-static loading, applied by hydraulic actuators (Park, 1988). The cyclic test result was then evaluated using the acceptance criteria stated in ACI 374.1-05 (*Acceptance Criteria for Moment Frames based on Structural Testing and Commentary*).

This chapter presents the behaviour of the PCBC connection (Specimen P2). The aim of this chapter is to investigate the structural behaviour of the precast concrete beam-to-column connection using interlocking bars subjected to quasi-static loading (Specimen P2). The results will then be compared with those of the connection which was subjected to static loading (Specimen P1).

Within this chapter, the material properties of Specimen P2, the set-up of the quasi-static loading system in the laboratory, and the behaviour of the connection in terms of crack-pattern, hysteresis load-deflection curves, energy dissipation, and stiffness degradation will be presented. Also, the theoretical nominal moment of the precast beam will be presented.

5.2 Acceptance Criteria

ACI 374.1-05 (*Acceptance Criteria for Moment Frames based on Structural Testing and Commentary*) provides a standard or acceptance criteria for evaluating the behaviour of the beam-column connection specimens of a moment resisting frame. The assessment is done on the hysteresis loops of the load-drift ratio relationship of the test specimens. The connections should fulfil the following requirements; for the third cycle at 0.035 of drift ratio:

1. The peak load in the positive and negative direction should not be less than 0.75 times the maximum load (E_{max}) for the same loading direction (see Figure 5-1);
2. The relative energy dissipation ratio (β) shall not less than 1/8; and
3. The secant stiffness from a drift ratio of -0.035 to a drift ratio of +0.035 shall not be less than 0.05 times the stiffness at the initial drift ratio (see Figure 5-3).

The Relative Energy Dissipation ratio (β) is defined as the ratio of actual to ideal energy dissipated by test specimen under the cyclic loading. The definition of relative energy dissipation ratio (β) according to ACI code is the ratio of the area of the hysteresis loop (A_h) to the area of a circumscribed parallelogram defined by the initial stiffness during the first cycle and the peak resistance, as presented in Figure 5-2 and Equation (5-1).

$$\beta = \frac{A_h}{(E_1 + E_2)(\theta_1' + \theta_2')} \quad (5-1)$$

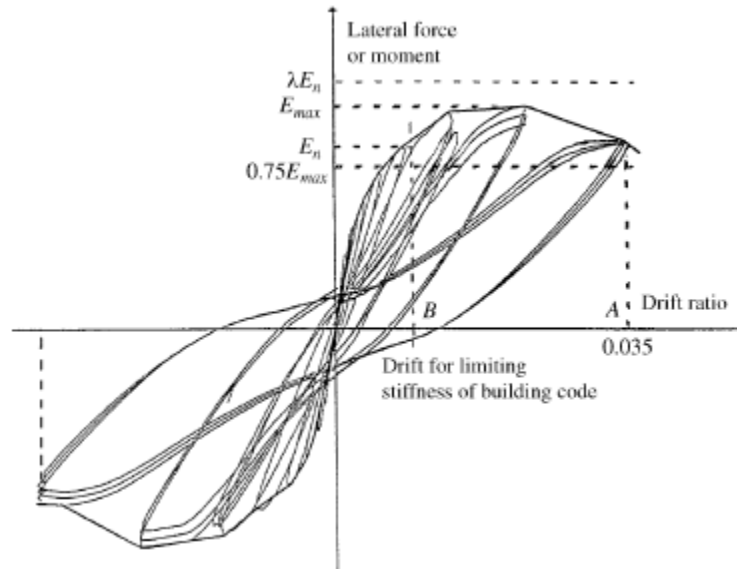


Figure 5-1 Quantities used in evaluating acceptance criteria (ACI 374.1-05, 2005)

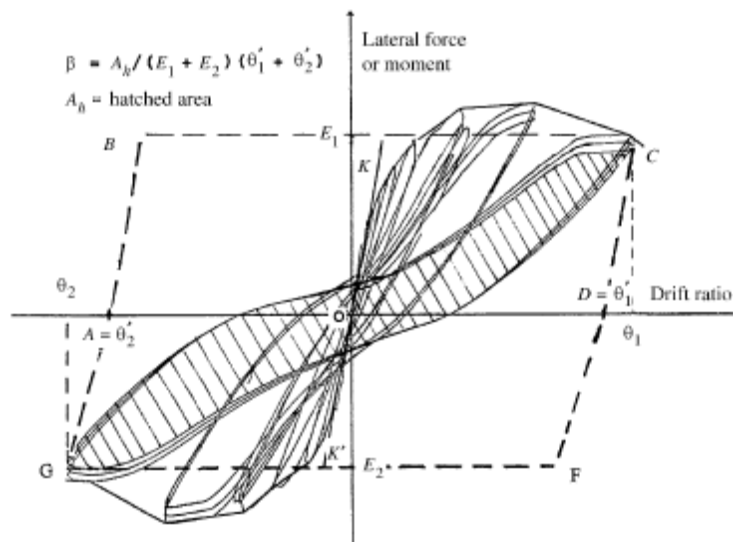


Figure 5-2 Relative Energy Dissipation Ratio (β) based on ACI 374.1-05 (2005)

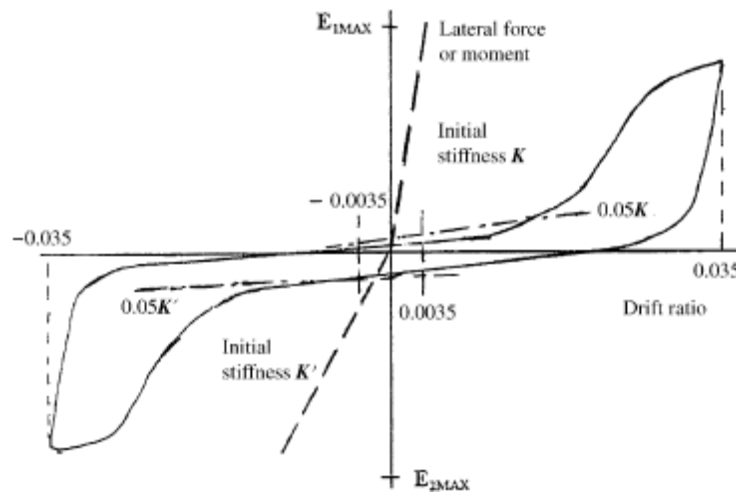


Figure 5-3 Unacceptable hysteretic behaviour (ACI 374.1-05, 2005)

5.3 Detail of Test Specimen P2

5.3.1 Geometry and reinforcement detail

Specimen P2 has similar reinforcement and dimensions to that of Specimen P1, although the reinforcement does differ slightly. Due to congestion experienced in the CIP beam core of Specimen P1, the number of interlocking bars was reduced from 4 interlocking bars (4 D12) to 3 bars (2 D16 and 1 D12) for Specimen P2. The reinforcement ratio in CIP beam core in both specimen P1 and P2 were similar (1.21% and 1.37% for specimen P1 and P2, respectively). Figure 3-4 and 3-6 in Chapter 3 presents the reinforcement details of Specimen P2.

5.3.2 Test setup and instrumentation/loading procedure

As explained in Chapter 3, the test set-up differed slightly from that used by previous researchers, (i.e. Figure 5-4(a) to Figure 5-4(b)). In this case, both the column ends were restrained by steel plates which were bolted to the test rig, while the beam end was free. The load was applied vertically

to the tip of beam. No vertical axial load was applied to the top of the column since this tends to enhance the joint shear strength; hence, this is a worst loading case scenario (Park, 1994).

A quasi-static loading was subjected to Specimen P2 using displacement control; displacements of 3, 8, 12, 18, 24, 36, 48, and 60 mm were used, as shown in Figure 5-5. For each displacement 2 cycles of quasi-static loading were applied. After the 2nd cycle at 60 mm displacement, the test specimen still appeared to be in good condition. At this stage, there was no significant peak load degradation; all peak loads at all cycles after displacement level of 12mm were higher than 75% of the maximum load at both loading directions. To finish the test, the load was applied in the negative direction (going down) until failure (maximum-displacement at failure was 97 mm).

The crack development at every level of displacement was recorded on the test specimen using different colours to indicate the different loading directions. Photographs were also taken at load step.

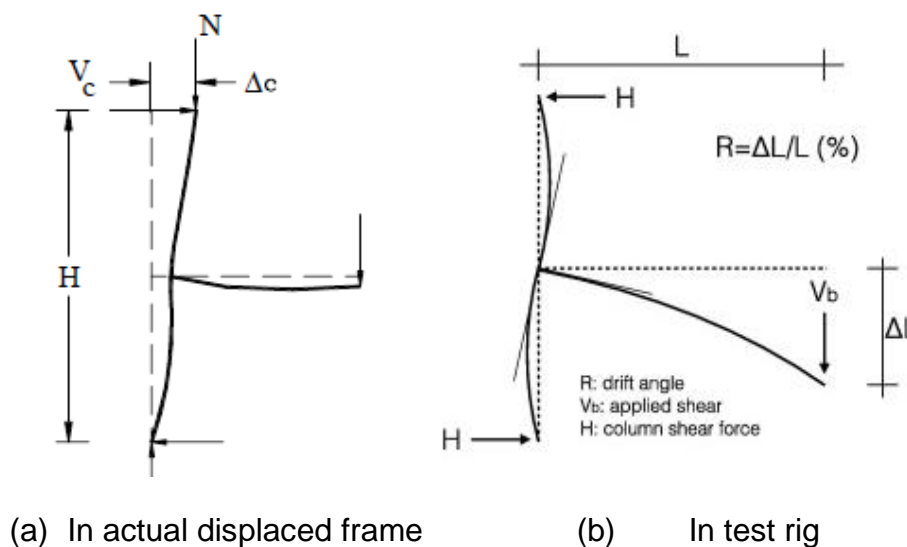


Figure 5-4 Exterior beam-column joints (Said and Nehdi, 2004; Kalogeropoulos et al., 2016)

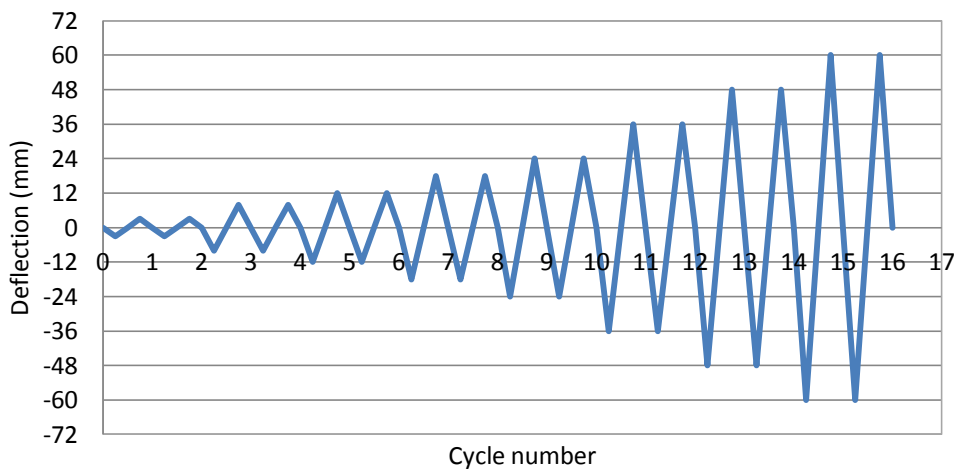


Figure 5-5 Load history for reversed cyclic load test used for Specimen P2

5.3.3 Mechanical properties of concrete

The precast elements were cast using normal concrete with a compressive strength of 30MPa. The cast-in-place (CIP) concrete had a compressive strength of 45MPa. A maximum size of 10mm coarse aggregate was used for the CIP concrete to ensure that the fresh concrete filled the congested section. The concrete slump was between 75 and 125mm.

Table 5-1 shows the compressive strengths, modulus of elasticity and modulus of rupture of the concretes. The compressive strength was obtained from 100 mm x 100 mm x 100mm cubes.

Yield strength of the steel reinforcing bars was 500MPa with a standard deviation of 30MPa.

Table 5-1 Average value of mechanical properties of concrete of Specimen P2

Mechanical properties	Precast Beam		Precast Column		CIP Connection	
	MPa	SD (MPa)	MPa	SD (MPa)	MPa	SD (MPa)
Average of Cube Strength	40.95	5.09	55.87	2.51	50.86	0.87
Average of Modulus of Elasticity	30697	186	28940	1473	31518	1279
Average of Flexural Strength	4.03	0.23	5.42	0.78	5.99	0.11

5.4 Test Results

5.4.1 Failure mode

Figure 5-6 shows the crack-pattern of Specimen P2 which was subjected to a quasi-static loading. The red mark indicates the cracks due to negative loading (downward), while the blue mark indicates the cracks due to positive loading (upward). The first crack occurred on the top surface of the beam core at a load of 15kN, during the first cycle of negative loading (at the displacement level of 3mm). Further new cracks on the top surface of the beam core continued to develop at displacement levels of 8mm, 18mm, 24mm, and 36mm during negative loading, along the connection region (see Figure 5-6 (a)).

The cracks developed in the wall of the precast U-beam from the displacement level of 8mm until 36mm. The cracks due to negative loading were the extension of the crack in the top surface of the beam core.

Cracks in the joint-core initially appeared during the first cycle of the 8mm displacement level. The cracks then extended forming an “X” crack pattern in the joint core; the propagation of cracks stopped at the displacement level of 36mm (DR = 3.5%). A thin delamination crack in the gap between the joint core in the column (CIP-concrete) and the precast concrete column (top and bottom part) occurred at the displacement level of 18 mm (see Figure 5-7).

After the displacement level of 36mm (DR = 3.5%), no more cracks developed in the joint core; the cracks were concentrated in the beam adjacent to the column. As can be seen in Figure 5-8, the crack-width of the top surface of the beam core was 7mm (at the displacement level of 60mm, 2nd cycle); at the end of the test (at -97mm of deflection) this crack width had widened to 12mm. Elsewhere in the joint, at the displacement level of -60mm, the crack opening between the U-beam and the column was 15mm (Figure 5-9) and the part of the U-beam supported by the corbel was crushed (Figure 5-10). At the end of the test (at -97mm of displacement) the opening between the U-beam and the column was 20mm (see Figure 5-9).

To sum up, at the end of the test, there was no significant damage in the joint core, whereas the beam end adjacent to the column face experienced wide cracks on the top surface of the beam core (Figure 5-8) and crushed at the part of the U-beam supported by the corbel (Figure 5-10). Therefore, it can be concluded that the PCBC Specimen P2 experienced a ductile failure with the plastic hinge forming in the beam.



(a) at the end of displacement level of 60mm (2nd cycle)



(b) at the end of test (97mm of deflection)

Figure 5-8 Crack width on the beam core of Specimen P2



(a) at displacement level of -60mm



(b) at the end of test (maximum deflection was -97 mm)

Figure 5-9 Opening between the precast U-beam and the column



Figure 5-10 U-beam condition Specimen P2 at the end of displacement level of 60 mm (2nd cycle)

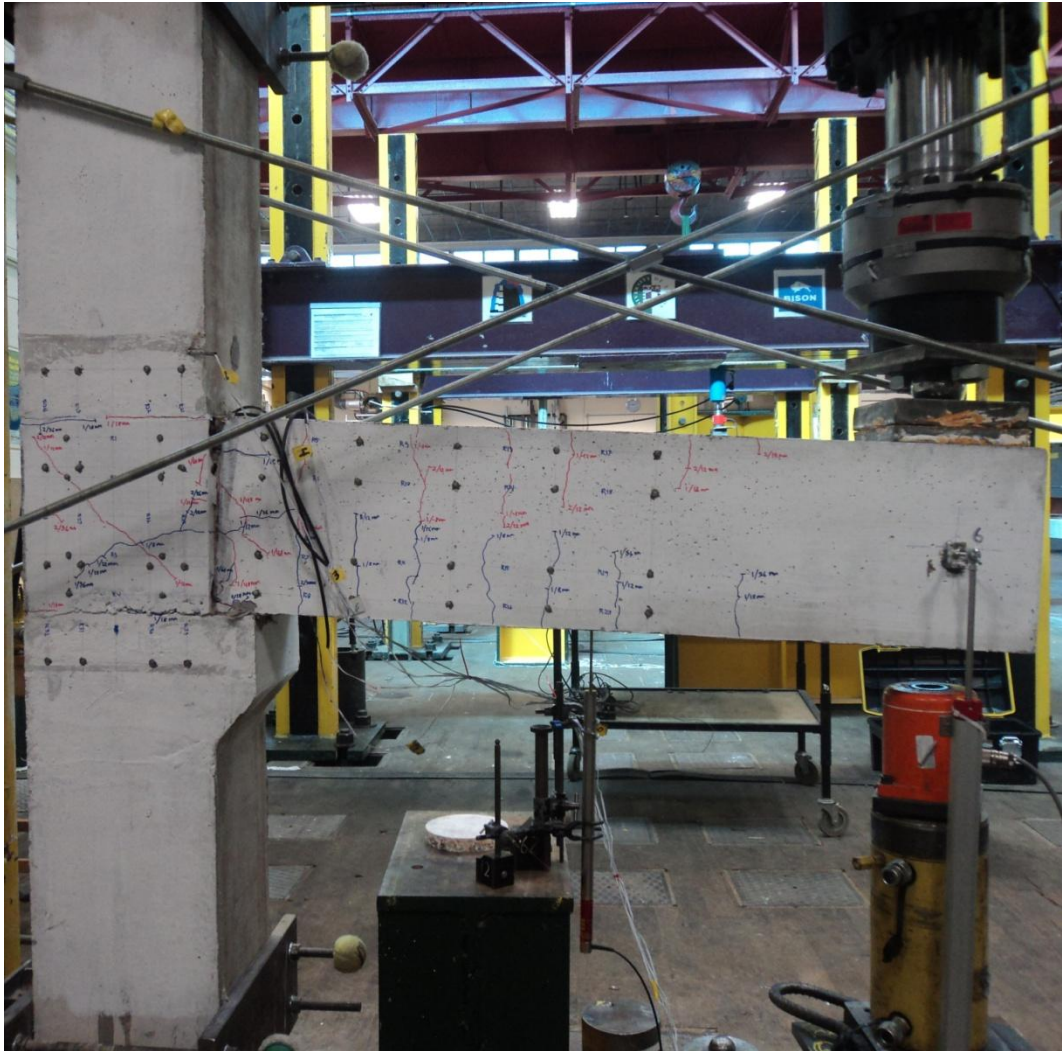


Figure 5-11 Crack-pattern on the beam-column connection (Specimen P2)

5.4.2 Load-deflection curves

Figure 5-12 illustrates the beam tip load-deflection curves for Specimen P2. Two full cycles were applied at each level of displacement. Table 5-2 presents the peak loads for every cycle throughout the test.

Table 5-2 Peak load for every cycle of testing of Specimen P2

Deflection (mm)	Maximum Load (kN)			
	Negative-1st cycle	Positive-1st cycle	Negative-2nd cycle	Positive-2nd cycle
3	-20.62	16.64	-19.94	16.44
8	-39.66	30.14	-36.58	29.14
12	-50.54	41.77	-47.82	39.96
18	-63.95	51.53	-58.23	47.51
24	-65.39	49.89	-56.01	45.59
36	-67	49.9	-56.36	46.64
48	-64.92	48.64	-54.1	46.95
60	-61.82	47.97	-56.05	47.28
DTF	-70.33			
mm	-97			

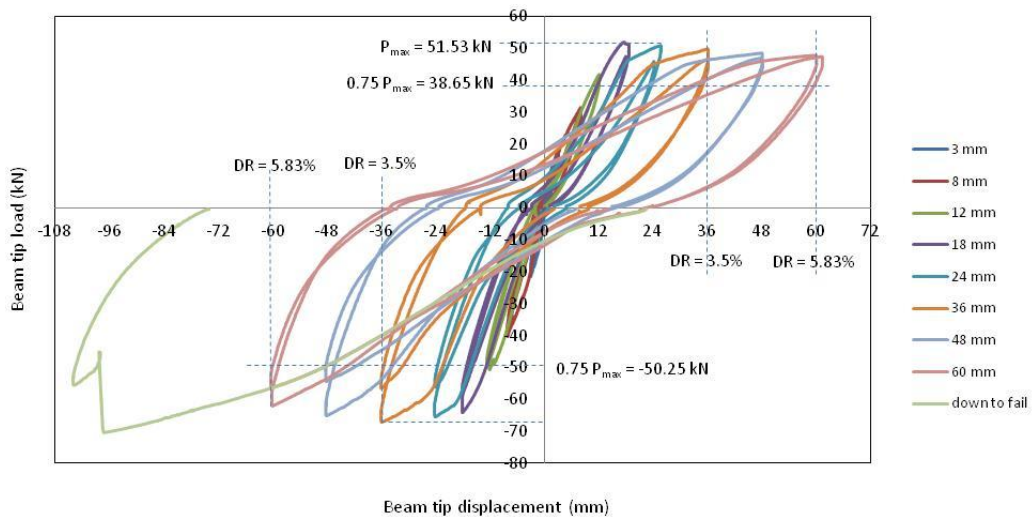


Figure 5-12 Load-displacement relationship of Specimen P2

As we can see in Table 5-2, the maximum loads at 2nd cycle at each displacement level is lower than those at 1st cycle. When the joint was loaded at the first cycle at a specific displacement level, the cracks occurred in the tension zone which causes a reduction in the member stiffness. Therefore, the slope of the curve was less at the next cycle, which results in a lower maximum load at the observed displacement level. Figure 5-14 presents the load vs. deflection loops at the displacement level of 18mm. It can be seen that the loop at the 1st cycle had a higher maximum load and stiffness in comparison with those at the 2nd cycle. Nevertheless, the stiffness reduction does not affect the flexural strength of the member, but it does result in a greater deflection (Park and Paulay, 1975).

The reduction in the stiffness of the member was mainly caused by the Bauschinger effect of the steel reinforcement bar. Due to reverse loading, the yield strength of the steel at the next cycle is lower than the initial yield strength, as can be seen in Figure 5-13. The Bauschinger effect happened in both compression and tension loading. In Specimen P2 at the displacement level of 18mm (see Figure 5-15), the strain of the top interlocking bar is 3100 micro strain (i.e. higher than the yield strain) resulting in a different maximum load of the joint, where the maximum load at the 1st cycle is higher than that at the 2nd cycle.

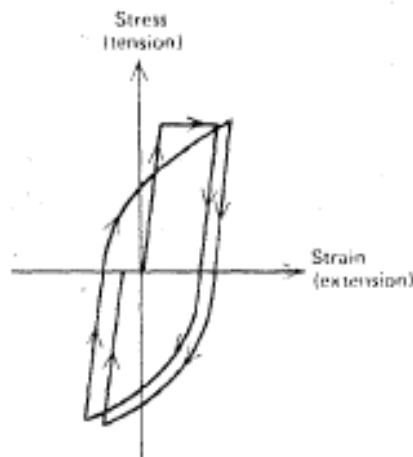


Figure 5-13 Bauschinger effect for steel under reverse loading (Park and Paulay, 1975)

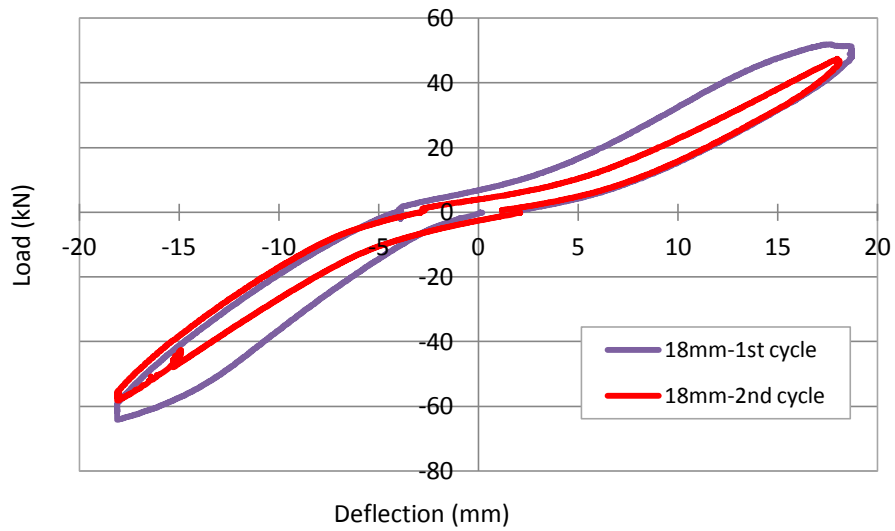


Figure 5-14 Load vs. deflection loops of Specimen P2 at the displacement level of 18mm

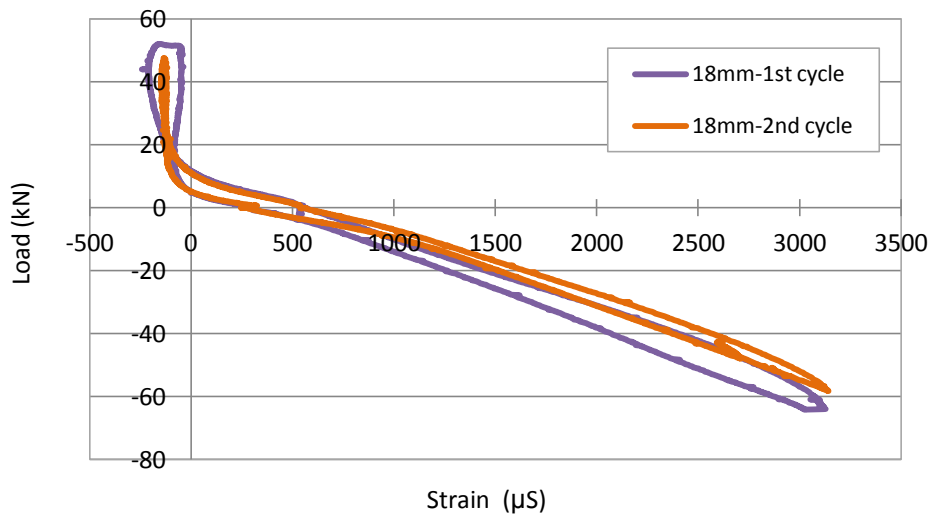


Figure 5-15 Load vs. strain of top longitudinal bar of Specimen P2 at the displacement level of 18mm

5.5 Discussion

5.5.1 Beam-column connection behaviour with reference to the ACI Acceptance Criteria

The seismic performance of this new PCBC-connection was evaluated using ACI 374.1-05 (*Acceptance Criteria for Moment Frames Based on Structural Testing and Commentary*). Table 5-3 presents the evaluation of Specimen P2 in comparison with the acceptance criteria stated in ACI 374.1-05.

The hysteresis loop, as shown in Figure 5-12, appeared stable from the beginning of the test until the last cycle at the deflection level of 60 mm. There was no significant strength degradation after the peak load. All peak loads at all cycles are higher than 75% of the maximum load in both loading direction (i.e. 50.25kN and 38.65kN for negative and positive loading, respectively).

The maximum load data in Table 5-2 shows that the maximum load for every negative loading cycle was higher than in the positive loading. Some reasons are considered as a possible cause.

First, due to the corbel, the distance between the point load and the critical moment point on the beam (the moment arm length) in the negative loading ($L=1030\text{mm}$) was shorter than that in the positive loading ($L=1100\text{mm}$). Secondly, the bottom wall of the precast U-beam increases the beam stiffness below the x-axis of the beam cross section. Therefore, the stiffness of the composite beam in negative loading is greater than the stiffness in positive loading.

All peak loads at each deflection increment were more than 75% of the maximum load in both the negative and positive loading. Particularly at the displacement level of 36mm (or 0.035 of DR), the ratios of the peak load of the second cycle ($P_{2\text{nd}}$) to the maximum load (P_{max}) in each

direction are $(-56.36\text{kN})/(-67\text{kN}) = 0.84$ (in negative loading) and $46.64\text{kN}/51.53\text{kN} = 0.91$ (in positive loading), as shown in Table 5-3. Thus, the connection fulfilled the requirements stated in ACI 374.1-05, that the peak load of the last cycle of the drift ratio of 3.5% should be not less than 0.75 of the peak load.

The ACI 374.1-05 requires that the relative energy dissipation ratio shall not be less than 0.125 at the end of the last cycle of the drift ratio (DR) of 3.5% (0.035). The definition of the relative energy dissipation ratio (β) according this code is the ratio of the area of the hysteresis loop to the area of a circumscribed parallelogram defined by the initial stiffness during the first cycle and the peak resistance (load), as presented in Figure 5-2 and Equation (5-1). The calculation of the relative energy dissipation ratio (β) of beam-column Specimen P2 used the load vs. deflection curve at the displacement level of 36mm as presented in Figure 5-16. The area of the hysteresis loop (A_h) is 1300kNmm; the area of the parallelogram is 5781.01kNmm. By using Equation (5-1), the relative energy dissipation ratio (β) of Specimen P2 is $1300/5781.01 = 0.225$, which satisfies the requirements of ACI 374.1-05.

The secant stiffness is evaluated at the peak-to-peak stiffness of the load-displacement curves. Increasing the displacement level caused a decrease in the stiffness of Specimen P2 due to the formation of cracks in the composite material. ACI 374.1-05 requires that the secant stiffness at a drift ratio of 3.5% (from positive to negative loading) should not be less than 0.05 times the initial stiffness. According to Figure 5-16, the initial stiffnesses in the positive direction (K) and in the negative direction (K') are 5 and 8.5714, respectively. The secant stiffness of Specimen P2 from -3.5% of DR to +3.5% is 1.4315. Therefore, the ratio of $K_{0.035}$ to the initial stiffness in the positive direction ($K_{0.035}/K$) is $1.4315/5 = 0.2863$, while in the negative direction, $(K_{0.035}/K') = 1.4315/8.5714 = 1.167$. As shown in Table 5-3, the ratios of $K_{0.035}/K$ and $K_{0.035}/K'$ are more than 0.05, which means the requirements stated in ACI 374.1-05 have been satisfied.

Furthermore, the ratios of secant stiffness at the displacement level of ± 60 mm ($DR = \pm 5.83\%$) to the initial stiffness in both directions are $0.8643/5 = 0.173$ (in the positive direction) and $0.8643/8.5714 = 0.101$ (in negative direction), which are still higher than the required 0.05.

Table 5-3 Comparison between test results of P2 and Acceptance Criteria ACI 374.1-05

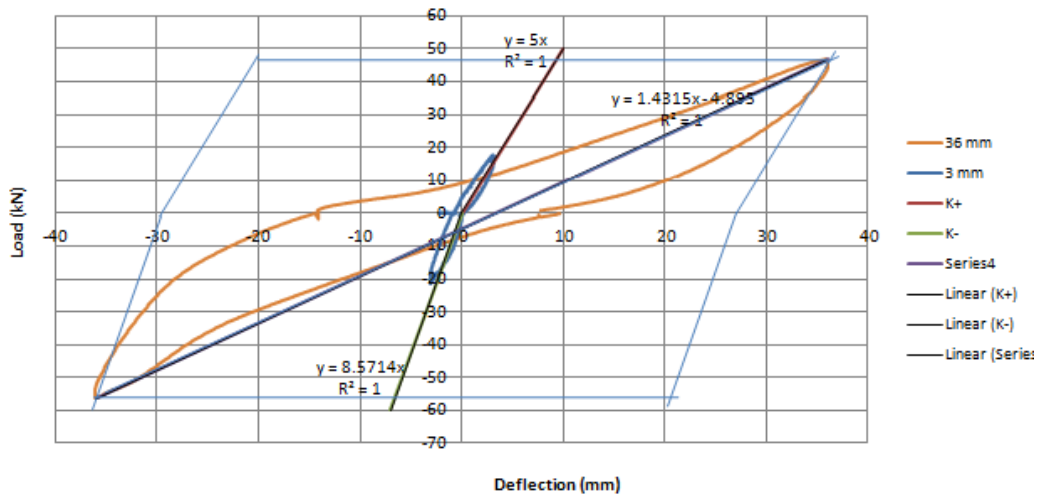
Items	Specimen P2	Acceptance Criteria*
P_{2nd}/P_{max}		
Negative loading	0.84	≥ 0.75
Positive loading	0.91	≥ 0.75
β	0.225	≥ 0.125
$K_{0.035}/K$	0.2863	≥ 0.05
$K_{0.035}/K'$	0.167	≥ 0.05

*) ACI 374.1-05 (2005)

β = relative energy dissipation ratio

K and K' = initial stiffness for positive and negative loading for first cycle.

$K_{0.035}$ = secant stiffness at drift ratio of 3.5%.



The area of hysteresis loop (A_h) = 1300

The area of parallelogram = 5781.01

Using Eq. (5-1), $\beta = 1300/5781.01$

Figure 5-16 Load-deflection curve (at 2nd cycle) of Specimen P2 at drift ratio of 3.5% (equal with deflection level of 36mm)

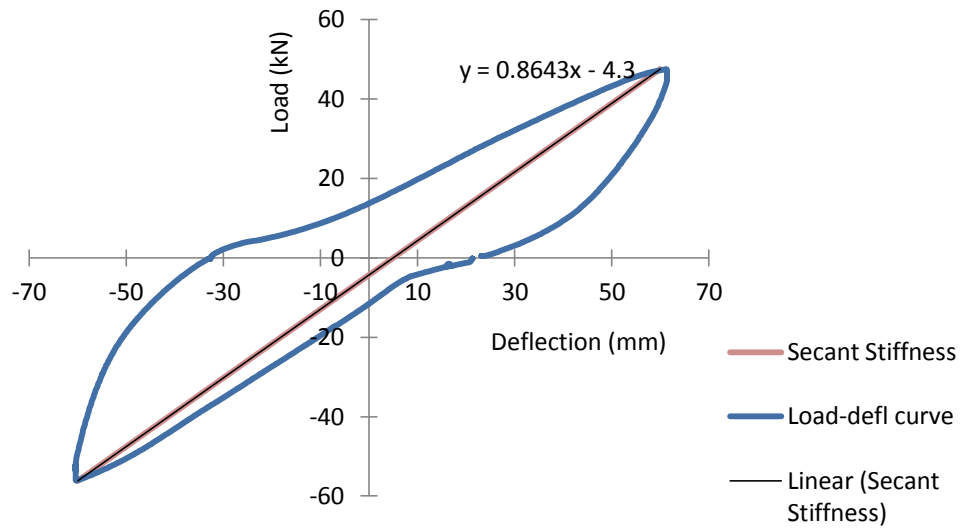


Figure 5-17 Secant stiffness at 2nd cycle of 60 mm displacement (±5.83% of DR)

5.5.2 Theoretical calculation of nominal moment of beam

A theoretical calculation of the beam nominal moment capacity is presented in this section. To reflect the cyclic load, the calculations have been done for both the negative and positive nominal moment. Table 5-4 presents the data of Specimen P2 which is used for the calculation. The calculation is performed according to the data at 1st cycle of the deflection level of 18mm in which the maximum load happened.

Table 5-4 Data of the composite beam of Specimen P2

Steel Reinforcing Bars		f_y	500 MPa	
		E_s	200000 MPa	
	Area (mm ²)	Strain at the max load of 18mm displacement (μ S)		
			1 st cycle, negative load	1 st cycle, positive load
A_{s1}	514.96	ϵ_{s1}	3028.960	-145.606
A_{s2}	514.96	ϵ_{s2}	1184.060	5917.560
A_{s3}	235.50	ϵ_{s3}	-960.517	881.008
Concrete		Cube strength (MPa)	0.8 of cube strength (MPa)	
CIP beam core		50.86	40.69	
U-Beam		40.95	32.76	
Maximum load (experimental)			(kN)	
Negative load at 18 mm of deflection			-63.95	
Positive load at 18 mm of deflection			51.53	

In term of the negative moment capacity, the calculation used the same assumptions to those used in the Specimen P1 calculation which are:

- both the U-beam and the beam core behave monolithically (compositely),
- the equilibrium existed between the tension forces carried by both the top and bottom interlocking bars,
- Compressive forces carried by the longitudinal bars of the U-beam and the compression block resulted from the bottom wall of the U-beam.

Figure 5-18 presents the strain and stress profiles of the composite beam component of Specimen P2 under negative loading.

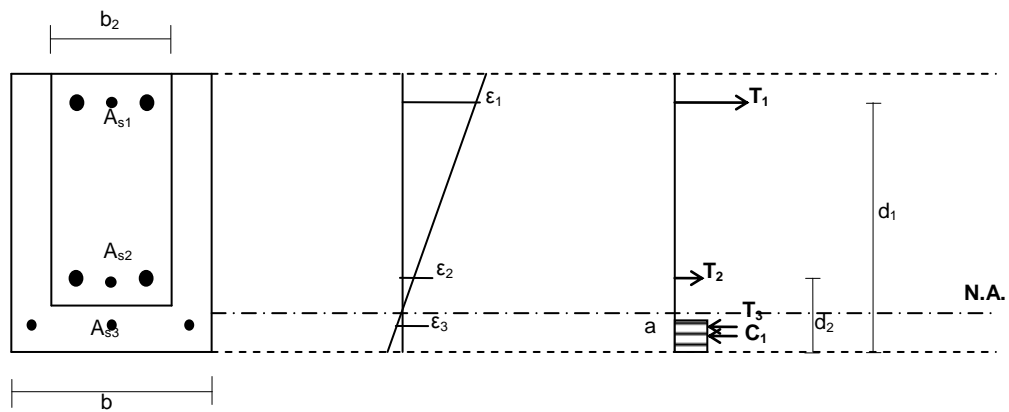


Figure 5-18 Strain and stress profile of the composite beam of Specimen P2 at the displacement level of 18mm (negative bending moment)

Notation:

$$b = 250mm$$

$$b_2 = 150mm$$

$$d_1 = 245mm$$

$$d_2 = 105mm$$

$$f_{s1} = f_y = 500 MPa$$

$$f_{s2} = \varepsilon_{s2}E_s = 1184.06 \times 10^{-6} \times 200,000 = 236.812 MPa$$

$$f_{s3} = \varepsilon_{s3}E_s = -960.517 \times 10^{-6} \times 200,000 = -192.103 MPa$$

Thus, the tension forces are:

$$T_1 = A_{s1}f_y = 452.16 \times 500 = 257480 \text{ N}$$

$$T_2 = A_{s2}f_{s2} = 452.16 \times 236.812 = 121948.7 \text{ N}$$

$$T_3 = A_{s3}f_{s3} = 235.5 \times -192.103 = 45240.35 \text{ N}$$

a can be obtained by equating the tension forces and compression forces.

$$C_c + T_3 = T_1 + T_2$$

Assume that T_3 is working on the resultant point of C_c to make the calculation easier.

$$0.85 f'_c ab + T_3 = T_1 + T_2$$

$$0.85 \times 32.76 \times a \times 250 + 45240.35 = 257480 + 121948.7$$

$$a = \frac{257480 + 121948.7 - 45240.35}{0.85 \times 32.76 \times 250} = 48.0 \text{ mm}$$

$$M_n = T_1(d_1 - \frac{a}{2}) + T_2(d_2 - \frac{a}{2})$$

$$M_n = 66.78 \text{ Nmm}$$

Hence, the theoretical ultimate load of beam is

$$P_n = \frac{66.78}{1.03} = 64.18 \text{ kN}$$

The maximum load obtained from the experiment is **63.95 kN (negative loading)**.

The assumptions to analyse the nominal moment of the beam under positive loading are:

- Both the beam core (C_{bc}) and the wall of the U-beam (C_{Ub}) contributed to the compression resistance.

- Although the top interlocking bars experienced compression, this was ignored. This is because their positions were very close to the neutral axis (see Figure 5-19).
- The longitudinal bars of the U-beam contributed to the tension resistance (T_3), (this was based on the strain gauge data).
- The bottom interlocking bars yielded (T_2), based on the strain gauge data.

Figure 5-19 presents the strain profile and stress profiles of the composite beam component of Specimen P2 when subjected to the positive bending moment. The equilibrium equation is,

$$C_{bc} + C_{Ub} = T_2 + T_3 \quad (5-2)$$

C_{bc} = Compression force resulted from the beam core.

$$C_{bc} = 0.85 f'_{c2} b_2 a$$

C_{Ub} = Compression force resulted from the wall of the U-beam.

$$C_{Ub} = 0.85 f'_{c1} b a$$

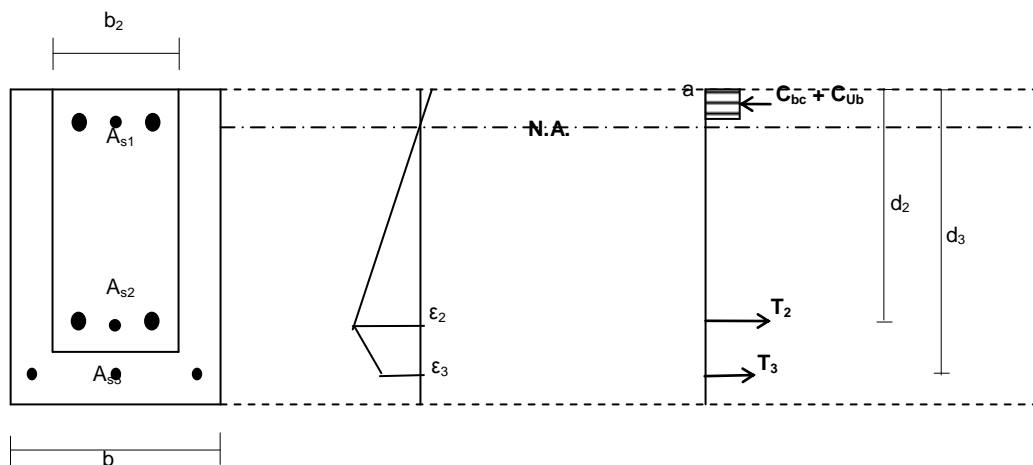


Figure 5-19 Strain and stress profile of the composite beam of Specimen P2 at the displacement level of 18mm (positive bending moment)

Notation:

$$b = 250\text{mm}$$

$$b_2 = 150\text{mm}$$

$$d_2 = 195\text{mm}$$

$$d_3 = 275\text{mm}$$

$$f_{s1} = f_y = 500 \text{ MPa}$$

$$f_{s2} = f_y = 500 \text{ MPa}$$

$$f_{s3} = \varepsilon_{s3} E_s = 881.008 \times 10^{-6} \times 200,000 = 176.2 \text{ MPa}$$

Thus, the tension forces are:

$$T_2 = A_{s2} f_{s2} = 452.16 \times 500 = 257480 \text{ N}$$

$$T_3 = A_{s3} f_{s3} = 235.5 \times 176.2 = 41495.48 \text{ N}$$

a can be obtained by equating the tension forces and compression forces.

Assume that both C_{bc} and C_{Ub} are working at the same point to make the calculation easier.

$$C_{bc} + C_{Ub} = T_2 + T_3$$

$$0.85 f'_{c2} b_2 a + 0.85 f'_{c1} b a = T_2 + T_3$$

$$a = \frac{T_2 + T_3}{0.85 f'_{c2} b_2 + 0.85 f'_{c1} b}$$

$$a = \frac{257480 + 41495.48}{0.85 \times 40.69 \times 150 + 0.85 \times 32.76 \times 100} = 36.85 \text{ mm}$$

$$M_n = T_2 \left(d_2 - \frac{a}{2} \right) + T_3 \left(d_3 - \frac{a}{2} \right)$$

$$M_n = 56.11 \text{ Nmm}$$

Hence, the theoretical ultimate load of beam is

$$P_n = \frac{56.11}{1.1} = 51.95 \text{ kN}$$

The load maximum obtained from experimental is **51.53kN (positive loading)**.

Table 5-5 presents a comparison of the calculated maximum loads with the experimental maximum loads. It can be seen that the analytically determined maximum loads are very similar to the experimentally measured values. The ratios of analytical to experimental are nearly 1 for both the negative and positive loading. It can be concluded that the assumption above could be considered to use in predicting the load capacity of the composite beam of Specimen P2.

Table 5-5 Comparison of the maximum load of Specimen P2

At 18 mm of deflection	Load (kN)		$\frac{\text{Analytical load}}{\text{Experimental Load}}$
	Analytical	Experimental	
Negative loading	-64.83	-63.95	1.014
Positive loading	51.01	51.53	0.989

5.5.3 Internal behaviour of Specimen P2

In order to evaluate the internal behaviour of precast concrete beam-column specimen (P2), several electrical strain gauges were installed on several reinforcement bars of the beam-column specimen as presented in Figure 5-20. The strain gauges SG1, SG2 and SG3 were attached on the top and bottom interlocking bars and the longitudinal bar of the U-beam, respectively. The strain gauges SG4 and SG6 were installed on the stirrups of the CIP beam and the joint core, respectively. SG5 was used for measuring the strain of the longitudinal bar of the precast column. Unfortunately, SG4 malfunctioned before the test.

The strain responses of the reinforcement bars due to a quasi-static load are presented in Figure 5-21-Figure 5-27. The cyclic loading was applied on the beam-column specimen in 8 displacement levels (i.e. 3mm, 8mm, 12mm, 18mm, 24mm, 36mm, 48mm, 60mm); each level consisted of 2 cycles. Therefore, there are 16 cycles in total (denoted on the horizontal axis of the figures below).

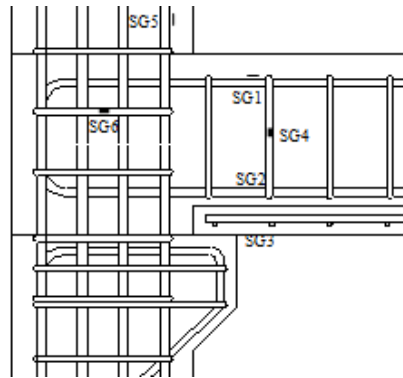


Figure 5-20 Location of strain gauges on the reinforcing bars of Specimen P2

5.5.3.1 The longitudinal bars of the beam

The interlocking bars in the PCBC specimen were designed to yield during the test, as a plastic hinge was expected to happen. The reinforcement ratio of the beam was lower than the maximum reinforcement ratio, to ensure that ductile failure occurred in the beam. Figure 5-21, Figure 5-22 and Figure 5-23 present the strain responses of the top and bottom interlocking bar and the longitudinal bar of the precast U-beam, respectively.

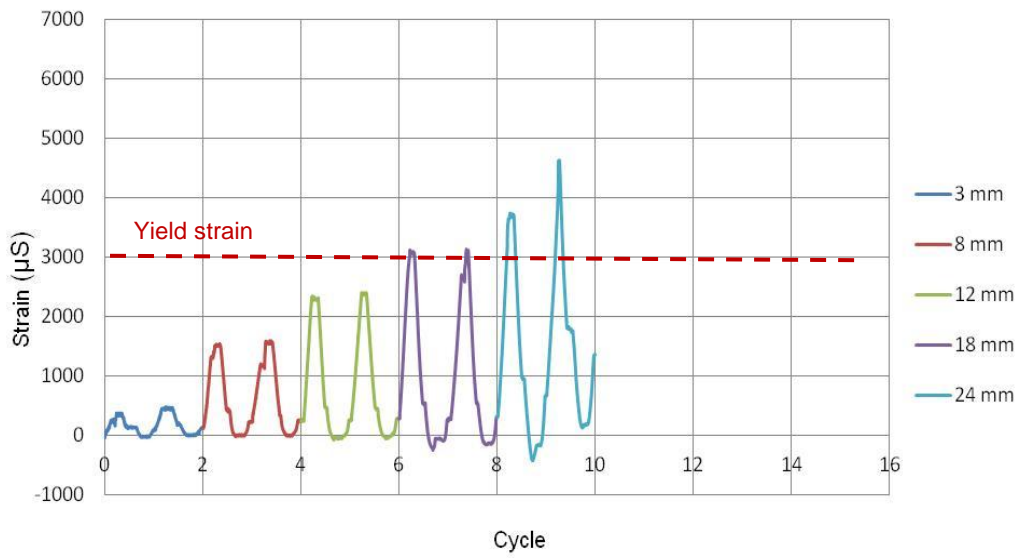


Figure 5-21 Strain response of the top interlocking bar of the beam in Specimen P2

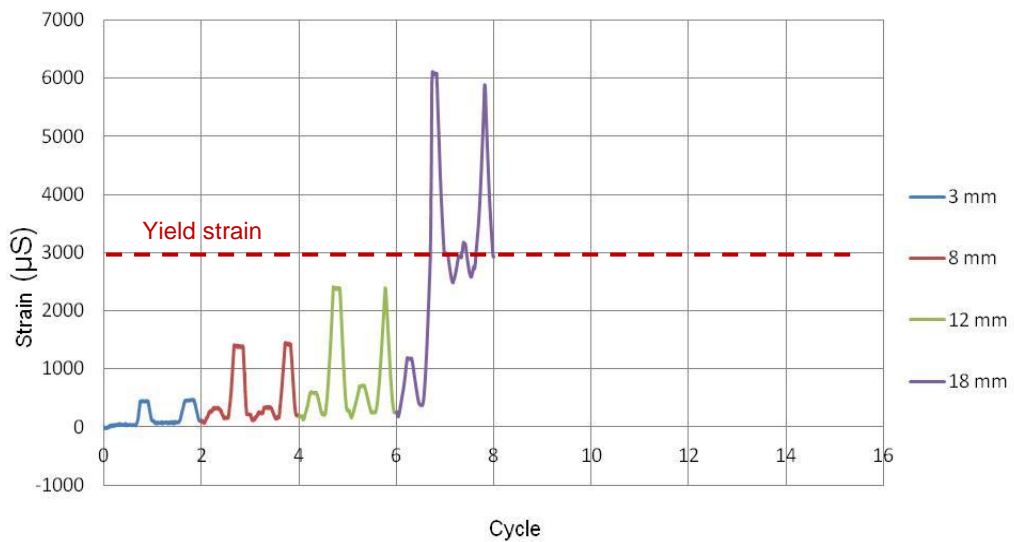


Figure 5-22 Strain response of the bottom interlocking bar of the beam in Specimen P2

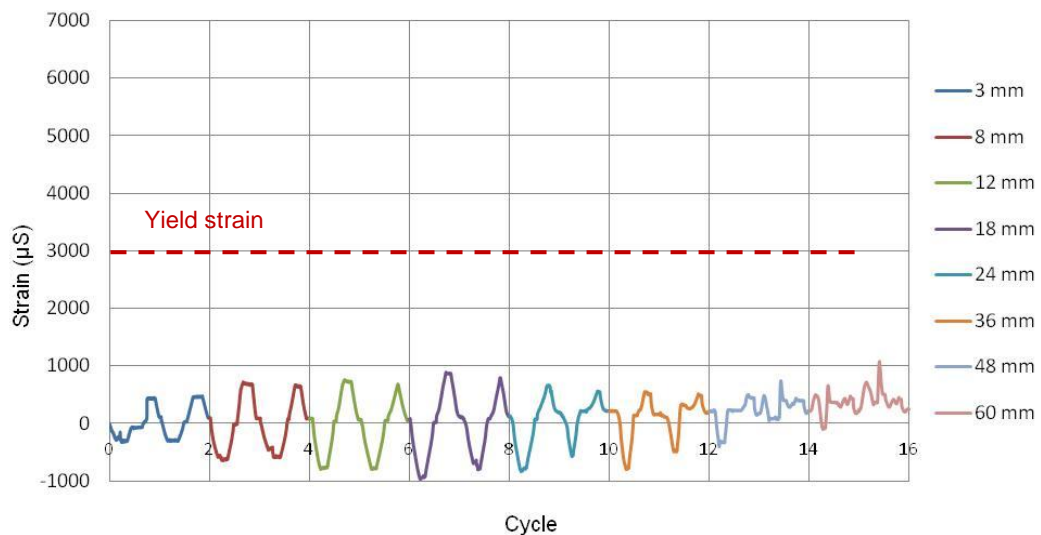


Figure 5-23 Strain response of the longitudinal bar of the precast U-beam in Specimen P2

As can be seen in Figure 5-21 the top interlocking bars (represented by SG1) started to yield at the displacement level of 18mm under negative loading (downward). In positive loading, the top interlocking bars did not experience yield strain until the specimen failure.

On the other hand, the bottom interlocking bar (SG2) experienced yield strain at the displacement level under positive loading (upward). Figure 5-22 shows that this bar always experienced tensile strain throughout the test. In contrast with the top interlocking bar, the bottom interlocking bars never yielded in the negative loading.

Both SG1 and SG2 malfunctioned after reaching the yield phase. Figure 5-21 and Figure 5-22 show that after the deflection level of 24mm the strain gauges did not work properly.

Different from SG1 and SG2, SG3 (the strain gauge of the longitudinal bar of the U-beam) did not yield until the specimen failed (see Figure 5-23). The strain varied between -1000 and 1000 micro strain which were much lower than the yield strain (i.e. 3000 micro strain). This is because the longitudinal bars of the U beam were not connected to the joint-core (they

were discontinued or stopped at the column face) which was unable to transfer the stresses to the joint core.

5.5.3.2 The longitudinal bars of the column

Figure 5-24 and Figure 5-25 present the strain response of the longitudinal bar of the precast column which was subjected to the cyclic loading. The column was designed to remain elastic during loading to ensure the plastic hinge occurred in the beam (strong column-weak beam principle). It can be seen in Figure 5-24 the longitudinal bar of the column still remained elastic with the strain varying between -200 and 250 microstrain, which means the longitudinal bar of the column did not yield throughout the test.

From the strain data (SG5) it can be concluded that when the negative loading (downward) was applied, the longitudinal bars of the column experienced tensile strain, which meant tensile stresses worked on them and the column bent to the right. Similarly, when the positive loading (upward) applied, the column would bend to the left.

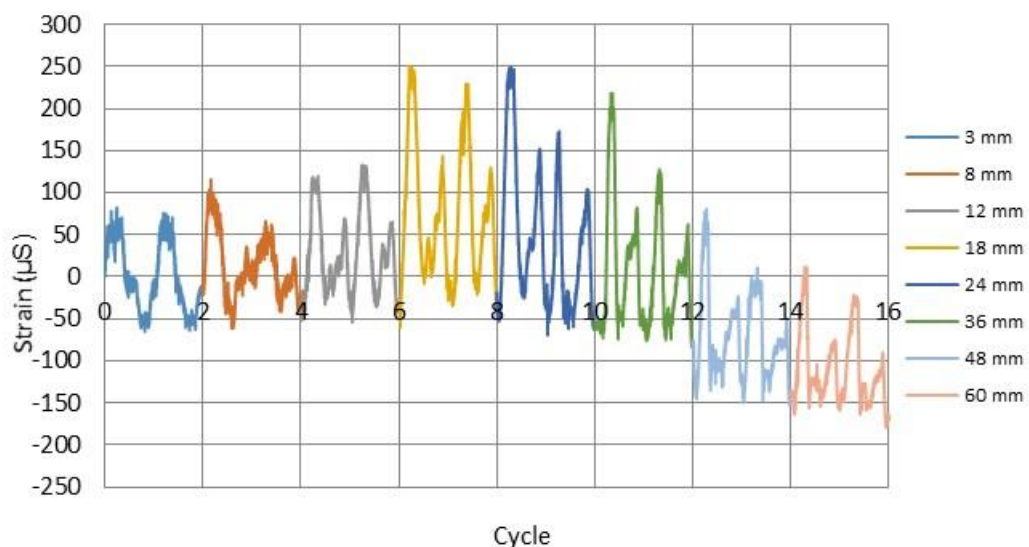


Figure 5-24 Strain response of longitudinal bar of the precast column of Specimen P2

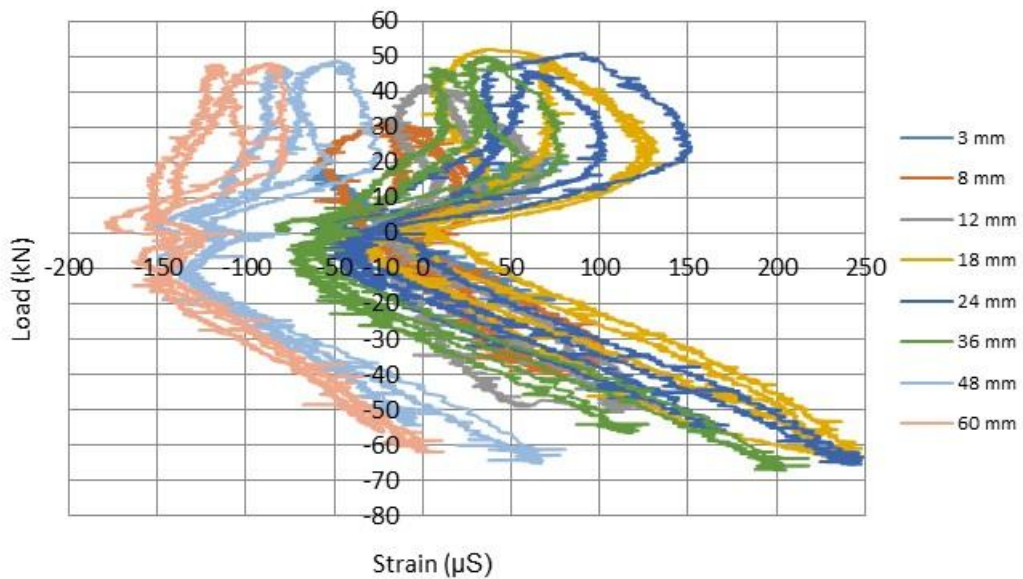


Figure 5-25 Load vs. strain response of longitudinal bar of the precast column of Specimen P2

5.5.3.3 The stirrup of the joint core

Two stirrups were installed in the joint core of Specimen P2. Figure 5-26 and Figure 5-27 present the strain response of the joint core stirrup (top part) in Specimen P2. The stirrup experienced tensile strain in both loading directions. The strains of the stirrup under negative loading are higher than those under positive loading which is related to the position of the observed stirrup (it was the top stirrup in the joint core). Evaluation of the strain data up to the beam-column specimen failure showed that the strain of the stirrup never reached yield strain. It means that the spacing stirrups of 100mm in the joint core were enough to resist the shear force during the test.

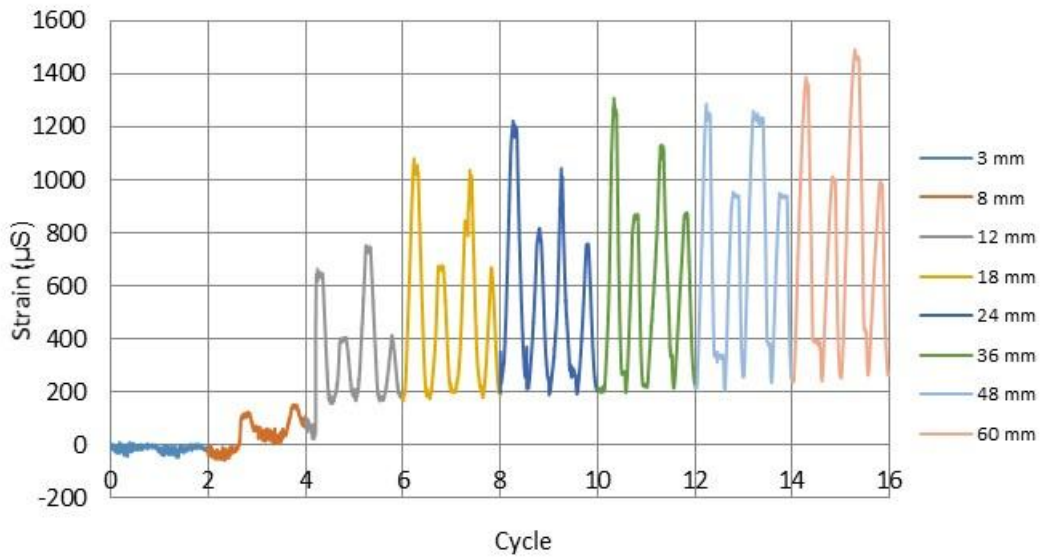


Figure 5-26 Strain response of the joint stirrup (top) in Specimen P2

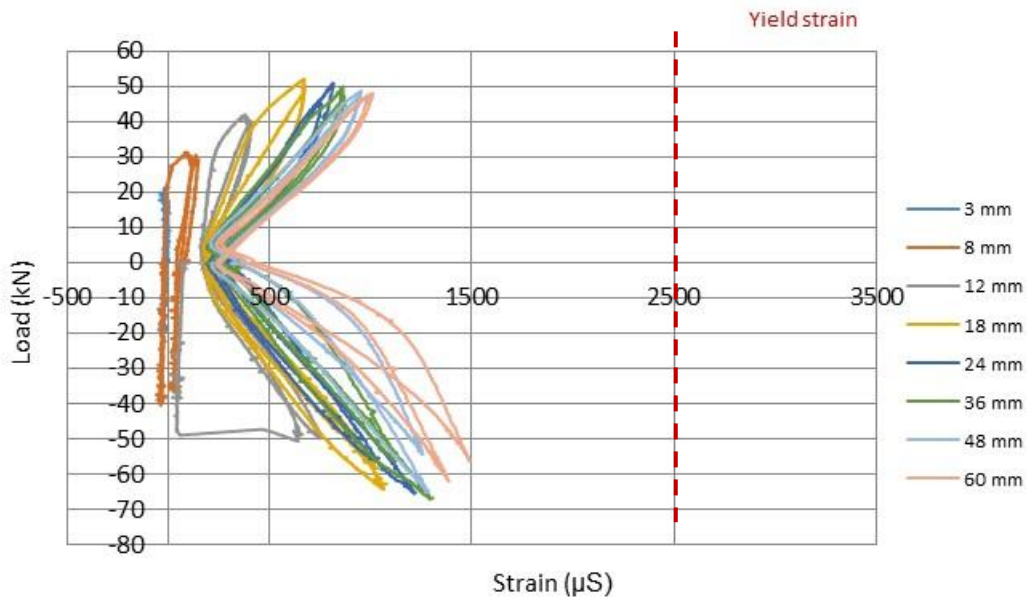


Figure 5-27 Load vs. strain response of the joint stirrup (top) in Specimen P2

From the analysis above, it can be concluded that only the top and bottom interlocking bars reached the yield phase during the test while the other reinforcement bars remained elastic. It showed that the beam, particularly

the beam end adjacent to the column face, was a weaker part of the joint system which allowed the plastic hinge to form. This fact also confirms that the beam-column joint specimen P2 fulfilled the strong column-weak beam principle.

5.6 Conclusions

Based on the result of the Specimen P2 test, several conclusions can be made:

1. Specimen P2 performed well under quasi-static loading. The connection exhibited a flexural failure mode and behaved monolithically until failure.
2. The first crack occurred on the top surface of the beam core at a load of 15kN during the first cycle of loading. The cracks propagated on the beam and were typically flexural cracks. These cracks occurred within the connection region and in the wall of the U-precast beam.
3. Even though the loading produced an 'X' crack pattern in the joint core of Specimen P2 under quasi-static loading, no more cracks developed in the joint core after the deflection level of 36mm; after 36mm, the cracks were concentrated in the beam adjacent to the column (the plastic hinge was formed in the beam). At this stage the stirrups in the joint core were still elastic whereas the interlocking bars in the beam had a strain that was much larger than the yield strain. This shows that the design meets the strong column-weak beam principle.
4. The structural behaviour of Specimen P2 under a quasi-static loading was evaluated using ACI 374.1-05 (Acceptance Criteria for Moment Frames Based on Structural Testing and Commentary), in terms of the strength degradation, relative energy dissipation ratio and the

stiffness degradation. The evaluation shows that the beam-column connection satisfies the acceptance criteria in ACI 374.1-05.

5. The length of the interlocking bars, with the development length of 800mm from the column face, are considered enough to distribute the internal stresses in the beam column connection under cyclic loading. The interlocking bars experienced yield strain at the displacement level of 18mm in both loading directions.
6. Similar with Specimen P1, there was a good bond between the precast concrete and the cast-in-situ concrete in Specimen P2 at least until the yield phase. At this stage (i.e. the deflection level of 18mm), analytical calculations have been performed on the composite beam section of Specimen P2 and generated the theoretical maximum loads (negative and positive) which are very similar with the experimental maximum load (less than 2% of differences).

Chapter 6

Precast Concrete Beam-Column Connection Incorporating with Steel Fibre Reinforced Concrete

6.1 Introduction

The next stage of this study was to investigate the effect of steel fibre reinforced concrete (SFRC) as the cast-in-place (CIP) connection on the structural behaviour of the precast concrete beam-column connection.

PCBC Specimen P2 satisfied the requirements stated in the ACI Code. However, Specimen P2 showed several cracks in the cast-in-place connection before testing, i.e. the cracks on the concrete surface and the interface between the wall of the precast U-beam and the beam core, which were caused by plastic shrinkage and drying shrinkage. In addition, the hysteresis loops of Specimen P2 seemed to have similar pattern with the hysteresis loops presented in Figure 6-1(a) rather than Figure 6-1(b), so theoretically, the joint behaviour was controlled by the bond slip of the longitudinal bars within the joint core. Because of that, there was still a possibility to improve the performance of the joint and hence, steel fibres were introduced.

SFRC has very good mechanical properties in comparison with the plain concrete (no steel fibre), especially in terms of tensile strength, shrinkage, etc. Also it has been shown that the use of SFRC in structures, particularly in beam-column connections, improves the seismic performance in terms of shear strength, ductility and energy dissipation (Naaman and Reinhardt, 2003; Parra-Montesinos, 2005).

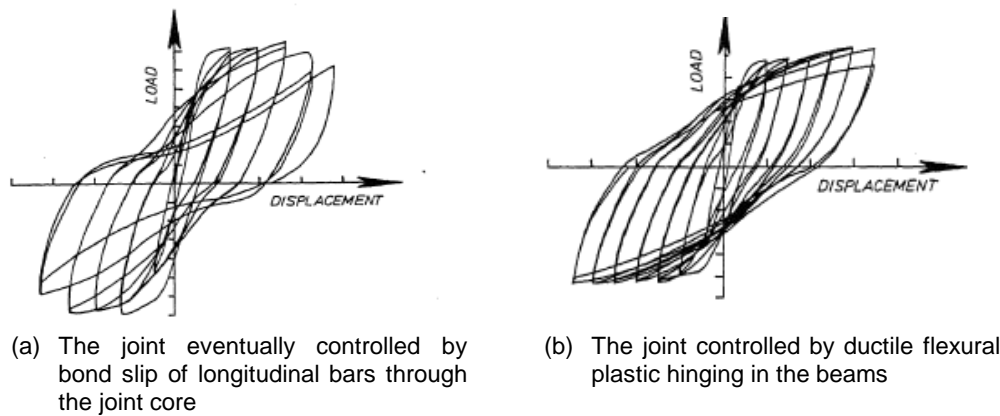


Figure 6-1 Typical measured hysteresis loops for reinforced concrete beam-column sub-assemblages Park (1988)

The aim of this study was to introduce the steel FRC as the cast-in-place material in the PCBC connection, in order to improve the joint behaviour in terms of the initial cracks and crack propagation, energy dissipation and ductility, without the need for additional bars, which would potentially cause reinforcement congestion in the connection.

This chapter presents the test results of the precast concrete beam-column connection incorporating SFRC as the CIP-connection. The investigated steel fibre volume fractions (V_f) were 0.5% (Specimen P3) and 1% (Specimen P4). As with Specimen P2, Specimen P3 and P4 were subjected to a quasi-static loading. The results of both beam-column joints were then compared to those of Specimen P2 (the beam-column connection with the plain concrete; $V_f = 0\%$, as CIP-connection). This was to understand the effect of percentage of steel fibre in the CIP-connection to the structural behaviour of precast concrete beam-column connection, in terms of the energy dissipation, the stiffness degradation and crack-propagation.

Beam-column specimens P3 and P4 are identical to beam-column Specimen P2 (barring the CIP concrete) having the same details in terms of the reinforcement detail, the location of strain gauges and procedure of

making and building elements in the laboratory. The details are presented in Chapter 3.

6.2 Material

The material composition used for the concrete mixes of the precast concrete elements for beam-column specimens P3 and P4 were identical to those of Specimen P2. While, there were differences in the material composition of the CIP-concrete in terms of the amount of steel fibres used in the concrete mix. Table 6-1 shows a comparison of the material proportion of the CIP-concrete of specimens P2, and P3 and P4. Table 6-2, Figure 6-2 and Figure 6-3 show the specification of the steel fibres used in this study.

Table 6-1 Material composition of CIP-connection of specimens P2, P3 and P4

Materials	P2	P3	P4
Coarse aggregate (kg/m ³)	1028.4	1028.4	1028.4
Fine aggregate (kg/m ³)	685.6	685.6	685.6
Cement (kg/m ³)	441	441	441
Water (kg/m ³)	210	213	213
Steel fibre (kg/m ³)	-	39.25	78.5
Slump	165	150	85
w/c	0.47	0.52	0.52

Table 6-2 Properties of the steel fibres

Brand	Dramix RC 65 35 BN
Length (l_f)	35 mm
Diameter (d_f)	0.55 mm
Aspect ratio (l_f/d_f)	65
Tensile strength	1345 N/mm ²
Young's Modulus (E_{mod})	210000 N/mm ²



Figure 6-2 Steel fibres

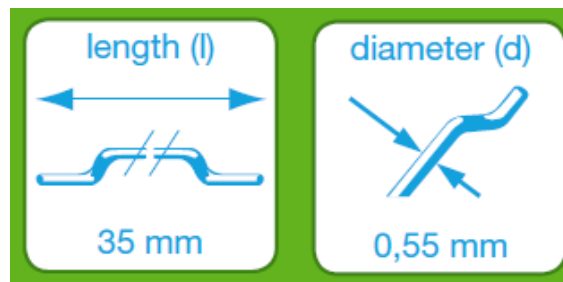


Figure 6-3 Dimensions of the steel fibre

The CIP connection of Specimen P3 contained 0.5% steel fibre by volume, while Specimen P4 used 1.0% steel fibre in the CIP-connection. These percentages were chosen based on existing literature, to present the affectivity of steel fibres to structural behaviour of the precast concrete beam-column connection.

Soubra and Naaman (1993) concluded that an adequate improvement in cracking can be achieved using only 30-40 kg/m³ steel fibre dosage. While Paine and Peaston (2002) determined that 1 - 2% volume fraction (V_f) of the steel fibre is an ideal value to adequately improve the performance of the reinforced concrete beams. Hartman (1999) tested 12 steel fibre reinforced concrete (SFRC) beams using Dramix-65/35-BN type steel fibre. Two different dosages of steel fibre, i.e. 60 kg/m³ and 90kg/m³ were used in that study. The conclusion was the SFRC beams having 60 kg/m³

of steel fibre have a greater ratio of the measured ultimate load to the theoretical ultimate load. Altun et al. (2007) also investigated the effect of steel fibre dosage on the mechanical properties of concrete and RC beams. They compared two different compressive strengths (C20 and C30) and 3 different steel dosages (0 kg/m^3 , 30 kg/m^3 , 60 kg/m^3). Generally, the highest value of the mechanical properties of concrete (compressive strength, split tensile strength, modulus of elasticity) and the measured ultimate load of reinforced concrete beams is achieved using concrete with 60 kg/m^3 steel fibre dosage. However, there is only a slight improvement in the compressive strength and modulus of elasticity between the specimens with steel fibre dosage of 30 kg/m^3 and those of 60 kg/m^3 .

6.3 Test Results

6.3.1 Mechanical properties of concrete

In this section a comparison of the mechanical properties of concrete used for making the beam-column joint specimens is made. The properties of compressive strength, modulus of elasticity and modulus of rupture are considered.

6.3.1.1 Compressive strength

Table 6-3 presents the average cube strength of the precast units and the CIP connection for Specimen P2, P3 and P4.

Even though the concrete mixes of the precast concrete elements had the same material proportion (see Table. 3-4 in Chapter 3), the compressive strength varied. This was because the moisture content of aggregate material (coarse aggregate and sand) was different for each mix. The

moisture condition of the aggregates depend on the porosity of the aggregates and the moisture condition of the storage area. Commonly, aggregates will have a moisture content which is either below or above the absorption limit; the absorption of the aggregate is the amount of water that will be absorbed. The moisture content of the aggregate can increase or decrease the water-cement-ratio and affect the strength and durability of the concrete. The standard deviation of the concrete used for each element varies between 0.87 and 5.09. The average of the compressive strength of the concrete presented in Table 6-3 satisfied requirements stated in BS8110, as presented in Equation (6-1).

$$f_m = f_k + k \times s \quad (6-1)$$

- where, f_m = target mean strength
 f_k = characteristic strength (i.e. 30MPa for precast elements and 45MPa for CIP-connection)
 k = constant (k=1.64 for defective level of 5%)
 s = standard deviation

Table 6-3 Average of compressive strengths

Specimen		Average Compressive Strength (MPa)	Standard Deviation (MPa)
P2	Beam	40.95	5.09
	Column	55.87	2.51
	CIP	50.86	0.87
P3	Beam	36.82	1.15
	Column	42.83	2.62
	CIP	47.36	1.29
P4	Beam	50.58	2.29
	Column	51.35	3.75
	CIP	60.26	1.29

The compressive strength of the precast concrete varies between 36.82MPa (P3-Beam) and 55.87MPa (P2-Column). The compressive strength of the CIP-concrete varies between 47.36MPa (P3-CIP) and 60.26MPa (P4-CIP). The compressive strength of the CIP-concrete in each beam-column specimen unit was always higher than the precast beams.

6.3.1.2 Modulus of elasticity

The modulus of elasticity test was obtained using cylinder specimens (dia. 150mm and height 300mm). Table 6-4 presents the average modulus elasticity of each mix.

The modulus of elasticity of the precast elements varied between 28GPa and 31.3GPa, while the CIP connection varied between 31.518GPa and 42.679GPa.

Table 6-4 Average modulus of elasticity

Specimen		Average of Modulus of Elasticity (GPa)
P2	Beam	30.697
	Column	28.940
	CIP	31.518
P3	Beam	30.461
	Column	28.009
	CIP	33.782
P4	Beam	31.304
	Column	29.841
	CIP	42.679

6.3.1.3 Modulus of rupture/flexural strength

Four-point bending tests were carried out to obtain the flexural strength of the concrete beam/prism. The prisms ($100 \times 100 \times 500 \text{ mm}^3$) were simply supported; the prism span was 300mm. Particularly for the CIP connection of Specimen P3 and P4, which contained steel fibres, an LVDT was placed at the mid-span of each prism to measure the deflection. Figure 6-4 presents the setup of the flexural test of the prism. The load and deflection of the prism were recorded throughout the test. The flexural strength, also known as the Modulus of Rupture, is calculated according to Equation (6-2) below,

$$f_t = \frac{Pl}{bh^2} \quad (6-2)$$

With reference to Equation (6-2) and Figure 6-4,

P = maximum load of test

b = the prism width = 100mm

h = the prism height = 100 mm

l = the prism span = 300mm

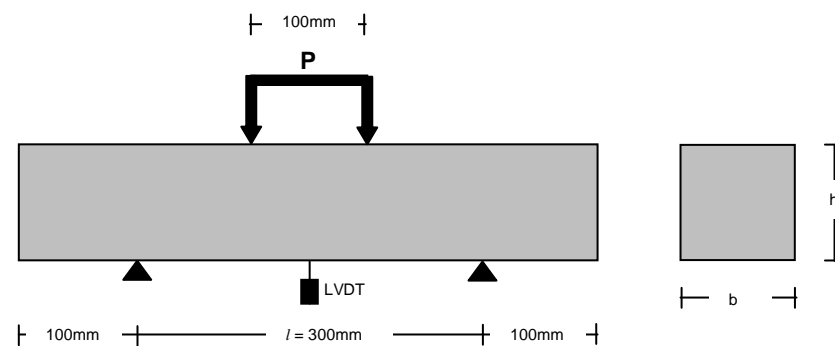


Figure 6-4 Flexural test set-up



(a) Plain concrete



(b) Steel fibre reinforced concrete

Figure 6-5 Failure mode of the flexural test of the prism

Figure 6-5 shows the failure mode of the prism concrete. The plain concrete prisms ($V_f = 0\%$) failed suddenly once the first crack occurred and fractured into two parts. On the other hand, the FRC prisms exhibited cracks but did not fully fracture (the load was stopped once the primary crack formed). This is because the random steel fibres bridge the cracks, control the cracks from developing and widening through the de-bonding and pulling-out mechanism (Maidl and Dietrich, 1995) and so no sudden fracture occurred.

Table 6-5 shows the average modulus of rupture of the different parts of the beam-column specimens P2, P3 and P4. Figure 6-6 presents the

load-deflection curves of the three parts of Specimen P3 (i.e. the precast column, precast beam and the CIP connection). The load-deflection curves for Specimen P4 are presented in Figure 6-7.

For each type of concrete, 3 prisms were tested; for the cast-in-situ concrete, CIP P3 consisted of CIP P3-1, CIP P3-2, CIP P3-3 (number 1, 2 and 3 denoted the number of the flexural tests, i.e. there were 3 in total). CIP P4 consisted of CIP P4-2, CIP P4-3; unfortunately, there was a data failure in the recording of the load - deflection of the CIP P4-1 test.

Table 6-5 Average modulus of rupture (MOR)

Specimen		Average of MOR (MPa)	SD (MPa)
P2	Beam	4.03	0.23
	Column	5.42	0.78
	CIP	5.99	0.11
P3	Beam	5.36	0.24
	Column	5.21	0.41
	CIP	6.06	0.18
P4	Beam	5.88	0.10
	Column	5.65	0.22
	CIP	7.76	1.30

From Figure 6-6 and Figure 6-7 it can be seen that the plain concrete (precast beam and column of specimens P3 and P4) is a brittle material, with a sudden failure as the first crack occurred. This means that the first-crack load is the peak load.

A better performance was observed for the steel fibre reinforced concrete (SFRC) used in the CIP connection of the PCBC specimens P3 and P4. The curves for the CIP of P4 ($V_f = 1.0\%$) showed that, after cracking the load continued to increase. Once the peak load was achieved, the load decreased gradually with the beam exhibiting significant deflection. Whereas, the CIP connection curve of Specimen P3 ($V_f = 0.5\%$) showed

that after cracking, the load decreased gradually accompanied by large deflection. Both SFRC material with $V_f = 0.5\%$ and 1.0% showed better ductility in comparison to the plain concrete material.

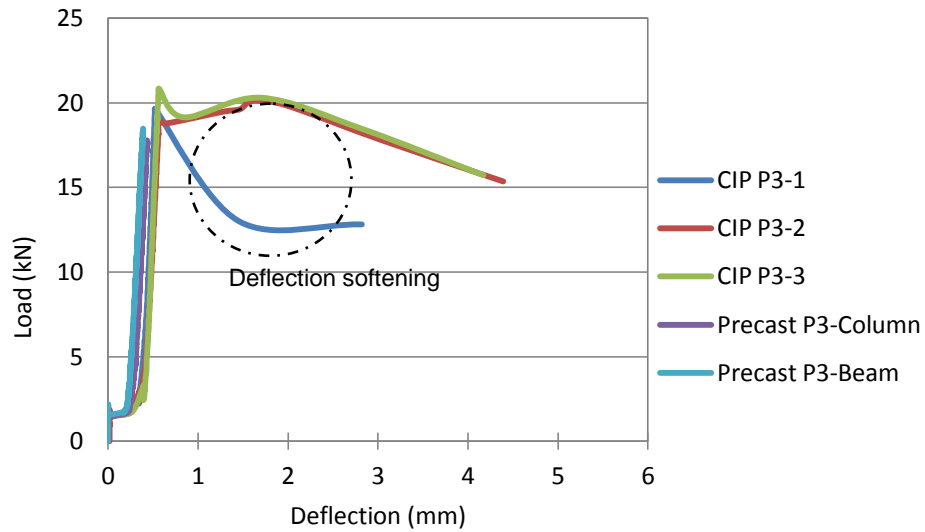


Figure 6-6 MOR test of PCBC Specimen P3

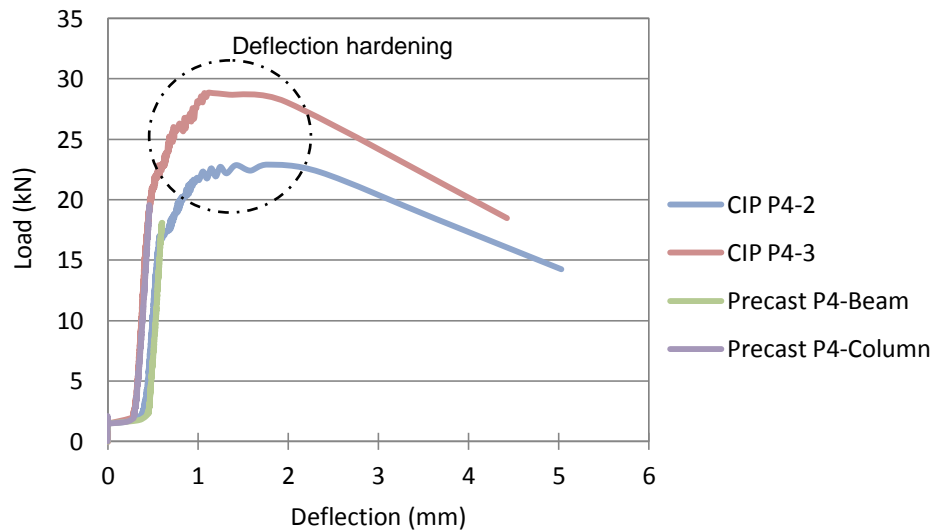


Figure 6-7 MOR test of PCBC Specimen P4

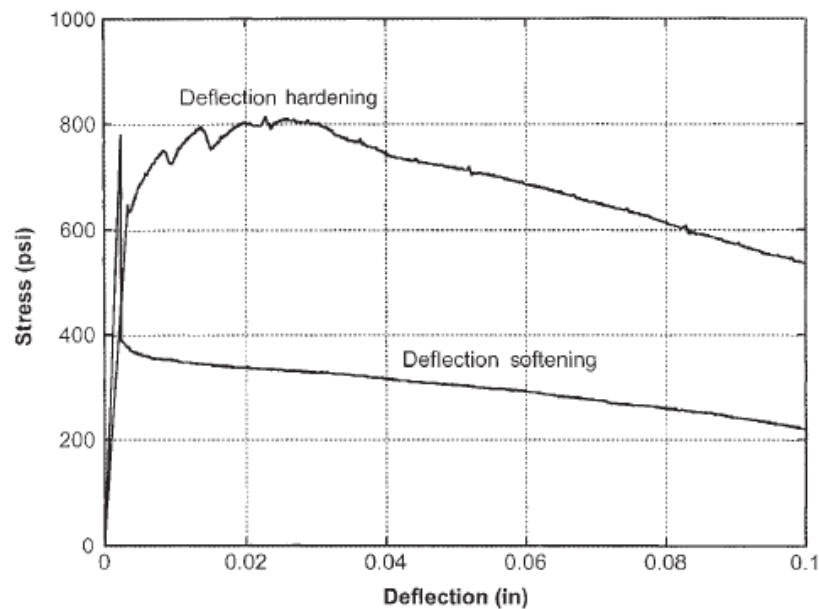


Figure 6-8 Deflection-hardening and deflection-softening behaviour (Naaman and Reinhardt, 1996)

The post-cracking behaviour of fibre reinforced concrete (FRC) under flexure can be classified into either deflection-hardening or deflection-softening, as presented in Figure 6-8 (Naaman and Reinhardt, 1996).

Referring to this classification, the CIP connection curves of Specimen P4 could be categorized as deflection-hardening, as the peak load was higher than the first-crack load. The CIP connection curves of Specimen P3 could also be categorized as deflection-hardening, even though the first-crack load and the peak load are similar. However, CIP P3-1 curve (Figure 6-6) showed deflection-softening behaviour. This was thought to be because the upper-side of the prism of CIP P3-1 when casting (i.e. the weak side of the prism) was placed in the machine so that it became the loaded (compression) face. ASTM C 1609 requires that the prism should be placed in the machine such as the parts of the prism in contact with the mould when casting are on the top and bottom; this ensures that the effect of any weak concrete resulting from the casting and floating process is reduced.

Table 6-6 Comparison of the mechanical properties of the CIP connection of the PCBC specimens

	P2 ($V_f = 0\%$)	P3 ($V_f = 0.5\%$)	P4 ($V_f = 1.0\%$)	Increase compared to Specimen P2 (%)	
				P3	P4
Average of compressive Strength (MPa)	50.86	47.36	60.26	-6.88	18.48
Average of MOR (MPa)	5.99	6.06	7.76	1.17	29.55
Average of MOE (MPa)	31518.93	33782.16	42679.92	7.18	35.41

Table 6-6 presents a comparison of mechanical properties of the CIP connection. Adding 0.5% of steel fibre by volume to the concrete only caused a slight increase in comparison with plain concrete in terms of the compressive strength, modulus of rupture and modulus of elasticity (i.e. -6.88%, 1.17% and 7.18%, respectively). However, adding 1.0% of steel fibre by volume of concrete increased the compressive strength, modulus of rupture and modulus of elasticity significantly (i.e. 18.48%, 29.55% and 35.41%, respectively).

A slight decrease in terms of the compressive strength (i.e. -6.88%) of the CIP-P3 concrete was caused by the amount of water added to the concrete mix. As can be seen in Table 6-1, the CIP-P3 mix contained more water (i.e. 213kg/m³) compared with the CIP-P2 mix (i.e. 210kg/m³). This was done in order to maintain the workability of the fresh concrete due to the inclusion of the steel fibres.

The effect of steel fibres on the compressive strength is not too significant. Oh (1992) found that the compressive strength increase was about 17% when steel fibres ($V_f = 2\%$) were added to the concrete, and less than 10% at $V_f = 1\%$. Altun et al. (2007) found that the addition of 30kg/m³ of steel fibre decreased the compressive strength of C30 concrete by approximately 11.5%. It can be concluded that a fibre volume fraction of

0.5% by volume (i.e. 39.35kg) caused a small effect on the compressive strength.

6.3.1.4 Energy absorption

The energy which could be absorbed by the specimen during the loading can be calculated as it is equal to the area under the load-deflection curves (Shannag and Ziyad, 2007). Energy absorption also indicates how much energy of the structural members to damage when subjected to static or dynamic load (Marthong and Marthong, 2016). Figure 6-9 presents a comparison of the load-deflection curves for the SFRC prisms with $V_f = 0.5\%$ (CIP P3) and 1.0% (CIP P4). It is observed that the area under the load-deflection curves of the SFRC specimen with $V_f = 1.0\%$ had the largest area, followed by the SFRC specimen with $V_f = 0.5\%$.

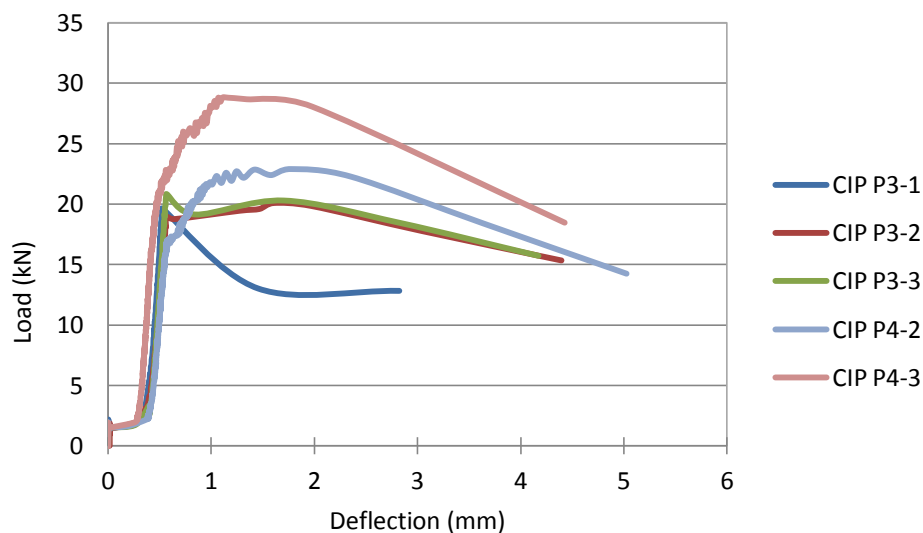


Figure 6-9 Load-deflection comparison between CIP connections of Specimen P3 ($V_f = 0.5\%$) and P4 ($V_f = 1.0\%$)

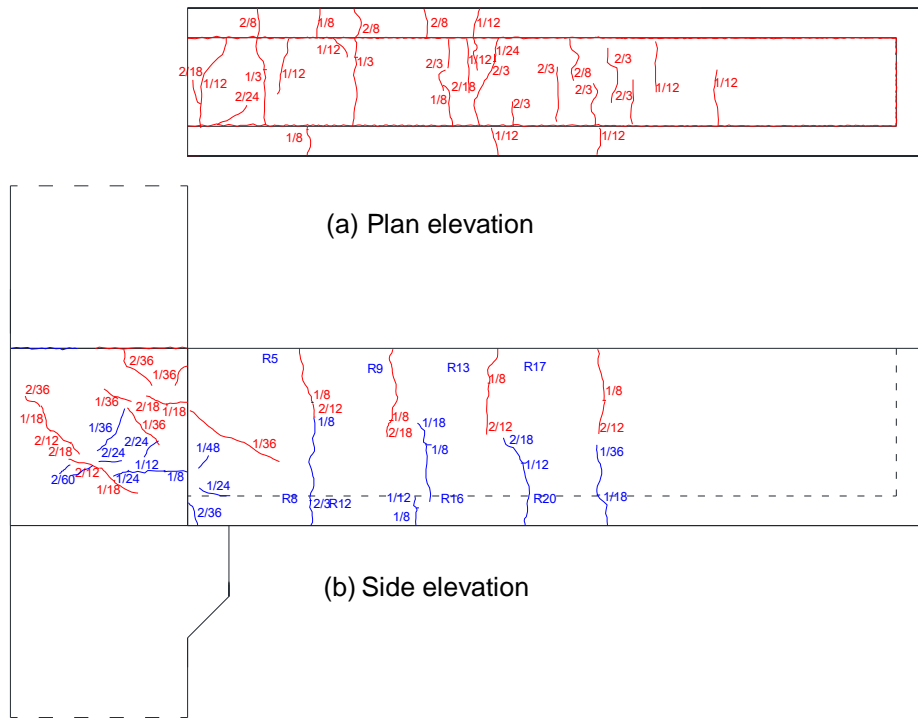


Figure 6-11 Crack pattern of beam-column Specimen P4

6.3.2.2 Load-Deflection Curves

The load-deflection hysteretic loops of the PCBC connections of Specimen P2, P3 and P4 are presented in Figure 6-15, Figure 6-16 and Figure 6-17, respectively. The load was applied at the beam tip, and the deflection was measured at the beam tip. Table 6-7 presents a comparison of the peak load at every cycle for specimens P2, P3 and P4.

After the testing of the PCBC specimens P3 and P4, and once the experimental data was analysed, it was discovered that there were errors in the output of the load cell of the positive loading (upward direction). This resulted in reduced positive loads at all deflection levels. The load-deflection loops containing the errors are presented in Figure 6-13 and Figure 6-14.

Fortunately, after each specimen P3 and P4 was tested, the load cell of the positive loading was calibrated. Hence, a scale factor could be

determined which allowed to modify the load data. Scale factors of 1.7 and 1.65 were obtained for the positive loading of specimen P3 and P4, respectively. The positive load data were then adjusted by multiplying all the positive loads with the scale factor – assuming a linear relationship. The result of the adjusted load-deflection loops of specimens P3 and P4 are presented in Figure 6-16 and Figure 6-17.

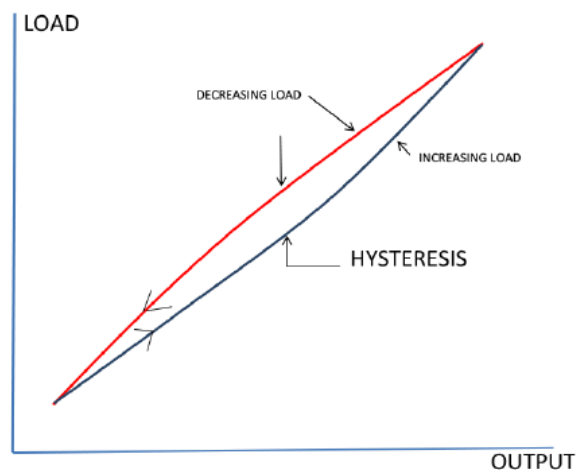


Figure 6-12 Applied load vs. load cell output readings (National Weighing & Sampling Association, 2013)

The assumption of a linear relationship was also investigated and it was found that when applying the cyclic load the load cell did not work linearly (see Figure 6-12). This means that by multiplying the output loads by the scale factor, smaller load-deflection loops than the actual response will be generated. As such, the actual energy dissipation of specimens P3 and P4 will be bigger than those presented in Figure 6-16 and Figure 6-17. The implication of this modification in terms of the stiffness degradation and the energy dissipation will be discussed later in Section 6.3.2.3 and 6.3.2.4.

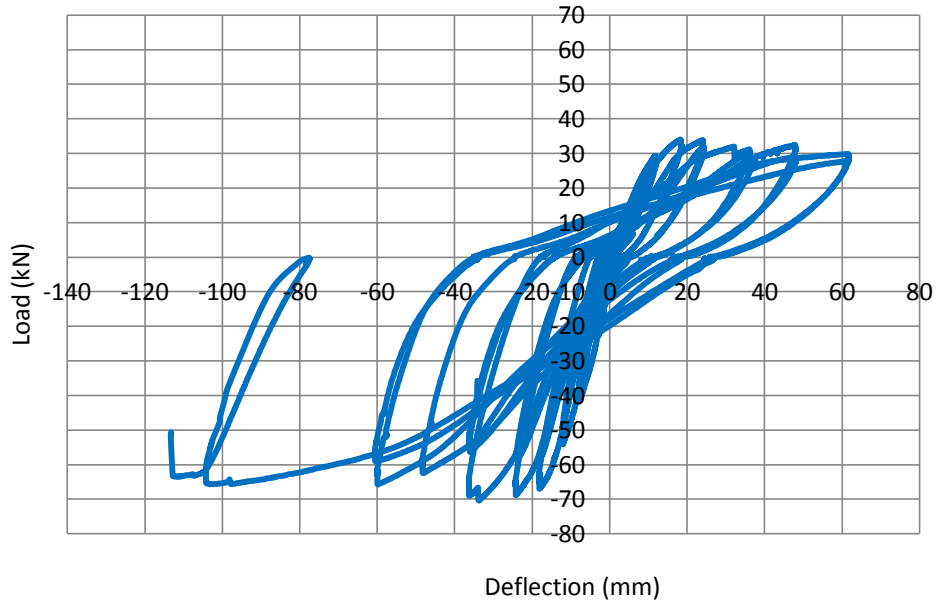


Figure 6-13 Load-deflection hysteresis loops of PCBC Specimen P3 containing the errors in the positive load

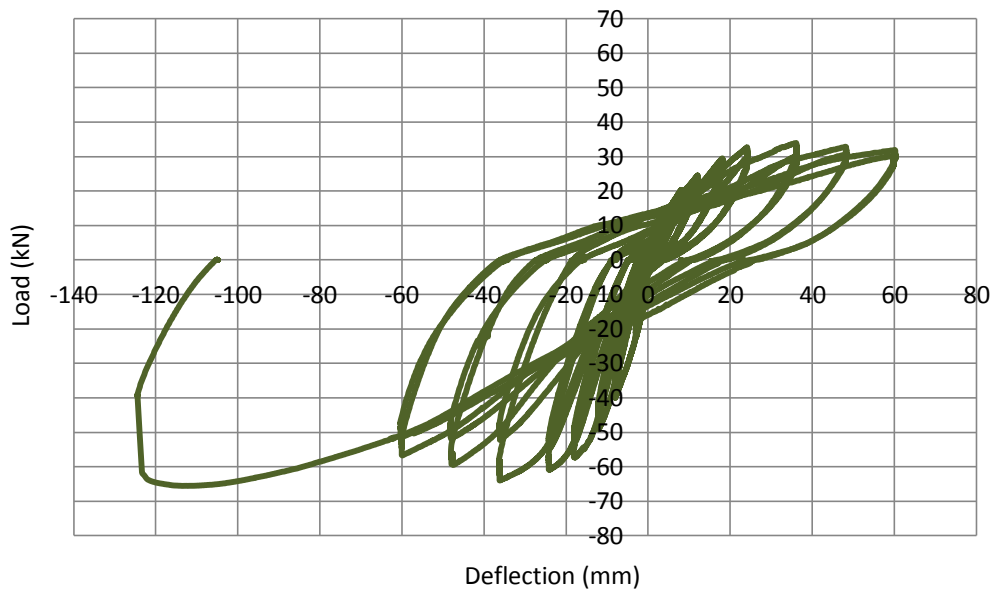


Figure 6-14 Load-deflection hysteresis loops of PCBC Specimen P3 containing the errors in the positive load

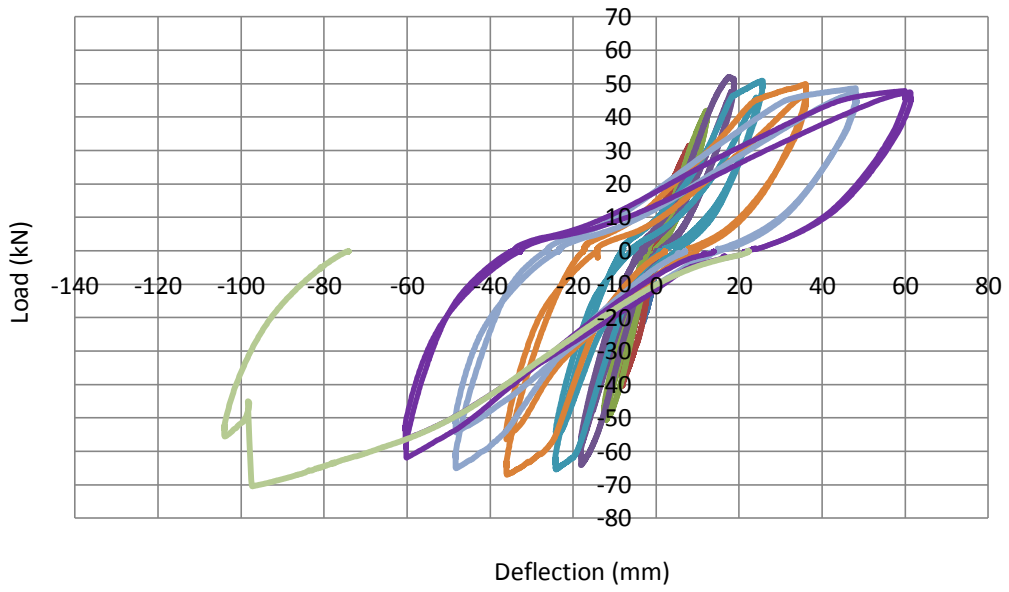


Figure 6-15 Load-deflection hysteresis loops of PCBC Specimen P2

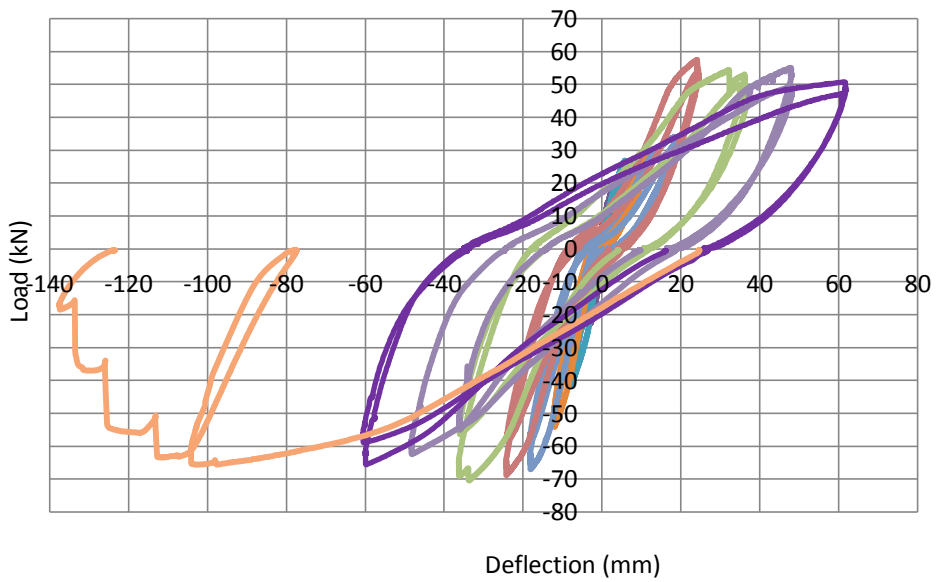


Figure 6-16 Load-deflection hysteresis loops of PCBC Specimen P3

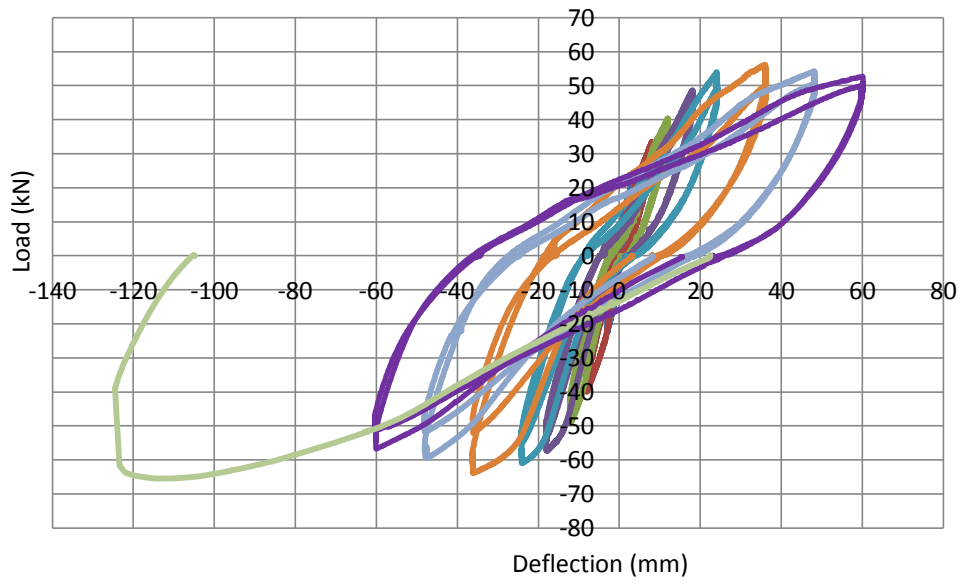


Figure 6-17 Load-deflection hysteresis loops of PCBC Specimen P4

6.3.2.3 Stiffness degradation

Stiffness degradation in this study was measured using the secant stiffness (K_{sec}) principle (peak-to-peak stiffness), which were calculated at every displacement level (3, 8, 12, 18, 24, 36, 48 and 60mm). Secant stiffness is defined as the slope of the straight line between the maximum load of the positive and negative direction, at the last cycle of each displacement level or drift ratio level (Ertas et al., 2006; Said and Nehdi, 2004). Figure 6-18 describes how to calculate the secant stiffness. Table 6-8 presents the secant stiffness of beam-column specimen P2, P3 and P4 at the last cycle of each displacement level. The values presented in Table 6-8 were plotted as a stiffness-deflection relationship as presented in Figure 6-19, and used to compare the stiffness degradation of the beam-column specimens from one cycle to the following cycle.

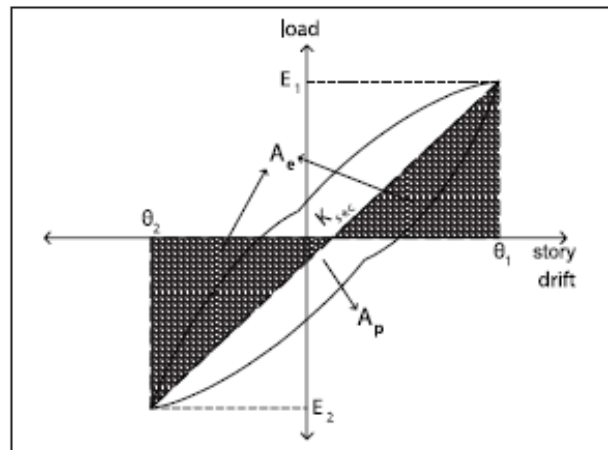


Figure 6-18 Secant stiffness (Ertas et al., 2006)

Table 6-8 Secant stiffness of specimen P2, P3, P4

Deflection (mm)	Stiffness (kN/mm)		
	P2	P3	P4
3	6.063	6.621	6.867
8	4.133	3.815	4.221
12	3.657	3.235	3.496
18	2.937	2.504	2.738
24	2.116	2.335	2.107
36	1.43	1.378	1.405
48	1.052	1.165	1.061
60	0.86	0.881	0.846

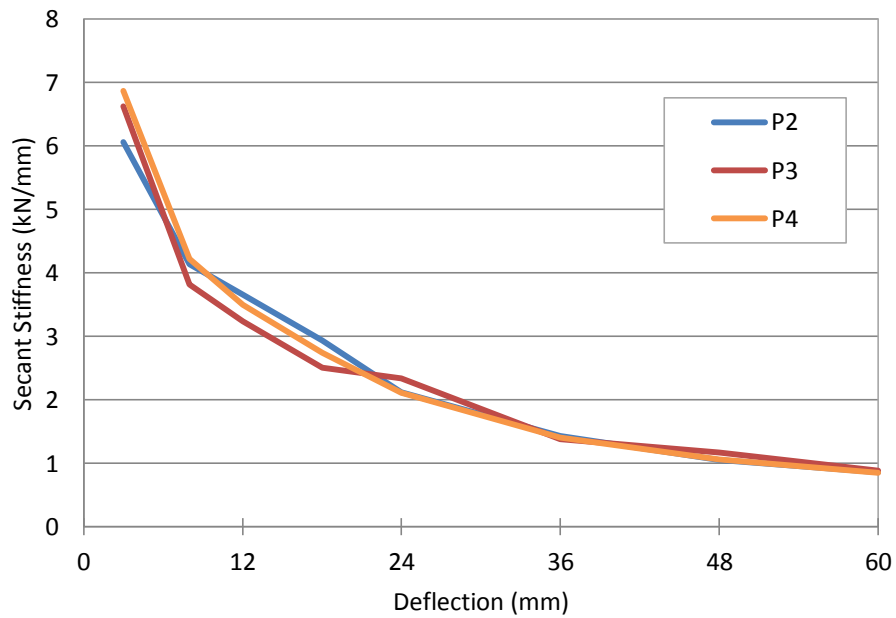


Figure 6-19 Secant stiffness degradation of the PCBC specimens

Figure 6-19 shows that as the deflection increases, the stiffness decreases. The stiffness degradation of specimens P2, P3 and P4 have a similar pattern, particularly at higher displacement level, from 36mm to 60mm of displacement. At the beginning of the test (the deflection level of 3mm), P4 had the highest secant stiffness.

The effect of steel fibre on the stiffness degradation was only apparent at the beginning of test (from deflection level of 3mm to 24mm), (see Figure 6-19). From deflection level of 36mm to 60mm, the curves appear similar. However, the connection with steel fibres absorb more energy (the loops were fatter in comparison with the connection without steel fibre). More energy absorption is also indicated by the extended flatter part of the curve representing the plastic behaviour.

This finding is also in agreement with Ganesan et al. (2014a) and Marthong and Marthong (2016). Ganesan et al. (2014a) studied the effect of hybrid fibres (a combination of steel crimped fibres and polypropylene fibres) on the structural behaviour of exterior beam-column joints. There were 12 High Performance Concrete (HPC) joints subjected to cyclic loading, with variations in the fibres as: (i) crimped steel fibre ($V_f = 0.5\%$ and 1%); (ii) polypropylene fibres ($V_f = 0.1, 0.15$ and 0.2%), as presented in **Table 6-9**. As can be seen in Figure 6-20, they found that the addition of the hybrid fibres improved the initial stiffness of the joint. HHRHPC5 specimen (1% of steel fibres and 0.15% of polypropylene fibres) has the highest initial stiffness. The polypropylene fibres bridge the micro cracks whereas the steel fibres intercept the macro cracks.

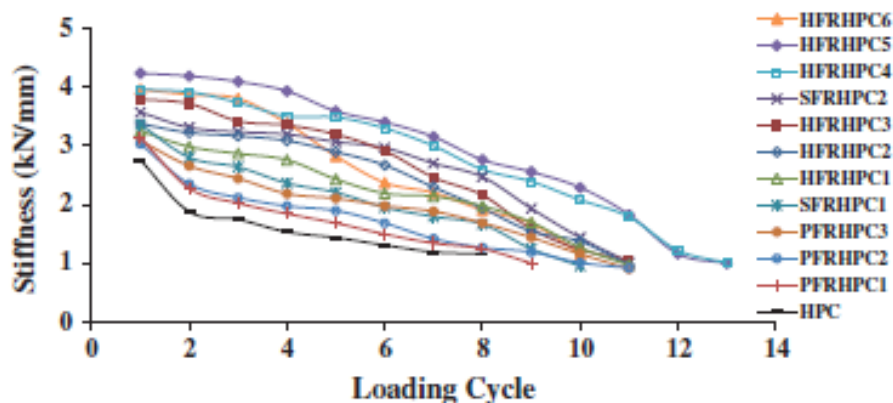


Figure 6-20 Stiffness degradation (Ganesan et al., 2014a)

Table 6-9 Detail of specimens (Ganesan et al., 2014a)

No.	Designation of specimens	Volume fraction of fibres (%)	
		Steel	Polypropylene
1	HPC	0	0
2	PFRHPC1		0.10
3	PFRHPC2		0.15
4	PFRHPC3		0.20
5	SFRHPC1	0.5	0
6	HFRHPC1		0.10
7	HFRHPC2		0.15
8	HFRHPC3		0.20
9	SFRHPC2	1	0
10	HFRHPC4		0.10
11	HFRHPC4		0.15
12	HFRHPC4		0.20

Marthong and Marthong (2016) studied the effect of the addition of Polypropylene Terephthalate (PET) fibre-reinforcement to the concrete, which was only applied in the joint region. Six exterior beam-column specimens were cast and tested. Three of them were reference specimens, namely: beam weak in flexure (BWF), beam weak in shear (BWS) and column weak in shear (CWS). Three similar specimens were cast with the addition of PFRC in the joint region, namely BWFSF, BWSSF and CWSSF. Figure 6-21 presents the effect of fibres on the stiffness degradation. It can be seen that the PET fibres improved the initial stiffness of the joint.

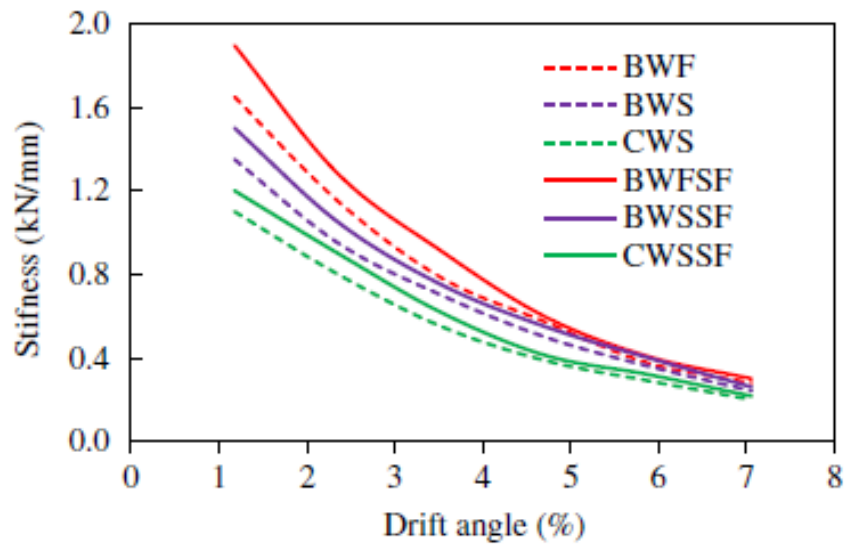


Figure 6-21 Stiffness degradation (Marthong and Marthong, 2016)

6.3.2.4 Energy dissipation

The energy dissipation of a structure indicates the ability of a structure to resist the earthquake loading through inelastic deformation. Greater energy dissipation will improve the seismic performance of a structure.

Energy dissipation was calculated as the area enclosed by the hysteretic loops in the corresponding beam tip load vs. deflection graphs (Said and Nehdi, 2004; Parastesh et al., 2014). Cumulative energy dissipation during the reverse cyclic load test was calculated by summing the energy dissipated in consecutive load-displacement loops throughout the test (Said and Nehdi, 2004), as presented in Figure 6-22.

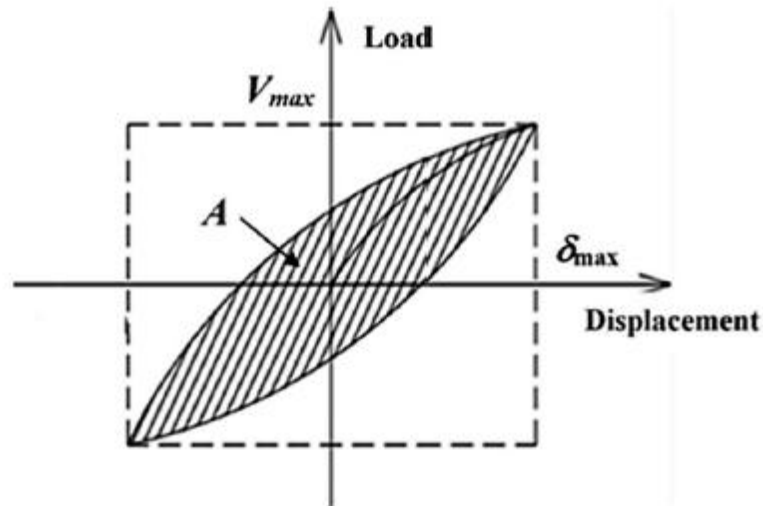


Figure 6-22 Definition of normalized dissipated energy normalizing hysteretic energy dissipation at each load cycle (Parastesh et al., 2014)

Figure 6-23 presents the cumulative energy dissipation (CED) of PCBC specimens P2, P3 and P4. It is clear that PCBC specimens with steel fibres had higher CED than PCBC specimen without fibres (Specimen P2). Here, it was found that all specimens had similar CED until the deflection level of 18mm, after that the curve of Specimen P2 dropped below that of the curves of specimens P3 and P4. The curve of Specimen P4 is approximately equal to that of Specimen P3 from the beginning of test, but P3 had slightly higher CED than P4 at the last deflection level (60mm).

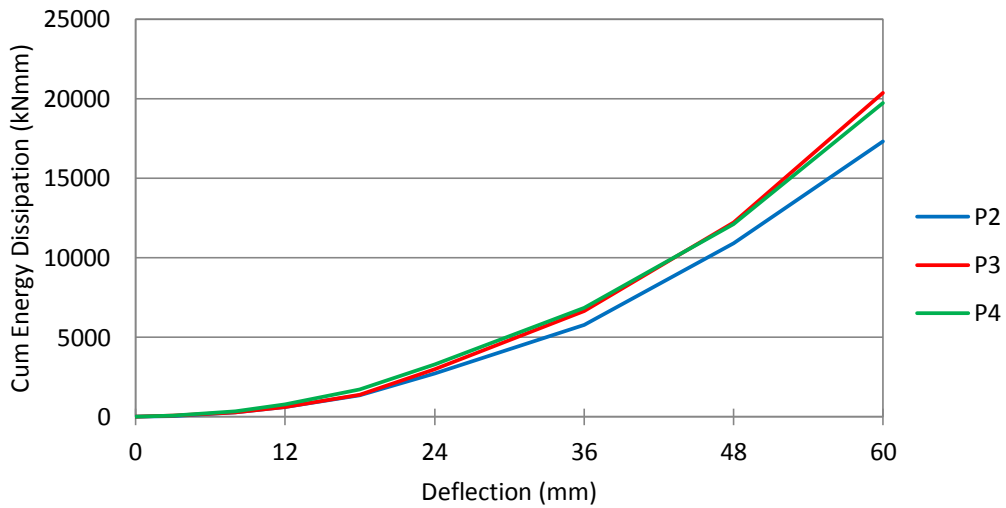


Figure 6-23 Cumulative energy dissipation of PCBC specimens

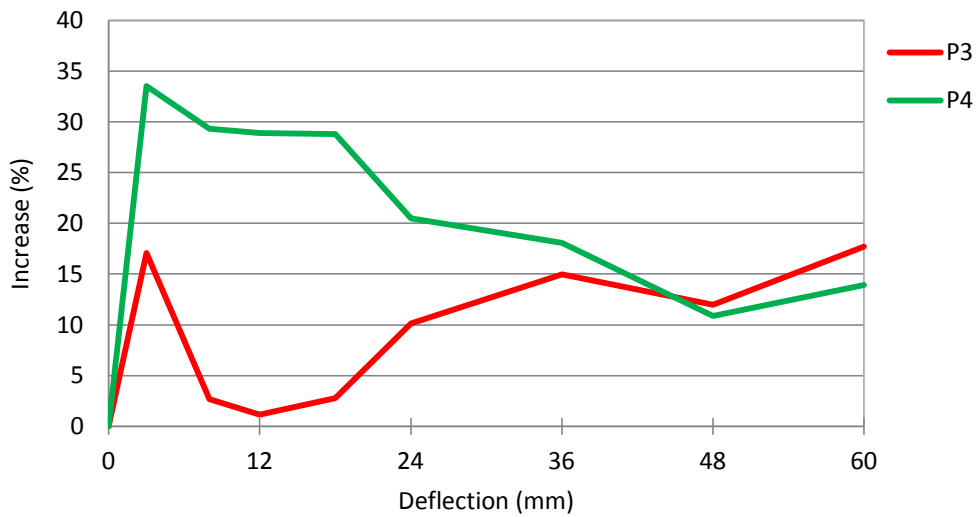


Figure 6-24 Percentage increase of cumulative energy dissipation (refer to Specimen P2)

Figure 6-24 illustrates the percentage increase in term of CED at each deflection level. It can be seen that Specimen P4 registered the highest increase of CED at the beginning of the test (at the deflection level of 3mm), after that the curve decreased as the deflection level increased. On the other hand, the percentage of Specimen P3 increased from a deflection level of 18mm to the end. It seems there was a problem in Specimen P4, which will be discussed in Section 6.4.2.2.

In order to eliminate the effects of the concrete strength variation in different beam-column specimens (see Table 6-3), the calculated energy dissipations were normalized with respect to the area of elastic-perfectly plastic rectangular block at each cycle using Equation (6-3) and Figure 6-22 (Parastesh et al., 2014; Hidalgo and Jordan, 1996).

$$\text{Normalized Energy Dissipation (NED)} = \frac{A}{4V_{max}\delta_{max}} \quad (6-3)$$

where:

V_{max} is the average of the maximum load.

δ_{max} is the average of displacement for positive and negative loading directions.

A is the area enclosed by the hysteretic loops (see Figure 6-22).

Figure 6-25 compares the normalising energy dissipation (NED) of PCBC specimens P2, P3 and P4. Specimen P4 has the highest result, particularly at the beginning of the test, where more cracks were developed at this stage. This can be seen by observing the crack propagation in Figure 6-26 as Specimen P4 had more cracks at the beginning of the test in comparison with other beam-column specimens.

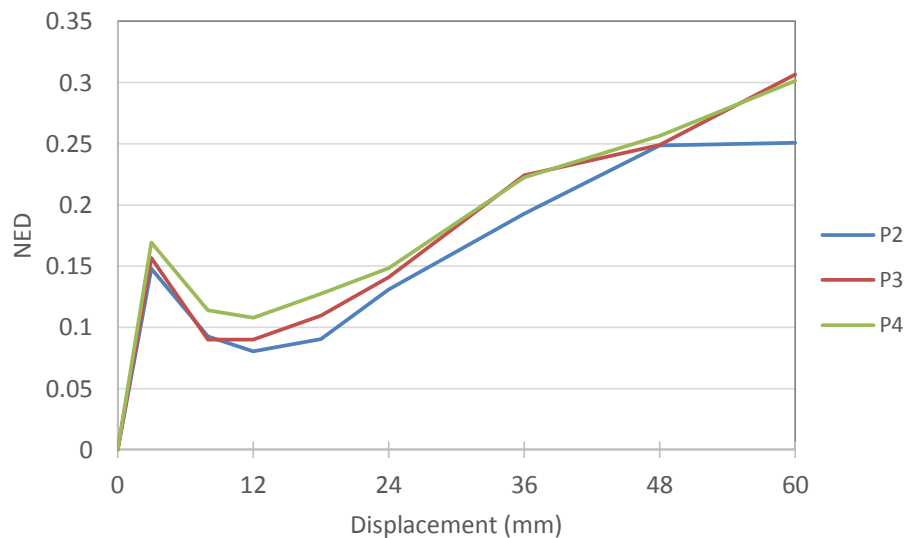


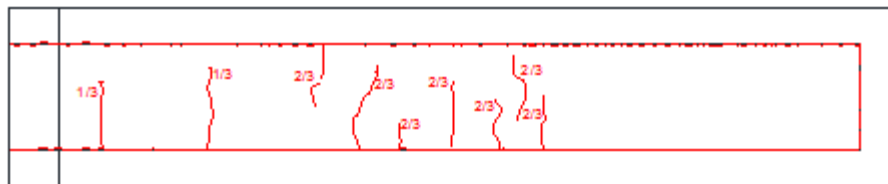
Figure 6-25 Normalized energy dissipation (NED) of PCBC specimens P2, P3 and P4



(a) Specimen P2



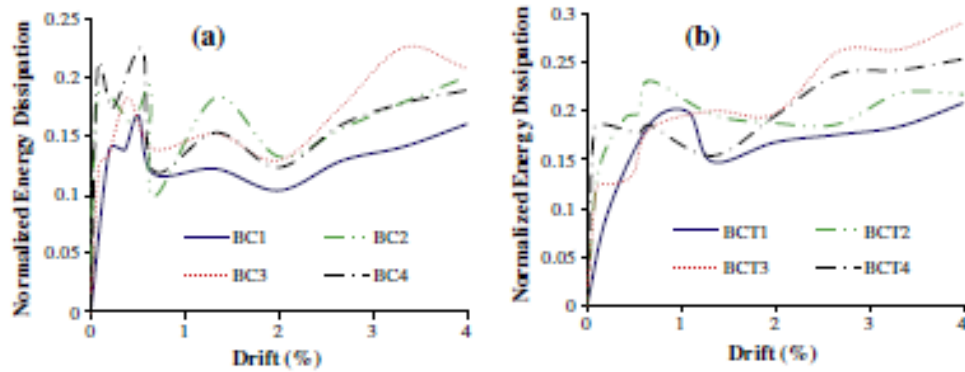
(b) Specimen P3



(c) Specimen P4

Figure 6-26 Crack-pattern on the top surface of the beam core (CIP-concrete) at the deflection level of 3mm

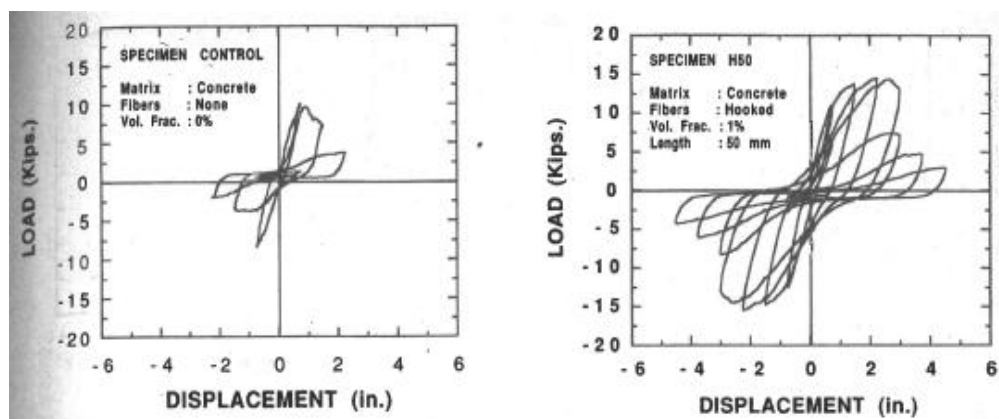
This result is also in agreement with Parastesh et al. (2014). They investigated the effect of the type of stirrups (open and closed) and the stirrup spacing in precast concrete beam-column connections. Figure 6-27 shows the normalized energy dissipation (NED) of the specimens. BC1 and BCT1 indicate the monolithic interior and exterior beam column joint, respectively, which were used as reference specimens. BC2, BC3 and BC4 are interior precast concrete beam-column specimens, whereas BCT2, BCT3 and BCT4 are exterior precast concrete beam-column specimens. Their conclusion was that all precast specimens had higher initial slope in corresponding NED and Drift ratio (see Figure 6-27), as initial cracks at the beam-column joint interface developed earlier in precast connections.



(a) interior connection (BC1 was monolithic) (b) exterior connections (BCT1 was monolithic)

Figure 6-27 Normalized energy dissipation capacity of PCBC specimens (Parastesh et al., 2014)

From Figure 6-23, Figure 6-24 and Figure 6-25, even though the curves of the specimens P2, P3 and P4 seem similar, there was a small increase in terms of the cumulative energy dissipation. However, these results are not as clear when compared with the results shown by Soubra and Naaman (1993). Figure 6-28 shows a comparison of the load-deflection curves between the precast beam-column sub-assemblages with cast-in-place connections without fibres (a) and with 1% of steel fibres (b). It is shown that there is a significant improvement in the load-deflection curve, which means in the energy dissipated as well. The possible problem in Specimen P4 will be discussed in Section 6.4.2.2.



(a) CIP connection with $V_f = 0\%$ (b) CIP connection with $V_f = 1\%$

Figure 6-28 Load-deflection curves of precast concrete beam-column specimens (Soubra and Naaman, 1993)

6.4 Discussion

This section discusses the evaluation of precast beam-column specimens using steel fibre reinforced concrete (SFRC) for the cast-in-place (CIP) connection in accordance with the acceptance criteria stated in ACI 374.1-05. It also discusses the effect of steel fibre content on the structural behaviour of the precast concrete beam-column (PCBC) specimens.

6.4.1 Beam-column connection behaviour with reference to the ACI Acceptance Criteria

The same calculation process has been performed for Specimens P3 and P4 as was done for Specimen P2 in Chapter 5.

Table 6-10 shows the ratio of the peak load at the second cycle (P_{2nd}) at the deflection levels of 36mm, 48mm and 60mm for each loading direction (positive and negative) to the maximum load (P_{max}). The peak loads for each cycle are also presented in this table. The results show that the ratio of P_{2nd}/P_{max} at the deflection levels of 36mm, 48mm and 60mm are higher than 75% of P_{max} for each direction and satisfy the acceptance criteria in ACI 374.1-05.

Table 6-11 presents the calculation of Relative Energy Dissipation (β) of Specimen P2, P3 and P4, analogous with the calculation of energy dissipation ratio for Specimen P2, which has done in Chapter 5. The hatched area is the area closed by the second cycle curve at the deflection level of 36mm (equal to 0.035 of drift ratio). The parallelogram is defined by the initial stiffness during the first cycle and the peak load (see Figure 5-2 in Chapter 5). The results are that all specimens have higher Relative Energy Dissipation Ratio than the minimum requirements.

Table 6-10 Ratio of the maximum load at the second cycle to the maximum load for each loading direction

Name of Specimen		P2	P3	P4	Conclusion
P _{max} at neg. direction		-67.00	-68.95	-63.79	
P _{max} at pos. direction		51.53	57.39	56.07	
Deflection (mm)	Loading direction	P _{2nd} /P _{max}			Acceptance Criteria: ≥ 0.75
36	Negative	0.84	0.82	0.82	Satisfy
	Positive	0.91	0.86	0.88	Satisfy
48	Negative	0.81	0.91	0.82	Satisfy
	Positive	0.91	0.86	0.89	Satisfy
60	Negative	0.84	0.85	0.81	Satisfy
	Positive	0.92	0.82	0.89	Satisfy

Table 6-11 Calculation of Relative Energy Dissipation Ratio (β)

PCBC Specimen	Hysteresis loop area (1)	Parallelogram area (2)	β (3)=(1)/(2)	
P2	1300	5781.01	0.23785	> 0.125
P3	1580	5905.45	0.26755	> 0.125
P4	1540	5926.58	0.25985	> 0.125

From Table 6-9 and Table 6-10, it can be seen that the maximum load and the hysteresis loop area of Specimen P4 is smaller than Specimen P3. This is an unexpected result considering Specimen P4 had a higher volume percentage of steel fibre than Specimen P3. The possible problem in Specimen P4 will be discussed in Section 6.4.2.2.

Table 6-12 presents the calculation of the ratio of the secant stiffness (peak-to-peak stiffness) to the initial stiffness for each direction at the first cycle of the applied load at the displacement level of 36mm (or equal to 0.035 of the drift ratio). The data of $K_{0.035}$, K and K' were taken from the load-deflection curves of each specimen.

Table 6-12 Ratio of the secant stiffness at a drift ratio of 0.035 to the initial stiffness

	P2	P3	P4
$K_{0.035}$	1.4306	1.3784	1.4058
K	5	5.5556	6.6667
K'	8.5714	8.5714	8.5714
$K_{0.035}/K$	0.28612	0.24811	0.210869
$K_{0.035}/K'$	0.16690	0.160814	0.164011

Table 6-13 Result of Specimen P2, P3 and P4 with reference to the Acceptance Criteria in ACI 374.1-05

Specimen Items	P2	P3	P4	Acceptance Criteria*
P_{2nd}/P_{max}				
Negative loading	0.84	0.82	0.82	≥ 0.75
Positive loading	0.91	0.86	0.88	≥ 0.75
β	0.23785	0.26755	0.25985	≥ 0.125
$K_{0.035}/K$	0.28612	0.24811	0.210869	≥ 0.05
$K_{0.035}/K'$	0.16690	0.16085	0.164011	≥ 0.05

* ACI 374.1-05

β = relative energy dissipation ratio

K and K' = initial stiffness for positive and negative loading for first cycle.

$K_{0.035}$ = secant stiffness at a drift ratio of 3.5%.

Finally, a summary of the ratio P_{2nd}/P_{max} , β , $K_{0.035}/K$ and $K_{0.035}/K'$ for all beam-column connections subjected to a quasi-static load are presented in Table 6-13. All results show that they satisfy the requirements of acceptance criteria in ACI 374.1-05.

6.4.2 The effect of the steel fibre in the CIP-connection on the behaviour of the beam-column connections

All PCBC specimens showed similar structural behaviour in terms of hysteretic load-deflection curves, secant stiffness degradation and the amount of dissipated energy during every cycle, as can be seen in Figure 6-15-Figure 6-25.

Table 6-14 Maximum load of specimens P2, P3 and P4 for each loading direction

Type of loading	P2	P3	P4	An increase compared to P2 (%)	
				P3	P4
Negative loading	67.00	68.95	63.79	2.96	-4.79
Positive loading	51.53	57.39	56.07	11.37	8.81

6.4.2.1 Comparison between P2 and P3

Specimen P3 with SFRC ($V_f = 0.5\%$) performed slightly better than Specimen P2. Specimen P3 achieved 2.96% (negative loading) and 11.37% (positive loading) greater maximum load than Specimen P2 (see Table 6-14).

This improvement was due to the existences of the steel fibres in the CIP-connection (the beam core and the joint core). This result is in good agreement with the mechanical properties of the CIP-connection material as presented in Table 6-6, which shows that there are increases in terms of modulus of elasticity and modulus of rupture due to the existences of the steel fibres.

6.4.2.2 Comparison between P3 and P4

From a comparison of the various cube strength (Table 6-6), it was found that by adding 1% steel fibre by volume to the concrete, the strength could be increased significantly. It was expected that Specimen P4 would perform better than Specimens P2 and P3 due to the greater fibre content. However, this was not the case which suggests that there was a problem with Specimen P4.

From the tests, it could be seen that there was a possible 'bonding' problem in PCBC Specimen P4, between the precast U-beam and the beam CIP core. When manufacturing the precast U-beam, the tape was stuck on some parts of the polystyrene (see Figure 6-29 (b)), instead of without tape on the polystyrene as have done on other beam-column specimens (see Figure 6-29 (a)). The tape might reduce the bond at the interface between the old concrete surface (the precast U-beam) and the new cast-in-situ concrete (the beam core). This has the potential of reducing the strength of the beam-column connection as composite behaviour may be lost.

This bonding problem affected the amount of energy absorbed in Specimen P4, so that it generated the lower energy dissipation in comparison with Specimen P3 (see Figure 6-23, Figure 6-25 and Table 6-11). This problem also caused the curve of Specimen P4 in Figure 6-24 to decrease (while the curve of Specimen P3 increased).



(a) Specimen P1, P2, P3, P5



(b) Specimen P4

Figure 6-29 Manufacturing the U-beam

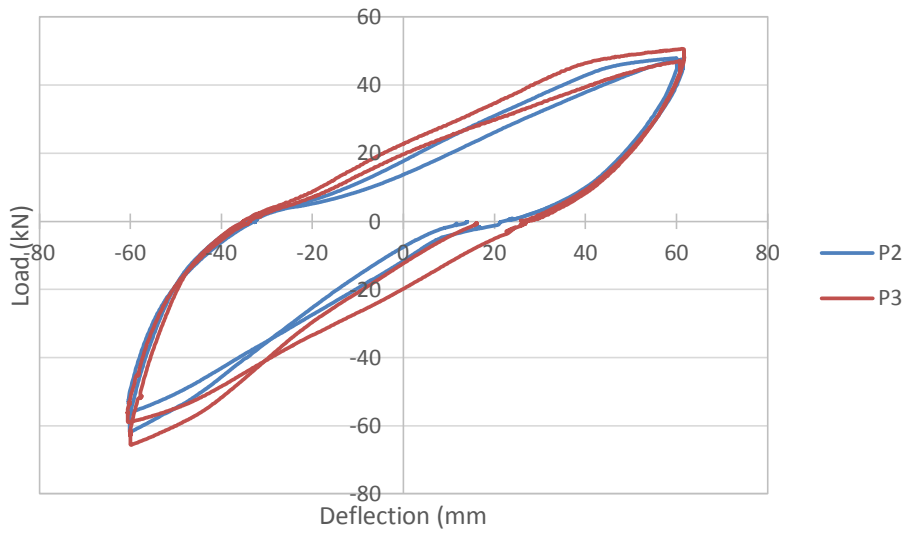
Steel fibres contained within the concrete performed should delay the crack propagation. As a comparison, the cracks on PCBC Specimen P2 (with plain concrete as CIP connection) appeared straight away and occurred at one load level (see Figure 6-30 (a)), whereas the cracks in Specimen P4 appeared shorter and spread-out on the surface (see Figure 6-30 (b)). This behaviour is in agreement with the data of the MOR test, which showed the first crack in the plain concrete ($V_f = 0\%$) is followed by a sudden-drop in the load-deflection curve (see Figure 6-7: precast concrete). On the other hand, when the first crack occurs in SFRC ($V_f = 1.0\%$), it is followed by a deflection hardening characteristic (see Figure

The existences of steel fibre in the concrete of the CIP-connection could improve the energy dissipation capacity of the PCBC joint. The analysis of the load-deflection hysteresis loops using CED and NED (see Figure 6-23 and Figure 6-25), shows that Specimen P4 has the highest value in terms of CED and NED in comparison with those of specimens P2 and P3.

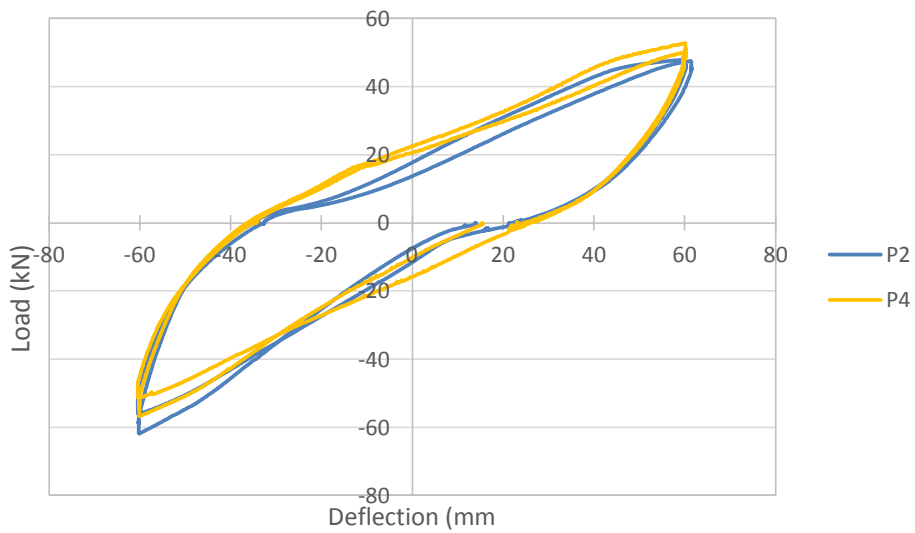
Figure 6-31 compares the load-deflection curves of the PCBC specimens P2, P3 and P4 at a deflection level of 60mm. It was found that the existence of steel fibres in the CIP connection caused a wider load-deflection loop, which also means the higher energy dissipation.

This behaviour is also in agreement with the study of Soubra and Naaman (1993). They tested four precast concrete beam-column connections with various fibre content. The PCBC specimens were subjected to a quasi-static loading. The result showed that the load-deflection curves of the highest fibre content ($V_f = 2\%$) had wider load-deflection hysteretic loops. In conclusion, the higher steel fibre content used in the CIP-connection in this study should give better structural behaviour in terms of the ductility and energy dissipation.

Mindess et al. (2003) and Van Chanh (2004) also concluded that the addition of fibres into the concrete are not there to improve strength (even though there is a little improvement), but primarily to control cracking and improve the toughness or energy absorption capacity. However, this did not really appear in Specimen P4 due to the bonding problem between the precast U-beam and the CIP beam core.



(a) Comparison between Specimen P2 and P3



(b) Comparison between Specimen P2 and P4

Figure 6-31 Load-deflection curves of Specimen P2 P3 and P4 at the displacement level of 60mm

The composite behaviour of the connection relies on the bond strength between the old (precast) concrete and the new concrete. In this study, the bond performance is presented by comparing the curvatures obtained from the electrical resistance strain gauges (attached on the interlocking

bars within the beam core) and the DEMEC gauges (attached on the concrete surface of the U-beam at Position I). The curvatures of specimens P2, P3 and P4 at the deflection level of 3mm, 8mm and 12mm (under negative loading) are presented in Figure 6-32. Those curvatures of the beam core and the precast U-beam are similar which suggests that the CIP beam core and the precast U-beam behaved compositely. However, under cyclic loading the bond strength decreased after the deflection level of 8mm.

As can be seen in Figure 6-32, the increase of steel fibre volume fraction in the CIP beam core decreased the curvature of the beam at the same load level, which is in agreement with the result of Lim et al. (1987) . The curves of Specimen P4 have the smallest differences, which means that the steel fibres increase the bond strength between the CIP beam core and the precast U-beam. This is because the steel fibres within the concrete decrease the drying shrinkage and reduce micro-cracks at the interface between the old and new concrete which lead to increase the bond strength of the interface.

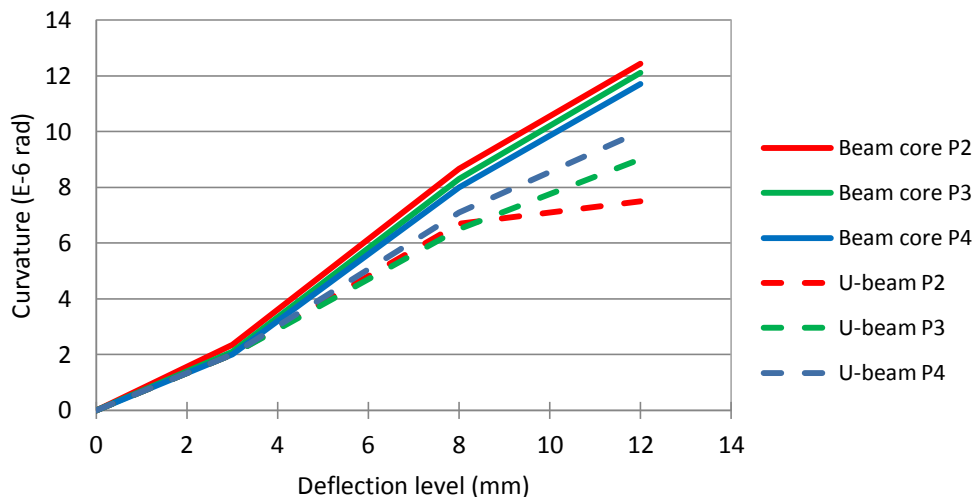


Figure 6-32 Curvatures of the beam core and the precast U-beam for specimens P2, P3 and P4

6.5 Conclusions

Based on the result of the Specimen P2, P3 and P4 tests, several conclusions can be made:

1. All beam-column specimens, which were subjected to a quasi-static loading, exhibited good structural behaviour and satisfied the acceptance criteria for moment resistant structures stated in ACI 374.1-05.
2. The use of steel fibre reinforced concrete in CIP-connection in this study was proven and can increase the energy dissipation and ductility of the exterior precast concrete beam-to-column connection.
3. The addition of 0.5% of steel fibre by volume could change the properties of concrete from a brittle material to a more ductile material with a little deflection-hardening characteristic (showed in MOR test). This means that once the tensile stress exceeds the tensile stress capacity of the concrete, the first crack occurred, but the steel fibres slowed-down the crack propagation.
4. The implementation SFRC with $V_f = 0.5\%$ as a CIP material in this study could improve the maximum load, stiffness degradation and energy dissipation in comparison with the precast concrete beam-column connection with plain concrete as a CIP.
5. Adding steel fibre by volume of 1.0% could change the properties of the CIP concrete from a brittle material to a more ductile material with deflection-hardening characteristic (showed in MOR test). This means that once the tensile stress exceeds the tensile stress capacity of the concrete, the first crack occurred, but the stress still increases. In the meantime, the steel fibres, which were spread out in the concrete-matrix, prohibit the crack extension until they were pulled-out from the matrix.

6. The implementation SFRC with $V_f = 1.0\%$ as CIP material in this study appears to improve the maximum load, stiffness degradation and energy dissipation, in comparison with either the precast concrete beam-column connection with plain concrete as CIP material (Specimen P2) or with SFRC-0.5% (Specimen P3). Unfortunately, the test result showed that the beam-column specimen with CIP material ($V_f = 1.0\%$) had a slightly lower value than the beam-column specimen with CIP material ($V_f = 0.5\%$); this was in terms of the maximum load, secant stiffness degradation and energy dissipation. This is thought to be due to the lower bond strength at the interface between the old concrete (the precast U-beam) and the new concrete (the beam core-CIP concrete), which was potentially reduced due to the tape which was stucked on the polystyrene when manufacturing the precast U-beam of Specimen P4, which caused a smooth surface inside of the precast U-beam.
7. However, it was clear from the tests that the steel fibres postponed and slowed down the crack propagation, resulting in the shorter cracks in the joint core and the top surface of the beam core of Specimen P4. This behaviour was in agreement with the deflection-hardening characteristic found from the MOR test.
8. By using NED, which eliminated the effects of the concrete strength variation and CED, the contribution of steel fibre with $V_f = 1.0\%$ in the CIP material of the precast beam-column connection (Specimen P4) showed the highest among other beam-column specimens.

Chapter 7

Precast Concrete Beam-Column Connection under Sustained Loading

7.1 Introduction

In the previous chapters, the static and quasi-static responses of the new precast concrete beam-column (PCBC) connections have been investigated. The conclusion was that the new PCBC joint performed well under both static and quasi-static loading. In order to get more complete information regarding the behaviour of the connection, the next study is to investigate the serviceability behaviour of the PCBC connection, i.e. under long-term loading.

Monitoring the long-term behaviour under a sustained load of reinforced concrete beams is important. The deflection of a beam under sustained load is affected by both shrinkage and creep; the deflection increases as the time increases. Many researchers have studied the behaviour of the beam-column joints under static and short-term loading. However, the information and knowledge about their long-term behaviour is still limited.

This chapter presents the behaviour of the PCBC connection (Specimen P5). The aim of this chapter is to investigate the structural behaviour of the precast concrete beam-to-column connection using interlocking bars under sustained load (Specimen P5), in terms of the deflection of the beam, both immediate and long-term deflections, and the crack-pattern. The experimental results of Specimen P5 will also be compared with those predicted by the theoretical approaches.

7.2 Detail of Test Specimen P5

PCBC Specimen P5 had the same geometry and reinforcement detail as those of Specimen P2, P3 and P4, (see Figure 3-4 and 3-6 in Chapter 3), as well as the same material composition as presented in Table 3-4 Chapter 3. There were 2 concrete mixes, i.e. for the precast concrete beam and column (a design compressive strength of 30MPa) and for the cast-in-place (CIP) connection (a design compressive strength of 45MPa).

7.2.1 Mechanical properties of the concrete

Several samples were made for each concrete mix in order to determine the mechanical properties. Table 7-1 shows the averages of compressive strength, modulus of elasticity and flexural strength of the concretes of Specimen P5.

Table 7-1 Average value of mechanical properties of concrete of Specimen P5

Mechanical properties	Precast Beam		Precast Column		CIP Connection	
	MPa	SD (MPa)	MPa	SD (MPa)	MPa	SD (MPa)
Average of Cube Strength	44.58	1.87	49.01	2.96	55.02	2.71
Average of Modulus of Elasticity	27000	2609	28600	1666	30700	910
Average of Flexural Strength	4.73	0.24	4.48	0.43	4.62	0.29

7.2.2 Test setup and instrumentation/loading procedure

7.2.2.1 Instrumentation and test setup

PCBC Specimen P5 had a similar test set-up and instrumentation to Specimen P1. The vertical load was applied on the beam end in the negative direction (downward), which represented the gravity load. While, there was no axial load applied on the precast column.

One LVDT was located under the beam end to measure the deflection of the beam. The data were recorded automatically every 15 minutes for 120 days of sustained loading.

Several DEMEC points were mounted on the surface of PCBC P5 in order to measure the strain of the concrete surface, as presented in Figure 7-8 and Figure 7-9. The measurement of the strains was taken manually using a digital DEMEC strain gauge at specific days.

7.2.2.2 Loading procedure

The long-term test of Specimen P5 was done according to the following procedure. A load from a hydraulic system was applied gradually at the beam end of PCBC Specimen P5 with the loading rate of 0.2-0.5 mm/min until a load of 20kN was reached, which was within the Serviceability Limit State (SLS) range for the joint, i.e. where the steel stress should be around 200MPa. Once attained, the load was sustained for 120days. During the test, the long term deflection and the strains of the concrete surface were taken in order to evaluate the behaviour of the beam-column connection under long-term loading. Also, the crack propagation was observed during the test.

7.3 Test Results

7.3.1 Immediate and long-term deflection

Figure 7-1 and Figure 7-2 present the immediate and the long-term deflection, respectively, of PCBC Specimen P5. The total deflection at the age of 90days consisted of the immediate and the long-term deflection. The immediate deflection was defined as the deflection that happened once a load of 20kN was applied to the beam, whereas the long-term deflection was the deflection that happened after a load of 20kN was sustained for 120days. Therefore, it can be specified that the immediate, the long-term, and the total deflection of PCBC Specimen P5 were 3.9mm, 6.2mm and 10.1mm, respectively.

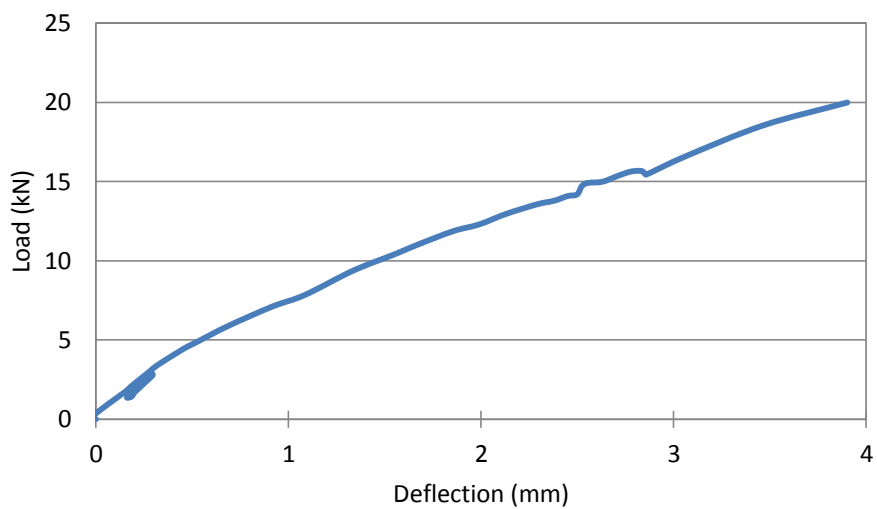


Figure 7-1 Load vs. deflection of Specimen P5 due to an initial load of 20kN (immediate deflection)

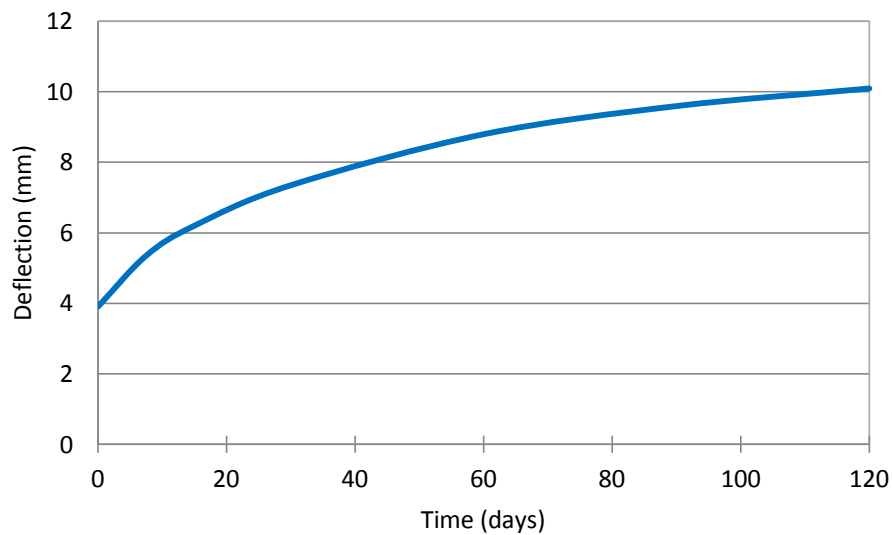


Figure 7-2 Long-term deflection of PCBC Specimen P5

7.3.2 Observation of cracking

Before the load was applied, several cracks had already appeared in Specimen P5, particularly in the beam core (cast-in-place connection) and the interface between the wall of the precast U-beam and the beam core. It is thought that these cracks occurred because of the restrained shrinkage of the concrete, either the internal shrinkage (due to the steel reinforcement) or the external shrinkage (due to the mould), which generated tensile stresses in the concrete. The initial crack widths located in the middle of the beam core length varied between 1-2 Divisions (i.e. 0.02-0.04mm), the width of the cracks located in the beam core (in line with the corbel tip) was 10 Divisions (i.e. 0.2mm). The width of the cracks at the interface varied between 5-10 Division (i.e. 0.1 – 0.2mm).

According to Nawy (2000), the shrinkage of the concrete can be distinguished become two types, i.e. autogenous shrinkage and drying shrinkage. The autogenous shrinkage occurred a few hours after the casting or during the hardening process of concrete. This is caused by the loss of water by evaporation from the exposed concrete surfaces, or by

absorption by the aggregates. Cracks in the concrete surfaces occur because of shrinkage laterally on its upper layers (i.e. at/near its surface) were restrained by the layers beneath. The cracks due to autogenous shrinkage can be avoided by keeping the surface of concrete continuously wet (i.e. 100% relative humidity) (Taylor, 2014; Concrete Society, 2014).

Drying shrinkage occurs because of the reduction in the capillary water of the concrete due to evaporation. The exterior part of the concrete element shrinks more rapidly than the interior, which leads to tensile stresses developing in the outer skin of the concrete and compressive stresses in the interior. When the tensile stress exceeds the tensile strength of the concrete, cracks will develop. The loss of capillary water will result in a volume reduction of the concrete (MacGregor, 1992).

Referring to the above definitions, it can be concluded that the CIP beam core experienced both autogenous and drying shrinkage, which caused the formation of fine cracks in the surface of the CIP beam core and the fine gaps at the interface between the precast U-beam and the CIP beam core. This is because the curing of the CIP connection was not done properly; the relative humidity of the curing method was less than 100%. The fine gaps at the interface were assumed to form only in the top surface of the composite beam because it was exposed which therefore enabled the concrete to shrink more rapidly.

Figure 7-6 - Figure 7-5 present the crack distribution of the precast concrete beam-column joint Specimen P5 after the test. The first crack occurred on the surface of the beam core, in line with the tip of the corbel at a load of 13.5kN during the initial load of 20kN applied (see Figure 7-3). Several flexural cracks occurred in the beam core and the wall of the U-beam during the initial load applied, as can be seen in Figure 7-4(a) and Figure 7-7(a).

During the sustained load of 20kN applied to the beam tip for 90days of testing, several new cracks developed in the beam core and the precast

U-beam as presented in Figure 7-4(b), Figure 7-7(b) and Figure 7-5. Similar with what happened in Specimen P1, all cracks were distributed at the distance of the plastic hinge length stated in the ACI 318-08 (2008), i.e. $2 \times$ the depth of beam (h) from the column face (600mm). No cracks occurred in the joint core/column (see Figure 7-6).

Further cracks developed under sustained loading because of the effect of the shrinkage and creep. The new cracks happened both in the CIP beam core and the wall of the precast U-beam.

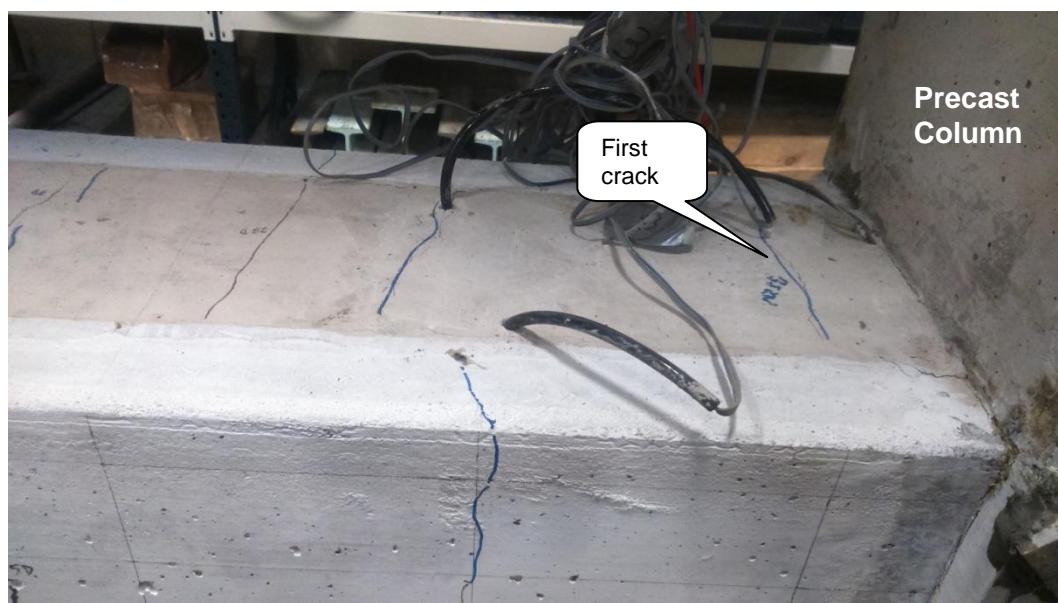
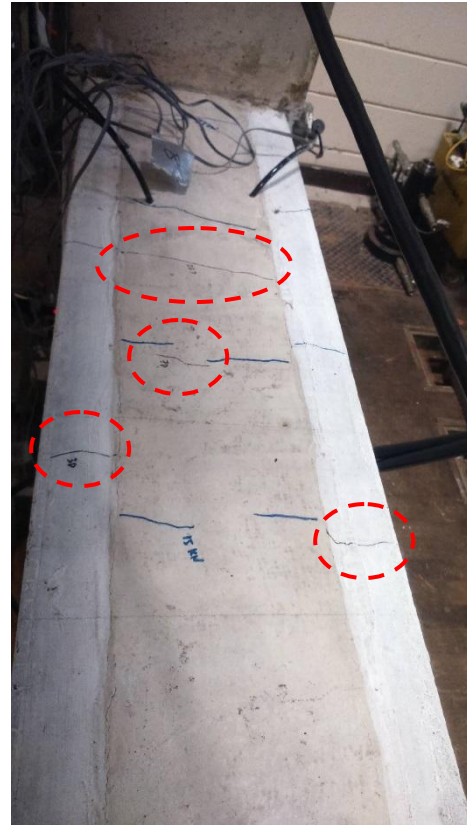


Figure 7-3 First-crack in the beam core of Specimen P5



(a) After a load of 20kN applied



(b) At the end of the test

Figure 7-4 Crack-pattern in the beam core

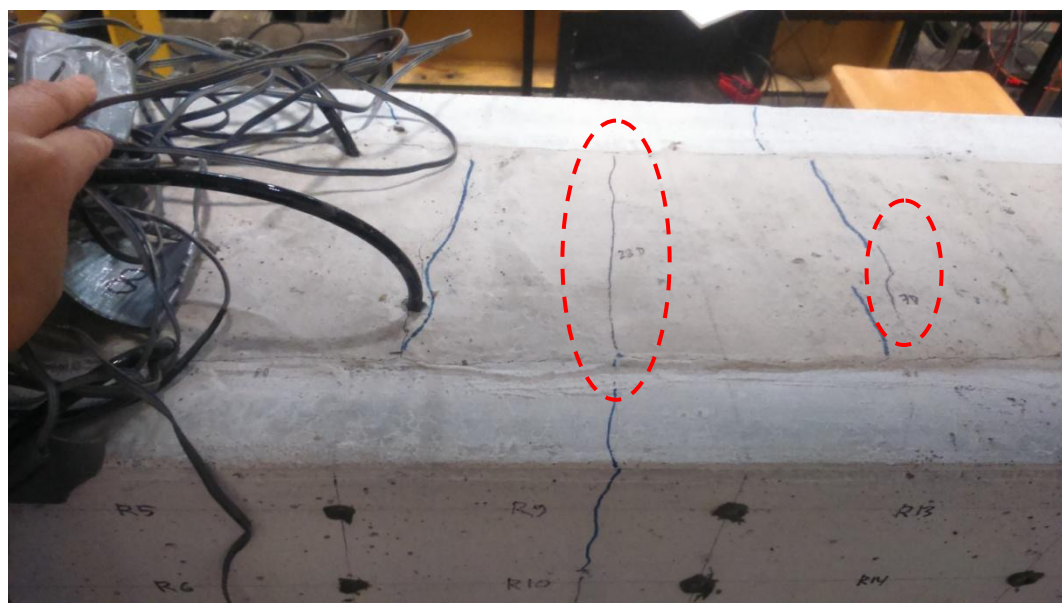


Figure 7-5 Crack-pattern of the beam at the end of the test

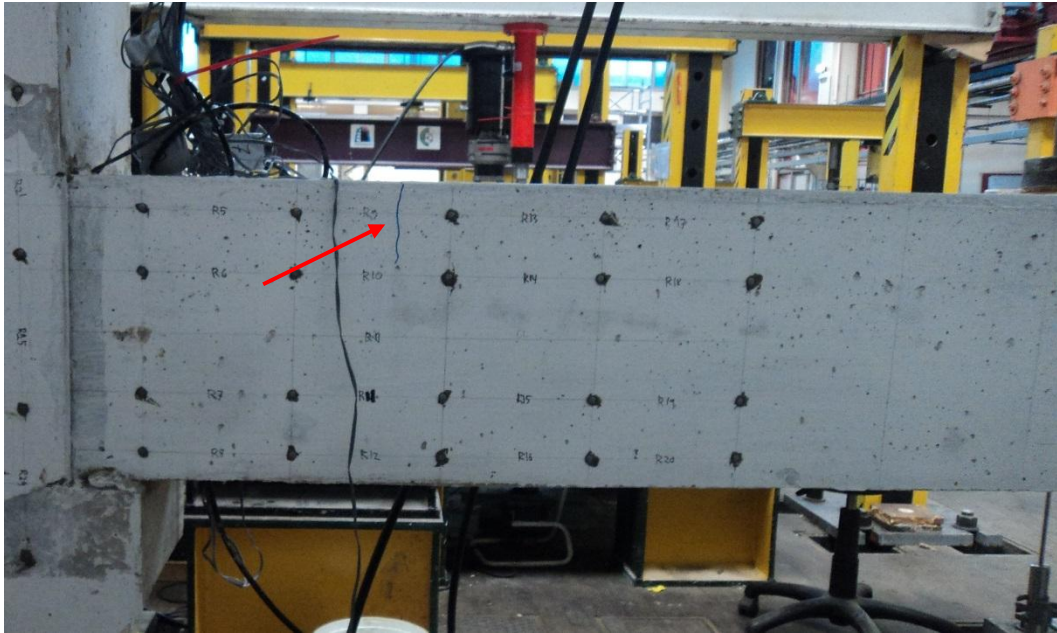


(a) After a load of 20kN applied

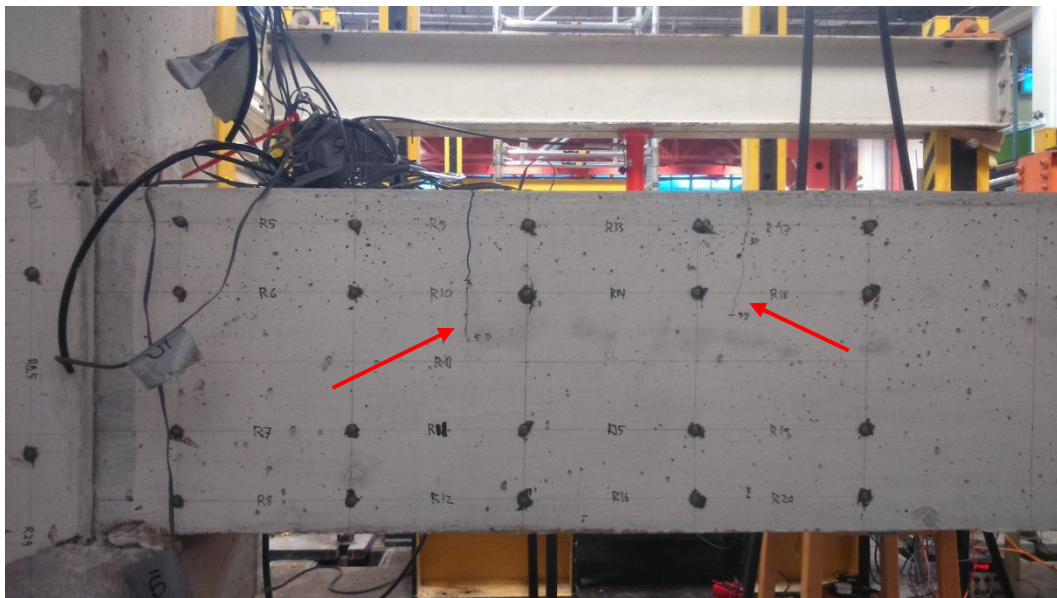


(b) At the end of the test

Figure 7-6 No cracks occurred in the joint core/column



(a) After a load of 20kN applied



(b) At the end of the test

Figure 7-7 Crack-pattern in the U-beam

7.3.3 Strain development (long-term creep strain) of the U-beam

The concrete surface strains were measured using a digital DEMEC strain gauge. Figure 7-8 and Figure 7-9 present the horizontal and vertical position of the DEMEC points on the U-beam of Specimen P5. Each position consisted of 4 levels. The top and bottom levels represented the level of the longitudinal bars of the beam and column. Figure 7-10 to Figure 7-17 show the total concrete strain developed under the sustained load of 20kN. The strains presented in these figures include the immediate strain, which is defined as the strain occurring immediately when the load is applied to the beam.

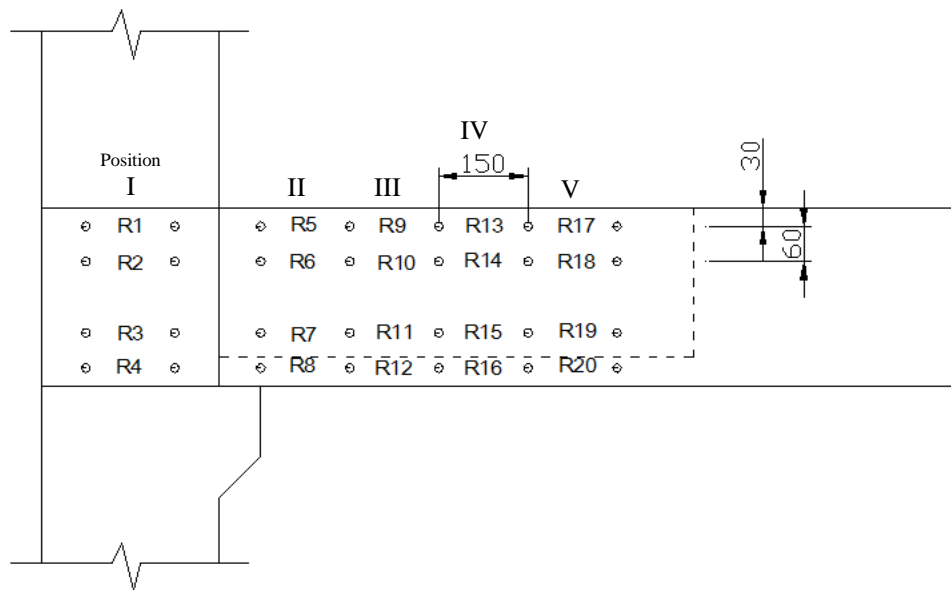


Figure 7-8 Position of DEMEC points in the joint core and the U-beam of Specimen P5 (horizontally)

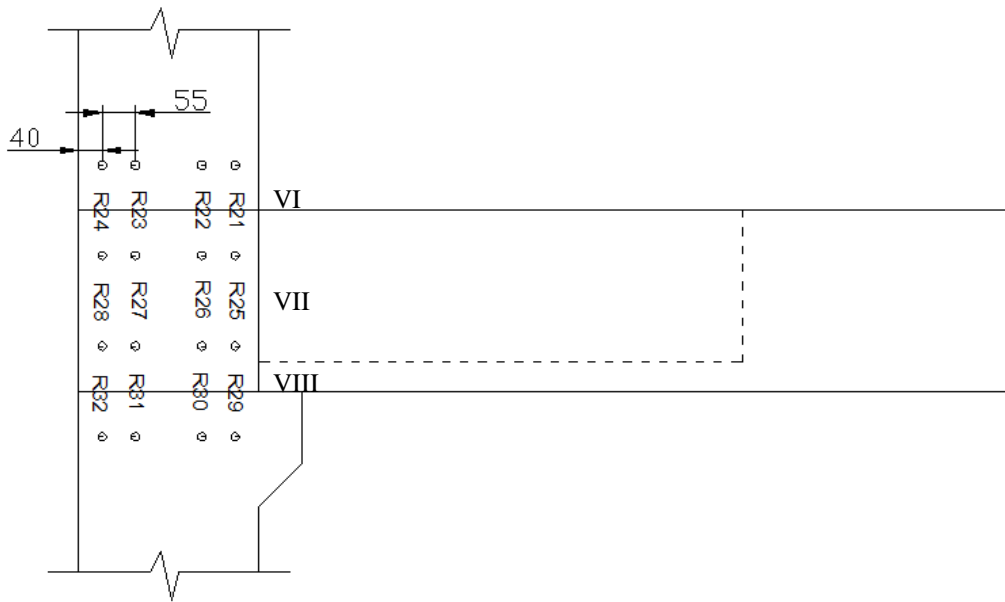


Figure 7-9 Position of DEMEC points in the joint core of Specimen P5 (vertically)

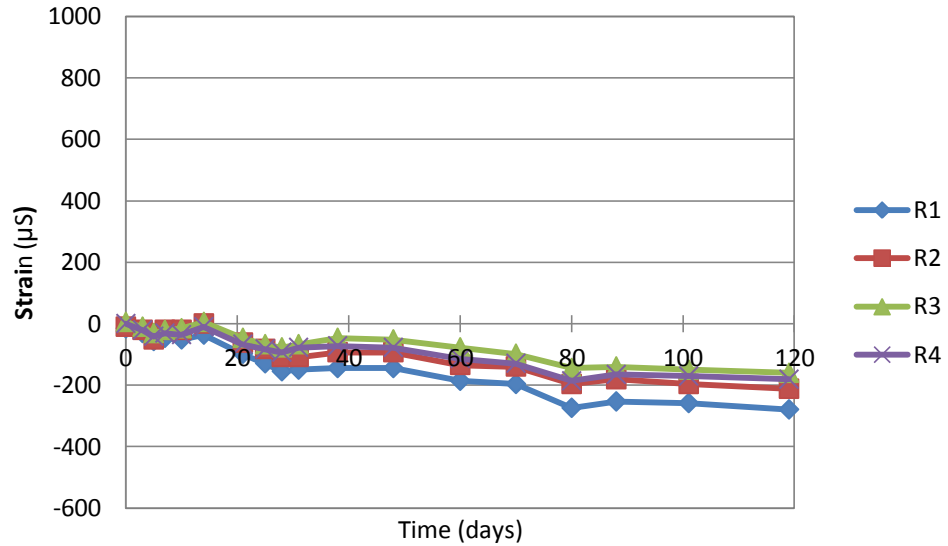


Figure 7-10 Strain development of Position I (the joint-core) of Specimen P5

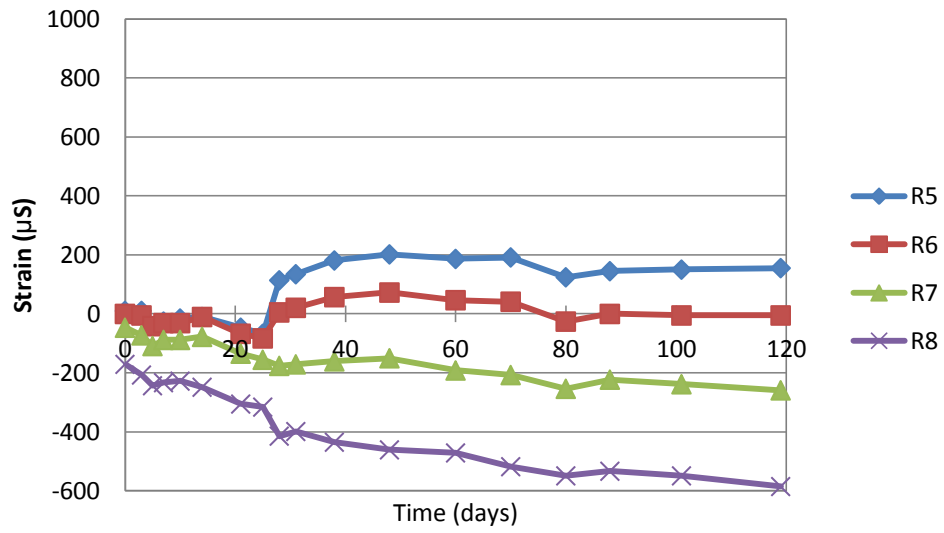


Figure 7-11 Strain development of Position II (the U-beam) of Specimen P5

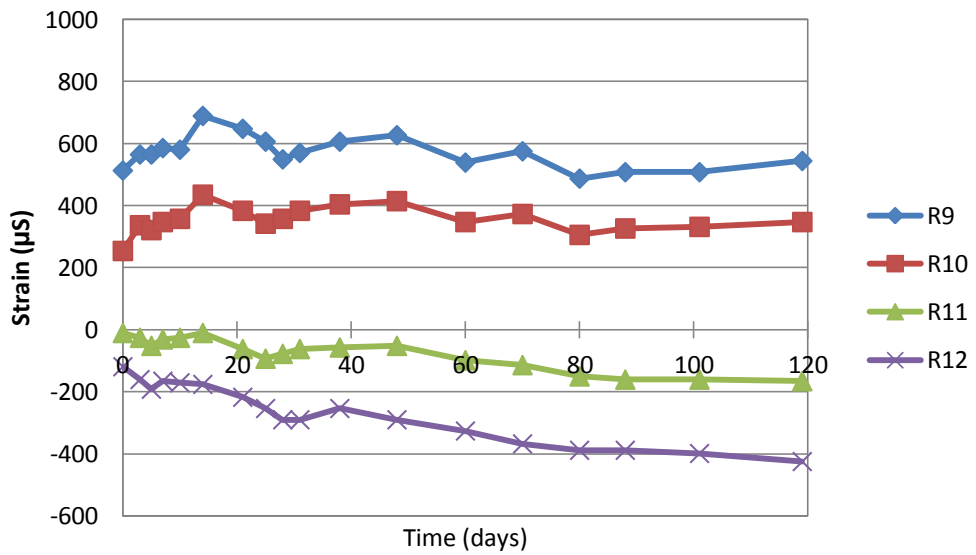


Figure 7-12 Strain development of Position III (the U-beam) of Specimen P5

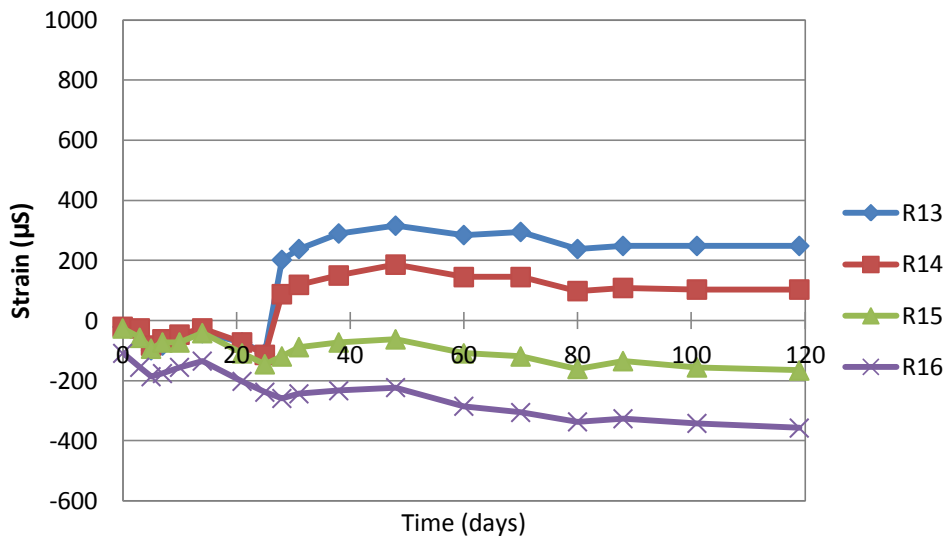


Figure 7-13 Strain development of Position IV (the U-beam) of Specimen P5

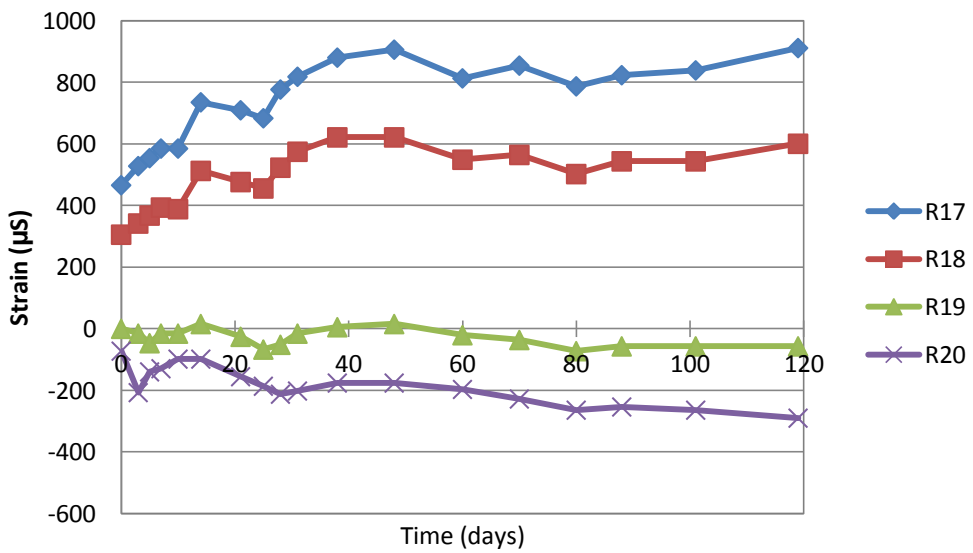


Figure 7-14 Strain development of Position V (the U-beam) of Specimen P5

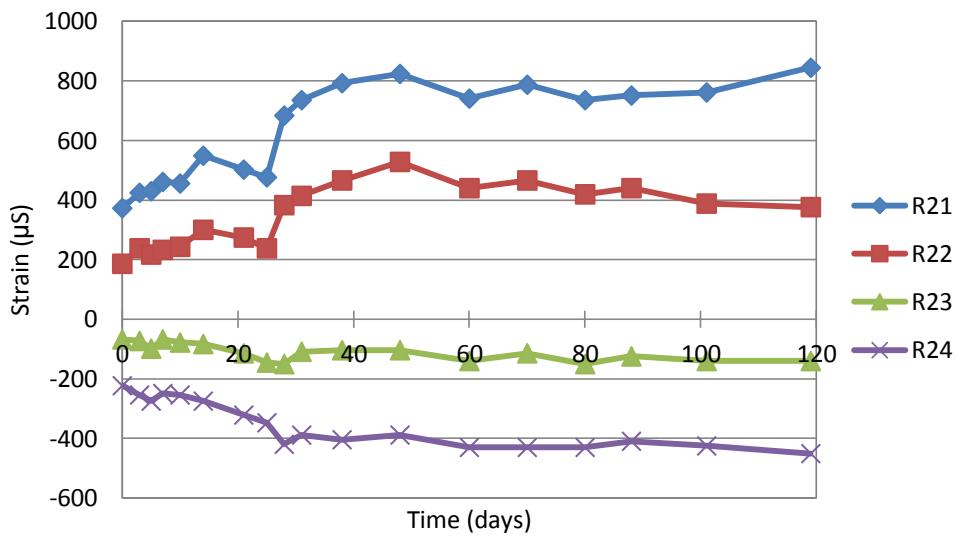


Figure 7-15 Strain development of Position VI (the joint core) of Specimen P5

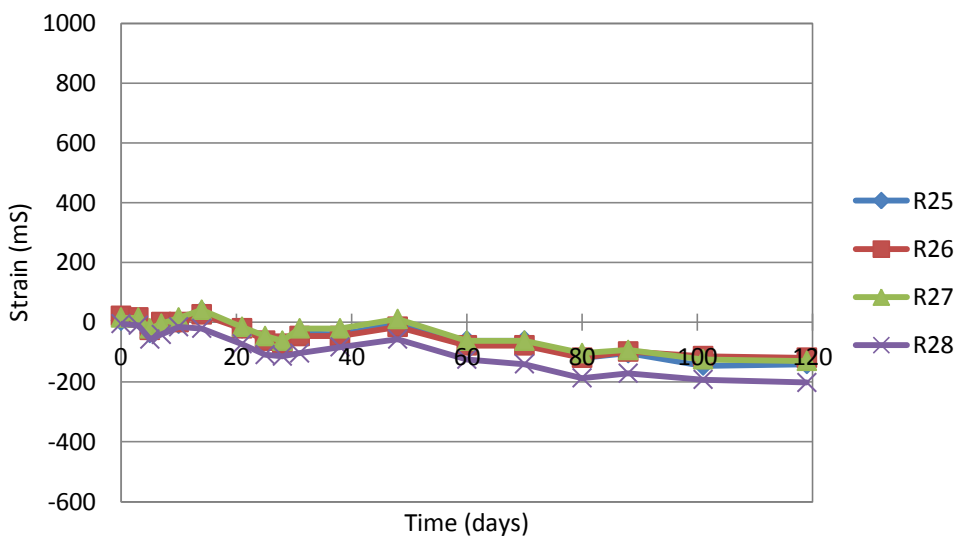


Figure 7-16 Strain development of Position VII (the joint core) of Specimen P5

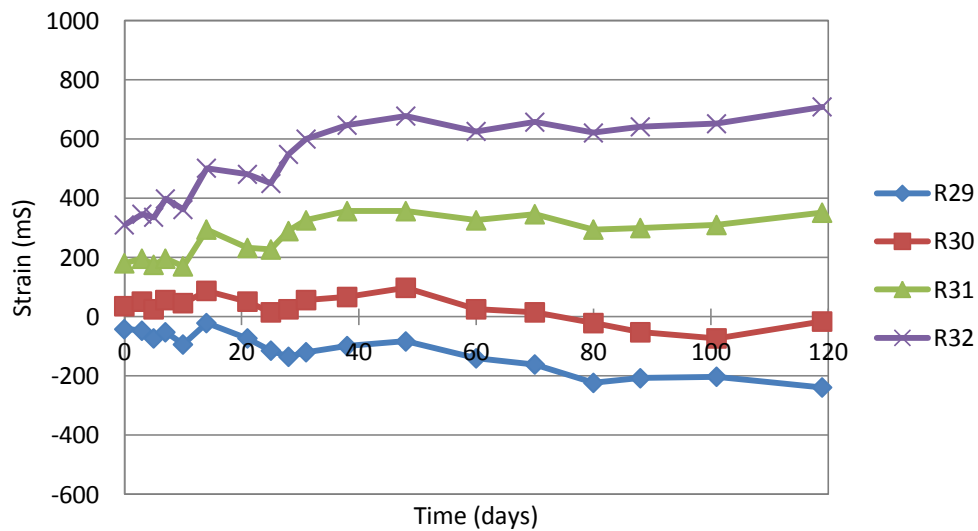


Figure 7-17 Strain development of Position VIII (the joint core) of Specimen P5

The curvature of the U-beam calculated from the strain data from Figure 7-10 to Figure 7-17 will be presented in Section 7.4.

Figure 7-18, Figure 7-19 and Figure 7-20 present the development of concrete strain increase at Position I, III and V of Specimen P5 and compare them with those of Specimen P1 (PCBC specimen under static loading). The development of concrete strain with time of Specimen P5 was calculated by reducing the total measured strains by the strains measured immediately after the beam was preloaded by 20kN

All levels in Position I (the joint core – R1 to R4) experienced compressive strains (see Figure 7-18). In Specimen P5, R1 had the highest compressive strain while R1, R2 and R3 had similar strains. This behaviour was similar with those of Specimen P1, although the strains at R3 and R4 of Specimen P1 were nearly zero. The strains of R3 and R4 in Specimen P5 were bigger due to the effect of shrinkage and creep.

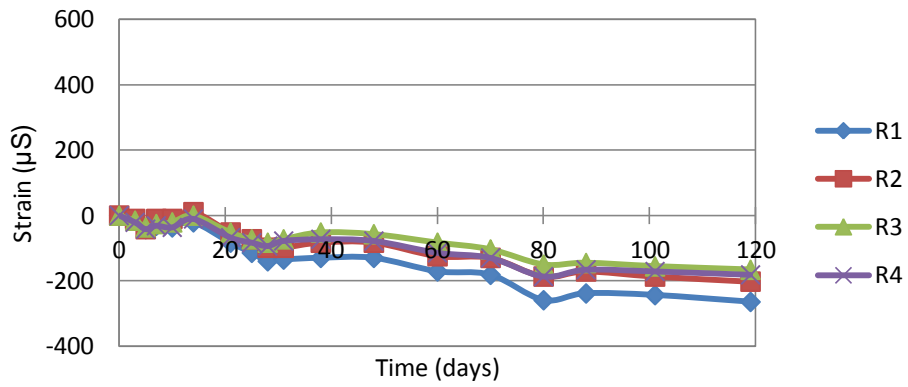
In Figure 7-19, Specimen P5 has similar values in terms of the compressive and tensile strain with those of Specimen P1. At Position III,

there is a short extension crack in Specimen P5 due to the sustained loading (see Figure 7-7).

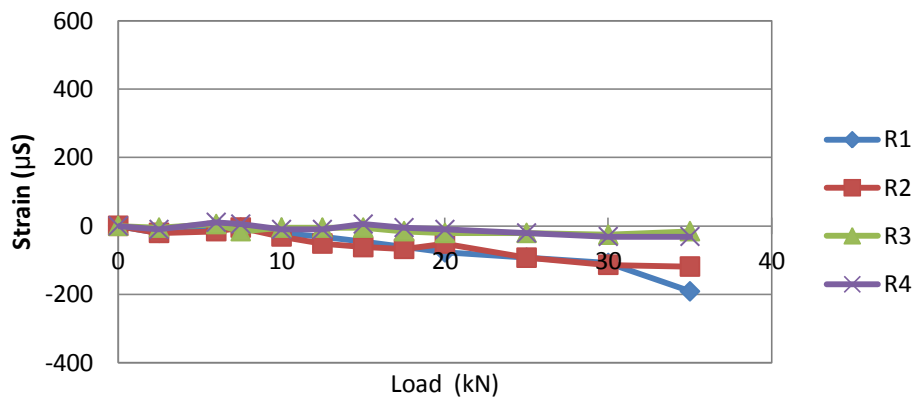
In Figure 7-20, specimens P5 and P1 have similar values in compression, but different values in tension. The tensile strains of Specimen P5 are bigger because there was a new vertical crack developed at this position due to the sustained loading (see Figure 7-7).

It can be concluded, that there were similarities in the development of compressive strain between specimens P1 and P5. Whereas, the tensile strain development were really influenced by the time dependent effect (i.e. creep and shrinkage).

The values of compressive and tensile creep depend on the level of applied stress in the tension and compression zone. In fact, the actual tensile creep is not equal to the actual compressive creep at Serviceability Limit State. Forth (2015) developed a method of predicting the tensile creep of unreinforced concrete. He found that the on the basis of equal stresses, the tensile creep is on average between 2 or 3 times greater than the compressive creep. However, when considering a cracked flexural reinforced concrete member, the applied compressive stress is much higher than the tensile stress at the Serviceability Limit State (SLS). The maximum average stress in the compression zone is typically around 5-16MPa (assuming an elastic distribution across the compression zone). Whereas, the maximum stress in the tension zone is around 3MPa (in concrete between cracks) or 1MPa on average.

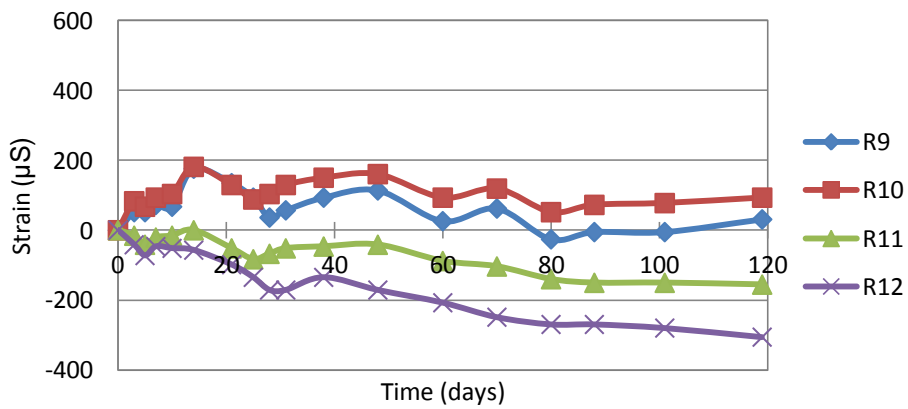


(a)



(b)

Figure 7-18 Position I (the joint core): (a) The rate of strain increase of Specimen P5; (b) The strain development of Specimen P1



(a)

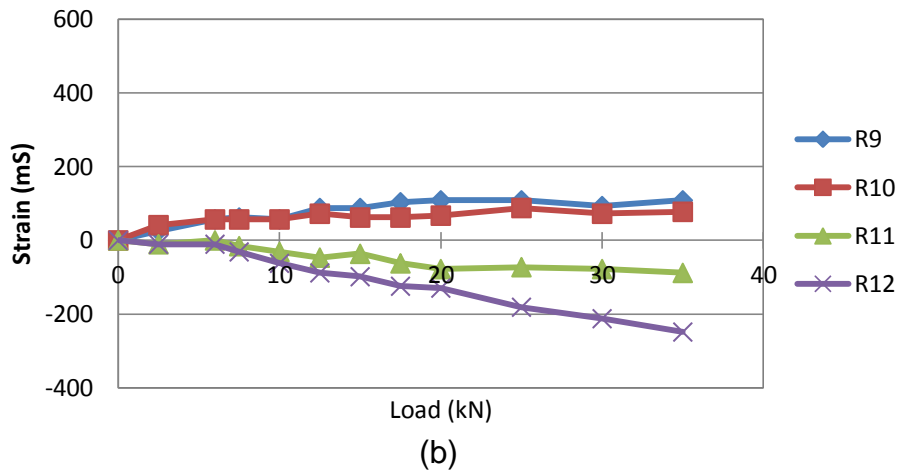


Figure 7-19 Position III: (a) The rate of strain increase of Specimen P5; (b) The strain development of Specimen P1

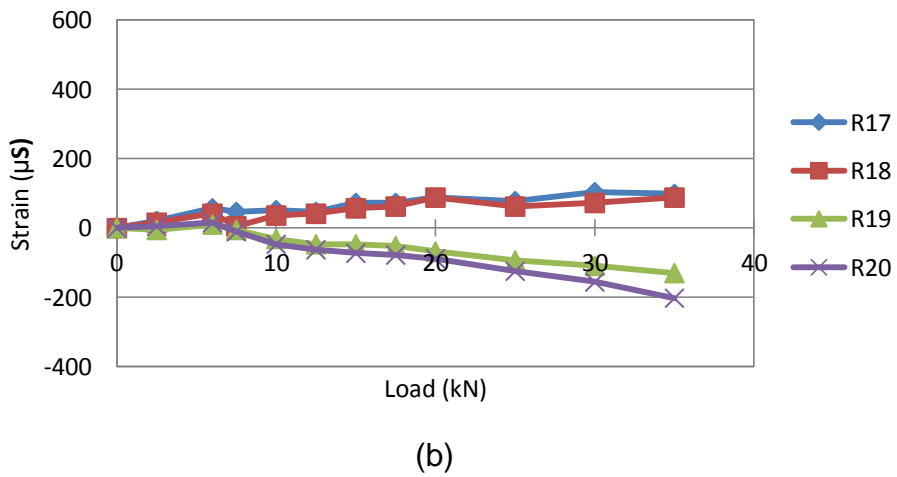
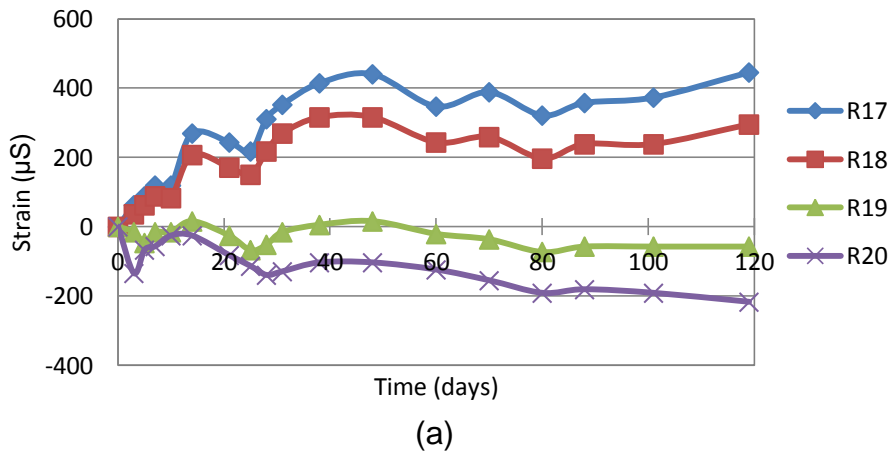


Figure 7-20 Position V: (a) The rate of strain increase of Specimen P5; (b) The strain development of Specimen P1

7.4 Discussion

7.4.1 Theoretical immediate deflection

A theoretical calculation of the immediate deflection (Δ_i) of Specimen P5 will be presented in this section. Equation (7-1) is used to calculate the deflection of the beam of the beam-column connection (Park and Paulay, 1975; Hasan et al., 2011).

$$\Delta_i = \int \frac{M}{E_c I_e} x dx \quad (7-1)$$

Where, M is the applied moment, E_c is modulus elasticity of concrete, I_e is effective inertia of the cracked beam section and x is the distance of element dx from the location of calculating deflection.

The effective moment of inertia (I_e) was used in the deflection calculation after the beam section cracked. Branson (1965) proposed an expression for I_e (see Equation (7-2)), which is the average of the inertia moment of the un-cracked (I_{ucr}) and fully-cracked section (I_{cr}) of a reinforced concrete beam. This approach is adopted by ACI 318-05 (ACI 2005), AASHTO LRFD (AASHTO 2005), CSA A.23.3-04 (CSA 2004), AS 3600 (SAA 1994) and TS 500 (TS 2000), by setting $m = 3$ in Equation (7-2)(Kalkan, 2013).

$$I_e = \left(\frac{M_{cr}}{M_a}\right)^m \cdot I_{ucr} + \left[1 - \left(\frac{M_{cr}}{M_a}\right)^m\right] \cdot I_{cr} \quad (7-2)$$

Where, M_{cr} is the cracking moment, M_a is the applied moment.

However, Alshaikh and Al-Zaid (1993) found that the value of m decreases as the reinforcement ratio of beam (ρ) increases. They proposed the following equation for m is,

$$m = 3 - 0.8\rho \quad (7-3)$$

Branson (1965) developed an expression for the effective moment of inertia empirically by testing the simply-supported reinforced concrete beams with reinforcement ratio (ρ) between 1-2%, which accurately estimate the deflections of the reinforced concrete beams with $\rho > 1\%$.

Further, Bischoff (2005) found that there were errors in the estimation of the effective moment of inertia moment in Branson's expression for the case of a reinforced concrete beam with a low reinforcement ratio, which was caused by the overestimation of the tension stiffening of the concrete. Branson's approach provided an accurate approach for the beams with $\rho > 1\%$, but for $\rho < 1\%$, it produced a stiffer response than the actual response, or in other words, overestimated the effective moment of inertia which resulted in the underestimation of the deflection.

Bischoff (2005) developed an effective moment of inertia expression, which is a weighted average of the flexibilities of the un-cracked and cracked portions of a reinforced concrete beam, as presented in Equation (7-4) as follows:

$$I_e = \frac{I_{cr}}{1 - \left(1 - \frac{I_{cr}}{I_g}\right) \left(\frac{M_{cr}}{M_a}\right)^2} \quad (7-4)$$

In this study, the immediate deflection of the PCBC Specimen P5 test will be compared with the analytical load-deflection curves obtained from Branson's and Bischoff's approaches.

Figure 7-21 presents the load-deflection of Specimen P5, which consists of the experimental curve, Branson's curve and Bischoff's curve. The figure also presents the un-cracked and fully cracked responses obtained from the analytical calculation. The un-cracked and cracked responses were obtained by introducing the gross moment of inertia (I_g) or un-

cracked moment of inertia (I_{ucr}) and fully-cracked section (I_{cr}) in the deflection equation.

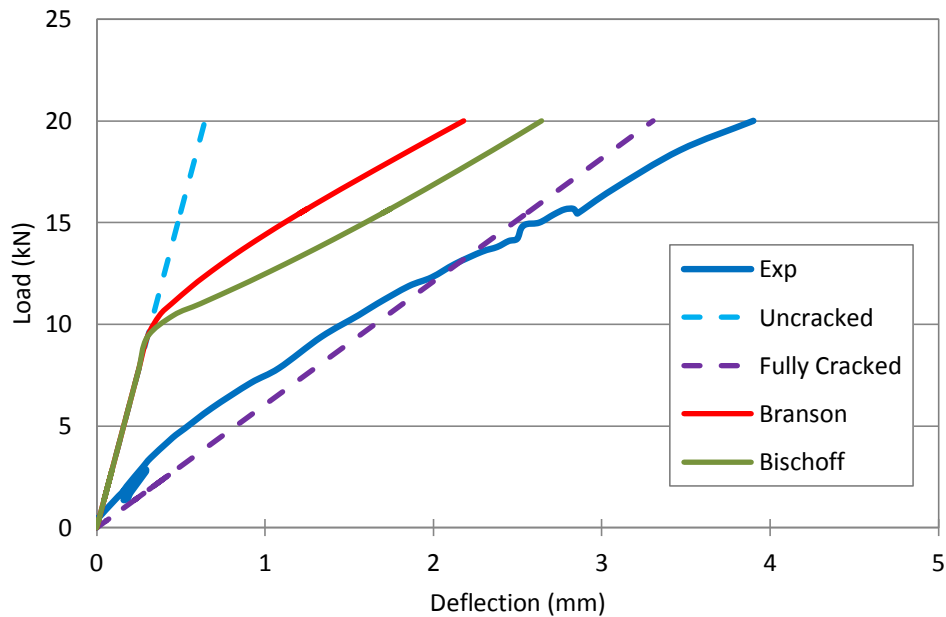


Figure 7-21 Theoretical and experimental of the load vs. deflection relationship

Branson's method yielded a smaller deflection in comparison with Bischoff's method. Both curves obtained from Branson's and Bischoff's method are much stiffer than the experimental curve.

The initial part of the experimental curve presented in Figure 7-21 lies above the fully cracked line, then, at a load of 12.5kN the curve crossed the fully cracked line. It is unexpected condition because the sample was not completely cracked. Theoretically, the ideal experimental load-deflection response is shown in Figure 7-22, since the experimental curve lies between the analytical un-cracked and fully cracked lines.

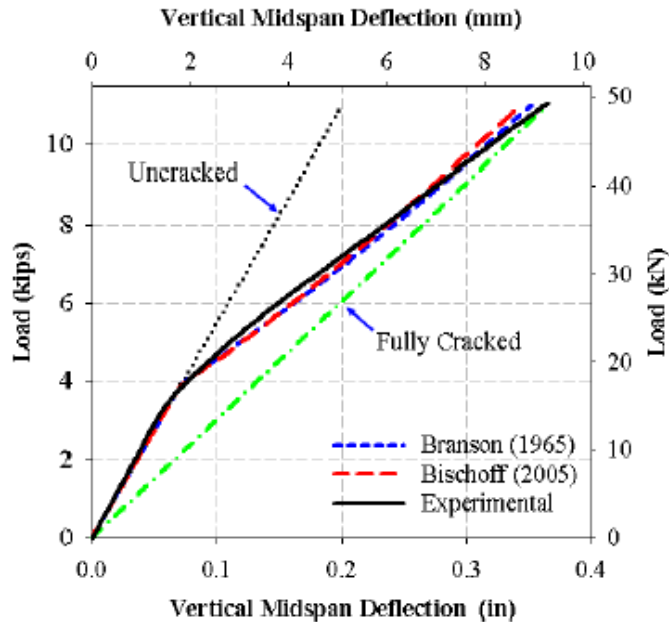


Figure 7-22 Ideal load-deflection curve (Branson, 1977)

The equations used to obtain the deflection of the beam were developed based on the monolithic reinforced structure's behaviour. In fact, the precast U-beam; where the deflection was measured, was not monolithically connected to the precast column. The precast U-beam was not perfectly fixed to the column which enabled to generate larger deflection at the beam tip. Therefore, the percentage of the joint rigidity of the PCBC connection in comparison with the monolithic joint can be defined.

In order to find the rigidity factor of the PCBC connection, a comparison of the load-deflection responses under static loading between the PCBC connection (obtained from experimental result of Specimen P1 as presented in Chapter 4) and the monolithic beam-column joint (obtained from finite element analysis) has been performed as presented in Figure 7-23 (the explanation about the finite element modelling result will be presented in Chapter 8). It can be seen that the monolithic beam-column joint response is stiffer than that of PCBC connection. The ratio of the secant stiffness of the curves of the PCBC connection and monolithic joint is 1.50. It means that to having a similar load-deflection response with the

monolithic joint, the deflection obtained from the PCBC specimen (under static loading) should be divided by 1.5, or multiplied by 0.67.

To validate the factor of 1.5, the deflection values of the monolithic beam-column joint were multiplied by 1.5, as presented by the dashed line in Figure 7-23. The figure shows that the dashed line coincided with the PCBC curve until the maximum load. It can be concluded that the rigidity percentage of the exterior PCBC connection is 1/1.5 or 67%.

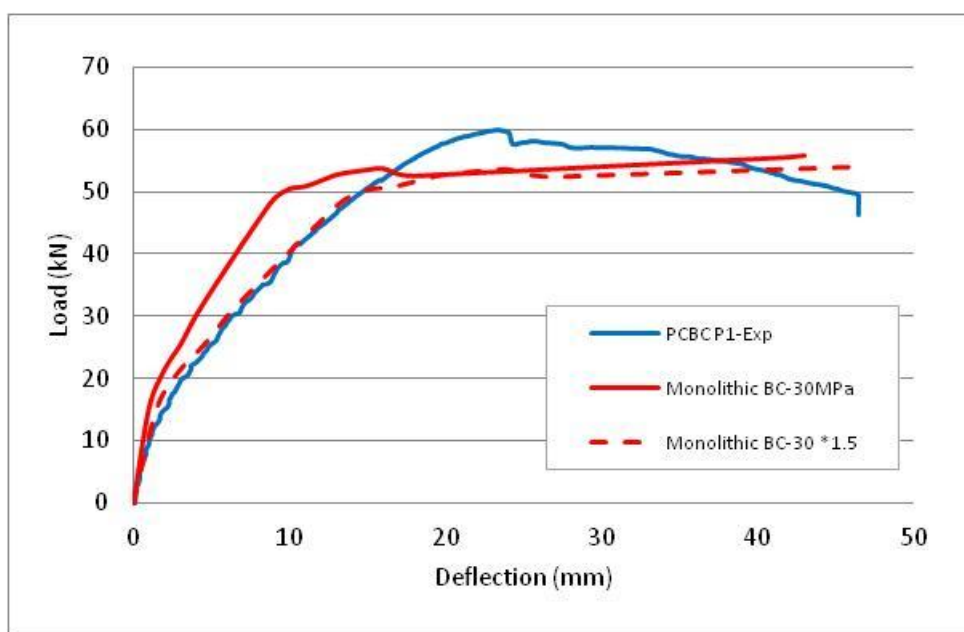


Figure 7-23 Comparison between PCBC and MBC (monolithic beam-column) joint

The curves presented in Figure 7-21, then, are fixed by multiplying the theoretical deflections with a factor of 1.5. The new load-deflection curves are presented in Figure 7-24.

It is shown in Figure 7-24 that the experimental curve lies between the analytical un-cracked and fully cracked lines. Branson's and Bishoff's methods provide close agreement with the experimental deflection. At a load level of 20kN, the theoretical deflections are 3.3mm (Branson's

method) and 3.9 (Bischoff's method); the method proposed by Bischoff (2005) provides the same deflection with the experimental result.

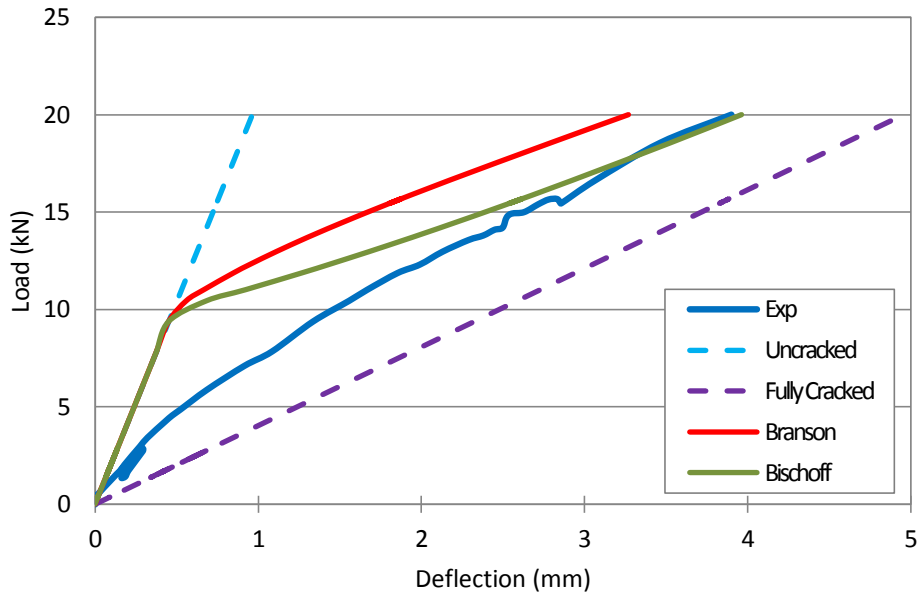


Figure 7-24 Theoretical (including the rigidity factor of 0.67) and experimental of the load vs. deflection relationship

The result above is in agreement with the study done by Kalkan (2013). He studied the use of the effective moment of inertia (I_g) proposed by Branson (1965) and Bischoff (2005) in the analytical deflection calculation of reinforced concrete beams. The methods were applied to calculate the deflection estimations of 10 reinforced concrete beams with medium to high reinforcement ratios ($\rho > 1\%$) which were tested by Kalkan (2009), then compared the deflection estimations with the actual deflections. He concluded that the method proposed by Bischoff (2005) provides slightly better result with the experimental deflection rather than the method proposed by Branson (1965).

The difference between the experimental result and the predicted behaviour up to first crack (10kN) is thought to be due to the fact that the

beam core (CIP connection) was cracked before the test began (as was explained in Section 7.3.2).

7.4.2 Theoretical long-term deflection

One of the objectives of this study is to evaluate the long-term deflection obtained from the precast concrete beam-column Specimen P5 test using current code equations, such as ACI-318 (2008), EMM (Neville et al., 1983), Branson's method (Branson, 1977) and EC2.

The American Concrete Institute Building code (ACI committee 318-2011) provides the following equations to calculate the long-term deflection of a beam:

$$\Delta_{(cr+sh)} = \lambda_{\Delta} (\Delta_i)_{sus} \quad (7-5)$$

$$\lambda_{\Delta} = \frac{\xi}{1 + 50\rho'} \quad (7-6)$$

Where, $\Delta_{(cr+sh)}$ is the long-term deflection due to creep and shrinkage, Δ_i is the initial deflection corresponding to the sustained load level; λ_{Δ} is a long-term coefficient which depends on the duration of the sustained load, ξ is the time-dependent factor (according to Figure 7-25) and ρ' is the compression reinforcement ratio:

$$\rho' = \frac{A_s'}{bd} \quad (7-7)$$

Total deflection of a beam is the sum of the immediate deflection and the long-term deflection, which is given by:

$$\Delta_{tot} = \Delta_i + \Delta_{(cr+sh)} \quad (7-8)$$

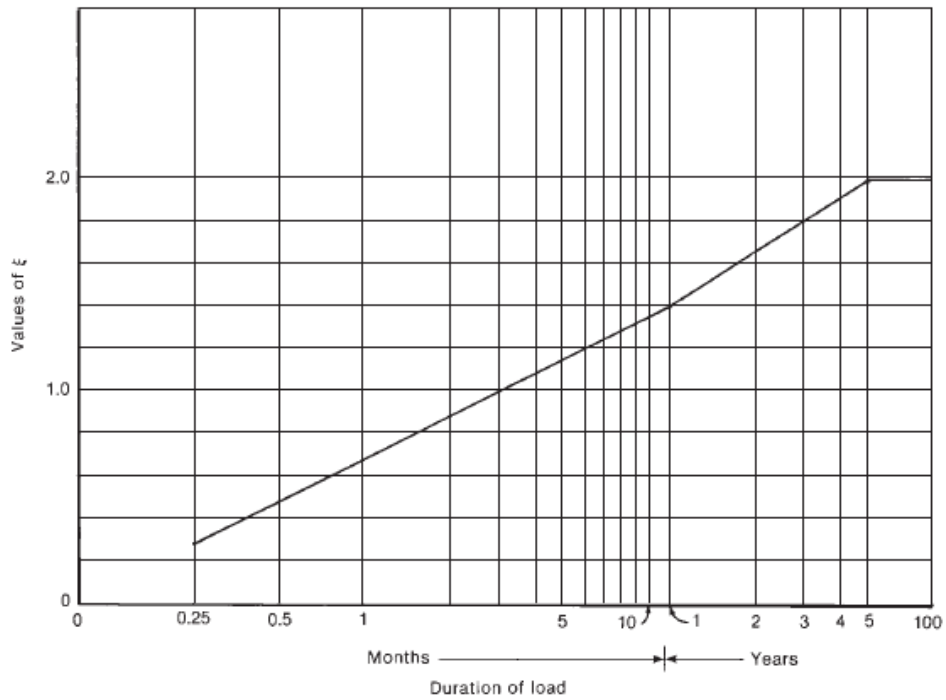


Figure 7-25 Time dependent factor (MacGregor, 1992)

The Effective Modulus Method (EMM) uses the effective modulus of elasticity to allow for the creep effect on the reinforced concrete beam (Neville et al., 1983) as given in the following equation:

$$E_e(t) = \frac{E_c(t_0)}{[1 + \phi(t, t_0)]} \quad (7-9)$$

Where, $E_c(t_0)$ is modulus of elasticity at 28 days and $\phi(t, t_0)$ is creep coefficient.

The effective modulus of elasticity is substituted into the I_{cr} equation then the new I_e will be obtained. This new values of I_e and $E_e(t)$ are then used to calculate the long-term deflection using the following equation,

$$\Delta_{sus} = K_a \frac{M_{max} l^2}{E_e(t) I_e} \quad (7-10)$$

K_a is a factor which depends on the loading and support conditions.

In the Adjusted Effective Modulus Method (AEMM), the reduction coefficient was applied to the creep coefficient in the effective modulus of elasticity (Equation (7-9)). The expression of the adjusted effective modulus (E_{ea}) is presented in Equation (7-11). The reduction coefficient $\chi(t, t_0)$ for normal strength is 0.8 (Ezeldin and Shiah, 1995; Gilbert, 1999). Furthermore, the adjusted effective modulus elasticity E_{ea} is used to replace E_c in Equation (7-10).

$$E_{ea}(t) = \frac{E_c(t_0)}{[1 + \chi(t, t_0)\phi(t, t_0)]} \quad (7-11)$$

Branson's method has similar equations with those of ACI-318 in terms of the long-term deflection calculation. This method specifically takes into account the creep coefficient of the concrete within the deflection calculation.

Long-term deflection caused by creep (Δ_{cr}) is

$$\Delta_{cr} = K_{\phi} \phi(t, t_0) \Delta_i \quad (7-12)$$

$$K_{\phi} = \frac{0.85}{1 + 50\rho'} \quad (7-13)$$

Where, K_{ϕ} is the reduction factor which is affected by the compression reinforcement ratio of the beam (ρ'); $\phi(t, t_0)$ is creep coefficient of the concrete and Δ_i is the immediate deflection corresponding to the sustained load level.

EC (EN, 2004) provides an expression to predict the long term deflection (δ_s) of a reinforced concrete beam as presented in Equation (7-14). This equation allows tension stiffening in a beam due to the un-cracked portions (between cracks).

$$\delta_s = \zeta\delta_c + (1 - \zeta)\delta_u \quad (7-14)$$

$$\zeta = 1 - \beta \left(\frac{M_{cr}}{M} \right)^2 \quad (7-15)$$

Where, δ_u is deflection assuming an un-cracked section (i.e. use I_u), δ_c is deflection assuming a fully cracked section (i.e. use I_c), ζ = distribution coefficient which allows the effects of tension stiffening at the section, β is coefficient which accounts for the duration of the loading or of repeated loading (i.e. $\beta = 1.0$ for single short-term loading, $\beta = 0.5$ for sustained loading or repeated loading). M_{cr} is the moment which causes the first crack and M is the design moment.

The creep could increase the concrete strain with time. The deflection calculation allows the increase of the concrete stress by reducing the modulus of elasticity of the concrete (E_c) to an effective modulus of elasticity (E_e) as presented in Equation (7-9).

Figure 7-26 presents a comparison of long-term deflection between the experimental result and the predictions obtained from ACI-318, Branson's, EC2 and AEMM method. The immediate deflection (Δ_i) of 3.9mm (explained in the previous section) used in the analytical calculations

Currently, no literature exists which studied the behaviour of the beam-column connection under long-term loading. Therefore, there is no information regarding the accuracy of the current prediction methods for estimating the long-term deflection of a beam-column joint.

As seen in Figure 7-26, the EC2 method presented the highest time-dependent deflection in comparison with ACI-318, Branson and AEMM. The experimental result of the PCBC connection has larger deflections in comparison with the theoretical deflections. Unfortunately, no approaches have similar curves with that of the exterior PCBC connection. This would suggest that the approaches cannot be used for estimating the long-term

deflection of the PCBC connection, since the PCBC connection only has 67% of the joint rigidity (as explained in the previous section).

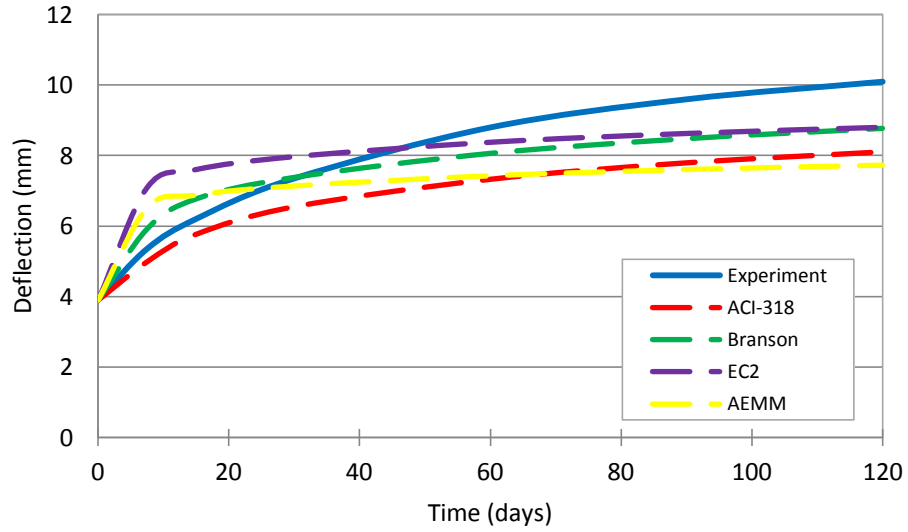


Figure 7-26 Comparison the test result of Specimen P5 and the predicted values

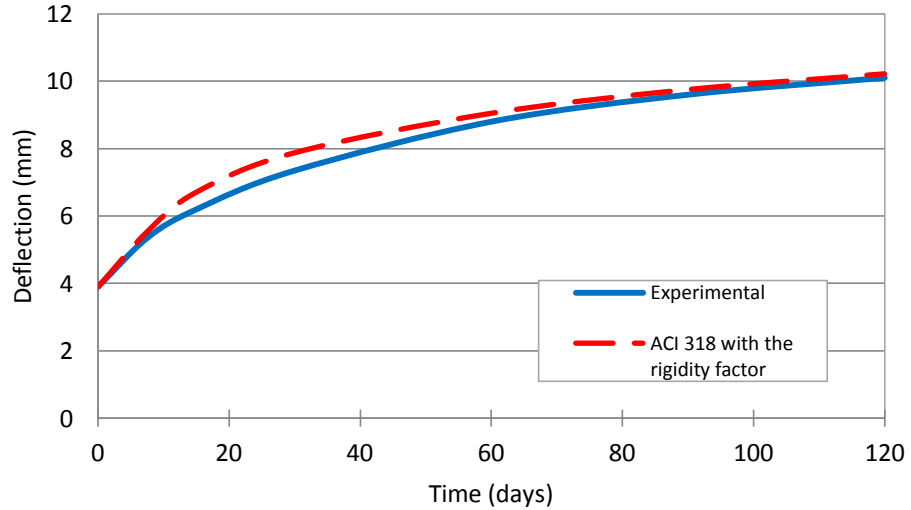


Figure 7-27 Theoretical and experimental deflection of Specimen P5 for the time-dependent factor (ξ) multiplied by 1.5

A modification was carried out in this study on the long-term deflection equation in order to get a closer result with the experimental long-term deflection. The long-term deflection proposed by ACI-318 (Equation (7-5)) was multiplied by a factor of 1.5 (i.e. $1/0.67$), which 67% is the percentage of the joint rigidity of the PCBC connection. By using the same equations (Equation (7-5) – (7-8)), the new estimation of long-term deflection was obtained. Figure 7-27 presents the experimental long-term deflection and the new estimation. It shows that the new estimation is in reasonable agreement with the experimental deflection when the long-term deflection is multiplied by 1.5 (i.e. $1/\text{the joint rigidity percentage}$). The reason of introducing the 0.67 into the time-dependent factors is because the precast concrete beam-column (PCBC) connection has different behaviour in term of long-term deflection development in comparison with the monolithic beam-column joint.

There are some possibilities that could cause the experimental deflection of the PCBC specimen greater than the theoretical deflections, i.e. the excessive cracks occurred in the beam, the loss of stiffness in the tension zone of the beam and the relative beam-column rotations.

In order to investigate how much the loss of tension stiffening in the beam, the theoretical calculation was performed according to Higgins et al. (2013). Figure 7-28 presents the moment-curvature relationship (after 120 days under sustained load) for the PCBC Specimen P5. The un-cracked and cracked lines were constructed using Equation (7-16) and (7-17), respectively. The moment-curvature curve was made according to Expression 7.18 and 7.19 of Eurocode 2 with $\beta = 0.5$ for long-term loading (see Equation (7-18) and (7-19)). The curve and lines were calculated using 120 days effective concrete modulus (E_e) mentioned in Equation (7-9).

$$\varphi_{ucr} = \frac{M}{E_e I_{ucr}} \quad (7-16)$$

$$\varphi_{cr} = \frac{M}{E_e I_{cr}} \quad (7-17)$$

$$\zeta = 1 - \beta \left(\frac{M_{cr}}{M} \right)^2 \quad (7-18)$$

$$\varphi_s = \zeta \varphi_{cr} + (1 - \zeta) \varphi_{ucr} \quad (7-19)$$

Where, φ_{ucr} and φ_{cr} are the values of the curvatures calculated for the un-cracked and fully cracked condition, respectively. β is a coefficient (i.e. $\beta = 1.0$ for short-term loading, $\beta = 0.50$ for sustained loading).

The 120 days beam curvatures were calculated using the strain profiles presented in Figure 4-25. The measurement of the strains of the beam was taken at a load of 20kN or equal to a bending moment of 20.6kNm. The maximum curvature presented in Figure 7-32 (Position V) is plotted in the moment-curvature relationship in Figure 7-28. It can be seen that the plot (“x”) lies in between the un-cracked and fully cracked lines, which means that no excessive loss of tension stiffening occurred in the beam.

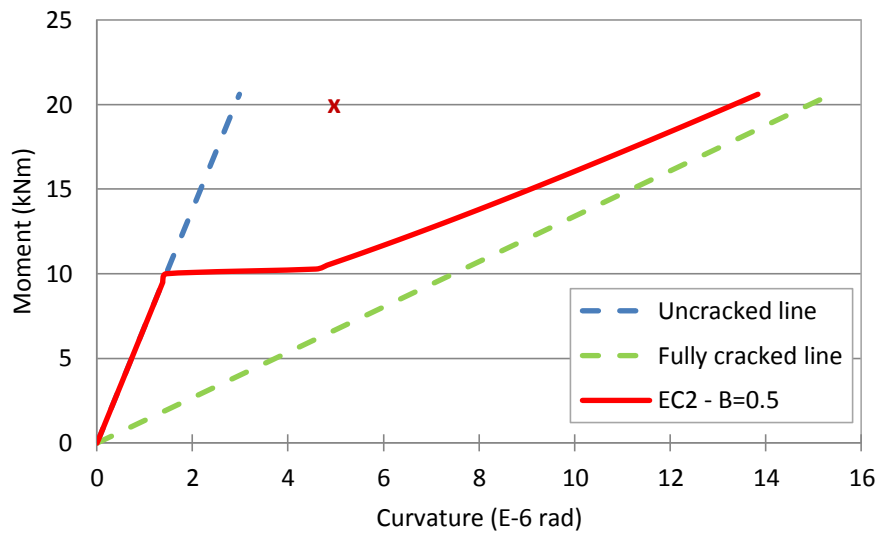


Figure 7-28 Moment-curvature relationship

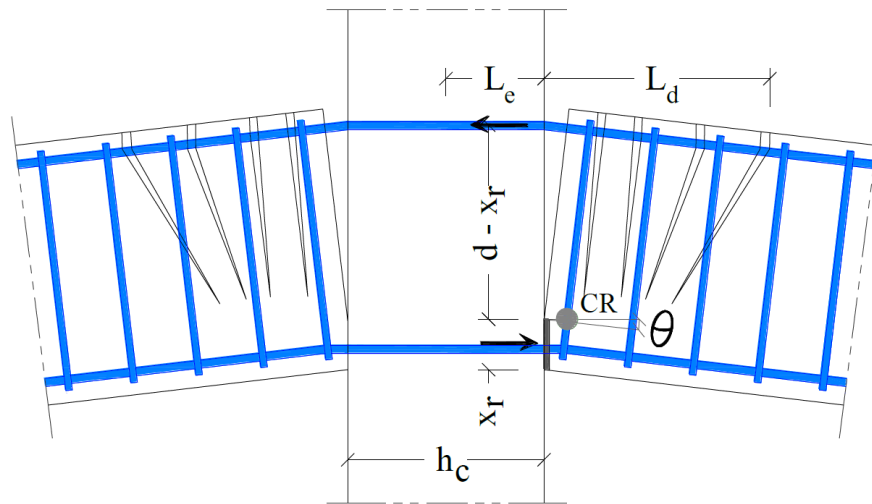


Figure 7-29 Deformation configuration of composite beam-column connection (Hasan et al., 2011)

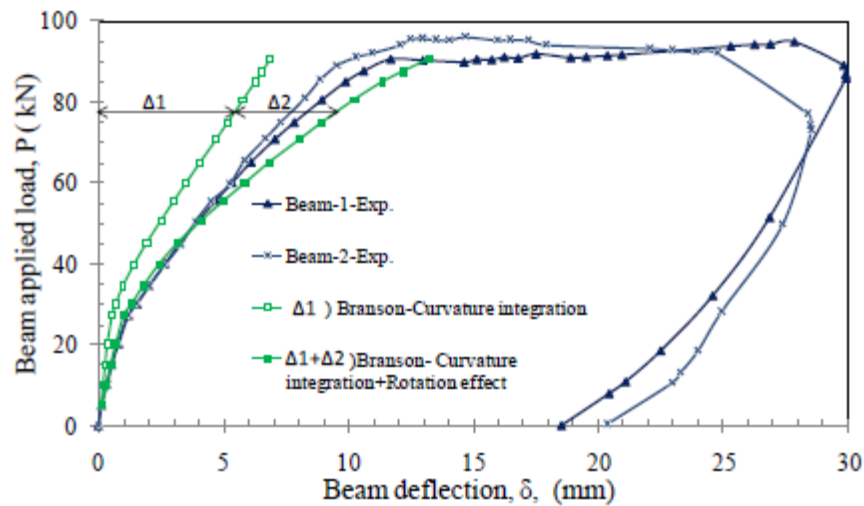


Figure 7-30 Load-deflection relation of GR1 (Hasan et al., 2011)

However, the development curvature shown in Figure 7-32 represents the curvature of the wall of the precast U-beam only, instead of the curvature of the CIP beam core. So, there is possibility that much loss of tension stiffening occurred in the beam core which was cast monolithically with the joint core. This could cause the beam-column rotation, which generate the additional deflection in the beam tip. This is in agreement with Hasan et al. (2011) who studied semi-rigid precast concrete beam-column

connections under gravity loading. A theoretical investigation was performed to predict the load-deflection curve of the beam-column connection as presented in Figure 7-30, where Δ_1 is the elastic deformation using moment inertia effective proposed by Branson and Δ_2 is the deflection due to the beam-column rotation effect. He concluded that the relative beam-column rotation (θ) caused the additional deflection.

The rotation of beam-column joint is similar with the joint rigidity percentage, which have discussed in Section Theoretical immediate deflection. The rotation did not stop when the initial loading was applied, but continued during sustained loading, which resulted bigger deflection on the Specimen P5. Thus, it is relevant to apply a factor of 1.5 (i.e. 1/the percentage joint rigidity) in Equation (7-5) to represent the effect of the beam-column rotation.

The joint rigidity percentage of the precast concrete beam-column connection in comparison with the monolithic beam-column joint will be different depending on the type of the connection. It is influenced by the stiffness of the reinforced concrete element, which is determined by some factors such as the dimension of the reinforced concrete element, the concrete and the steel strength, the percentage and the layout of the reinforcement bars.

7.4.3 Long-term curvatures of the U-beam

As with PCBC Specimen P1, Figure 4-25 and Equation (7-20) were used to calculate the curvatures of the beam using the strain data presented in Figure 7-10 to Figure 7-17. The curvatures which developed in the joint core and the U-beam are presented in Figure 7-32.

$$\frac{1}{r} = \frac{Ra + Rb}{240} \quad (7-20)$$

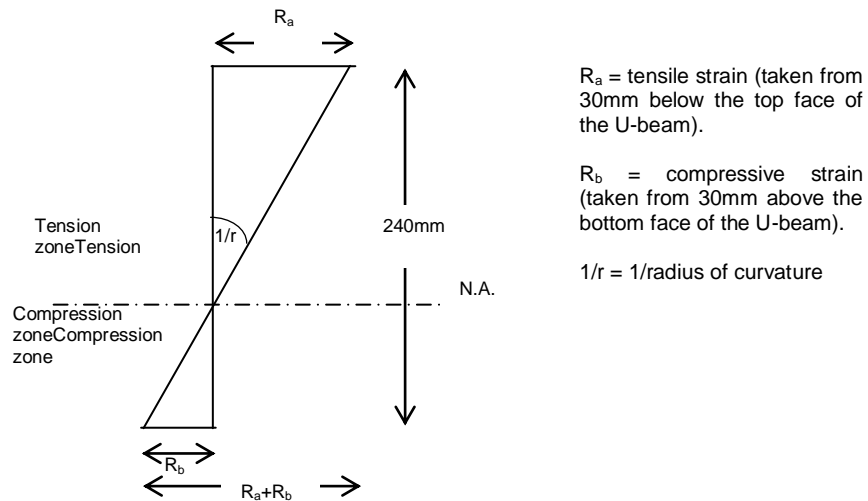


Figure 7-31 Strain profiles of the beam (Higgins et al., 2013)

Figure 7-32 shows that the curvatures at Position II-VI (the U-beam) increased with time. The curvatures at III and V are bigger than those at II and IV, because vertical cracks occurred in regions III and V (see Figure 7-7). The curvatures at II and IV appear to be similar, with a dramatic increase at the age of 30 days; at this stage the cracks occurred on the top surface of the beam core.

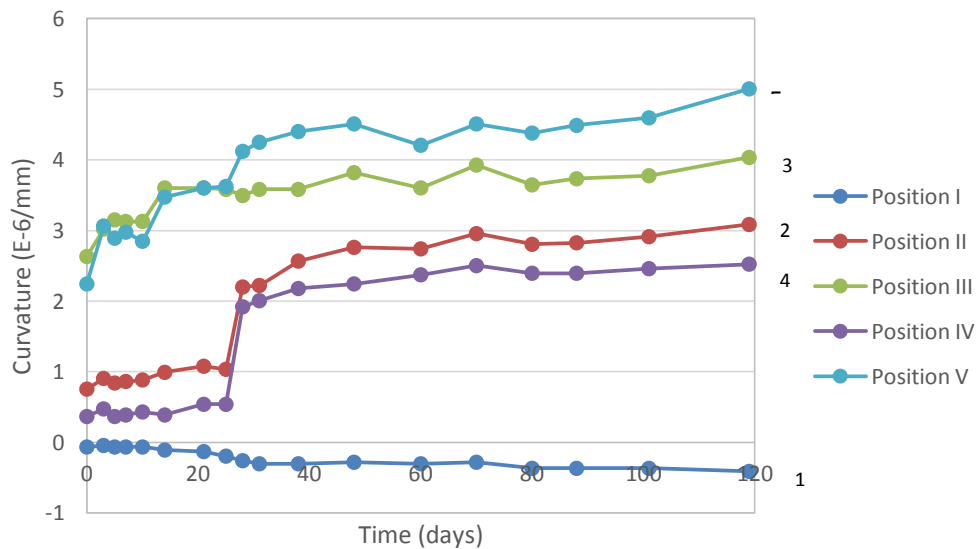


Figure 7-32 Curvature developments of the surface strain of the U-beam of Specimen P5

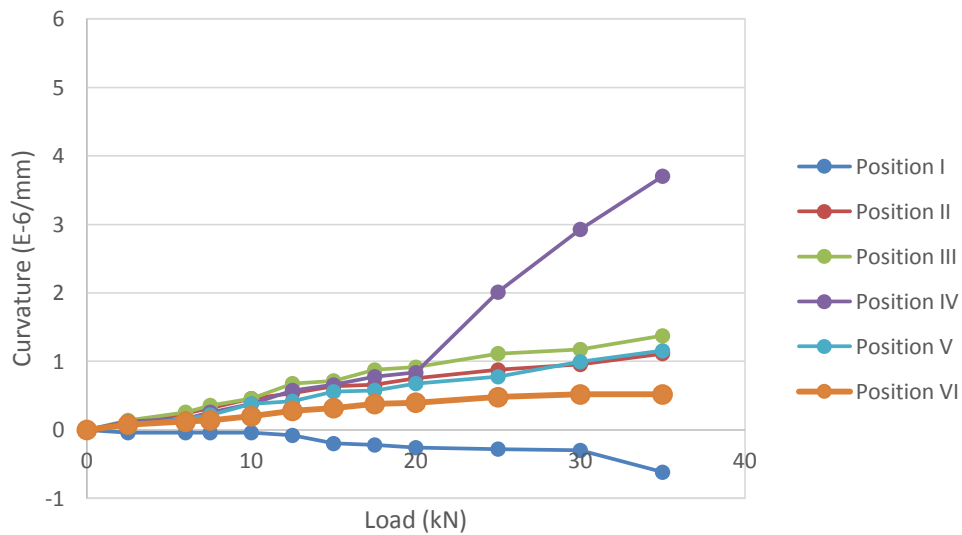


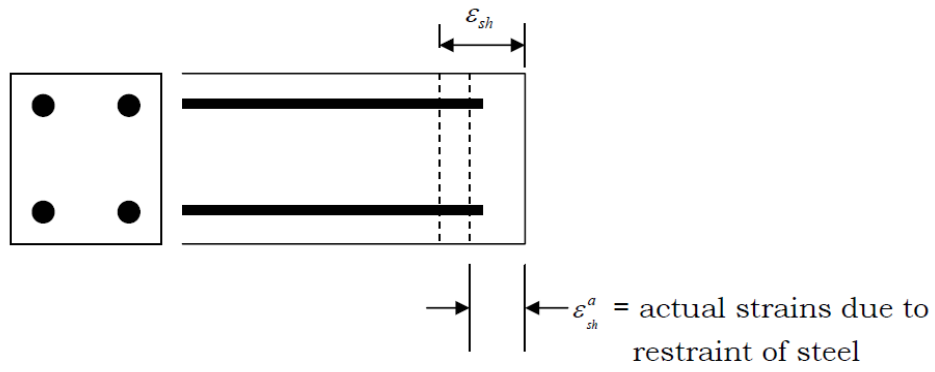
Figure 7-33 Curvatures of the surface strain of the U-beam of Specimen P1

The curvature at Position I (the joint core), as presented in Figure 7-32, decreased as the loading time increased. This behaviour is similar with the beam-column joint Specimen P1 under static loading, i.e. the joint experienced a compression strut mechanism, which has been discussed in Chapter 4.

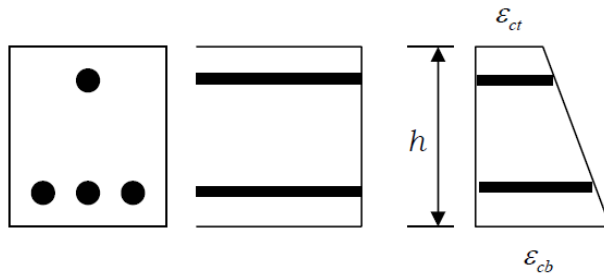
The exterior PCBC connection has bigger curvatures when subjected to a sustained load of 20kN (Figure 7-32) in comparison with those under short time loading (Figure 7-33). This is caused by the effect of creep and shrinkage due to long-term loading.

Theoretically, the effect of shrinkage on the reinforced concrete beam with symmetrical reinforcement causes uniform stress distribution. As presented in Figure 7-34 (a), due to uniform strain distribution, the zero curvature results.

Different from the symmetrical beam, the composite beam (i.e. the precast U-beam and the CIP beam core) used in this study had unsymmetrical reinforcement. Using the same analogy with the beam presented in Figure 7-34 (b), the composite beam experienced non-uniform stress distribution due to shrinkage, and hence, a curvature resulted.



b. Symmetrical reinforced beam



c. Unsymmetrical reinforced beam

Figure 7-34 Shrinkage effect on the reinforced concrete beam

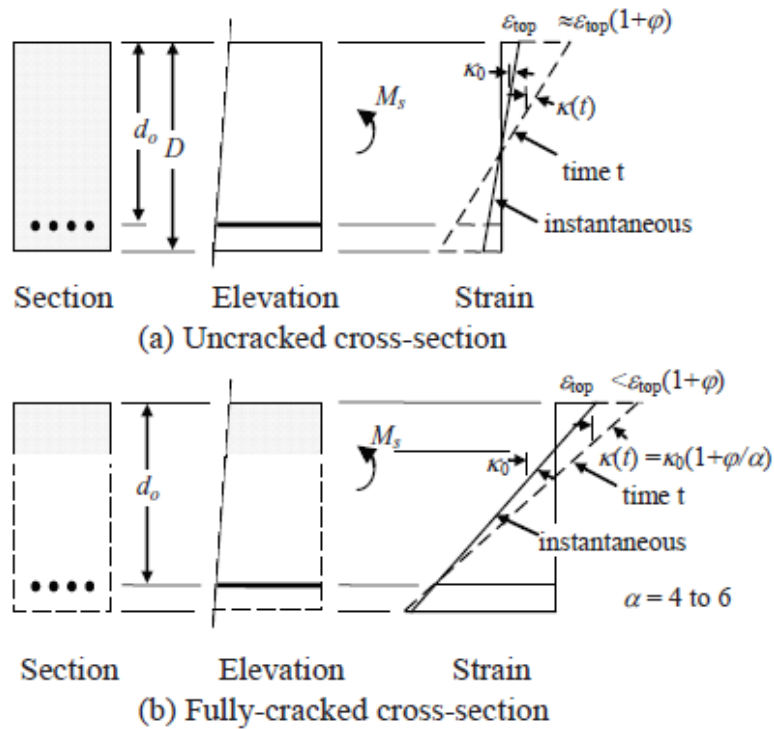


Figure 7-35 Effects of creep on the strain a single reinforced section in bending (Gilbert, 2011)

The effects of creep on a reinforced concrete beam, both un-cracked and cracked, are presented in Figure 7-35. The interaction of the compression and tension zone works according to the compatibility requirement that plane sections must remain plane. The neutral axis depth varied along the beam length depending on the un-cracked and the cracked sections. For the un-cracked section (Figure 7-35-a), creep increases the compressive and tensile strain, which also increases the curvature as well. The higher tensile creep is reduced by the restraint of the reinforcement. For the cracked section of a singly reinforced beam (Figure 7-35-b), creep in the compression zone increases the compressive strain. The tensile strain remains the same because there is no concrete to creep. Therefore, creep increases the neutral axis depth (measured from the top surface in Figure 7-35) and also the curvature, but reduces the compressive stress level.

Finally, the effect of shrinkage and the gradual development of creep strain in the compression zone of the composite beam section increased the curvature, which leads to an increase in the deflection of the beam. The effects of shrinkage and creep are additive. The neutral axis (NA) position is influenced by these phenomena. Due to shrinkage, the symmetrical reinforced concrete beam section (under positive moment) has the same shrinkage strains in both the compression and tension zone, consequently, the NA drops and the curvature remains same. Whereas, in un-symmetrically reinforced concrete beam sections (i.e. tension reinforcement is greater than compression reinforcement), the shrinkage in the tension zone is lower than in the compression zone (due to the greater restraint to movement offered by the tension steel), hence, the NA drops slightly and the curvature gets bigger. Due to creep, at the same stress level, the tensile creep is greater than the compressive creep. In this stage, the NA moves upward and the curvature is greater. However, the compressive stress is much higher than the tensile stress; this causes the compressive creep to be greater than the tensile creep. Hence, the NA drops and the curvature is bigger. By assuming the principle of superposition with respect to those phenomena, it can be said that the NA

position can potentially remain the same or move slightly depending on the quantity and the arrangement of the reinforcement. The curvature becomes greater due to shrinkage and creep effects.

7.5 Conclusions

The conclusions of this chapter are:

1. Precast concrete beam-column connection Specimen P5 behaved in a similar manner to conventional reinforced concrete members under long-term loading. Flexural cracks occurred within the plastic hinge region of the beam. No cracks occurred in the joint core and the precast column.
2. Several cracks appeared in the top surface of the CIP beam core and also, fine gaps appeared at the interface between the precast U-beam and the CIP beam core – this was probably because of autogenous and drying shrinkage.
3. The concrete strain development under sustained loading is influenced by shrinkage and creep.
4. It was found that the joint rigidity percentage of the PCBC connection is 67% in comparison with a fully monolithic beam-column joint.
5. The joint rigidity percentage of 67% was introduced in the equations which are used to predict the immediate deflection of the PCBC connection. The method proposed by Branson (1965) and Bischoff (2005) resulted in stiffer load-deflection curves in comparison with the experimental curve due to a static load of 20kN. Bischoff's method yielded the same deflection as the experimental result at a load of 20kN.

6. The current prediction methods (ACI-318, EC2, AEMM, Branson's method) underestimated the long-term deflection of Specimen P5 in comparison. This is because the precast U-beam was not perfectly monolithic with the column, which, therefore meant a larger deflection at the beam tip was generated.
7. Tension stiffening occurring in the CIP beam core could cause the beam-column rotation. The rotation continued during sustained loading which generated bigger deflection on the beam tip. Because of that, introducing the joint rigidity percentage into the time-dependent factor (ζ) used in the ACI method is relevant. This approach resulted a new estimate which is in agreement with the experimental long-term deflection of the PCBC connection.
8. Due to creep, the curvatures of the U-beam increased as the time increased. In contrast, the curvature of the joint core decreased as the time increased because the compression strut mechanism happened in the joint core due to the negative bending moment. These curvatures were similar to those of the PCBC connection under static loading (Specimen P1).

Chapter 8

Finite Element Modelling

8.1 Introduction

This chapter presents the finite elements modelling of the exterior and interior precast concrete beam-column (PCBC) connections using interlocking bars using MIDAS FEA software package.

The objective of this chapter is to predict the load-deflection behaviour of the exterior PCBC connection using finite elements modelling and validate the numerical results with the experimental data. Furthermore, this study is performed in order to provide a numerical model that can be used to investigate the effect of further parameters on the behaviour of the connection.

Firstly, the FE model was developed and validated using the experimental results of the PCBC Specimen P1 (exterior PCBC connection under static loading). Then, it was used to simulate the FE model under cyclic loading. The results were compared with the experimental result of Specimen P2.

Secondly, the FE model of the monolithic beam-column joint was developed in order to find the relative joint rigidity of the PCBC connection by comparing the results of the numerical and the experimental results.

Finally, in order to investigate the structural behaviour of the interior PCBC connection (as presented in Figure 1-3, Chapter 1), the FE model for interior PCBC was developed using the same material constitutive models used in the exterior PCBC model.

Within this chapter, the element types used in the FE model, material constitutive models, loading and boundary conditions are presented.

8.2 Material Constitutive Model

8.2.1 Concrete

Midas FEA provides 8 constitutive models of material, i.e. Elastic, Rankine, Tresca, Von Mises, Drucker Prager, Mohr Coulomb, Total Strain Crack and user supplied material (see Figure 8-1). For modelling the concrete used in this study, as discussed below, the Total Strain Crack model was considered to be the most suitable to simulate crack propagation in concrete.

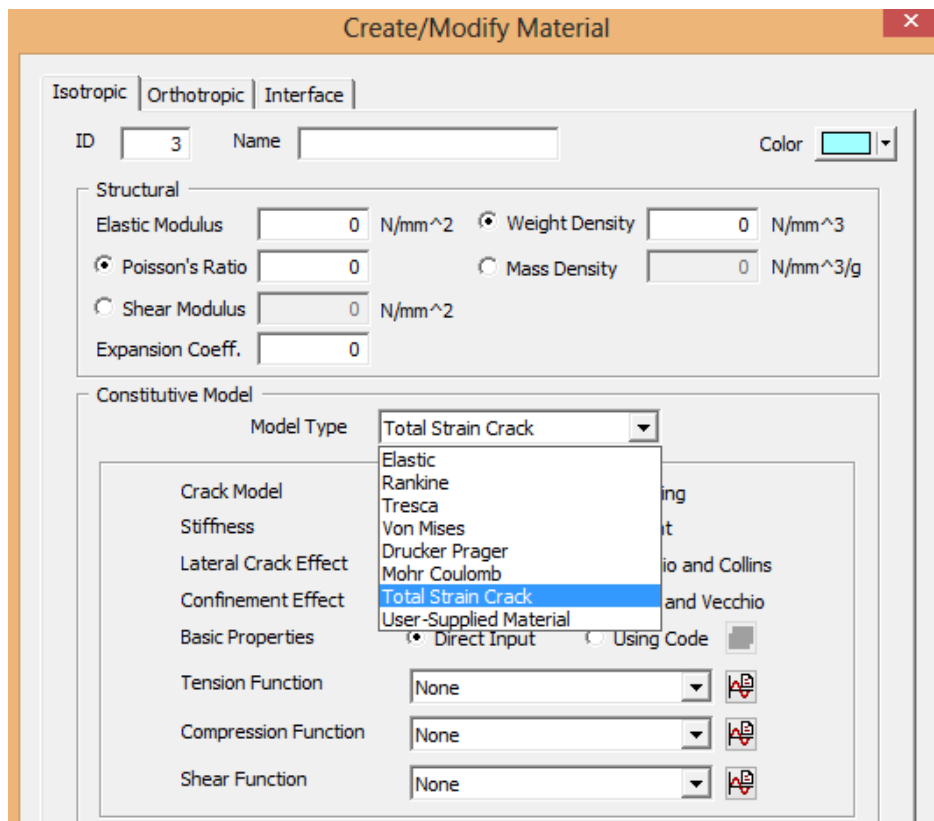


Figure 8-1 Constitutive model of material provided by Midas FEA

The Total Strain Crack model is based on the Modified Compression Field Theory proposed by Vecchio and Collins (1986). The Modified Compression Field considers the tensile stress of cracking concrete, whereas the Compression Field theory is ignored. The Total Strain Crack model uses a smeared approach in predicting the reinforced concrete element response with three uniaxial material models for tension, compression and shear. The three-dimensional extension to this theory is proposed by Selby and Vecchio (1993) to account for the effect of lateral cracking (Ngekpe et al., 2016). The Total Strain Crack model provides two methods: the fixed crack model and the rotating crack model depending on the reference crack axes. The shear stiffness of the cracked concrete is gradually reduced due to the progressive damage of the concrete; this is modelled by using a shear retention factor.

This study will use the Total Strain Crack model with the configuration of the fixed crack model including secant stiffness, lateral crack effect (Vecchio and Collins, 1986), and the confinement effect (Selby and Vecchio, 1993), as presented in Figure 8-2. Compressive strength, tensile strength and shear model implemented is defined as follows.

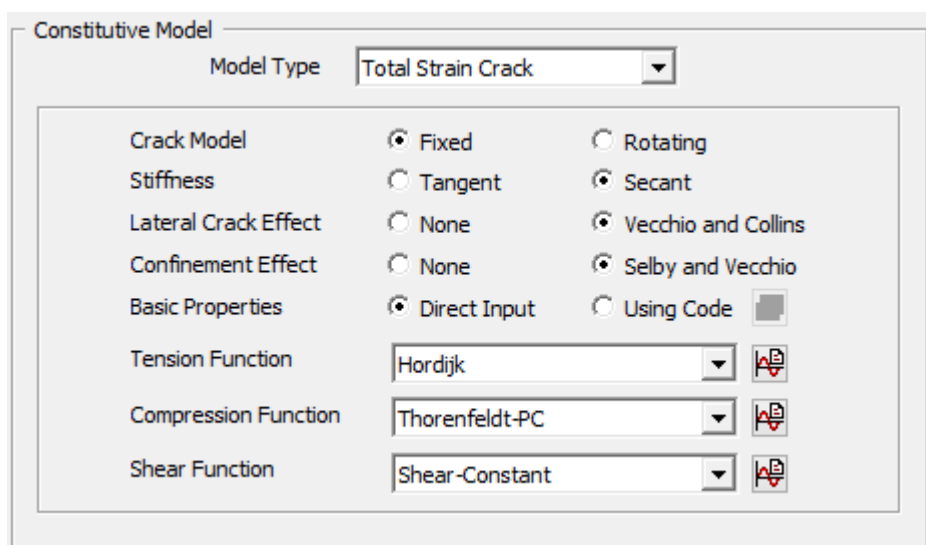


Figure 8-2 Total strain crack parameters used in this study

The models proposed by Thorenfeldt et al. (1987) and Hordijk (1991) were used for modelling the uniaxial compressive and tensile behaviour, respectively. Those models were used by Brunesi et al. (2015) and Bandara et al. (2016) which resulted in a numerical result which had a good agreement with the experimental results.

The model proposed by Thorenfeldt et al. is presented in Figure 8-3. The compressive model is influenced by lateral cracking. If the concrete is cracked in the lateral direction, the compressive stress and strain are reduced with the factor of $\beta_{\epsilon_{cr}}$ (for the peak strain) and with the factor $\beta_{\sigma_{cr}}$ (for the peak stress). The reduction factor of $\beta_{\sigma_{cr}}$ is presented in Figure 8-4 (Vecchio and Collins, 1993), whereas the factor of $\beta_{\epsilon_{cr}}$ is equal to 1 (MIDAS, 2010).

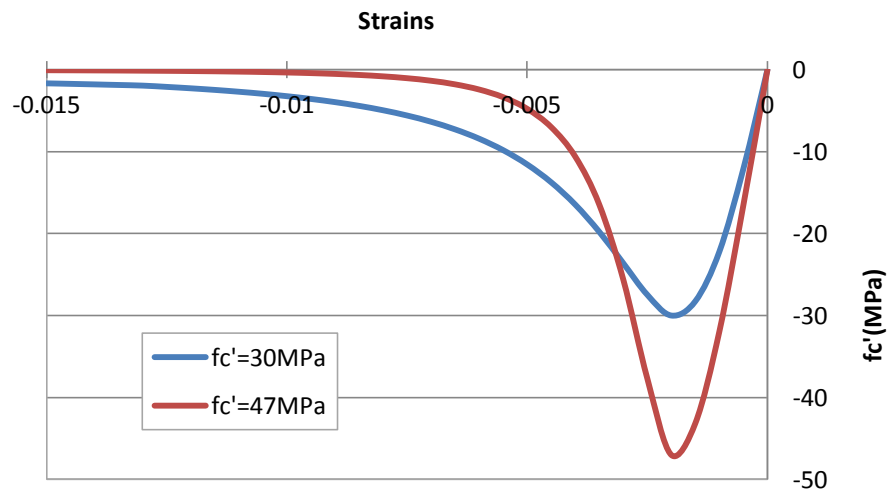


Figure 8-3 Thorenfeldt compression curve (Thorenfeldt et al., 1987)

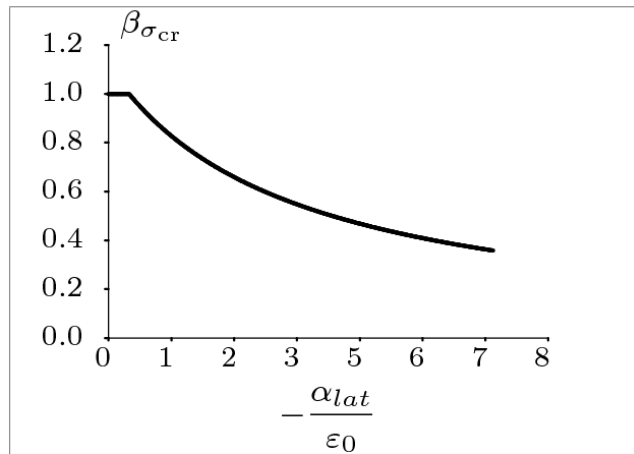


Figure 8-4 Reduction factor due to lateral cracking (Vecchio and Collins, 1986)

Hordijk (1991) proposed an expression for softening behaviour of concrete which results in a crack stress equal to zero at a crack width $\Delta u_{n,ult}$, as presented in Figure 8-5. This model was used for the tensile behaviour. The hysteresis model of Hordijk (1991) is presented in Figure 8-6. It shows that unloading and reloading follow the different paths. The ultimate crack strain is defined by Equation (8-1).

$$\Delta u_{n,ult} = 5.136 \times \frac{G_f^I}{f_t} \quad (8-1)$$

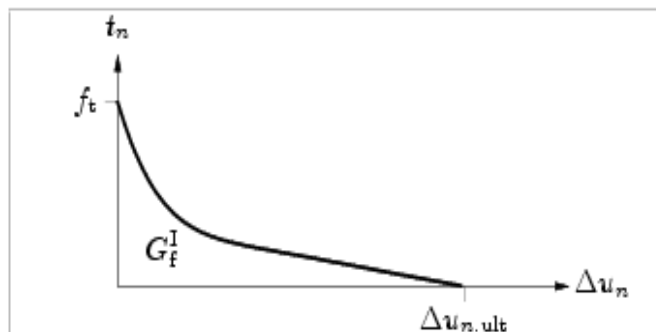


Figure 8-5 Hordijk tension model (Hordijk, 1991)

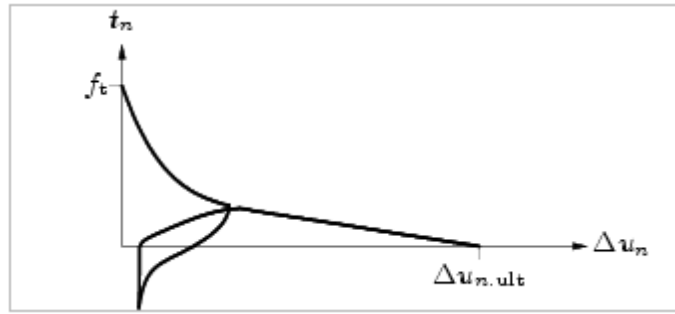


Figure 8-6 Hysteresis model (Hordijk, 1991)

The fracture energy (G_f) is defined as the amount of energy required to create one unit area of crack surface (Ngekepe et al, 2016). The fracture energy used in this modelling is obtained from equations proposed by CEB-FIP (1993), as presented in Equation (8-2) and (8-3).

$$G_{f0} = 0.024 \frac{0.0053 d_{max}^{0.95}}{8} \quad (8-2)$$

$$G_f = G_{f0} \left[\frac{f_{cm}}{10} \right]^{0.7} \quad (8-3)$$

Where,

d_{max} = maximum aggregate size

G_{f0} = the base fracture energy

f_{cm} = the mean compressive strength of cylinder

In the fixed crack concept, the shear behaviour of the concrete is modelled with the shear stiffness reducing after cracking (G^{cr}). The reduction factor from the initial elastic shear modulus (G) is referred to as the shear stiffness reduction or shear retention factor (β), where $0 \leq \beta \leq 1$. Therefore, the reduced constant shear stiffness is calculated as: $G^{cr} = \beta G$ (see Figure 8-7). For the rotating crack concept, the shear retention factor can be assumed equal to one (MIDAS, 2010).

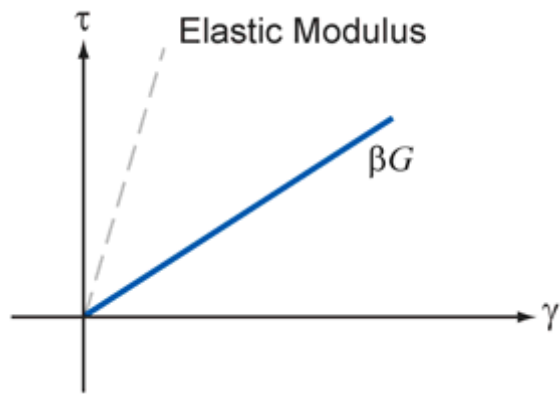


Figure 8-7 Shear stiffness model

8.2.2 Steel reinforcement

The embedded reinforcement was used for modelling the longitudinal and transverse reinforcement bars, with the assumption that there is a perfect bond between the reinforcement bar and the concrete (Ngekpe et al., 2016; Barbosa and Ribeiro, 1998; Hasan, 1994; Ibrahim and Mubarak, 2009; Mahmood, 2007).

The Baushinger's effect in the steel reinforcement under cyclic loading is included by using Menegotto-Pinto model (Menegotto and Pinto, 1973), as presented in Figure 8-8.

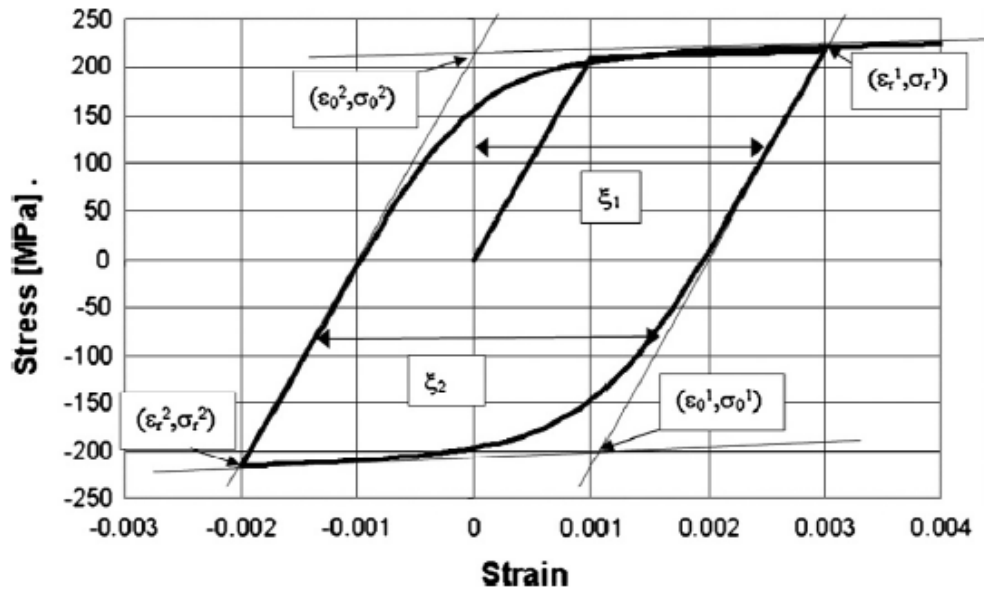


Figure 8-8 Model proposed by (Menegotto and Pinto, 1973)

The stress-strain relationship is defined as:

$$\sigma^* = b\varepsilon^* + \frac{(1-b)\varepsilon^*}{(1+\varepsilon^{*R})^{1/R}} \quad [MPa] \quad (8-4)$$

Where,

$$\sigma^* = \frac{\varepsilon - \varepsilon_r}{\varepsilon_0 - \varepsilon_r} \quad \sigma^* = \frac{\sigma - \sigma_r}{\sigma_0 - \sigma_r} \quad (8-5)$$

In Figure 8-8, σ_0 and ε_0 are the stress and strain values at the point where two asymptotes meet; σ_r and ε_r are the stress and strain values at the point where the last strain reversal with equal stress takes place. R is a parameter which influences the shape of the transition curve and allows a good representation of the Baushinger's effect. After each strain reversal, the parameters of σ_0 , ε_0 , σ_r , ε_r and R are updated. Furthermore, the strain hardening ratio (b) is calculated as ratio between slope E_1 and E_0 .

The corresponding value of the stress-strain behaviour of the reinforcement bars obtained from the tests is incorporated in this model. The Von Mises yield criterion combined with elastic-plastic behaviour with strain hardening was used for reinforcement.

8.3 Modelling of Exterior PCBC Connection

8.3.1 FE model

The finite element model of the exterior precast concrete beam-column specimen was developed in the MIDAS FEA programme. Solid element (auto-mesh) type (see Figure 8-9) was used to model the precast concrete beam-column (PCBC) specimen; this is because the reinforced concrete element (i.e. precast column with corbel, precast U-beam and the cast-in-place (CIP) connection) have variation in shape and dimension. Using auto-mesh solid, the meshes are generated automatically for selected solids (shapes).

A sensitivity analysis was carried out to investigate the mesh size that is suitable for modelling the exterior PCBC connection. The analysis compared 4 sizes of meshes, i.e. 25mm, 50mm, 75mm, and 100mm (see Figure 8-10). The result of the sensitivity analysis is presented in Figure 8-15.

Reinforcement elements were used to model the longitudinal and transverse reinforcement bars, as presented in Figure 8-14.

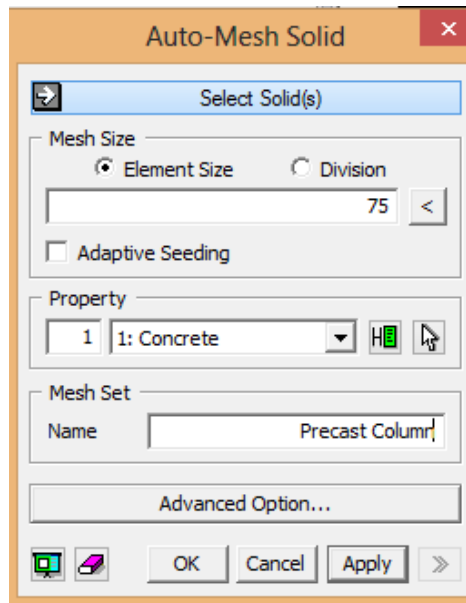
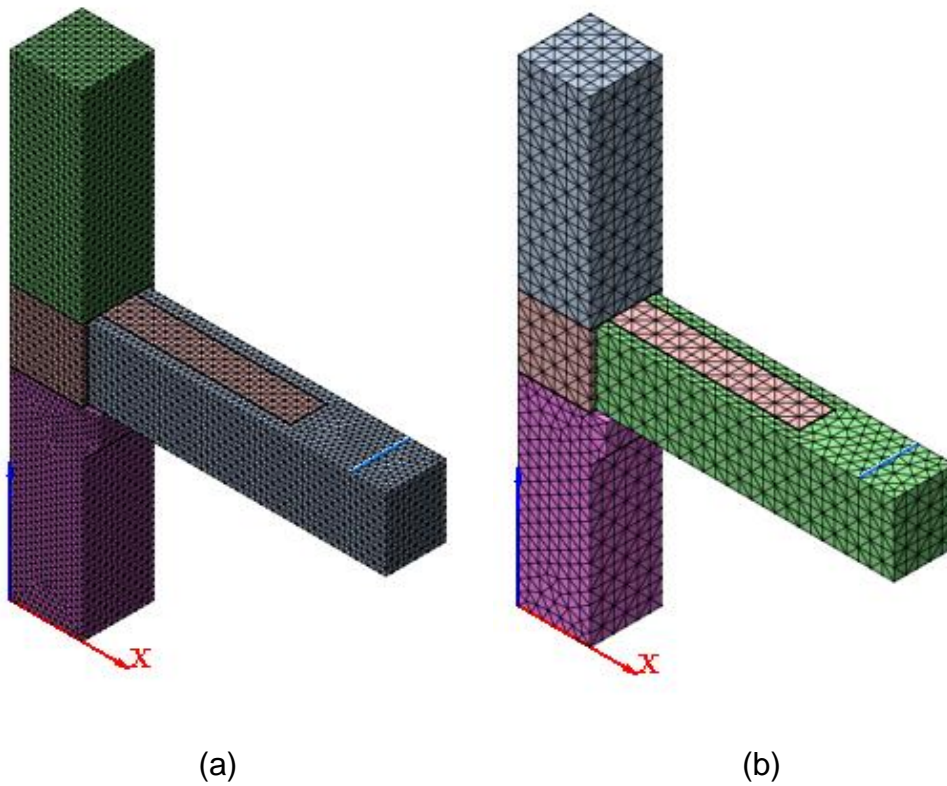


Figure 8-9 Auto-mesh Solid in Midas FEA



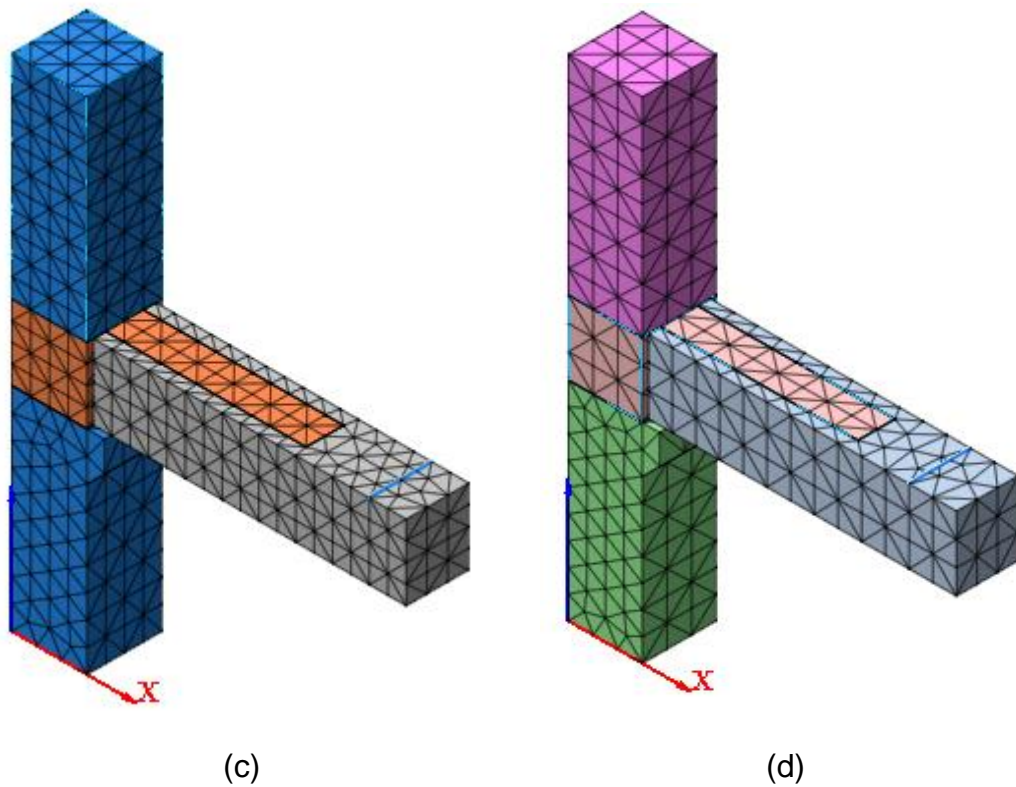


Figure 8-10 FE meshes of the exterior PCBC connection: (a) 25mm, (b) 50mm, (c) 75mm and (d) 100mm

To separate the CIP concrete and the precast concrete in the model, two-dimensional interface elements were applied to represent the interaction between the precast concrete and the CIP concrete, as illustrated in Figure 8-11. ACI 318-08 (Sec. 11.6) stated that shear-friction provisions are to be applied to consider shear transfer across a given plane, such as an interface between dissimilar material, or interface between two concretes cast at different times. The mesh size of the interface was the same as the mesh size used for precast and CIP elements.

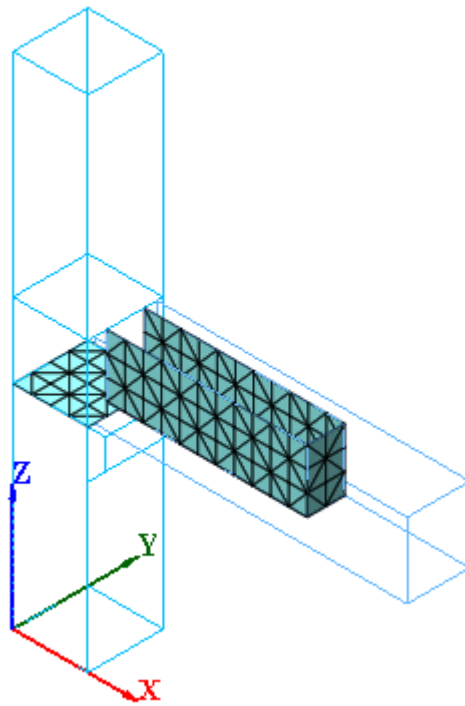


Figure 8-11 Interface mesh

Coulomb friction was implemented for interface elements. This model is used for the interface between two parts of a structure which is governed by a frictional behaviour (MIDAS, 2010).

Lampropoulos et al. (2007) investigated the behaviour of RC columns strengthened with RC layers and jackets. The interface between the old and new concrete was modelled using contact elements. The model used to define the behaviour of the contact elements is presented in Figure 8-12.

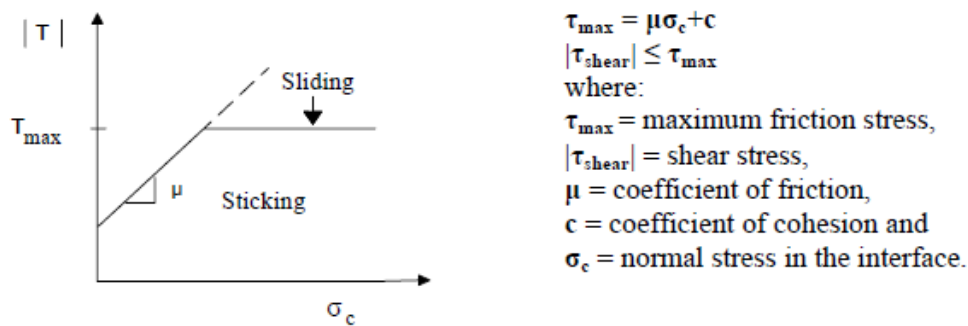


Figure 8-12 Shear stress against normal stress distribution at the interface (Lampropoulos et al., 2007)

Due to the lack of experimental data for the interface in this study, the value of normal stiffness and shear stiffness of interface between the old and new concrete were obtained from the model showed in Figure 8-12. Considering the angle of friction of the interface in this study was nearly 0, then the minimum value were taken as presented in Figure 8-13. The cohesion of the interface was taken to be 1.38 (Mattock and Hawkins, 1972).

A sensitivity analysis was carry out on the parameters of the interface, i.e. the angle of friction and the interface cohesion. The results are presented in Figure 8-16 and Figure 8-17.

Figure 8-13 Properties of interface elements used in MIDAS

The model of the boundary condition simulated the experimental set-up condition, i.e. on the column portion fixed by steel plates bolted into the test rig were modelled by two single line supports (fixed) which were provided at two sides of the upper and lower column. Figure 8-14 presents the boundary condition of the FE model of the exterior PCBC connection.

In this section, the FE model will be subjected to static loading and cyclic loading. The result, in term of load-deflection relationship, will be compared with the experimental result of Specimen P1 (for static loading) and Specimen P2 (for cyclic loading).

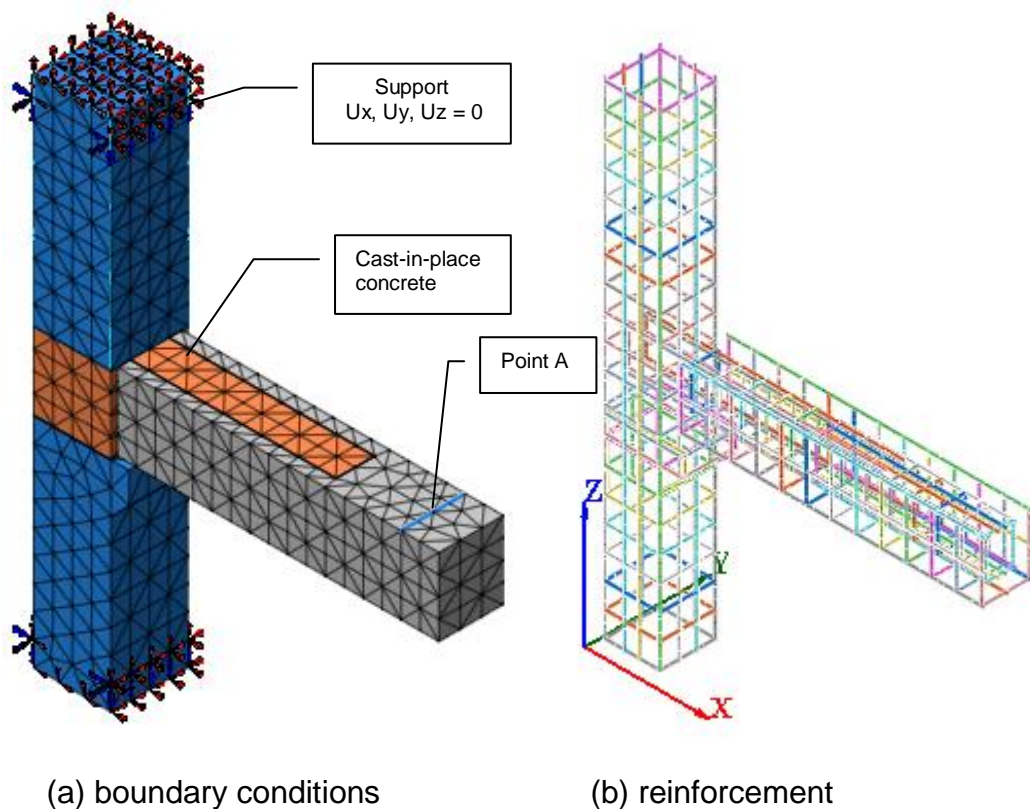


Figure 8-14 Boundary condition and reinforcement of exterior PCBC specimen

8.3.2 Results and discussion

8.3.2.1 Static loading

Nonlinear analysis using displacement based load control was performed to obtain the load-deflection relationship of the PCBC Specimen. The displacement was applied vertically downwards to the beam tip (at point A in Figure 8-14), which generated negative moments in the beam. The maximum displacement applied to the PCBC model was 50mm with the increment load of 1mm.

The mechanical properties obtained from the PCBC Specimen P1 tests, as presented in Table 8-1, were implemented in MIDAS FEA. The yield strength (f_y) of the steel reinforcement was 500MPa. Poisson's ratios were 0.3 for reinforcement steel and 0.16 for the concrete (Hawileh et al., 2010).

Table 8-1 Mechanical properties of concrete*

	Precast Concrete	CIP Concrete
Type of material	Isometric	Isometric
Modulus of elasticity	27000 N/mm ²	35300 N/mm ²
Compressive strength	30 N/mm ²	47 N/mm ²

*adopted from experimental data of PCBC Specimen P1 (as mentioned in Chapter 4)

Figure 8-15 presents the numerical load-deflection curves of 4 different mesh sizes, i.e. 25mm, 50mm, 75mm and 100mm, for the PCBC specimen under static loading in comparison with the experimental curve obtained from PCBC Specimen P1 (as explained in Chapter 4).

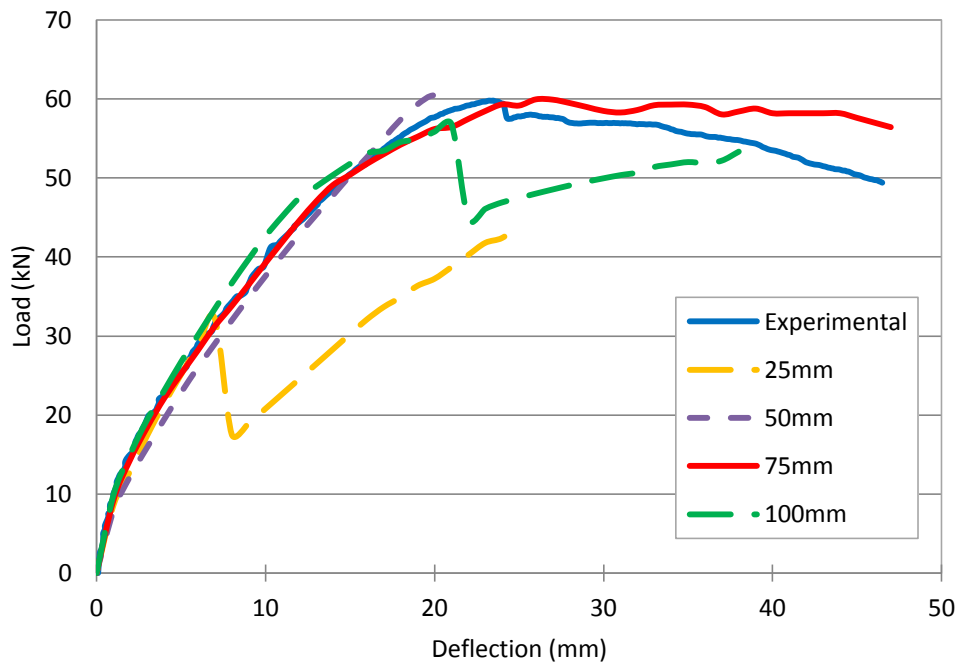


Figure 8-15 Comparison of load-deflection curves of PCBC connection between experimental and numerical results

It can be seen in Figure 8-15 that all numerical curves have similar slopes with the experimental curve at the elastic portion. However, the 25mm-curve dropped at the deflection of 7mm and increased again at the deflection of 8mm then stopped at the deflection of 25mm. The 50mm-curve stopped at the deflection of 22mm because the analysis was not converged in maximum number of iterations. The 75mm-curve shows a better result: the curve is coincident with the experimental curve until the yield point. The 100mm-curve is slightly stiffer than the experimental curve and dropped at the deflection of 21mm (at the yield point) and increased again at the deflection of 22mm and stopped at deflection of 38mm.

It shows that the model with the mesh size of 75mm provides the best result. The initial part of the numerical curve (mesh size 75mm) is coincident with the experimental until the yield load. The numerical curve has a small decrease after the yield point. In fact, after the yield point, the

experimental curve decreased due to the de-lamination between the CIP beam core and the wall of the precast U-beam (it has been discussed in Chapter 4).

To see the sensitivity of the results to the choice parameters of the interface between the CIP beam core and the precast U-beam, i.e. the angle of friction and the interface cohesion (presented in Figure 8-13), some analysis were carried out. Firstly, 3 different friction angles (i.e. 2, 3 and 5 degrees) were applied with the constant interface cohesion ($C = 1.38 \text{ N/mm}^2$). Secondly, 4 different interface cohesion (C) values were applied with the constant angle of friction (2 degrees). The results are presented in Figure 8-16 and Figure 8-17.

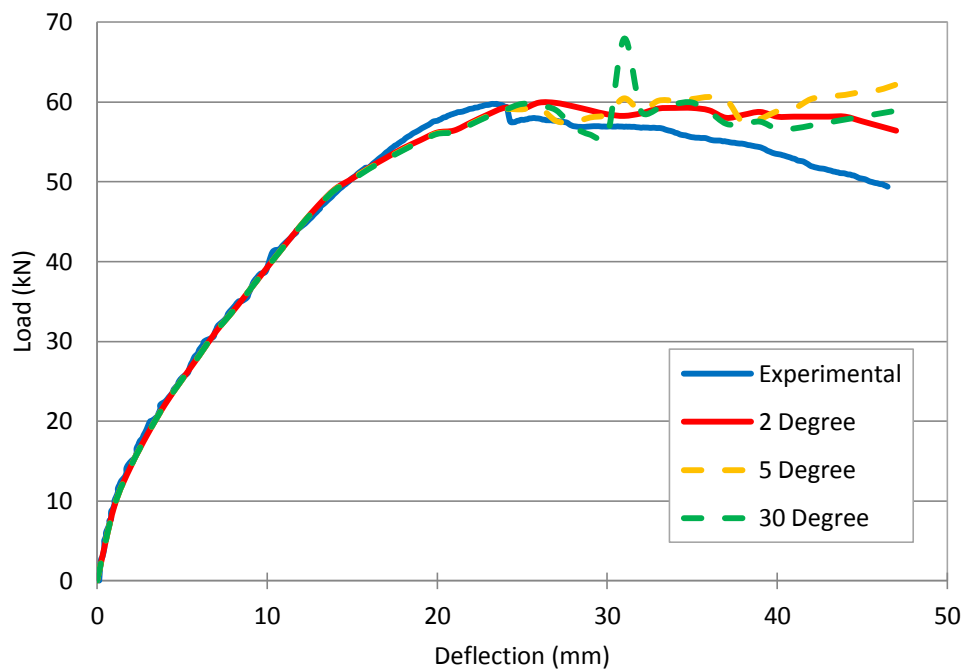


Figure 8-16 Load-deflection curves with different friction angle of the interface (i.e. 2, 5 and 30 Degrees).

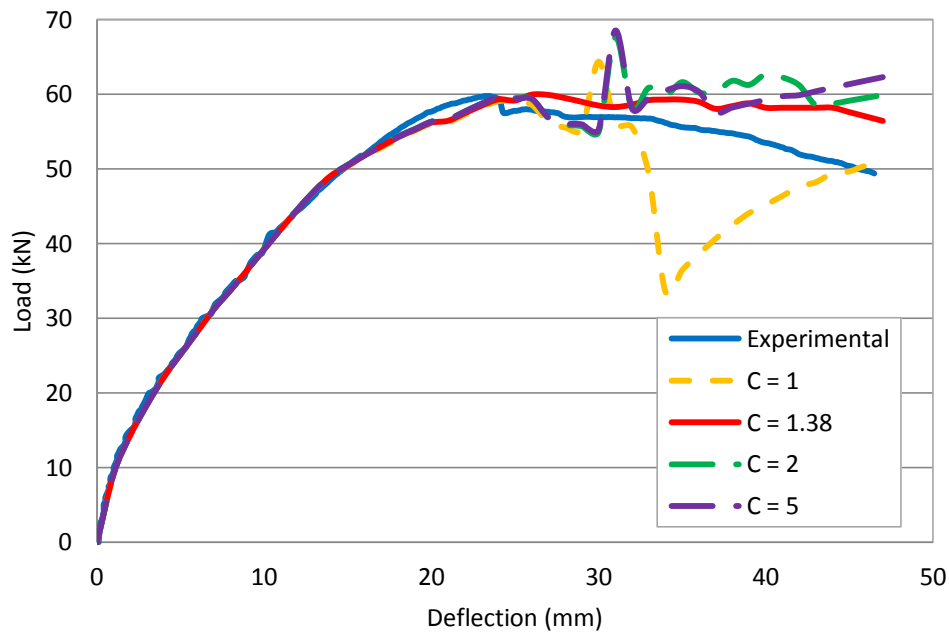


Figure 8-17 Load-deflection curves with different cohesion (C) of the interface (i.e. 1, 1.38, 2 and 5 N/mm²)

As can be seen in Figure 8-16 and Figure 8-17, all the numerical results have the same load-deflection curves in the elastic portion, which means that the change in the cohesion and the friction angle of the interface do not affect the load-deflection curve. The changes in these parameters only affects the post-elastic portion (after the yield point). The curve with the friction angle of 2 degrees and the interface cohesion of 1.38 N/mm² provides the result that is very close to the experimental result.

From the sensitivity analysis above, it can be concluded that the model of exterior PCBC connection with the mesh size of 75mm, the friction angle of 2 degrees and the interface cohesion of 1.38 N/mm² provides a load-deflection curve that is similar with the experimental result.

Figure 8-18 illustrates the stress distribution in the reinforcement of the PCBC connection under negative loading. The top longitudinal bars of the beam reach yield stage, whereas other reinforcement remains elastic. This is in a good agreement with the experimental data of PCBC Specimen P1 (explained in Chapter 4),

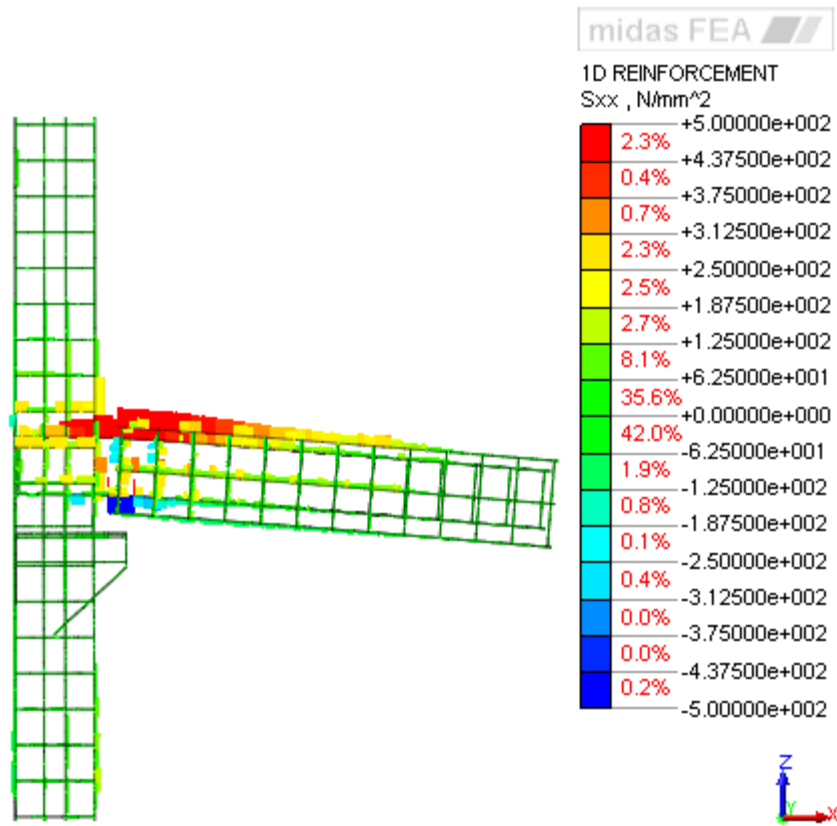


Figure 8-18 Reinforcement stresses at failure

Figure 8-18 illustrates the stress distribution in the reinforcement of the PCBC connection under negative loading. The top longitudinal bars of the beam reach yield stage, whereas other reinforcement remains elastic. This is in a good agreement with the experimental data of PCBC Specimen P1 (explained in Chapter 4),

In conclusion, the FE model could predict the behaviour in the elastic region until the yield point, but not accurately predict the behaviour after yield point. This is due to the lack of data of the interface properties between the precast concrete and CIP concrete.

8.3.2.2 Cyclic loading

In order to get the numerical cyclic behaviour, the FE model developed in the previous section was subjected to cyclic loading. The result will be compared with the experimental result of the PCBC Specimen P2.

MIDAS FEA software could not incorporate the cyclic model for concrete and steel reinforcements, therefore the same stress-strain relationship models used for concrete and steel reinforcement in the static analysis were applied in the cyclic analysis.

The same mechanical properties of concrete obtained from Specimen P2 tests (available in Chapter 5) were applied in the FE model. The interlocking bars were changed become 2D16 and D12, as Specimen P2 used.

The lateral load was applied on the beam tip using displacement control according to the loading history as presented in Figure 5-5. The vertical load was applied downward and upward to the beam tip, which is called as negative and positive loadings, respectively (see Figure 8-19). Two complete cycles were performed at each displacement level. During the test in the laboratory, the lateral displacement increments have been applied in a quasi-static reserve technique. Quasi-static cyclic loading tests have the advantages of requiring less complicated loading and recording equipment and giving more time to monitor the performance of the test specimens during the test (Park, 1994; Roehm et al., 2015).

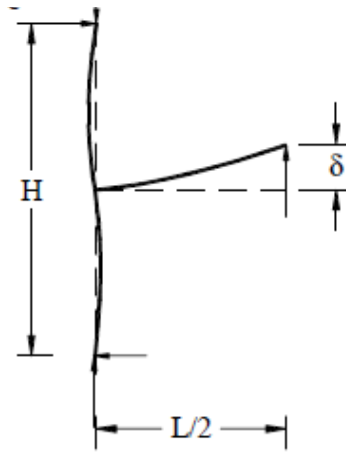


Figure 8-19 Cyclic loading used for the exterior PCBC connection

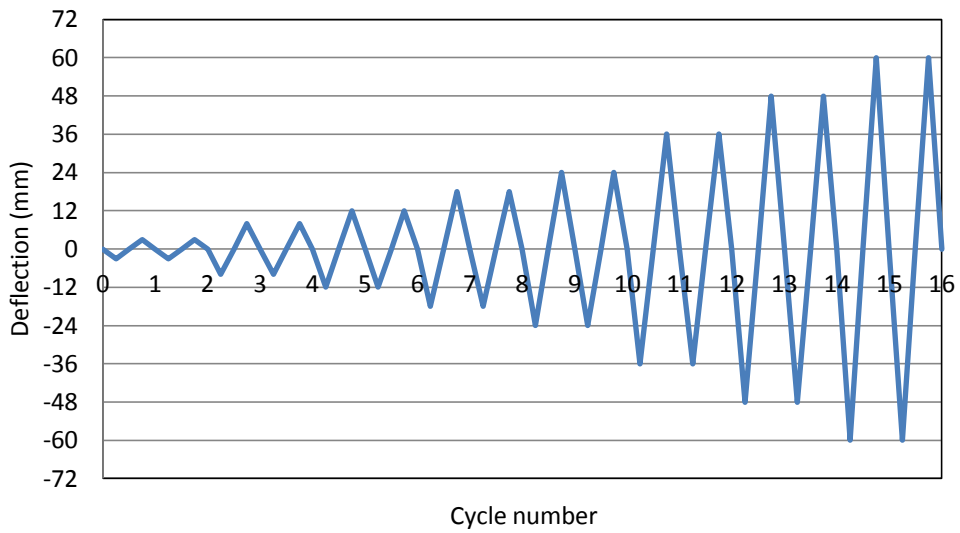


Figure 8-20 Load history for reversed cyclic load test used for Specimen P2

Figure 8-21 presents the hysteresis load-deflection loops obtained from the numerical and the experimental method. Figure 8-22 presents the envelope of the load –deflection relationship which connects the peak load of each displacement level; this is used for evaluating the structural stability of the joint (Nurjaman and Sidjabat, 2008; Said and Nehdi, 2004; Hawileh et al., 2010). As can be seen in Figure 8-21, the loops obtained from numerical method are not matching well with the loops of experimental method. This is because MIDAS FEA software could not accommodate the cyclic model for the concrete and steel reinforcement. As Hasan et al. (2011) stated that the correctness of the finite element model of reinforced concrete structure rely on the modelling of the stress-strain relationship of the concrete and steel reinforcement. However, the peak load at every displacement level is similar, as presented in Figure 8-22. The differences of peak loads between numerical and experimental method varies between 0.1 and 12.5%.

The stress-distribution of steel reinforcements due to the negative and positive moments is presented in Figure 8-23 and Figure 8-24. It shows that the longitudinal bars of the beam, especially at the beam end adjacent to the column face, reach yield stage before other reinforcement bars. This allows the plastic hinge formed in the beam. This result is in line with the result of the PCBC Specimen P2 (subjected to quasi-static loading) which has been discussed in Chapter 5.

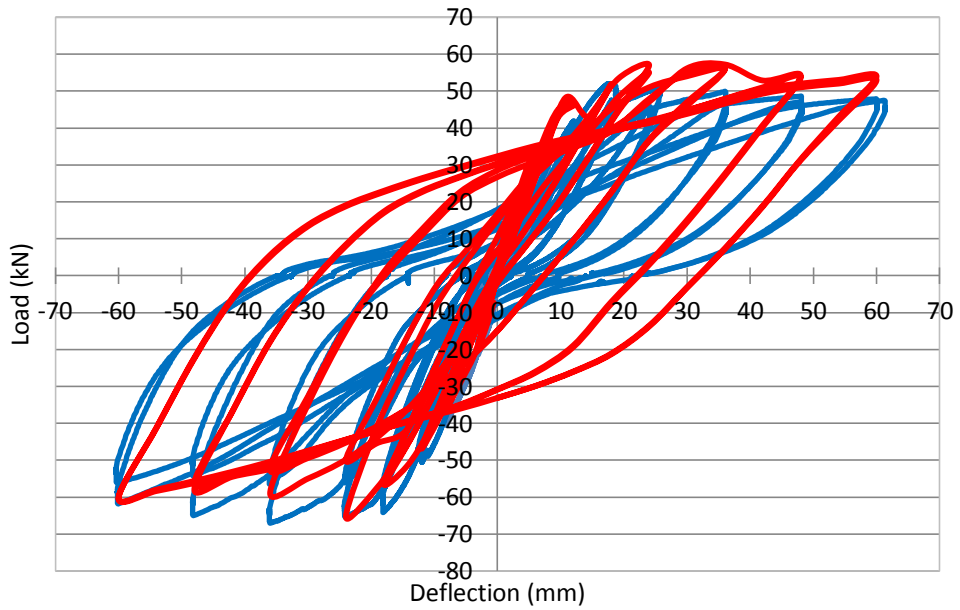


Figure 8-21 Comparison of load-deflection curves of PCBC connection between experimental and numerical results

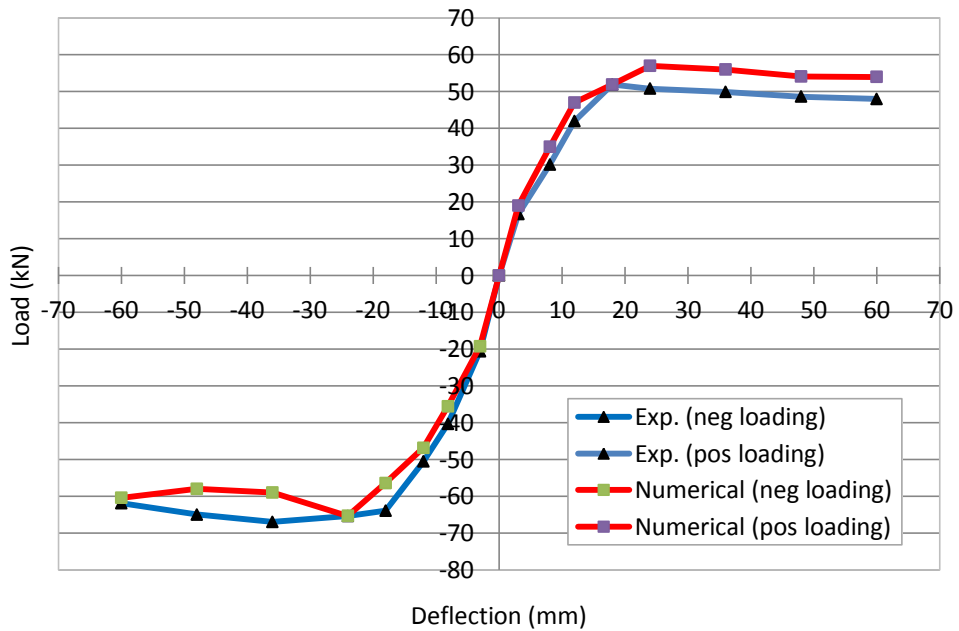


Figure 8-22 Load-displacement envelopes

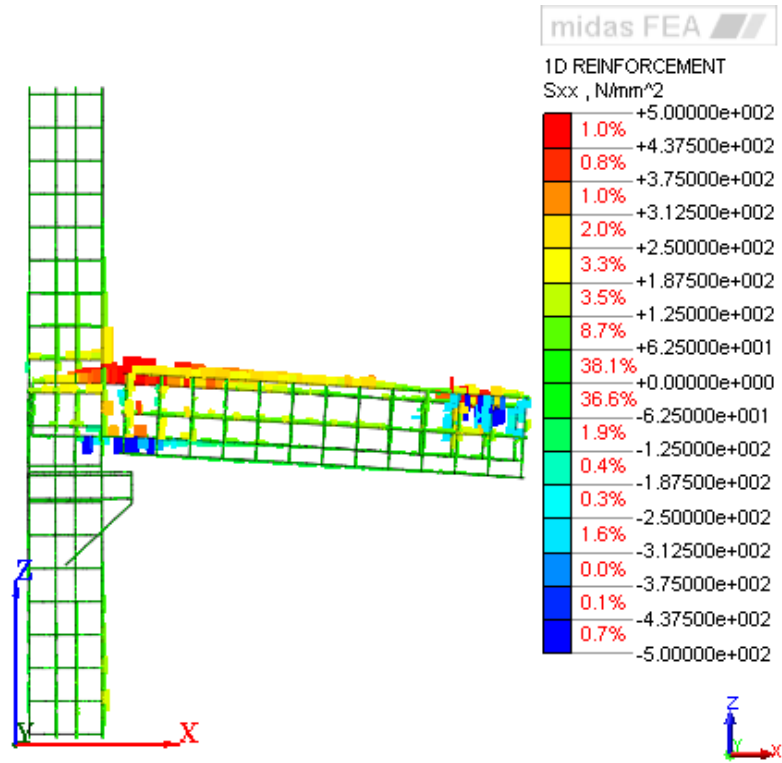


Figure 8-23 Reinforcement stresses at failure due to negative moment

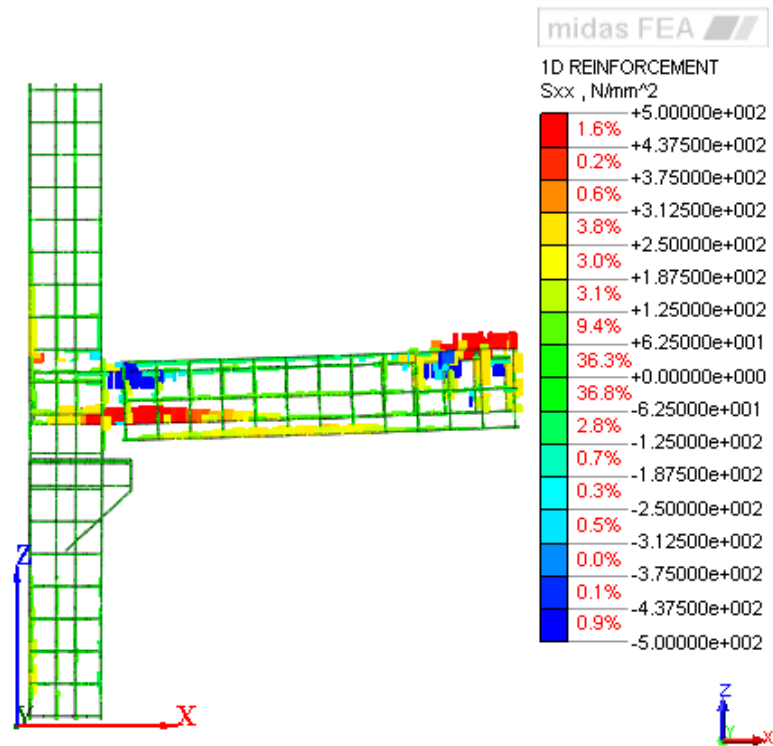


Figure 8-24 Reinforcement stresses at failure under positive moment

Conclusively, the FE model could not predict the hysteresis loop accurately because the software could not accommodate the cyclic model for the concrete and steel reinforcement. However, the FE model could predict the peak loads at each displacement level with the differences less than 12.5% in comparison with the experimental result.

8.4 Modelling of Monolithic Exterior BC Joint

8.4.1 FE model

In this study, it is important to know how much the relative joint's rigidity of the precast concrete beam-column (PCBC) connection developed in this study with respect to the monolithic beam-column joint. This could be determined by comparing the curves of experimental load-deflection of the PCBC connection and the monolithic beam-column joint.

In this study, there was no testing on the specimen of the monolithic beam-column joint experimentally. Therefore the load-deflection behaviour of the monolithic beam-column joint will be obtained from FE analysis. This section will present the FE analysis of the monolithic beam-column joint.

The FE model of the monolithic beam-column joint was built using the same principles as those used for the PCBC connection. Total strain crack strain model with configuration of fixed crack model, including lateral crack effect, confinement effect and secant stiffness were used. The Thorenfeld and Hordijk models were used to represent the compressive behaviour and tension softening of the reinforced concrete material. The compressive strength of concrete used in this model is 30MPa, i.e. the concrete strength of precast concrete elements.

The geometry and dimensions of the beam and the column were same with the PCBC connection. A slight change was introduced in the beam

reinforcement, i.e. there's no reinforcement in the precast U-beam. Figure 8-25 presents the FE mesh and reinforcement in the monolithic beam-column joint. The FE model of the monolithic beam-column joint was subjected to static loading.

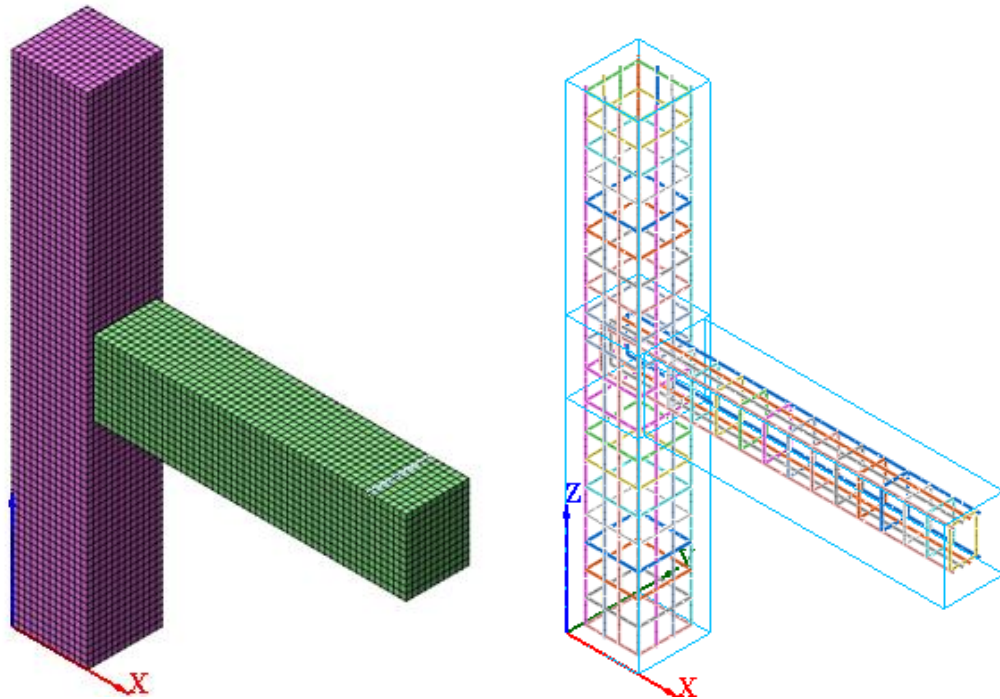


Figure 8-25 Mesh and reinforcement detail of the monolithic beam-column joint

8.4.2 Results and discussion

Figure 8-26 shows the load-deflection curves of the monolithic beam-column joint and the PCBC connection (obtained from Specimen P1 test). It can be seen that the monolithic curve is stiffer than the PCBC curve. It is because the precast U-beam was not monolithically connected to the precast column, which enabled to generate larger deflection at the beam tip.

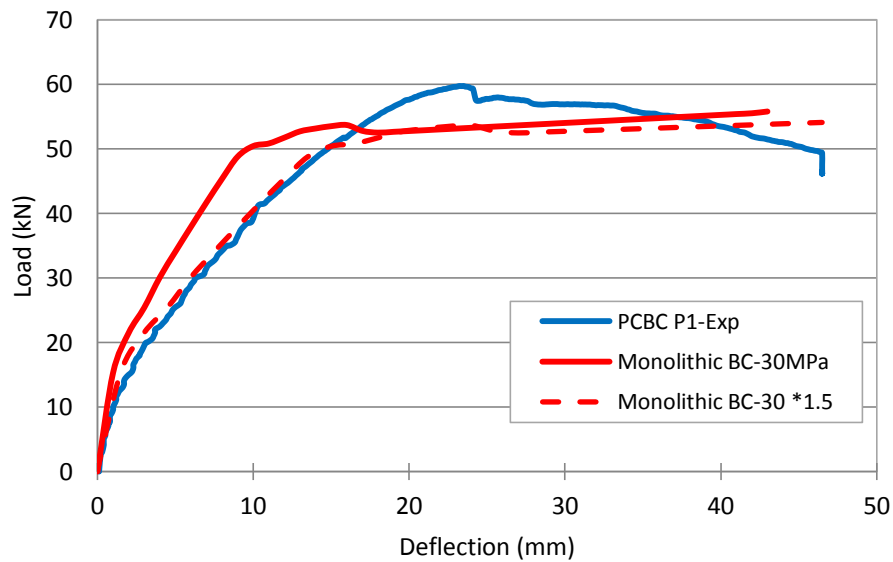


Figure 8-26 Comparison of load-deflection curves of PCBC connection and the monolithic beam-column joint

The joint rigidity percentage of the PCBC connection is obtained by dividing the secant stiffness of the curves of the PCBC connection with the monolithic joint. It is found that the joint rigidity percentage of the PCBC connection is 67% (it has been discussed in Chapter 7). It means that in order to have a similar load-deflection response with the monolithic joint, the deflection obtained from the PCBC specimen (under static loading) should be multiplied by 0.67.

To validate this claim, the deflection values of the monolithic beam-column joint were multiplied by 1.5 (i.e. obtained from $1/0.67$), as presented by the dashed line in Figure 8-26. The figure shows that the dashed line coincided with the PCBC curve until the maximum load. It can be concluded that the rigidity percentage of the exterior PCBC connection is $1/1.5$ or 67%.

8.5 Modelling of Interior PCBC Connection

8.5.1 FE Model

After validating the model of exterior PCBC specimen with the experimental result of PCBC Specimen P1, the next stage is to develop the FE model for the interior PCBC connection. The FE model of the interior PCBC connection was developed according to the precast concrete system concept illustrated in Figure 1-3 (Chapter 1). The model utilized the same beam used in the exterior PCBC model. The longitudinal reinforcement of the precast column was increased to ensure that the moment capacity of the column was bigger than the moment capacity of the beams. Figure 8-29 shows the reinforcement arrangements of the interior PCBC connection.

The same mechanical properties of materials applied to FE model of exterior PCBC connection above were also used for the interior model. The interior model will be subjected to a static loading. The cyclic loading on the interior PCBC model will not be performed in this study because Midas FEA could not predict the cyclic behaviour accurately (based on the FE analysis on the exterior PCBC connection in the previous section).

Figure 8-28 presents the FE meshes and boundary conditions of the interior PCBC connection. Two vertical loads are applied downward to both beam tips for static loading (see Figure 8-27).

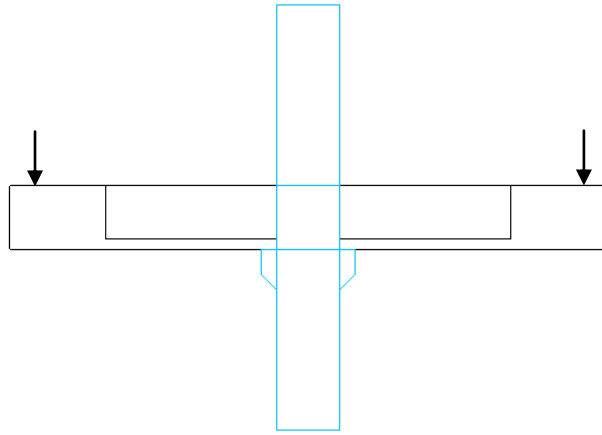


Figure 8-27 Loading arrangement of static loading for the interior PCBC connection

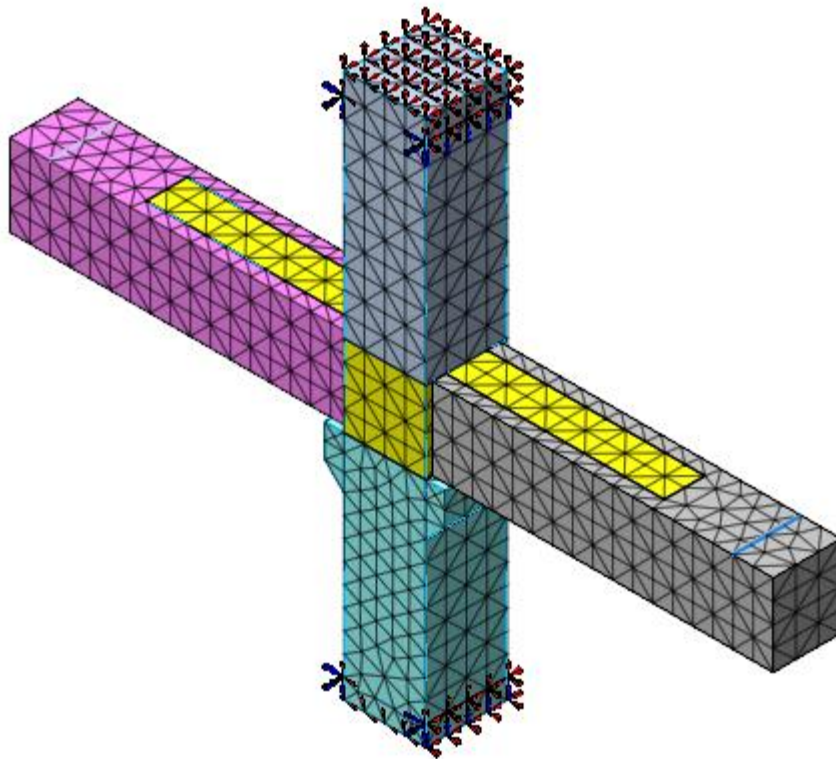


Figure 8-28 FE meshes and the boundary conditions of the interior PCBC connection

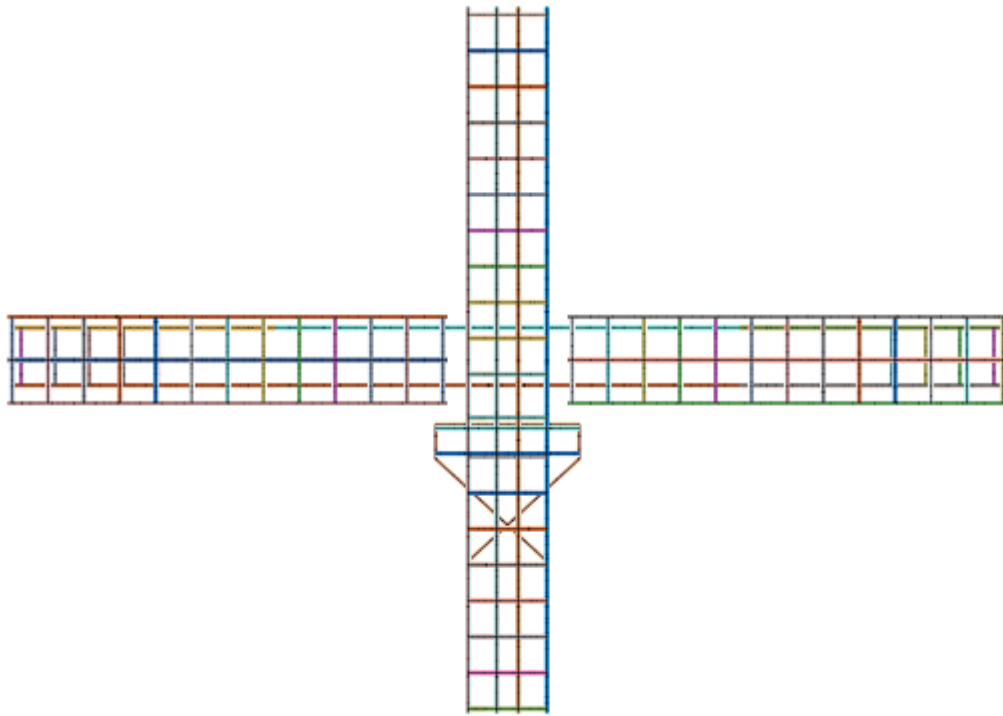


Figure 8-29 Reinforcement arrangement of the interior PCBC connection

8.5.2 Result and discussion

8.5.2.1 Static loading

Figure 8-30 presents the load-deflection relationship of the interior PCBC connection under static loading. Due to the symmetrical reinforcement and geometry, the curves of the right beam and the left beam are same. From that curves can be determined that the first crack load, the yield load and the maximum loads are about 15kN, 53kN and 60kN, respectively. The deflections of the beams are illustrated in Figure 8-31.

Figure 8-32 presents the stress distribution of the steel reinforcement in the interior PCBC connection. The top longitudinal bars of the right and left beams reach the yield stage earlier than the other reinforcement, which shows that the plastic hinges formed at the expected location.

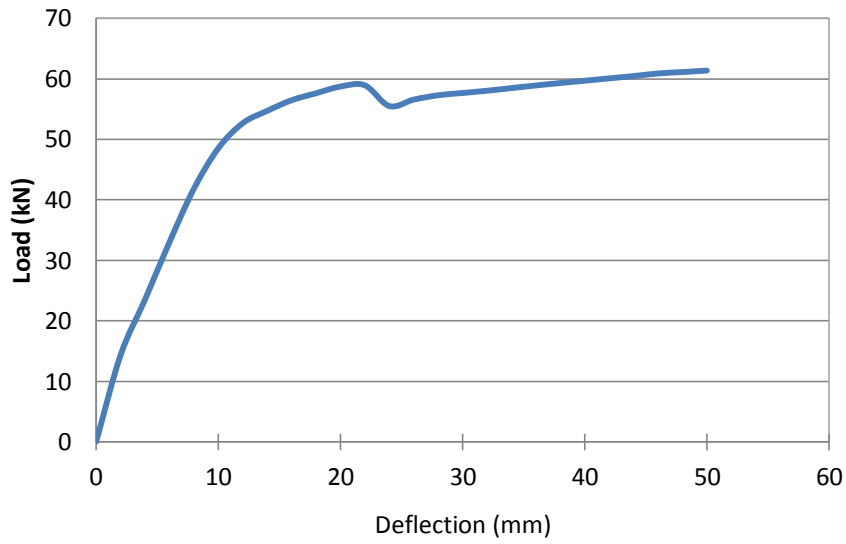


Figure 8-30 Load-deflection relationship of the interior PCBC connection under static loading

8

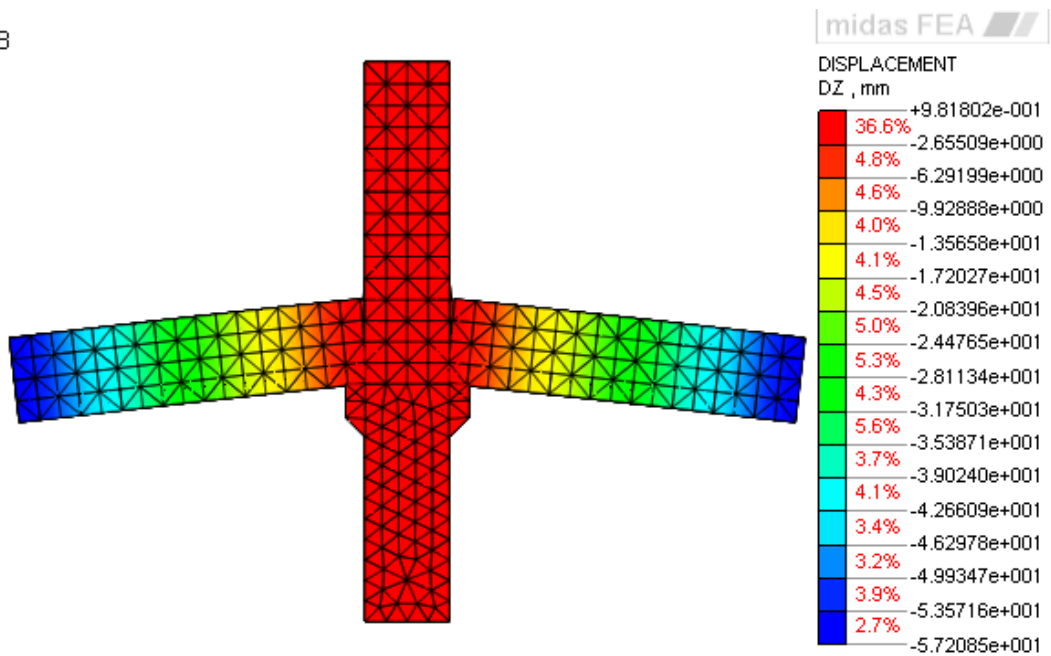


Figure 8-31 Deflection of the interior PCBC connection under static loading

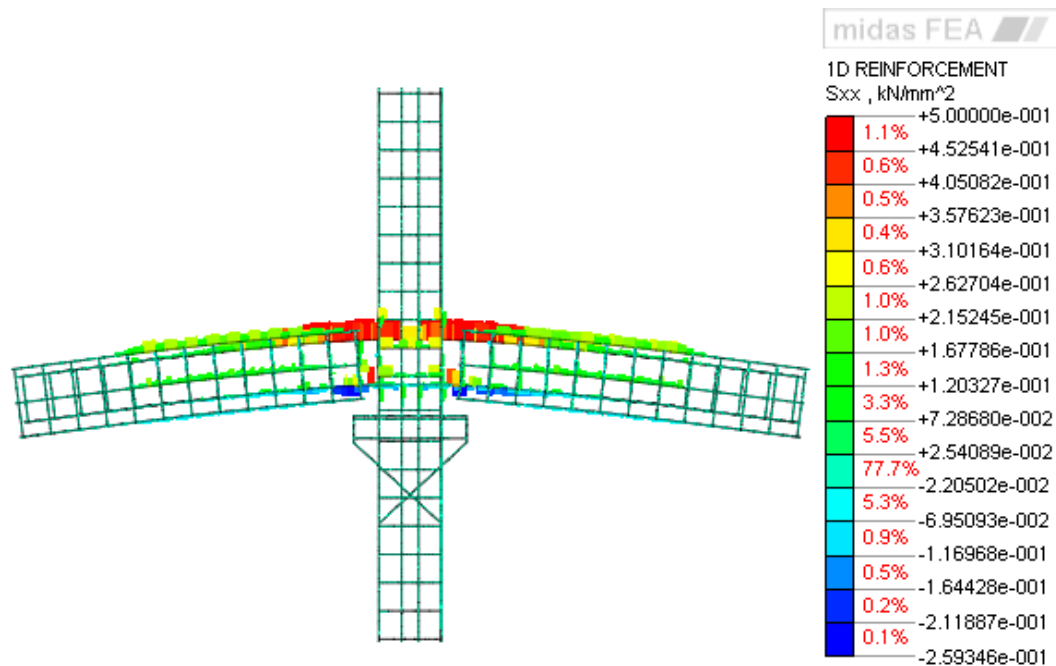


Figure 8-32 Reinforcement stresses of the interior PCBC connection under static loading

8.6 Conclusions

The conclusion of this chapter are:

1. The finite element modelling using Total Strain Crack model is fairly accurate to predict the load-deflection behaviour of the exterior PCBC connection under static loading until the yield point. It is thought that inaccurate prediction after the yield point is due to a lack of data of the interface properties.
2. The FE model of the exterior PCBC connection could not predict the hysteresis loop accurately because MIDAS FEA software could not accommodate the cyclic model for the concrete and steel reinforcement. However, the FE model could predict the peak loads

at each displacement level with the differences less than 12.5% in comparison to experimental result.

3. The longitudinal bars of the beam (adjacent to the column face) yielded before the other reinforcement, which means that the plastic hinge occurred in the beam rather than in the column. This confirms that the exterior PCBC connection fulfilled the strong column-weak beam principle.
4. The relative joint rigidity of the exterior PCBC connection is 67% in comparison with the monolithic beam-column joint.
5. The structural behaviour (in terms of the load-deflection relationship and the reinforcement stress distribution) of the interior PCBC connection subjected to static loading can be predicted using the finite element model which has been developed using the same principles applied when modelling the exterior PCBC connection. The results show that the interior PCBC connection behaved in a similar manner to conventional reinforced concrete members under static loading. The longitudinal bars of the beams yielded first, whereas the column reinforcement remained elastic until the end of test.

Chapter 9

Conclusions and Recommendation for Future Studies

9.1 Introduction

A new type of exterior precast concrete beam-column (PCBC) connection has been developed in this study. The connection system consisted of the precast beam, the precast column, interlocking bars and cast-in-place (CIP) concrete. Five exterior PCBC specimens have been tested experimentally with the variations in terms of types of loading (i.e. static, quasi-static and long-term loadings) and the steel fibre contents (i.e. 0%, 0.5% and 1%) contained in the CIP concrete. The structural behaviour in terms of load-deflection relationship, the failure mode, cracks propagation and the development strain in the reinforcing bars (especially in the interlocking bars) were investigated. Finite element modelling using MIDAS finite element software was developed to predict the load-deflection behaviour for an exterior and interior PCBC connection.

9.2 Conclusions

The main conclusions of this study can be summarised as follows:

1. Load-deflection behaviour

Due to static loading from the beginning until the yield point, the load-deflection curve behaved in a similar manner to traditional reinforced concrete elements. After reaching the yield point, the load decreased as the deflection increased until the maximum deflection

was reached. This is because, after yield, the bond between the CIP beam core and the precast U-beam had started to disintegrate.

Due to quasi-static loading, the load-deflection hysteresis loops appeared stable from the beginning of the test until the last cycle, which consisted of the deflection levels of 3, 8, 12, 18, 24, 36, 48 and 60mm. There was no significant strength degradation after the peak load. All peak loads at all cycles are higher than 75% of the maximum load in both loading directions. The structural behaviour of the exterior PCBC connection under quasi-static loading was evaluated using ACI 374.1-05 (Acceptance Criteria for Moment Frames Based on Structural Testing and Commentary), in terms of the strength degradation, relative energy dissipation ratio and the stiffness degradation. The evaluation shows that the beam-column connection satisfies the acceptance criteria in ACI 374.1-05.

2. Failure mode

Both due to static and quasi-static loadings, the connections exhibited a flexural failure mode, with the plastic hinges forming in the beam. Therefore, this design meets the strong column-weak beam concept.

3. Crack propagation

Under static loading, flexural cracks occurred within the plastic hinge region of the beam, while the joint had no significant cracks and the precast column was free from cracks.

Under quasi-static loading, an 'X' crack pattern was formed in the joint core, no more cracks developed in the joint core after the deflection level of 36mm; after 36mm, the cracks were concentrated in the beam adjacent to the column (the plastic hinge was formed in the beam). At this stage, the stirrups in the joint core were still elastic, whereas the interlocking bars in the beam had a strain that is much larger than the yield strain.

4. Interlocking bars

The interlocking bars connecting the joint core and the beam core can act as flexural reinforcement for the beam core. The development length of the interlocking bars, i.e. 800mm from the column face, is considered necessary to generate enough bond strength between the reinforcing bars and the concrete, so as to allow the interlocking bars to develop their tensile strength through to yield.

Due to static loading (negative loading), only top interlocking bars reached the yield stage, whereas other reinforcement were still elastic.

Due to quasi-static loading, the interlocking bars experienced yield strain at the displacement level of 18mm in both loading directions.

5. Composite behaviour

The precast U-beam and the CIP beam core behave as a composite beam (the evidence for this were the extension cracks from the beam core through the wall of the U-beam and the load-displacement curve). This was also shown by theoretical analysis. After the joint reached the yield phase, the bond strength of the interface between the precast U-beam and the beam core decreased.

The composite behaviour relies on the bond strength between the old and new concrete. In this study, the bond performance is presented by comparing the curvatures obtained from the electrical resistance strain gauges (attached on the interlocking bars within the beam core) and the DEMEC gauges (attached on the concrete surface of the U-beam at Position I). The curvatures of the beam core and the precast U-beam were similar which indicates that the CIP beam core and the precast U-beam were acting compositely. However, under cyclic loading the bond strength decreased after the deflection level of 8mm.

The increase of steel fibre volume fraction in the CIP beam core decreased the bond strength between the beam core and the precast

U-beam. This is because the steel fibres within the concrete decrease the drying shrinkage and reduce micro-cracks at the interface between the old and new concrete which lead to increase the bond strength of the interface.

6. Analytical calculations

The analytical calculation for Specimen P2 was performed with the assumption that there was a good bond between the precast concrete and the CIP beam core (which behave as a composite beam) – at least until the yield phase. The calculation generated the theoretical maximum loads (negative and positive) which are very similar with the experimental maximum load (less than 2% differences).

Conclusions regarding the use of SFRC for the cast-in-place (CIP) concrete:

1. The use of steel fibre reinforced concrete (SFRC) in the CIP connection in this study did not increase the peak load significantly but increase the energy dissipation and crack control.
2. The result of the modulus of rupture (MOR) tests showed that the addition of steel fibres by volume (i.e. 0.5% and 1%) could change the properties of concrete from a brittle material to a more ductile material with deflection-hardening characteristic (shown in the modulus of rupture test). Adding 0.5% and 1% of steel fibre by volume to the concrete increased the modulus of rupture by 1.17% and 29.55% respectively. The steel fibres slowed down crack propagation, prohibiting the crack extension until they were pulled-out from the matrix.
3. The implementation of SFRC with $V_f = 0.5\%$ as a CIP material in the exterior PCBC connection (Specimen P3) could improve the

maximum load, stiffness degradation and energy dissipation in comparison with the PCBC connection with plain concrete as a CIP.

4. The implementation of SFRC with $V_f = 1\%$ as a CIP material in the exterior PCBC connection (Specimen P4) resulted in a slightly lower value (i.e. the maximum load, secant stiffness degradation and energy dissipation) than the beam-column specimen with CIP material ($V_f = 0.5\%$). This is thought to be due to the lower bond strength at the interface between the old concrete (the precast U-beam) and the new concrete (the beam core-CIP concrete), which was potentially reduced due to the tape which was stucked on the polystyrene when manufacturing the precast U-beam of Specimen P4, creating a smooth surface inside the precast U-beam.
5. It is clear from the tests (Specimen P4) that the steel fibres (contained in CIP connection) have postponed and slowed down the crack propagation, causing the shorter cracks in the joint core and the top surface of the beam core. This behaviour is in agreement with the deflection-hardening characteristic resulted from the MOR test.
6. By using normalising energy dissipation (NED), which eliminated the effects of the concrete strength variation and cumulative energy dissipation (CED), the contribution of steel fibre with $V_f = 1\%$ in the CIP material of the precast beam-column connection (Specimen P4) showed the highest result among the other PCBC specimens.

Conclusions regarding the behaviour under sustained loading:

1. Before the test, several cracks appeared at the top surface of the CIP beam core with fine gaps developing at the interface between the precast U-beam and the CIP beam core- this was because of autogenous and drying shrinkage.

Due to sustained loading, the new flexural cracks developed within the plastic hinge region of the beam, which were caused by the effect of the shrinkage and creep.

2. The curvatures of the composite beam section under sustained loading increased due to shrinkage and creep effects, which led to an increase in the deflection of the beam. Thus, the deflection increased as the period of sustained loading increased.
3. The joint rigidity percentage of the PCBC connection is 67% in comparison with the monolithic beam-column joint. This is because the precast U-beam was not perfectly monolithic with the column, which, therefore, meant that a larger deflection at the beam tip was generated.
4. The joint rigidity percentage of 67% was introduced in the equations which are used to predict the immediate deflection of the PCBC connection. This resulted in a similar immediate deflection with the experimental result.
5. The current prediction methods (ACI-318, EC2, AEMM, Branson's method) underestimated the long-term deflection of the exterior PCBC connection, since the PCBC connection only has 67% of the joint rigidity.
6. The rotation of beam-column joint, which is similar with the relative joint rigidity, did not stop when the initial loading was applied, but continued during sustained loading, which resulted in a bigger deflection on the PCBC connection. Thus, it is relevant to apply a factor of 1.5 (i.e. $1/\text{the percentage joint rigidity}$) in Equation (7-5) to represent the effect of the beam-column rotation.

Conclusions regarding the design recommendation:

Currently, specific design recommendations for ductile precast connection are not available. From the test result, using ACI 318-2011 (the design recommendation for monolithic beam-column joint) as a conservative guide for designing the PCBC connection is relevant.

Several requirements (based on ACI 318-2011) were used for designing beam-column specimens with additional notes presented as follows:

1. The flexural strength of the column shall satisfy Equation (3-1). The over-strength factor in the reinforced concrete beam should not be less than 6/5 (Section 21.6.2.2 ACI 318-2011).

$$\sum M_{nc} \geq \sum \left(\frac{6}{5}\right) M_{nb} \quad (9-1)$$

Where,

$\sum M_{nc}$ = the sum of the nominal flexural strengths of columns framing into the joint, evaluated at the faces of the joint.

$\sum M_{nb}$ = the sum of the nominal flexural strengths of the beams framing into the joint, evaluated at the faces of the joint.

In this PCBC connection, $\sum M_{nb}$ was obtained from the longitudinal bars (interlocking bars) of the CIP beam core (the longitudinal reinforcement bars of the precast U-beam were not taken into account to calculate $\sum M_{nb}$ since they were not connected to the joint core). At the beam end, the CIP beam core should be designed to provide the negative moment flexural strength.

2. The column dimensions shall not be less than 20 times the largest diameter of the longitudinal bars of the beam, which extends through a beam-column joint (Section 21.7.2.3 ACI 318-2011). In this PCBC connection, the diameter of the interlocking bars of the CIP beam core was used to determine the column dimension.
3. The width of the beam framing into the joint shall be at least three-fourths the column width (Section 21.7.3.2 ACI 318-2011).

4. The longitudinal reinforcement ratio (ρ) of the column is 1%-6% (Section 21.6.3.1 ACI 318-2011)
5. The longitudinal reinforcement ratio (ρ) of the beam shall not be less than $1.4/f_y$ and not exceed 0.025 (Section 21.5.2.1 ACI 318-2011)
6. The embedment length of the longitudinal bars of a beam extended through the joint (l_{dh} in Figure 3-1) shall not be less than d , or 12 times the diameter of the longitudinal bars of the beam (Section 12.12.3 ACI 318-2011)
7. The development of standard hooks in tension (Section 12.5.1 ACI 318-2011)
8. The transverse reinforcements of joints shall have the same spacing with those of upper and lower columns (Section 21.7.3.1 ACI 318-2011)
9. Due to cyclic loading, the bond between the CIP beam core and the precast U-beam will be damaged. It is suggested that the transverse reinforcement of the CIP beam core at the beam ends (in the plastic hinge regions) should be designed to resist the design shear force.
10. The joint shear strength in the PCBC specimen was designed according to ACI 318-2011, as presented in Section 4.4.4 Chapter 4. This study showed that the joint behave well under static, cyclic and sustained loading.

Conclusions regarding finite element analysis behaviour:

1. The finite element modelling using Total Strain Crack model is sufficiently accurate to predict the load-deflection behaviour of the exterior PCBC connection under static loading until yield point. It is thought that inaccurate prediction after yield point is due to lack of data of the interface properties.

2. The FE model of the exterior PCBC connection could not predict the hysteresis loop accurately because MIDAS FEA software could not accommodate the cyclic model for the concrete and steel reinforcement. However, the FE model could predict the peak loads at each displacement level with the differences less than 12.5% of the experimental result.
3. The longitudinal bars of the beam (adjacent to the column face) yielded before the other reinforcement, which means that the plastic hinge occurred in the beam rather than in the column. This confirms that the exterior PCBC connection fulfilled the strong column-weak beam principle.
4. The structural behaviour, in terms of the load-deflection relationship and the reinforcement stress distribution, of the interior PCBC connection can be predicted using the finite element modelling which have been developed using the same principle with the model of exterior PCBC connection. The results show that the interior PCBC connection behaved in a similar manner to conventional reinforced concrete members under static loadings. The longitudinal bars of the beams yielded first, whereas the column reinforcement remained elastic until the end of test.

Overall, the exterior PCBC connection behaved in a similar manner to conventional in-situ cast reinforced concrete elements, either under static, quasi-static or long-term loadings. The connection has 67% joint rigidity in comparison with the monolithic beam-column joint. Therefore, it leads to have less secant stiffness or greater deflection. However, the connection satisfies the acceptance criteria stated in ACI 374.1-05.

In term of the technical process, the manufacturing of these precast elements (beams and columns) appears to be economical and easy to construct. The precast elements are easy to transport and they have

sufficient in-built tolerances to allow construction by comparatively unskilled staff.

Considering the structural performance and the technical process, this new connection can be expected to offer a better economical and practical method than those currently available.

9.3 Recommendation for Future Studies

There are some areas which need to be investigated in order to understand the structural behaviour of precast concrete beam-column (PCBC) connection.

1. Conducting further experimental tests on the exterior PCBC connection to see the effect of the following parameters, which were associated with the CIP connection, such as the length variation of CIP beam core/ interlocking bars, the beam reinforcement ratio and the steel fibre content.
2. Conducting further experimental tests on the exterior PCBC connection to see the effect several parameter, i.e. column size, beam size and beam reinforcement ratio.
3. Conducting further experimental tests on the exterior PCBC connection using a test set-up which represents an actual beam-column joint, i.e. lateral load (cyclic) and axial load (constant) applied on the top column.
4. Conducting further experimental tests on the interior PCBC connection to investigate the structural behaviour of the interior PCBC connection presented in Chapter 1.
5. The FE model needs to be improved by including more representative models for material properties of concrete and steel

reinforcement, to get better load-deflection behaviour after the yield point (under static loading) and hysteresis load-deflection loops (under cyclic loading).

References

- Abduh, M. 2007. Inovasi teknologi dan sistem beton pracetak di Indonesia: sebuah analisa rantai nilai. In: *Seminar dan Pameran HAKI, Indonesia*.
- ACI 318-08. 2008. Building Code Requirements for Structural Concrete (ACI 318-08) and Commentary. In: American Concrete Institute.
- ACI 318-11. 2011. Building Code Requirements for Structural Concrete (ACI 318-11) and Commentary. In: American Concrete Institute.
- ACI 374.1-05. 2005. *Acceptance Criteria for Moment Frames Based on Structural Testing and Commentary (ACI 374.1-05)*. American Concrete Institute, Farmington Hills Michigan,, USA.
- ACI 544.1 R. 1996. State-of-the-art report on fiber reinforced concrete. *ACI manual of concrete practice-Part. 5*.
- Al Chami, G., Theriault, M. and Neale, K. 2009. Creep behaviour of CFRP-strengthened reinforced concrete beams. *Construction and Building Materials*. 23(4), pp.1640-1652.
- Alshaikh, A.H. and Al-Zaid, R. 1993. Effect of reinforcement ratio on the effective moment of inertia of reinforced concrete beams. *Structural Journal*. 90(2), pp.144-149.
- Altun, F., Haktanir, T. and Ari, K. 2007. Effects of steel fiber addition on mechanical properties of concrete and RC beams. *Construction and Building Materials*. 21(3), pp.654-661.
- Arockiasamy, M., Chidambaram, S., Amer, A. and Shahawy, M. 2000. Time-dependent deformations of concrete beams reinforced with CFRP bars. *Composites Part B: Engineering*. 31(6), pp.577-592.
- Austin, S., Robins, P. and Pan, Y. 1999. Shear bond testing of concrete repairs. *Cement and concrete research*. 29(7), pp.1067-1076.
- Bandara, N.M.S.H., Bandara, I.M.L.R. and Wijesundara, K.K. 2016. Numerical simulation of prediction of shear strength of reinforced concrete beam using Total Strain-Crack model. In: *The 7th international conference in sustainable built environment, Sri Lanka*.
- Barbosa, A.F. and Ribeiro, G.O. 1998. Analysis of reinforced concrete structures using ANSYS nonlinear concrete model. *Computational mechanics-New trends and applications, Barcelona*.
- Bhatt, P. and Kirk, D.W. 1985. Test on an improved beam column connection for precast concrete. *ACI Journal*. pp.834-843.
- Bischoff, P.H. 2005. Reevaluation of deflection prediction for concrete beams reinforced with steel and fiber reinforced polymer bars. *Journal of Structural Engineering*. 131(5), pp.752-767.

- Branson, D.E. 1965. *Instantaneous and time-dependent deflections of simple and continuous reinforced concrete beams*. Alabama Highway Department, Bureau of Public Roads, Alabama (Department of Civil Engineering and Auburn Research Foundation, Auburn University, August 1963).
- Branson, D.E. 1977. *Deformation of concrete structures*. McGraw-Hill Companies.
- Brunesi, E., Nascimbene, R., Deyanova, M., Pagani, C. and Zambelli, S. 2015. Numerical simulation of hollow steel profiles for lightweight concrete sandwich panels. *Comput Concr.* 15(6), pp.951-972.
- Bull, D.K. and Park, R. 1986. Seismic resistance frames incorporating precast prestressed concrete beam shells. *PCI Journal*. pp.54-93.
- CEB-FIP. 1993. *Model Code 1990*. Comite Euro-International du Beton.
- Chao, S.-H., Naaman, A.E. and Montesinos, G.J.P. 2009. Bond behavior of reinforcing bars in tensile strain-hardening Fiber Reinforced Cement Composites. *ACI Structural Journal*. pp.897-906.
- Choi, H.K., Choi, Y.C. and Choi, C.S. 2013. Development and testing of precast concrete beam-to-column connections. *Engineering Structures*. 56, pp.1820-1835.
- Concrete Society. 2014. *Autogenous Shrinkage*. Framewood Road, Wexham, Slough, SL3 6PJ: Concrete Society.
- Elliott, K. 2002. *Precast concrete structures*. Elsevier.
- EN, -. 2004. *Eurocode 2: Design of concrete structures-Part 1-1: General rules and rules for buildings*.
- Ertas, O., Ozden, S. and Ozturan, T. 2006. Ductile connections in precast concrete moment resisting frames. *PCI Journal*. pp.2-12.
- Ezeldin, A.S. and Balaguru, P.N. 1992. Normal and high strength Fiber-Reinforced Concrete under compression. *Journal Mater Civil Engineering*. 4, pp.415-429.
- Ezeldin, A.S. and Shiah, T. 1995. Analytical immediate and long-term deflections of fiber-reinforced concrete beams. *Journal of Structural Engineering*. 121(4), pp.727-738.
- Forth, J. 2015. Predicting the tensile creep of concrete. *Cement and Concrete Composites*. 55, pp.70-80.
- Ganesan, N., Indira, P. and Abraham, R. 2007. Steel fibre reinforced high performance concrete beam-column joints subjected to cyclic loading. *ISET Journal of Earthquake Technology*. 44(3-4), pp.445-456.
- Ganesan, N., Indira, P.V. and Sabeena, M.V. 2014a. Behaviour of hybrid fibre reinforced concrete beam-column joints under reverse cyclic loads. *Materials & Design*. 54, pp.686-693.

- Ganesan, N., Indira, P.V. and Sabeena, M.V. 2014b. Bond stress slip response of bars embedded in hybrid fibre reinforced high performance concrete. *Construction and Building Materials*. 50(0), pp.108-115.
- GENÇOĞLU, M. and Eren, I. 2002. An experimental study on the effect of steel fiber reinforced concrete on the behavior of the exterior beam-column joints subjected to reversal cyclic loading. *Turkish Journal of Engineering and Environmental Sciences*. 26(6), pp.493-502.
- Ghosh, S.K., Nakaki, S.D. and Krishnan, K. 1997. Precast Structures in Regions of High Seismicity: 1997 UBC Design Provisions. *PCI journal*. 42(6), pp.76-93.
- Gibb, A.G. 1999. *Off-site fabrication: prefabrication, pre-assembly and modularisation*. John Wiley & Sons.
- Gilbert, R. 2011. The serviceability limit states in reinforced concrete design. *Procedia Engineering*. 14, pp.385-395.
- Gilbert, R.I. 1999. Deflection calculation for reinforced concrete structures—why we sometimes get it wrong. *Structural Journal*. 96(6), pp.1027-1032.
- Gillette, R.W. 1963. Performance of Bonded Concrete Overlays. In: *Journal Proceedings*, pp.39-50.
- Hartman, T. 1999. *Steel fiber reinforced concrete*. thesis, PhD Thesis, Department of Structural Engineering, Royal Institute of Technology, Stockholm, Sweden.
- Hasan, S., Elliot, K. and Ferreira, M.d.A. 2011. Experimental investigation on the moment continuity of precast concrete beam-column connections under gravity loads. In: *Symposium Prague*, pp.395-398.
- Hasan, S.A. 1994. *Finite element analysis of reinforced concrete deep beams*. MSc thesis, Salahdeen University, Erbil.
- Hawileh, R., Rahman, A. and Tabatabai, H. 2010. Nonlinear finite element analysis and modeling of a precast hybrid beam-column connection subjected to cyclic loads. *Applied mathematical modelling*. 34(9), pp.2562-2583.
- Hidalgo, P. and Jordan, R. 1996. Strength and energy dissipation characteristics of reinforced concrete walls under shear failure. In: *Proceedings of The Eleventh World Conference on Earthquake Engineering, Acapulco, Mexico*.
- Higgins, L., Forth, J.P., Neville, A., Jones, R. and Hodgson, T. 2013. Behaviour of cracked reinforced concrete beams under repeated and sustained load types. *Engineering structures*. 56, pp.457-465.
- Hong, S. and Park, S.-K. 2016. Long-term behavior of fiber-reinforced-polymer-plated concrete beams under sustained loading: Analytical and experimental study. *Composite Structures*. 152, pp.140-157.

- Hordijk, D.A. 1991. *Local approach to fatigue of concrete*. PhD thesis, Delft University of Technology.
- Ibrahim, A.M. and Mubarak, H.M. 2009. Finite Element Modeling of Continuous Reinforced Concrete Beam with External Prestressing. *European Journal of Scientific Research*. 30(1), pp.177-186.
- Indonesia, S.N. 2002. SNI-03-2847-2002-Tata Cara Perhitungan Struktur Beton Untuk Bangunan Gedung. *Jakarta: Badan Standar Nasional*.
- Jiang, C., Fan, K., Wu, F. and Chen, D. 2014. Experimental study on the mechanical properties and microstructure of chopped basalt fibre reinforced concrete. *Materials & Design*. 58, pp.187-193.
- Julio, E.N., Branco, F.A., Silva, V.D. and Lourenco, J.F. 2006. Influence of added concrete compressive strength on adhesion to an existing concrete substrate. *Building and environment*. 41(12), pp.1934-1939.
- Julio, E.N., Branco, F.A. and Silva, V.t.D. 2004. Concrete-to-concrete bond strength. Influence of the roughness of the substrate surface. *Construction and Building materials*. 18(9), pp.675-681.
- Kalkan, I. 2009. *Lateral torsional buckling of rectangular reinforced concrete beams*. thesis, Georgia Institute of Technology.
- Kalkan, İ. 2013. Deflection prediction for reinforced concrete beams through different effective moment of inertia expressions. *International Journal of Engineering*. 5(1).
- Kalogeropoulos, G.I., Tsonos, A.-D.G., Konstandinidis, D. and Tsetines, S. 2016. Pre-earthquake and post-earthquake retrofitting of poorly detailed exterior RC beam-to-column joints. *Engineering Structures*. Volume 109, pp.1-15.
- Kaung, J.S. and Wong, H.F. 2011. Effectiveness of Horizontal Stirrups in Joint Core for Exterior Beam-Column Joints with Nonseismic Design. *Procedia Engineering*. 14, pp.3301-3307.
- Kitayama, K., Kojima, C., Otani, S. and Aoyama, H. 1989. Behavior of reinforced concrete interior beam-column connection subjected to high shear. *Proceedings of The Japan concrete Institute*. 11(2), pp.531-536.
- Korkmaz, H.H. and Tankut, T. 2005. Performance of a precast concrete beam-to-beam connection subject to reversed cyclic loading. *Engineering Structures*. 27(9), pp.1392-1407.
- Kularni, S.M. and Patil, Y.D. 2013. A Novel Reinforcement Pattern for Exterior Reinforced Concrete Beam-Column Joint. *Procedia Engineering*. 51, pp.184-193.
- Lampropoulos, A., Tsioulou, O. and Dritsos, S.E. 2007. Effect of connection procedures on the behaviour of RC columns strengthened with RC layers and jackets. *Earthquake Resistant Engineering Structures VI*. 93, p399.

- Lee, M.K. and Barr, B.I.G. 2004. An overview of the fatigue behaviour of plain and fibre reinforced concrete. *Cement and Concrete Composites*. 26(4), pp.299-305.
- Li, B., Yip, W.K. and Leong, C.L. 2003. Hybrid-steel concrete connections under reversed cyclic loadings. In: *2003 Pasific Conference on Earthquake Engineering*.
- Lim, T., Paramasivam, P. and Lee, S. 1987. Analytical model for tensile behavior of steel-fiber concrete. *ACI Materials Journal*. 84(4).
- MacGregor, J.G. 1992. *Reinforced concrete: mechanics and design*.
- Mahin, S. and Bertero, V. 1976. Problems in establishing and predicting ductility in aseismic design. In: *Proceedings, International Symposium on Earthquake Structural Engineering*, pp.613-628.
- Mahmood, M.N. 2007. Nonlinear analysis of reinforced concrete beams under pure torsion. *Journal of Applied Sciences*. 7(22), pp.3524-3529.
- Maidl, B. and Dietrich, J. 1995. *Steel fibre reinforced concrete*. Ernst, Verlag für Architektur und technische Wissenschaften.
- Marthong, C. and Marthong, S. 2016. An experimental study on the effect of PET fibers on the behavior of exterior RC beam-column connection subjected to reversed cyclic loading. *Structures*. 5, pp.175-185.
- Mathey, R.G. and Watstein, D. 1961. Investigation of bond in beam and pull out specimens with high-yield-strength deformed bars. *Journal of the American Institute*. pp.1071-1090.
- Mattock, A.H. and Hawkins, N.M. 1972. Shear transfer in reinforced concrete—Recent research. *Pci Journal*. 17(2), pp.55-75.
- Maya, L.F., Zanuy, C., Albajar, L., Lopez, C. and Portabella, J. 2013. Experimental assessment of connections for precast concrete frames using ultra high performance fibre reinforced concrete. *Construction and Building Materials*. 48(0), pp.173-186.
- Mazzotti, C. and Savoia, M. 2007. Long-term behaviour of FRP-strengthened beams. In: *The 8th international symposium of fiber reinforced polymer reinforcement for concrete structures (FRPRCS/8), 16-18 July, Patras*. pp.1-10.
- Menegotto, M. and Pinto, P. 1973. Method of analysis for cyclically loaded rc frames including changes in geometry and non-elastic behaviour of elements under combined normal force and bending. In: *IABSE Congress Reports of the Working Commission*.
- MIDAS. 2010. Nonlinear and detail FE analysis system for civil structures- FEA analysis and algorithm manual (www.csfea.net).
- Mindess, S., Young, J.F. and Darwin, D. 2003. *Concrete*. Prentice Hall.

- Naaman, A. and Reinhardt, H. 2003. High performance fiber reinforced cement composites HPFRCC-4: International RILEM Workshop. *Materials and Structures*. 36(10), pp.710-712.
- Naaman, A. and Reinhardt, H. 2006. Proposed classification of HPFRC composites based on their tensile response. *Materials and structures*. 39(5), pp.547-555.
- Naaman, A.E. and Reinhardt, H.W. 1996. *High performance fiber reinforced cement composites 2 (HPFRCC2)*.
- Naderi, M., Sheibani, R. and Shayanfar, M. 2009. Comparison of different curing effects on Concrete strength. In: *3rd International Conference on concrete and development, Tehran, Iran*.
- Nawy, E. 2000. *Reinforced concrete: A fundamental approach*.
- Negro, P. and Toniolo, G. 2012. *Design guidelines for connections of precast structures under seismic actions. Report EUR 25377 EN, European Commission*.
- Neville, A.M., Dilger, W.H. and Brooks, J.J. 1983. *Creep of plain and structural concrete*. Construction press.
- Ngekpe, B.E., Ode, T. and Eluozo, S.N. 2016. Application of total-strain crack model in finite element analysis for punching shear at edge connection. *International Journal of Research in Engineering and Social Sciences*. pp.1-9.
- Noorhidana, V.A. and Forth, J.P. 2016a. An experimental study on precast concrete beam-to-column connection using interlocking bars. In: *The 2nd International Conference on Concrete Sustainability, Madrid, Spain*.
- Noorhidana, V.A. and Forth, J.P. 2016b. Precast concrete beam-to-column connection using interlocking bars, An alternative. *Concrete Plant International (CPI)*. December 2016.
- Nurjaman, H.N., Imran, I., Faizal, L. and Sidjabat, H.R. 2011. Standar Nasional Indonesia tentang metoda uji dan kriteria penerimaan sistem struktur rangka pemikul momen beton bertulang pracetak untuk bangunan gedung. In: *Seminar HAKI Jakarta, Indonesia*.
- Ochs, J.E. and Ehsani, M.R. 1993. Moment resistant connections in precast concrete frames for seismic regions. *PCI Journal*. 38(5), pp.64-75.
- Oh, B.H. 1992. Flexural analysis of reinforced concrete beams containing steel fibers. *Journal of structural engineering*. 118(10), pp.2821-2835.
- Paine, K. and Peaston, K.E.C. 2002. Flexural toughness as a measure of shear strength and ductility of prestressed fibre reinforced concrete beams. In: *Composite Materials in Concrete Construction: Proceedings of the International Seminar Held at the University of*

Dundee, Scotland, UK on 5-6 September, 2002: Thomas Telford, p.201.

- Parastesh, H., Hajirasouliha, I. and Ramezani, R. 2014. A new ductile moment-resisting connection for precast concrete frames in seismic regions: An experimental investigation. *Engineering Structures*. 70, pp.144-157.
- Park, H.G., Im, H.J., Eom, T.S. and Kang, S.M. 2008. An experimental study on beam-column connections with precast concrete U-shaped beam shells In: *The 14th World Conference on Earthquake Engineering, October 12-17,, Beijing, China*.
- Park, R. 1988. State of the Art Report Ductility Evaluation from Laboratory and Analytical Testing. In: *Ninth World Conference on Earthquake Engineering, August 2-9,, Japan*. pp.605-616.
- Park, R. 1994. Simulated seismic load tests on reinforced concrete elements and structures. In: *Earthquake Engineering, Tenth World Conference, Rotterdam*. pp.6681-6693.
- Park, R. and Keong, Y.S. 1979. Tests on structural concrete beam-column joints with intermediate column bars. *The New Zealand National Society for Earthquake Engineering*. 12(3).
- Park, R. and Paulay, T. 1975. *Reinforced Concrete Structures*, John Wiley & Sons, New York.
- Park, R. and Thompson, K.J. 1977. Cyclic load tests on prestressed and partially prestressed beam-column joints. *PCI Journal*. 22(5), pp.84-110.
- Parra-Montesinos, G.J. 2005. High-performance fiber-reinforced cement composites: an alternative for seismic design of structures. *ACI Structural Journal*. 102(5), p668.
- Paulay, T. and Scarpas, A. 1981. The behaviour of exterior beam-column joints. *Bulletin of the New Zealand National Society for Earthquake Engineering*. 14(3), p14.
- Paulson, K.A., Nilson, A.H. and Hover, K.C. 1991. Long-term deflection of high-strength concrete beams. *Materials Journal*. 88(2), pp.197-206.
- Priestley, M. and Park, R. 1987. Strength and ductility of concrete bridge columns under seismic loading. *ACI Structural Journal*. 84(1).
- Roehm, C., Sasmal, S., Novák, B. and Karusala, R. 2015. Numerical simulation for seismic performance evaluation of fibre reinforced concrete beam-column sub-assemblages. *Engineering Structures*. 91, pp.182-196.
- Said, A.M. and Nehdi, M.L. 2004. Behaviour of beam-column joints cast using self-consolidating concrete under reversed cyclic loading. In: *13th World Conference on Earthquake Engineering, August 1-6, , Canada*.

- Santos, P.M.D. and Júlio, E.N.B.S. 2011. Factors affecting bond between new and old concrete. *Materials Journal*. 108(4), pp.449-456.
- Seckin, M. and Fu, H. 1990. Beam-column connections in precast reinforced concrete construction. *ACI structural Journal*. 87(3).
- Selby, R.G. and Vecchio, F.J. 1993. 3D constitutive relations for reinforced concrete. *Tech, Rep.93-02 Department of Civil Engineering, Toronto, Canada*.
- Shannag, M.J. and Ziyad, T.B. 2007. Flexural response of ferrocement with fibrous cementitious matrices. *Construction and building materials*. 21(6), pp.1198-1205.
- Shin, H.-C. and Wan, Z. 2010. Interfacial properties between new and old concretes. In: *Second Int. Conf. on Sustainable Construction Materials and Technologies*.
- Sobuz, H.R., Ahmed, E., Sutan, N.M., Hasan, N.M.S., Uddin, M.A. and Uddin, M.J. 2012. Bending and time-dependent responses of RC beams strengthened with bonded carbon fiber composite laminates. *Construction and Building Materials*. 29, pp.597-611.
- Soroka, I., Jaegermann, C. and Bentur, A. 1978. Short-term steam-curing and concrete later-age strength. *Materials and Structures*. 11(2), pp.93-96.
- Soroushian, P. and Bayasi, Z. 1991. Fiber type effects on the performance of steel fiber reinforced concrete. *Materials Journal*. 88(2), pp.129-134.
- Soubra, K.S. 1993. Cyclic response of fibrous cast-in-place connections in precast beam-column subassemblages. *ACI Structural Journal*. 90(3).
- Soubra, K.S. and Naaman, A.E. 1993. Cyclic response of fibrous cast-in-place connections in precast beam-column subassemblages. *Structural Journal*. 90(3), pp.316-323.
- Soubra, K.S., Wight, J.K. and Maaman, A.E. 1991. Fiber reinforced concrete joints for precast construction in seismic areas. *ACI Structural Journal*. 88(2).
- Stanton, J.F., Hawkins, N.M. and Hicks, T.R. 1991. PRESSS Project 1.3: Connection classification and evaluation. *PCI journal*. 36(5), pp.62-71.
- Taylor, P.J. 2014. *Curing Concrete*. CRC Press.
- Thorenfeldt, E., Tomaszewicz, A. and Jensen, J. 1987. Mechanical properties of high-strength concrete and application in design. In: *Proceedings of the symposium utilization of high strength concrete: Tapir Trondheim Norway*, pp.149-159.

- Uma, S. and Prasad, A.M. 1996. Seismic behavior of beam column joints in reinforced concrete moment resisting frames. *Department of Civil Engineering, Indian Institute of technology Madras, Chennai.*
- Valcuende, M. and Parra, C. 2009. Bond behaviour of reinforcement in self-compacting concretes. *Construction and Building Materials.* 23(1), pp.162-170.
- Van Chanh, N. 2004. Steel fiber reinforced concrete. In: *Faculty of Civil Engineering Ho chi minh City university of Technology. Seminar Material*, pp.108-116.
- Vecchio, F.J. and Collins, M.P. 1986. The modified compression-field theory for reinforced concrete elements subjected to shear. In: *Journal Proceedings*, pp.219-231.
- Vecchio, F.J. and Collins, M.P. 1993. Compression response of cracked reinforced concrete. *Journal of structural engineering.* 119(12), pp.3590-3610.
- Vollenweider, B. 2004. Various Methods of Accelerated Curing for Precast Concrete Applications, and Their Impact on Short and Long Term Compressive Strength. *Concrete Technology.*
- Washa, G.W. and Fluck, P. 1952. Effect of compressive reinforcement on the plastic flow of reinforced concrete beams. In: *Journal Proceedings*, pp.89-108.
- Yee, A.A. 1991. Design considerations for precast prestressed concrete building structures in seismic areas. *PCI Journal.* 36(3), pp.40-55.